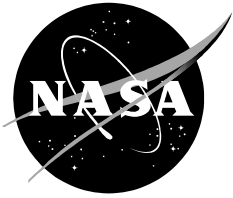**NASA/CR—2003–212799**

An Overview of Autogyros and The McDonnell XV-1 Convertiplane

Franklin D. Harris

October 2003

The NASA STI Program Office ... in Profile

Since its founding, NASA has been dedicated to the advancement of aeronautics and space science. The NASA Scientific and Technical Information (STI) Program Office plays a key part in helping NASA maintain this important role.

The NASA STI Program Office is operated by Langley Research Center, the lead center for NASA's scientific and technical information. The NASA STI Program Office provides access to the NASA STI Database, the largest collection of aeronautical and space science STI in the world. The Program Office is also NASA's institutional mechanism for disseminating the results of its research and development activities. These results are published by NASA in the NASA STI Report Series, which includes the following report types:

- TECHNICAL PUBLICATION. Reports of completed research or a major significant phase of research that present the results of NASA programs and include extensive data or theoretical analysis. Includes compilations of significant scientific and technical data and information deemed to be of continuing reference value. NASA counterpart of peer-reviewed formal professional papers, but having less stringent limitations on manuscript length and extent of graphic presentations.

- TECHNICAL MEMORANDUM. Scientific and technical findings that are preliminary or of specialized interest, e.g., quick release reports, working papers, and bibliographies that contain minimal annotation. Does not contain extensive analysis.

- CONTRACTOR REPORT. Scientific and technical findings by NASA-sponsored contractors and grantees.

- CONFERENCE PUBLICATION. Collected papers from scientific and technical conferences, symposia, seminars, or other meetings sponsored or co-sponsored by NASA.

- SPECIAL PUBLICATION. Scientific, technical, or historical information from NASA programs, projects, and missions, often concerned with subjects having substantial public interest.

- TECHNICAL TRANSLATION. English-language translations of foreign scientific and technical material pertinent to NASA's mission.

Specialized services that complement the STI Program Office's diverse offerings include creating custom thesauri, building customized databases, organizing and publishing research results ... even providing videos.

For more information about the NASA STI Program Office, see the following:

- Access the NASA STI Program Home Page at *http://www.sti.nasa.gov*

- E-mail your question via the Internet to help@sti.nasa.gov

- Fax your question to the NASA STI Help Desk at (301) 621-0134

- Telephone the NASA STI Help Desk at (301) 621-0390

- Write to:
  NASA STI Help Desk
  NASA Center for AeroSpace Information
  7121 Standard Drive
  Hanover, MD 21076-1320
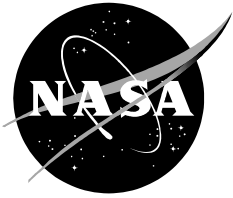
An Overview of Autogyros and The McDonnell XV-1 Convertiplane

Franklin D. Harris
University of Maryland
Dept. of Aerospace Engineering
College Park, MD 20742

Available from:

TABLE OF CONTENTS

THIS PAGE INTENTIONALLY BLANK

FOREWORD

About once a decade (since World War II), the subject of the autogyro and its many variants comes to our attention again. United States Army questions about its needs for a Future Transport Rotorcraft precipitated the review this time. On this occasion, Dr. Michael Scully (US Army AFDD) and Dr. William Warmbrodt (NASA Ames) raised the subject with me. They asked if I would prepare and give a seminar on the subject at NASA Ames, which I did on June 18 and 19, 2003. The seminar was titled "Let's Revisit Autogyros." At the seminar's conclusion, Dr. Scully suggested that the presentation material would be more archivalable if published as a NASA/USAAMCOM document. This report is in response to Dr. Scully's suggestion.

The report serves primarily as a summary to the seminar's many charts, tables and photographs. The seminar material itself is contained in the report as an Appendix. While the report is in normal portrait format, the Appendix is in landscape format. This appendix is numbered consecutively starting at page A-1. Lastly, the seminar included 16 additional topics in a section entitled Supplemental Data and Charts. The table of contents for these 16 supplemental topics is on page A–181.

In addition to the acknowledgements on page A–180 of the seminar, I especially want to thank Ray Prouty, Dick Carlson and Troy Gaffey for being at the seminar. Not only did they add technical explanations to several subjects addressed, they related personal recollections which were not lost on the young engineers who attended. Lastly, John Davis (US Army AFDD), who chaired the meeting, was very, very helpful in acquainting me with the modern "give a show projector" system. He also has taken custodial responsibility for all the material used in preparing and giving the seminar.

<div align="right">

Frank Harris
October 2003

</div>

THIS PAGE INTENTIONALLY BLANK

An Overview of Autogyros and the McDonnell XV–1 Convertiplane

Franklin D. Harris

INTRODUCTION

Autogyros, their technology and their compound helicopter derivatives, have become a minor (if not nonexistent) topic in the curriculum and apprenticeship of several generations of rotorcraft engineers. Names such as Cierva, Pitcairn and Kellett and aircraft such as the Rotodyne and Lockheed's AH–56 Cheyenne are, of course, still recalled. But the overwhelming attention for several decades has been on helicopter engineering and the more recently emerging tilt rotor technology. And yet, questions frequently arise about applying new technology to many concepts– but fewer experimental aircraft–that failed to live up to their promise. For example, the development of the Bell/Boeing V–22 Tiltrotor has been accompanied by thoughts that a lower risk development of an aircraft having less performance might well be a better investment strategy. These thoughts have, on more than one occasion, led to re-examining the potential of compound helicopters and even the wingless autogyro itself.

To respond to these thoughts, the questions they create and the re-examinations sought, today's rotorcraft engineers frequently must start from first principles because of insufficient background. Of course, the re-examinations encounter extravagant claims by zealous advocates, which hardly helps an objective study of quantitative results. Still in all, periodic re-examinations have considerable value.

It is with just these thoughts in mind that an overview of autogyros and, primarily, their performance has been prepared drawing from the many pages of the seminar, which are included as an appendix to this report. Following a brief historical assessment, the elementary aerodynamic technology of autogyro components (i.e. fuselages, wings, propeller, and rotors) is provided. Finally, a detailed re-examination of the McDonnell XV–1 Convertiplane is made. This re-examination allows (1) an application of the elementary aerodynamic technology, and (2) a discussion of an aircraft having considerable potential to fill the gap between helicopters and higher speed/range VTOLs such as the Bell/Boeing V–22 Tiltrotor.

HISTORY
(Appendix pages A–3 to A–25)

The autogyro[1] era began with Juan de la Cierva's development of his C–1 (from the latter part of 1919 to unsuccessful flight during October 1920). The 25 year era ended, for all practical purposes, by 1943 after the U.S. Army Air Corp selected the underpowered Sikorsky R–4 helicopter instead of the competing Kellett XO/YO–60 autogyro or the less satisfactory Pitcairn XO–61 autogyro. The choice was made primarily upon the fact that the helicopter could hover and the autogyro could not. A configuration comparison (A–14 & A–19) shows the XO/YO–60 bested the R–4 in every performance category. The rotor and control systems were functionally identical in that both aircraft had 3–blades and fully articulated hubs; both used collective and cyclic control. Laying cost aside, the discriminator was simply a short takeoff and landing (STOL) autogyro versus a vertical takeoff and landing (VTOL) helicopter.

The autogyro industry, while it existed, developed some 46 aircraft types and delivered about 450 rotorcraft. The aircraft's safety record was easily 5 times better than general aviation experience over the 25 year period. The cost per pound of weight empty varied from $3.50 for the Cierva C.30 (of which 180 were produced) up to about $8.00 for the Pitcairn PCA-2 (of which 25 were produced), these costs being in "back then dollars." The industry reduced the civil autogyro's initial weight empty to gross weight fraction from 0.81 to 0.58 by the end of the era. From a business point of view, our pioneers (a) created a flying machine other than an airplane, (b) acquainted the public with the aircraft and (c) pursued a vigorous product improvement program.

The technology foundation for all helicopters (and its still evolving industry) comes from the autogyro's research, development, production and field service era. Only a minimum of effort was required to list 10 fundamental technology contributions from which the helicopter industry now benefits (A–24). Cierva laid the initial technical foundation with his 2 volume notebook entitled "Engineering Theory of the Autogiro." These notebooks were edited by Dr. James A.J. Bennett, found their way into Dr. Richard Carlson's hands in the mid 1970s, who later sent a copy to the American Helicopter Society Library. The bulk of all follow on engineering work can now be found in pre 1940s technical society journals, NACA technical notes and reports and, from Britain, the Royal Aircraft Establishment and National Physical Laboratory research published as a British Aeronautical Research Council R & M.

Three particularly noteworthy reports stand out in the pre 1940s open literature. The first is H. Glauert's and C.N.H. Lock's R & M 1162 published in April 1928 and titled "A Summary of the Experimental and Theoretical Investigations of the Characteristics of an Autogiro." The second is John B. Wheatley's 1932 NACA TR 434 dealing with the "Lift and Drag Characteristics of Gliding Performance of an Autogiro [the Pitcairn PCA–2] as Determined in Flight." The third report, R & M 1859, deals with the Cierva's production C.30 Autogiro. It was published in March 1939 and titled "General Investigation into the Characteristics of the C.30 Autogiro."

---

[1] Peter W. Brooks (in his absolutely indispensable and comprehensive book "Cierva Autogiros" published by the Smithsonian Press) states in note 2, pg. 357 that the word Autogiro was a Cierva Company trademark, to be spelled with a capital A and with the "i". He further says the generic term is autogyro, with a lower case "a" and a "y". Ray Prouty, in private conversation, noted that autogiro is Spanish for autogyro in his dictionary.

It is generally known (within the rotorcraft community) that Cierva developed the flapping hinge for rotor blades before his early C–4 Autogiro was really flyable. Later, he introduced the lead–lag hinge. These two articulated joints insured that blade loads would be minimal in flight. These and other improvements were incorporated into his C.30 Autogiro, his most successful production configuration. What is not so commonly known is that the C.30's rotor blades were a significant departure from his earlier configurations. For example, an aerodynamic performance improvement was made by going from the C–6's 4 wide chord blades having 0.19 solidity to 3 narrow chord blades with 0.047 solidity on the C.30.[2] This reduction in solidity was accompanied by an airfoil thickness to chord ratio increased from the C–6's 11.4 percent to 17.1 percent for the C.30.

What is even less well known is that the C.30 used a highly cambered airfoil instead of the symmetrical airfoil of all preceding models. The airfoil's nose down pitching moment caused severe elastic twisting of the blade. Because of this adverse blade twisting, the C.30 experienced a forward tilt of the rotor as forward speed was increasing. This led to the adverse stick gradient shown in Figure 1. The elastic twisting became so severe at high speed, that the aircraft could not be pulled out of dive, which led to a fatal accident in January of 1935. Beavan and Lock successfully analyzed the "phenomena" and reported their results in R & M 1727 from which Figure 1 was taken.[3]
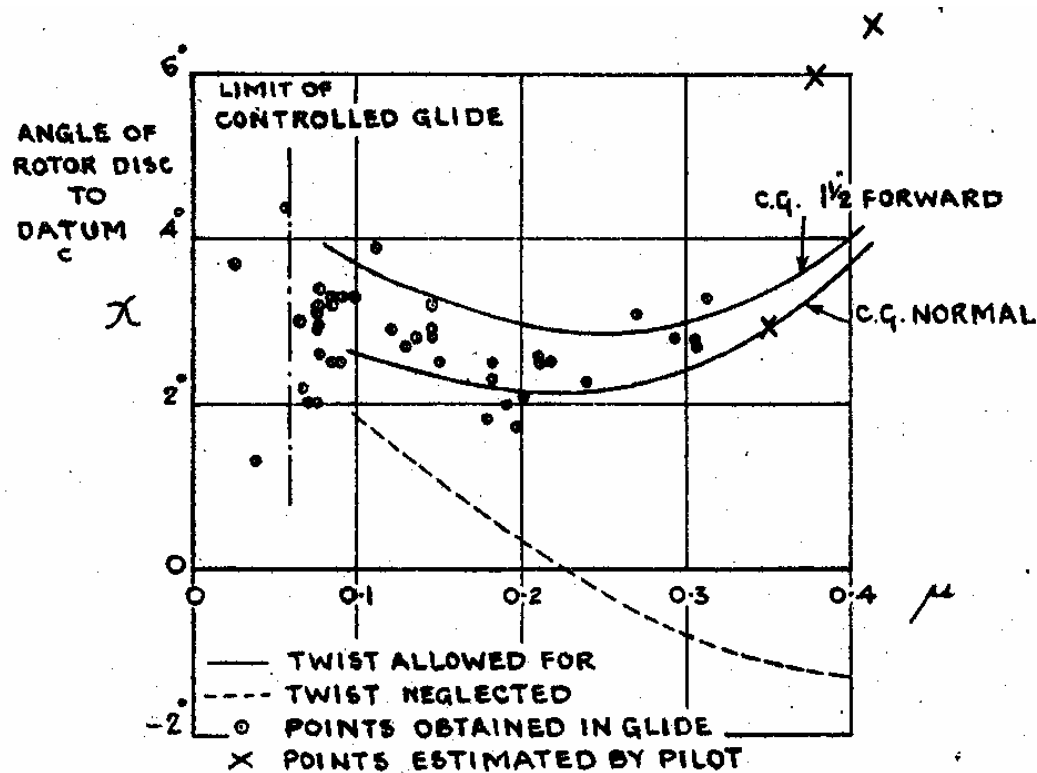
Figure 1. The Cierva C.30's Stick Gradient Became Adverse at High Speed Due to Blade Elastic Twisting Caused by a Highly Cambered Airfoil.

---

[2] Solidity is the ratio of total blade area to swept area. For rectangular blades, one blade's area is (chord × radius). The total blade area is simply number of blades times the area of one blade. The swept area is πR^2.

[3] See "The Effect of Blade Twist on the Characteristics of the C.30 Autogiro" Aeronautical Research Council of Great Britain, Reports and Memoranda No. 1727, April 1936.

Because of this adverse longitudinal stick position to trim the aircraft, the Cierva C.30 could not be certificated by today's FAA or MIL Std 8501A design standards. The use of cambered airfoils was quickly abandon in favor of symmetrical airfoils having virtually zero pitching moments. Today, only the most recent helicopters have returned, with care, to cambered airfoils that have a slight amount of trailing edge reflex to avoid significant airfoil pitching moments.

The addition of the lead–lag hinge solved blade bending moment problems, but, as is frequently the case, the hinge led to a disastrous downstream problem. The problem was ground resonance, the results of which are shown in Figure 2.

The addition of jump takeoff capability required over speeding the rotor on the ground. At the higher rotor speed, blade lead–lag motion coupled with aircraft rocking motion leading to a destructive conclusion within 5 seconds. Peter Brooks notes in his book that Bob Wagner of Kellett and Prewitt Coleman of NACA independently provided the industry with analysis that explained the "phenomena." The helicopter industry heeded this autogyro lesson.

Figure 2. The Kellett XR–2 Autogyro Before and After Ground Resonance.

4

The assessment of the engineering related literature suggests that the autogyro was quite capable of competing with general aviation airplanes of the era between WW I and the start of WW II; however, it was not competitive with military aircraft. The autogyro's maximum aircraft lift to drag ratio (not including propeller efficiency) was on the order of 5 to 6 (A–10 and A–15), though the rotor blades alone easily achieved a maximum L/D of 10 at high speed cruise. When the autogyro lift–drag ratio is defined as

$$\text{Aircraft } \frac{L}{D} = \frac{\text{Gross Weight (lbs)}}{\dfrac{550}{V_{fps}}\left[\text{Engine(s) Horsepower Required}\right]}$$

(which implicitly includes propeller efficiency, accessory and other losses), the autogyro's maximum aircraft L/D was roughly 3.5 (A–27).

Like general aviation aircraft of the period, the autogyro suffered from (a) excessive fuselage drag compared to the rotor's lifting efficiency, (b) non-retracting landing gear, (c) fixed pitch propellers of poor propulsive efficiency and (d) heavy weight reciprocating engines. In short, disregarding hub drag, the rotor system was not the detracting feature of the aircraft.

TECHNOLOGY ASPECTS
(A–26 to A–77)

After WW II, interest in what came to be called a convertiplane (aka, an autogyro with wings or a compound helicopter or an airplane with a rotor) was reawakened. The high speed limitations of helicopters were becoming evident and the gap in maximum speed between this rotary wing aircraft and the fixed wing airplane was widening. And it became necessary for rotorcraft engineers to apply airplane technology. That is, they added engineering of streamlined fuselages, efficient wings, variable pitch propellers and retractable landing gear to their growing knowledge of high advance ratio, high advancing tip Mach number rotors.

Component Aerodynamics

The elementary aerodynamics of fuselages, wings, rotors and propellers is covered with pages A–26 to A–57. Fuselage parasite drag is, as it has always been, the primary reason for an aircraft's poor performance. The seminar's pages compare fixed to rotary wing aircraft using the parameter, equivalent flat plate drag area, $f_e = D/q$, in units of square feet. Through evolution, today's modern helicopter fuselage is nearly on par with a fixed wing airplane fuselage, given that both aircraft have retracted landing gear (A–33 to A–36). But when the helicopter's rotor hub is included as part of the fuselage, helicopters (and by similarity, convertiplanes) suffer a substantial parasite drag area penalty. The current state of fuselage and hub drag is quite adequately summarized as

$$f_e = 1.65\left(\frac{\text{Gross Weight}}{1000}\right)^{2/3} + 0.85\left(\frac{\text{Gross Weight}}{1000}\right)^{2/3}$$

The first term accounts for a fuselage with retracted landing gear, the second term accounts for a rotor hub. Note that if the gross weight is equally shared by two rotors as in a tandem, side–by–side or synchropter configuration, the total hub parasite drag area is likely to be $2^{1/3} = 1.26$ greater than one hub carrying all of the gross weight. This latter result assumes, of course, equal design engineering skill.

The aerodynamic performance of a simple fixed wing is addressed on pages A–37 and A–38 and by the last equation on page A–39. Ludwig Prandtl fully explained basic wing lift and drag performance and his original work is available in NACA Technical Report No. 116. For initial convertiplane design studies, one hardly needs to read any other papers or books.

The elementary aerodynamic performance of a simple rotary wing is well understood by most rotorcraft engineers.[4] The convertiplane introduces an additional feature–an autorotating rotor– to an engineer who has only helicopter background. The helicopter engineer is quite comfortable with lifting and propelling rotor blade performance as described by the equation:

$$\text{Rotor Power Required} \left(\text{RHP}_{\text{Req'd.}} \right) = \frac{\text{Induced Power} \left(P_i \right) + \text{Profile Power} \left(P_o \right) + \text{Parasite Power} \left(P_p \right)}{550}$$

The helicopter rotor is tilted forward to produce a propelling force, $F_P = q\, f_e$, which leads to a parasite power, $P_P = V F_P$, at flight path velocity, V.

The convertiplane engineer sees the lifting rotor blades as creating a drag, D_R – not a propulsive force – and rearranges the helicopter engineer's equation to

$$\text{Rotor Drag} \left(D_R \right) = -F_P = -\frac{550\, \text{RHP}_{\text{Req'd.}}}{V} + \frac{P_i}{V} + \frac{P_o}{V} = T_R \sin \alpha_{\text{tpp}} + H_R \cos \alpha_{\text{tpp}}$$

Page A–29 provides a schematic showing the tip path plane (tpp) coordinate system. Now, if the rotor is in autorotation, $\text{RHP}_{\text{Req'd.}} = 0$. Then, for good measure, the convertiplane engineer can express autorotating rotor blade drag as an equivalent parasite drag area simply by dividing by dynamic pressure, q, where upon

$$\text{Rotor } f_e = \frac{D_R}{q} = \frac{P_i}{qV} + \frac{P_o}{qV} = \frac{T_R \sin \alpha_{\text{tpp}} + H_R \cos \alpha_{\text{tpp}}}{q}$$

To facilitate communication, the convertiplane engineer can, of course, always resort to helicopter notation so that

$$\text{Rotor } C_D = \frac{D_R}{\rho \left(\pi R^2 \right) V_t^2} = \frac{C_{Pi}}{V/V_t} + \frac{C_{Po}}{V/V_t} = C_T \sin \alpha_{\text{tpp}} + C_H \cos \alpha_{\text{tpp}}$$

No matter how the rotor blade drag equation is viewed, the convertiplane engineer is quite interested in rotor blade drag at advance ratios that are 2 or 3 times the maximum advance ratio which interests the helicopter engineer. The reason for the interest in two different advance ratio

---

[4] However, the preoccupation with isolated rotor blade performance has permitted a complete disregard of the blades plus hub system performance. Ignoring hub drag has led to virtually zero improvement in helicopter maximum cruise speeds for several decades.

regions is because there are two very different performance objectives. This point is illustrated with Figure 3. The helicopter engineer is designing a rotor system that must both lift and propel. He searches for the point of maximum lift to drag ratio. After several decades, this point general has been found near an advance ratio of 0.4 – if there is little compressibility involved.[5] When compressibility becomes a factor, the maximum L/D will occur closer to an advance ratio of 0.35. It is, of course, possible to force the rotor to perform at higher advance ratio as Figure 3 suggests, but the penalty is high solidity and reduced tip speed. One important reason the helicopter's cruise speed nearly doubled from, say a Sikorsky R-4 of 1943, to the modern helicopter is that design advance ratios approaching 0.4 became possible with increased installed power per pound of weight. Higher power loading was permitted by gas turbine engines. Going from an R-4's 0.2 advance ratio to 0.35 or 0.4 today about doubled the maximum rotor L/D as Figure 3 suggests. Of course, such streamlining as retractable landing gear was a key factor as well.

The convertiplane engineer's rotor performance objective is to defeat the conventional helicopter rotor's trend of poor performance at high speed caused by compressibility and blade stall. The typical approach has been to off load the rotor lift on to a wing, transfer the propulsion requirement on to a propeller (or some other propulsive device) and idle the rotor at a very low tip speed in autorotation. It is important to keep in mind that a rotor will not autorotate efficiently –if a all – without carrying some lift and operating at some slightly positive angle of attack. After several decades, this convertiplane approach has been reduced to a search for the rotor's minimum equivalent parasite drag area.
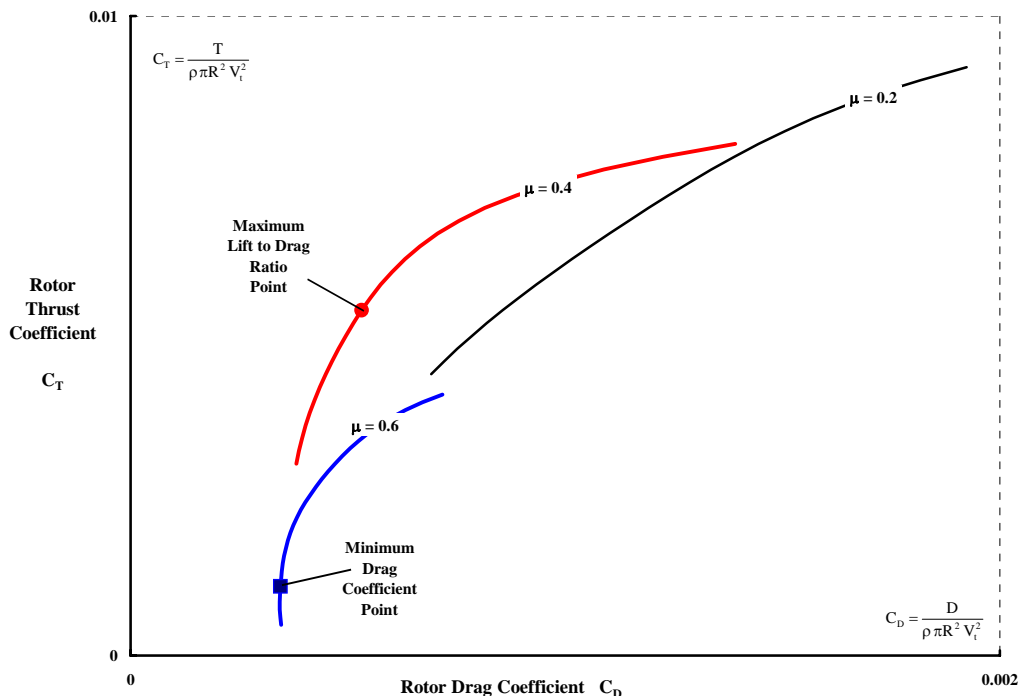
Figure 3. Typical Lift–Drag Polars for a Conventional Rotor.

[5] Ref.: F.D. Harris, "Rotary Wing Aerodynamics–Historical Perspective and Important Issues." Paper Given at AHS Southwest Region Specialists' Meeting on Aerodynamics and Aeroacoustics, Feb. 25-27, 1987. (Chairman: Tom Wood of Bell Helicopter). Contact Mike Scully for a copy.

These two different performance objectives can be examined another way as illustrated by Figures 4 and 5. First, consider the variation in rotor blade drag coefficient (helicopter notation) with advance ratio as shown in Figure 4. This is a calculated result for an autorotating rotor operating at a quite low rotor thrust coefficient, C_T, relative to the C_T for maximum L/D shown on Figure 3. From the helicopter engineer's point of view, this rotor has a minimum rotor total blade drag coefficient of $C_D = 0.00041$ at $\mu = 0.4$. Suppose the tip speed of this lifting and, if tilted forward, propelling rotor was 700 feet per second. At $\mu = 0.4$, the corresponding speed is 166 knots and the advancing tip Mach number would be 0.88. Now, suppose the rotor area is 1,600 square feet and the rotor is operating at sea level density. The rotor blade total drag would then be about 760 pounds at the minimum drag coefficient, $C_D = 0.00041$, as seen from Figure 4 for $\mu = 0.4$.

The convertiplane engineer is searching for the minimum drag point, *which is not the helicopter engineer's minimum drag coefficient point of $C_D = 0.00041$ at $\mu = 0.4$*. To illustrate this fundamental difference, suppose the rotor tip speed was slowed from 700 to 350 feet per second, still holding forward speed at 166 knots. The advance ratio would double to $\mu = 0.8$ and the advancing blade tip Mach number would drop to 0.77. The rotor total blade drag coefficient would rise to $C_D = 0.00056$ according to Figure 4. But with the same rotor area of 1,600 square feet and sea level density, the drag would be reduced to about 260 pounds from 760 pounds. This is an example of the carrot held out by a convertiplane. Of course, the drag of a wing to carry most of the convertiplane weight and the efficiency of the propeller to overcome the drag become very important if this favorable 500 pound rotor blade drag reduction is not completely eroded.

Figure 5 expresses this example by using drag divided by dynamic pressure, D/q in square feet, plotted versus advance ratio, which is the convertiplane engineer's preferred coordinate system. The exact same drag data leading to C_D in Figure 4 has been converted to D/q in Figure 5. The equivalent flat plate parasite drag area of this unloaded rotor drops from about 8 ft^2 at $\mu = 0.4$ to well under 3 ft^2 at $\mu = 0.8$. Figure 5 also shows that the equivalent drag area is not likely to drop much lower if advance ratio is increased to 0.9 or even 1.1 – at least according to this calculation, which has been made with CAMRAD II methodology.[6]

The difference in advance ratio interest leads to a poorly understood point about rotor induced drag (i.e., induced power divided by velocity). Most helicopter engineers dismiss induced power – and thus induced drag – as almost second order in importance based on classical teachings. In fact, calculations made with a rotor wake that recognizes and accounts for the rotor's non–uniform lift distribution in forward flight can now correct this classical view as pages A–42 to A–49 discusses. Figure 4, obtained with the CAMRAD II comprehensive code, points out that the minimum drag coefficient (in helicopter notation) of an autorotating rotor occurs around 0.4 advance ratio. It also shows that the induced drag coefficient does not diminish after 0.4 advance ratio.

---

[6] Johnson, W., "CAMRAD II Comprehensive Analytical Model for Rotorcraft Aerodynamics and Dynamics - Theory Manual," Johnson Aeronautics, Palo Alto, California, 1993.
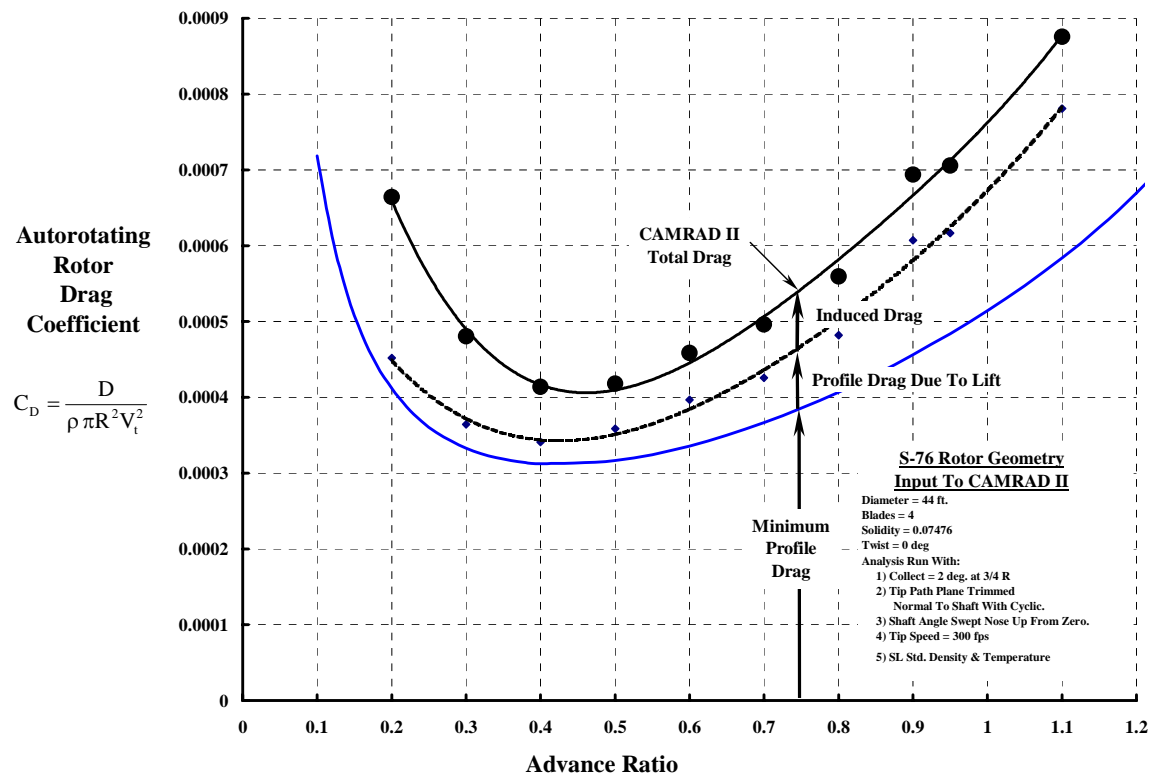
Figure 4. Calculated Autorotating Rotor Blade Drag Coefficient versus Advance Ratio.
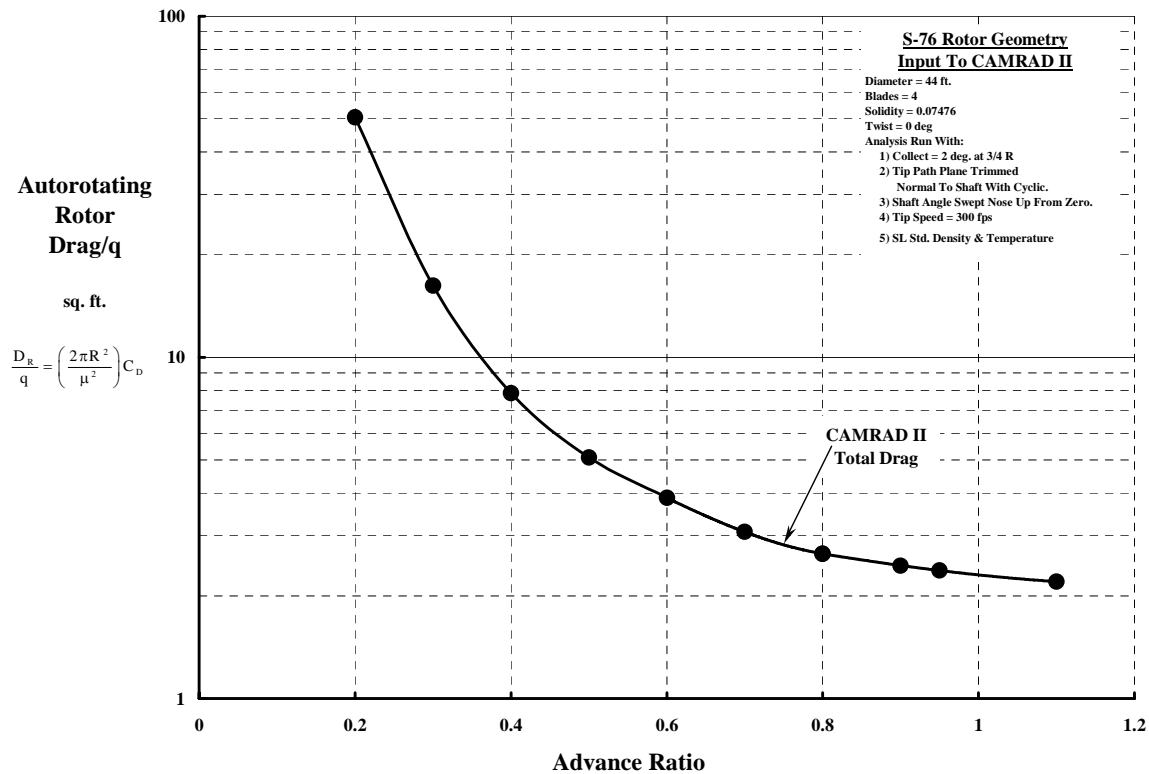
Figure 5. Calculated Autorotating Rotor Blade D/q versus Advance Ratio.

Another poorly understood point about the autorotating rotor and its blade drag has to do with minimum profile drag, which Figure 4 shows is the primary drag. The minimum profile drag is P_o/V, and P_o is the sum of two terms, ΩQ_o and VH_o (see Supplemental Data and Charts, A–181, Items 5 & 11). Now the autorotating rotor requires some upwards flow through the thrust carrying rotor disc. This upflow creates an accelerating torque, which balances the decelerating torque due airfoil drag. Since the decelerating torque due airfoil drag is Q_o, the energy per unit time, a power, is ΩQ_o. The balancing energy per unit of time is $V(T\alpha_o)$ and therefore,

$$T(\alpha_o) = \frac{\Omega Q_o}{V}$$

For autorotation to occur, some combination of rotor thrust and rotor angle of attack must exist. It is possible, of course, for a convertiplane to carry its gross weight on its wing and operate its rotor at zero thrust (and/or zero angle of attack); but then the required torque, Q_o, must be provided directly by shaft power and the propeller provides enough thrust to overcome H_o.

Another way of looking at this point about minimum profile drag follows this logic:

$$D_R = T_R \sin\alpha + H_R \cos\alpha$$

or, for small angle of attack,

$$D_R \approx T\alpha + H = T(\alpha_i) + T(\alpha_o) + H_i + H_o = D_i + \left[T(\alpha_o) + H_o\right] = D_i + D_o$$

Then the substitution of $T(\alpha_o) = \Omega Q_o / V$ gives

$$\text{Minimum Profile } D_R \equiv D_o = T(\alpha_o) + H_o = \frac{\Omega Q_o}{V} + H_o = \frac{\Omega Q_o + VH_o}{V} = \frac{P_o}{V}$$

The Seminar's, Supplemental Data and Charts, Item 11 (A–211 to A–215) addresses minimum profile power, P_o, in considerable length.

The last convertiplane component the seminar addresses is propeller performance (A–51 to A–56). The propeller became a reasonably efficient propulsive device when fixed pitch was replaced by a variable pitch mechanism. With this feature, propulsive efficiency well above 0.8 could be obtained over a very wide speed range. In fact, just when the jet engine and swept wing were gaining favor in the fixed wing industry, NACA thoroughly tested a 3-bladed, 9.75 foot diameter propeller, which demonstrated a propulsive efficiency of 0.88 at 400 knots (A–53 and A–54). One can contrast this modern, variable pitch propeller's efficiency with the YO–60's fixed pitch propeller efficiency shown on page A–17. A simple, empirical equation that captures a variable pitch propeller's performance (i.e., power required to produce a desired propulsive force) is given on page A–56.

Rotor Behavior at High Advance Ratio

Thrust and rigid blade flapping behavior is discussed in the seminar, pages A–59 to A–69. A reasonable body of work suggests that rotor flapping stability becomes a serious issue for advance ratios above 1.5. Both analysis and experiment confirm that 2 per flapping is a very destabilizing influence on rotor's behavior (A-67, 68). What is less well known, is that the change of thrust with collective pitch reverses sign as Figure 6, below, shows (See footnote 5).
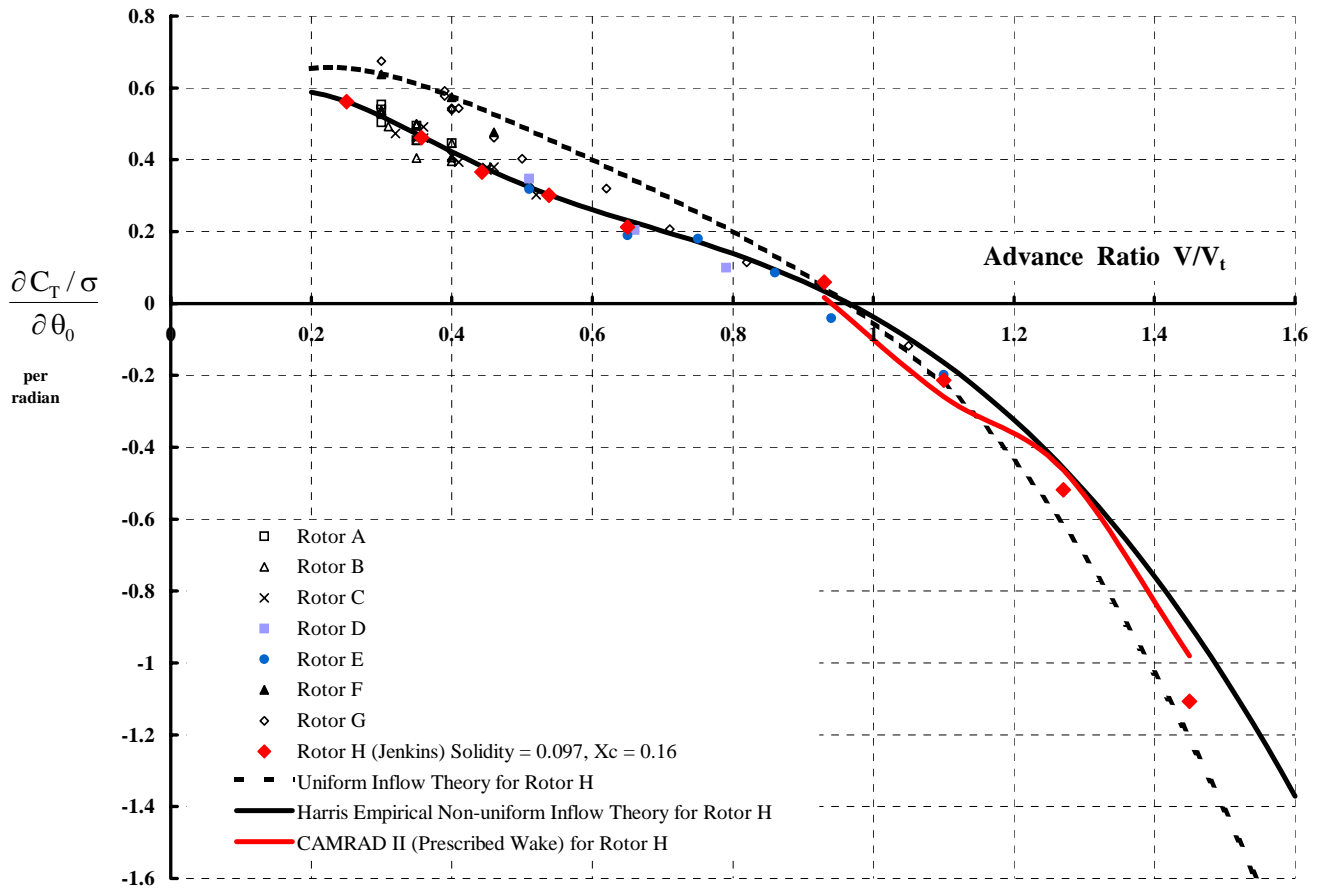
Figure 6. Thrust Sensitivity to Collective Pitch at Constant Tip Path Angle of Attack for Articulated and Teetering Rotors Having Little Pitch–Flap Coupling.

Limits to Rotor Lift and Propulsion

This technology aspect was explored using the CAMRAD II comprehensive code and the graphical results are provide, pages A–71 to A–76. When all issues such as loads, vibration, instabilities, etc. are laid aside, the articulated rotor's aerodynamic capability to both lift and propel is rather astounding – if power required is of little concern. The CAMRAD calculations were made for a Sikorsky S–76 isolated rotor. If this rotor, operating at 670 feet per second tip speed, was lifting an S–76 of 10,000 pounds gross weight and overcoming a parasite drag area of $f_e = 10$ square feet, then the calculated performance results are tabulated as

Speed	Rotor Horsepower	Tip Path Plane Angle of Attack	Lift/Drag Based on GW=10,000lbs & RHP	Advancing Tip Mach Number	Advance Ratio
198 kts	2,370 RHP	-14 deg	2.57	0.90	0.50
238	5,930	-23	1.23	0.96	0.60
278	9,490	-31	0.91	1.02	0.70
317	14,820	-36	0.66	1.08	0.80
357	No solution			1.14	0.90

These are rather discouraging results to the engineer searching for a high speed helicopter, but they are very motivating results to a convertiplane engineer. This is particularly so because overcoming 10 ft^2 of parasite area with an $\eta_P = 0.85$ propeller efficiency at 317 knots at sea level on a standard day (q = 342.3 psf) only requires

$$\text{RHP}_{fe} = \frac{q(f_e)V}{550\,\eta_P} = \frac{342.3(10)(1.69 \times 317.5)}{550(0.85)} = 3,900\,\text{hp}$$

Conclusions To Technology Aspects

1. Our autogyro pioneers build a solid foundation for us.

2, Many of the VTOL aircraft that have been studied are not easy to describe simply.

3. Elementary aerodynamics captures the performance of fuselages, wings, props and rotors.

4. There is a wealth of experimental data in the old NACA TRs, TNs, TMs, RMs, etc.

5. Theoretically, a conventional rotor can both lift and propel at speeds above 300 kts. It's just that inordinately large forward shaft tilts and enormous power is required, to say nothing about loads and vibration.

6. Around $\mu = 1$ conventional rotors experience a collective pitch control reversal if rolling moment equilibrium is maintained.

7. Rotor flapping instability caused by 2nd harmonic blade motion is a show stopper to very high advance ratio operation (i.e. $\mu = 1.5$ to 2.0 depending on configuration). Other potential instability problems are too numerous to list.

RE-EXAMINING THE XV–1
(A–78 to A–176)

The 1950s began with a U.S. Army and Air Force sponsored research program to find a high speed VTOL that complemented the helicopter.[7] The Services selected three concepts to pursue:

1. the XV–1 Convertiplane from McDonnell Aircraft Corp.'s Helicopter Division, which was a compound helicopter with pressure jet tip drive rotor, plus a wing and a propeller.

2. the XV–2 from Sikorsky, which had a 1 bladed rotor that would be stopped and stowed, plus a wing and two propellers,

3. the XV–3 from Bell, which had side-by-side tilting rotors, plus a wing.

A down select was made to the XV–1 and XV–3 designs and – you might say – the rest is history.[8] But that neglects the major contributions Kurt Hohenemser and Fred Doblhoff of McDonnell's Helicopter Division made to the technology of edgewise flying rotors operating in autorotation at high advance ratio.

Figure 7. The McDonnell Aircraft Corp., Helicopter Division's XV–1 Convertiplane.

During its development, the XV–1 was a classified program and the lack of details in the open literature reflects this Confidential status. Therefore, considerable help from several sources was turned to in preparing the seminar included in this report. First, two aircraft were built and flown and now they reside–intact–in museums; one at Fort Rucker and one in the Air and Space Museum

---

[7] The helicopter speed record as of April 1949 was 112.6 knots set by a Sikorsky S-52-1. A Piasecki YH-21 raised the record to 127 knots in September 1953. Westland's G–Lynx now holds the helicopter speed record at 216.3 knots, set on August 11, 1986. At this speed, the Lynx aircraft L/D was about 2.

[8] The XV-1 is one of the earliest aircraft on the ANSER V/STOL Aircraft and Propulsion Wheel (see Supplemental Data and Charts, Item 14, page A–229).

storage. Photos from the XV–1 stored at Ft. Rucker,[9] along with several sessions with Mr. Robert Head[10] clarified the key features of a very ingeniously designed rotor system. Secondly, the open literature provided (1) a well documented full scale wind tunnel test, (2) the Phase II Flight Evaluation report and (3) fortunately, several key papers by Hohenemser and others. Finally, two key McDonnell Aircraft Corporation reports authored by Kurt Hohenemser greatly expanded knowledge about the full scale testing that was done.

The XV–1 had 3 operating modes. In the first mode, the helicopter mode, the aircraft flew on the pressure jet tip drive units and the propeller was declutched and stationary. The design rotor speed of the 31 foot diameter rotor was nominally 410 rpm in the helicopter mode and was controlled by the pilot. An autogyro mode was adopted that captured the transition between the helicopter mode and the "airplane" mode. In the autogyro mode, the propeller was clutched in, the 3 tip drive units were turned off and the rotor autorotated at a nominal 325 rpm with collective pitch set to 6 degrees. The pilot controlled rotor rpm in the autogyro mode. In the airplane mode (110 to 125 knots and higher), the rotor rpm was reduced to a nominal 180 rpm and collective pitch was further reduced to 0 degrees. In the airplane mode, rotor rpm was controlled through longitudinal hub plane angle of attack, which was controlled by a flyball governor. The full scale wind tunnel test investigated only the autogyro and airplane modes. Flight testing, of course, included all three modes.

The XV-1's stiff inplane, bearingless and damperless rotor system changed its configuration when transitioning from helicopter/autogyro to airplane flight (A–81, 82,125, 127, and 138 to 150). Each blade was attached to the hub by 2 flex strap bundles, which gave an equivalent flapping hinge offset of 0.062R. A large diameter torque tube controlled feathering and provided the air passage to the blade. This torque tube was centered between the fore and aft flex strap bundles. The hub itself was gimbaled to the rotor mast.[11] The swashplate was mounted to a large diameter tube (called a "stem") and this "stem" was tilted for cyclic input. Blade cyclic feathering was introduced by directly controlling the swashplate plane relative to the aircraft, much as Cierva/Pitcairn/Kellett did on their direct control autogyros. In the helicopter and autogyro modes, the gimbal was free. The blades then had pitch–cone coupling of 65.5 degrees (i.e., 2.2^o pitch down for 1° cone up) and pitch–flap coupling of 15 degrees. In airplane mode, the hub and gimbal were both locked to the "stem" and the collective pitch was reduced to zero degrees. In this locked mode for airplane flight, the pitch–cone and pitch–flap coupling both became 65.5 degrees. Thus, in the airplane mode, the rotor system became a stiff inplane, bearingless and damperless main rotor system (A–81).

Full Scale Testing in NASA Ames 40 by 80 ft Wind Tunnel

Two tests were conducted in the large NASA wind tunnel at Ames Research Center. The first test evaluated the blades, hub and pylon with and without a dummy wing and cylindrical fuselage (A–80). No NACA report is available for this first test conducted during July and August of 1953.

---

[9] Photos courtesy of Larry Frakes, LTC Franco Villaneuvo, and Tim Smith with help from Fort Rucker Museum maintenance staff. They found the aircraft and partially disassembled it so details of the rotor system became clear.

[10] Bob Head, retired from Boeing Mesa and now living in Gilbert, Arizona, was intimately involved with the XV–1. His knowledge was invaluable in understanding just how the XV–1 and its rotor system worked.

[11] The Robinson R–22 and R–44 have a modern day equivalent of the XV–1 hub. These two helicopters are two bladed teetering (i.e. gimbaled) and each blade has its own flapping hinge.

However, Kurt Hohenemser authored "Full Scale Rotor Tests of the Air Force Convertiplane Model XV–1 in the NACA 40 x 80 foot Wind Tunnel at Moffett Field, California," McDonnell Aircraft Corporation Report No. 3379 and dated Feb. 4, 1954.[12]

The second test, conducted during five weeks in April and May of 1954, was reported both by NACA and by Hohenemser. NACA Research Memorandum RM A55K21a, entitled "Full-scale Wind Tunnel Tests of the Longitudinal Stability and Control Characteristics of the XV–1 Convertiplane in the Autorotating Flight Range" was authored by Mr. David H. Hickey and released May 17,1956 with a Confidential classification. Kurt Hohenemser's MAC Report No. 3599 is dated Nov. 1, 1954 and titled "The Characteristics of the Model XV–1 Convertiplane in Airplane and in Autogiro Phase Flight Conditions as Measured in the NACA 40 x 80 foot Wind Tunnel at Moffett Field, California."

Rotor System Test. Seminar pages A–79 to A–96 re-examine the "rotor alone" test data that Hohenemser reported in MAC Report No.3379. This first test evaluated the rotor system in both autogyro and airplane flight, with and without the dummy wing. The four configurations tested are described by Hohenemser as:

FWR (Wing On, Hub & Gimbal Locked, 0° Collective) (MAC 3379, Fig. 24–38)

FWR (Wing On, Hub & Gimbal Free, 6° Collective) (MAC 3379, Fig. 39–54)

FR (Wing Off, Hub & Gimbal Locked, 0° Collective) (MAC 3379, Fig. 55–69)

FR (Wing Off, Hub & Gimbal Free, 6° Collective) (MAC 3379, Fig. 70–85)

He also states that "the rotor was mounted on a rotor adapter of which the upper portion had the geometric shape of the prototype pylon and which carried a fixed wing of rectangular planform, constant thickness and zero washout in order to keep its manufacturing costs down. The fixed wing had the same area as the prototype wing and was located at the same distance from the rotor center." The rather non–representative fuselage was on for the whole test (A–80). During the test, collective pitch and longitudinal cyclic pitch were controlled from the control room. However, lateral cyclic was fixed at zero degrees throughout the test.

While the pressure jet tip drive units were not operated during the test period, the full scale prototype hardware operated free of instabilities up to the tunnel's 200 knot maximum speed capability with the rotor in the 180 rpm, airplane mode (hub & gimbal locked to the stem). This high speed point was an advance ratio of 1.15. Additionally, the rotor system was free of flutter "up to the maximum tested rotor speed of 480 rpm at 125 knots tunnel speed in the locked hub condition." The high rpm point was inadvertently obtained during "the rotor runaway caused by overloading the longitudinal power cylinder and excessive leakage of this cylinder when manual controlling the rotor incidence." Surely, one of the most gratifying proof of concepts must have been the excellent control of rotor speed exhibited by the flyball governor coupled to longitudinal hub plane tilt. In the airplane mode, the human (a remotely located rotor rpm controller) was a poor substitute for the onboard governor.

---

[12] The MAC reports are available with many thanks to Mr. Frederich W. Roos, Boeing Company, Phantom Works, St, Louis, Mo. The rotorcraft industry is very lucky that these two reports could be found. Mr. Roos found a third report by Hohenemser, MAC Report No. 3371 dated Jan. 1954, titled "The Development of a V–Tab Controller Floating Horizontal Tail for Rotary–Wing Aircraft." John Davis of the Army organization at NASA Ames now has the CD with all three reports.

The impact on loads and vibration of transitioning from the autogyro's 320 to 430 rpm range through a resonance range to the airplane's idling 180 to 200 rpm was quantified. It was expected that vibration would be very high, but of short duration. Loads did not exceed allowables. A relatively short list of redesign requirements was compiled that, because of this test's early timing, could be completed before first flight. The majority of the items dealt with subsystems such as the need to increase hydraulic pressure.

The discouraging aspects of the test were primarily aerodynamic in nature. For one thing, the "fixed wing had the effect of increasing all the rotor loads, including blade vertical bending moments by an appreciable amount." And, as is so often the case, "the hub drag was found to be much higher than estimated because of hub–pylon interference." As Figure 8 shows, drag from the hub, pylon and non-representative fuselage (and to a much lesser extent, the exposed wind tunnel struts) completely over shadowed the drag of the 3 blades at high advance ratio. Kurt Hohenemser said, in his 1952 AHS Forum paper: "Actually in a compound aircraft the drag of pylon and hub is of more importance than the drag of the rotating blades." One could reasonably add the fuselage and landing gear to Hohenemser's list.
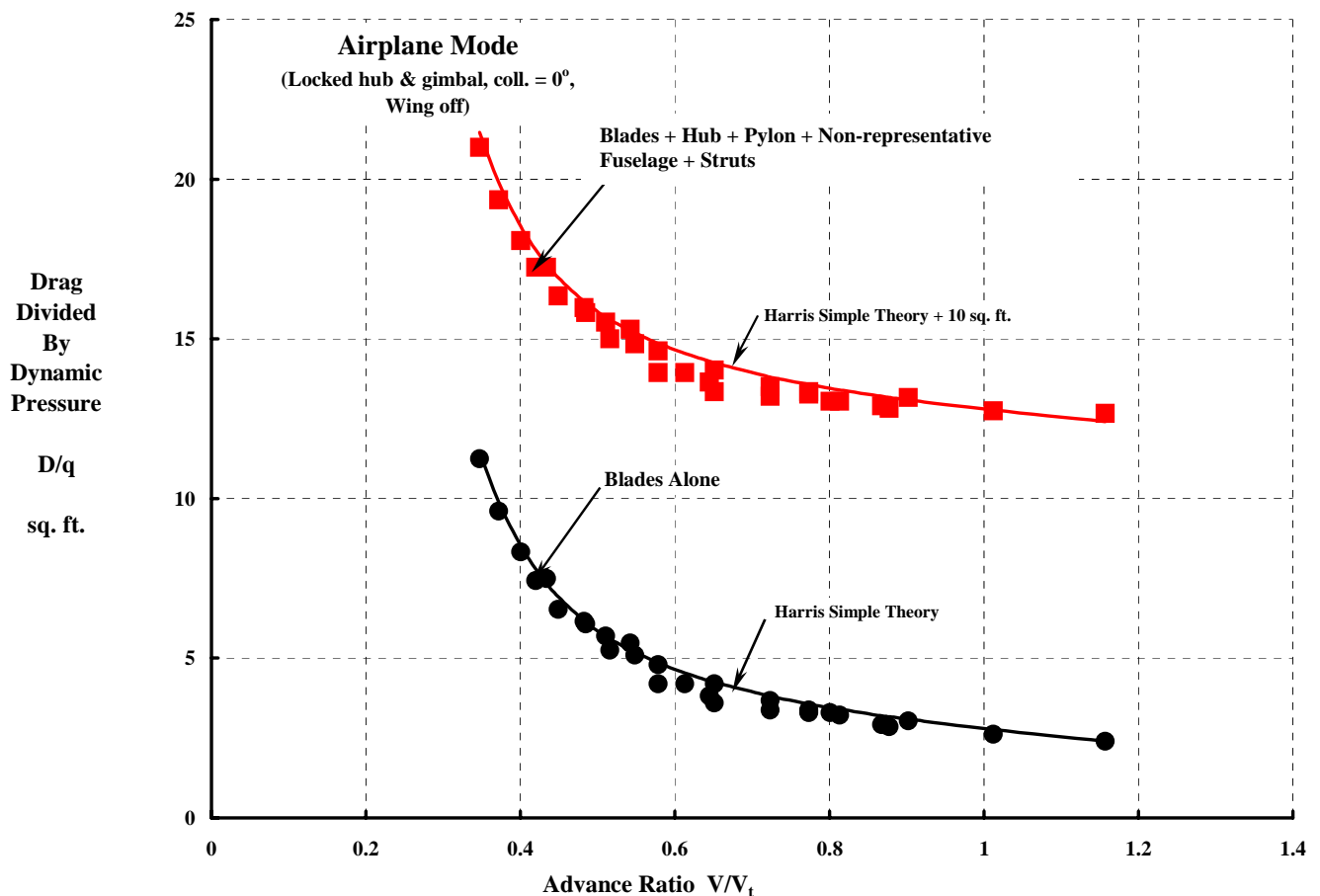
Figure 8. The XV–1's Blades and Hub + Pylon + Non–representative Fuselage Parasite Drag Area versus Advance Ratio.

The simple theory for blades alone drag referred to on Figure 8, the energy method, is nothing more than

$$\frac{D_R}{q} = \frac{K_i}{\pi}\left(\frac{L_R}{2Rq}\right)^2 + \frac{(b\,c\,R)C_{do}}{4}\left(\frac{1+4.65\mu^2+4.15\mu^4-\mu^6}{\mu^3}\right)$$

where $K_i = 1.075\,\mathrm{Cosh}\left(6.76\mu^2\right)$ for $\mu \le 0.5$

and $K_i = 1-29.332\mu+92.439\mu^2-51.746\mu^3$ for $0.5 \le \mu \le 1.0$

$b = 3$, $c = 17.5/12$ ft, $D = 31.0$ ft, $R = 15.5$ ft. $C_{do} = 0.01568$

which, strictly speaking, was semi–empirically created for untwisted rotor blades. The XV–1 blades had 8 degrees of washout, which creates an induced drag even though the total rotor lift is small or even zero (A–48). This is compensated for in this simple theory by an increase in the airfoil average drag coefficient, C_{do}. For the XV–1, a value of $C_{do} = 0.0124$ was derived from whirl stand tests done with the blades at zero degrees collective pitch at the ¾ radius (A–84). This compares to the $C_{do} = 0.01568$ used for forward flight in Figure 8.

From an operations point of view, this first XV–1 test clearly showed how sensitive rotor rpm and hence advanced ratio became at high speed. This key convertiplane factor is illustrated by Figure 9. The aircraft operator in the control room had very little trouble setting rotor speed in the low advance ratio, autogyro mode. However, in the high advance ratio airplane mode, the human operator was a very poor substitute for the flyball governor.
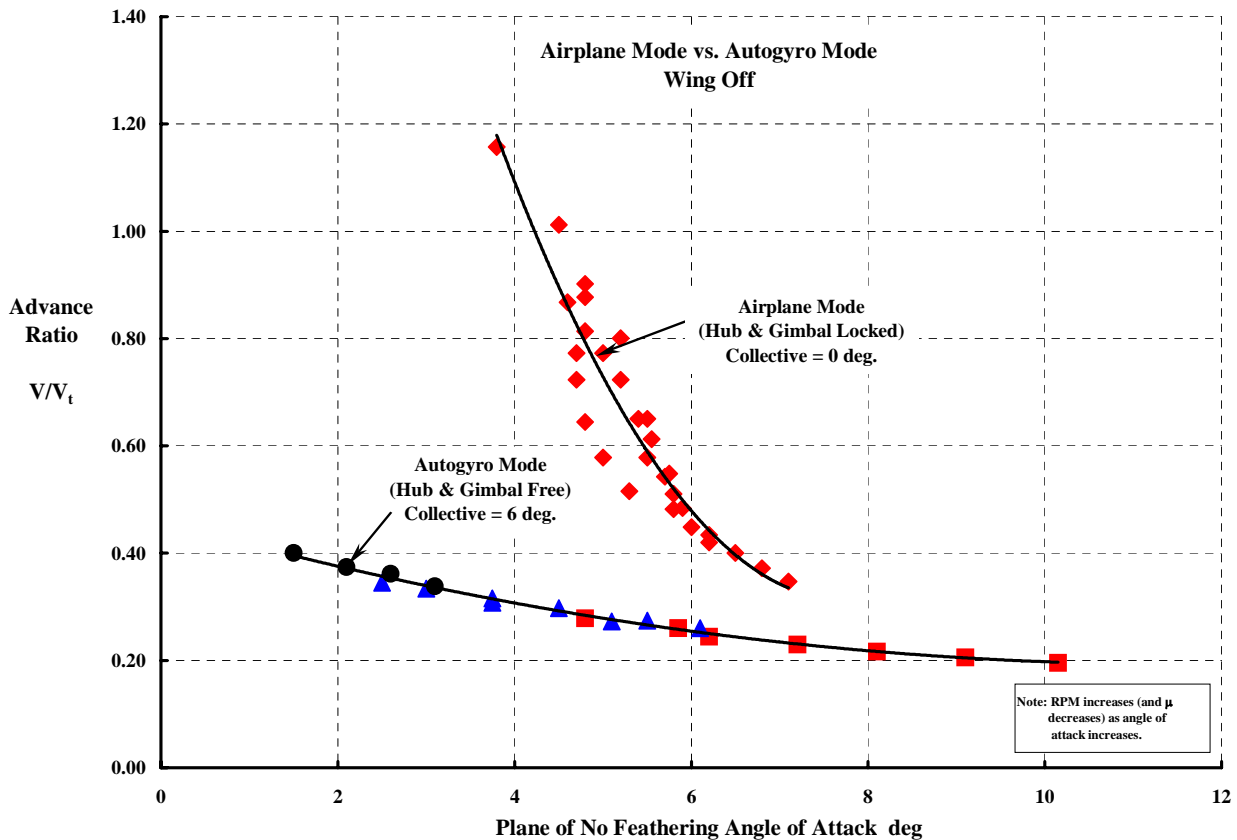
Figure 9. Rotor Speed Control Becomes Very Sensitive at High Advance Ratio.

Kurt Hohenemser ended his summary in MAC Report No. 3379 on a very positive note. He says: "The outcome of the full scale rotor tests has shown that the decision to conduct these tests as soon as a rotor became available was well made. A few malfunctions of the rotor could be eliminated during the test period by improvised modifications. A number of other rotor modifications will be incorporated in the rotor during the time between the full scale rotor tests and the completion of the prototype so that considerable development time will be saved."[13]

Complete Aircraft Test. Seminar pages A–96 to A–104 re-examine the full scale aircraft test data that Hickey and Hohenemser reported. Three configurations,

> 1. rotor off, prop off
> 2. rotor on, prop off (autogyro rpm = 325, airplane rpm = 180)
> 3. rotor on, prop on (autogyro rpm = 325, airplane rpm = 180)

were tested at very specific tunnel velocities (A–98). The pressure jet powering the main rotor was never operated in the tunnel. The basic aircraft (hub on, but blades off and prop off) achieved a maximum lift to drag ratio of 7.5 at a lift to dynamic pressure ratio of $L/q = 105$ square feet (A–103). With propeller off and rotor on, the L/D dropped to 5.0 with a nominal 325 rotor rpm (A–108). When the rotor speed was slowed down to 175 rpm and the propeller was off, L/D increased to about 6.5 (A–112).

The aircraft's lift variation with angle of attack (Figure 10) and equivalent parasite drag area variation with advance ratio (Figure 11) summarize the key aerodynamics learned from this second XV–1 test in the NASA 40 by 80 foot wind tunnel. The lift curve slope in airplane mode shows just how effective the 2.2 degrees of feather down to 1 degree of flap up coupling was in making the rotor nearly a transparent surface to the complete aircraft.

A summary of the XV–1's drag as measured in the full scale wind tunnel test, taken from the seminar, page A–101, is reproduced here as Figure 11. The equivalent parasite drag area (at a gross weight of nominally 5,300 pounds) dramatically benefits by high advance ratio operation. However, this benefit is nearly fully realized by an advance ratio of 0.8. Of course, if compressibility were a factor, the picture could be significantly different. But this was not the case for the XV–1. Note that at $\mu = 1$, the induced drag due to lift is easily twice the rotor minimum profile drag of the blades. Most importantly, note that parasite drag of the aircraft (without the rotor blades and propeller) dominates the configuration's performance trend at high advance ratio.

Figure 11 further emphasizes Hohenemser's point (MAC 3599) that "the most important result of the Moffett Field tests is the recognition of the drag problem as the most pressing for any future application of the rotary–fixed wing aircraft. Although the large amount of drag increase [over estimates made from small models] was found to be caused by the accumulation of many items, by far the most important single contribution of this drag increase was traced to pylon–rotor interference."

---

[13] Both of Kurt Hohenemser's reports contain a wealth of technical data reported in the detail and suitable format demanded of engineers – at least up to my generation. More importantly, critical hardware short comings that might have caused a crash in flight test are emphasized and problems yet to be overcome are fully divulged. Studying his reports was a great pleasure for me.
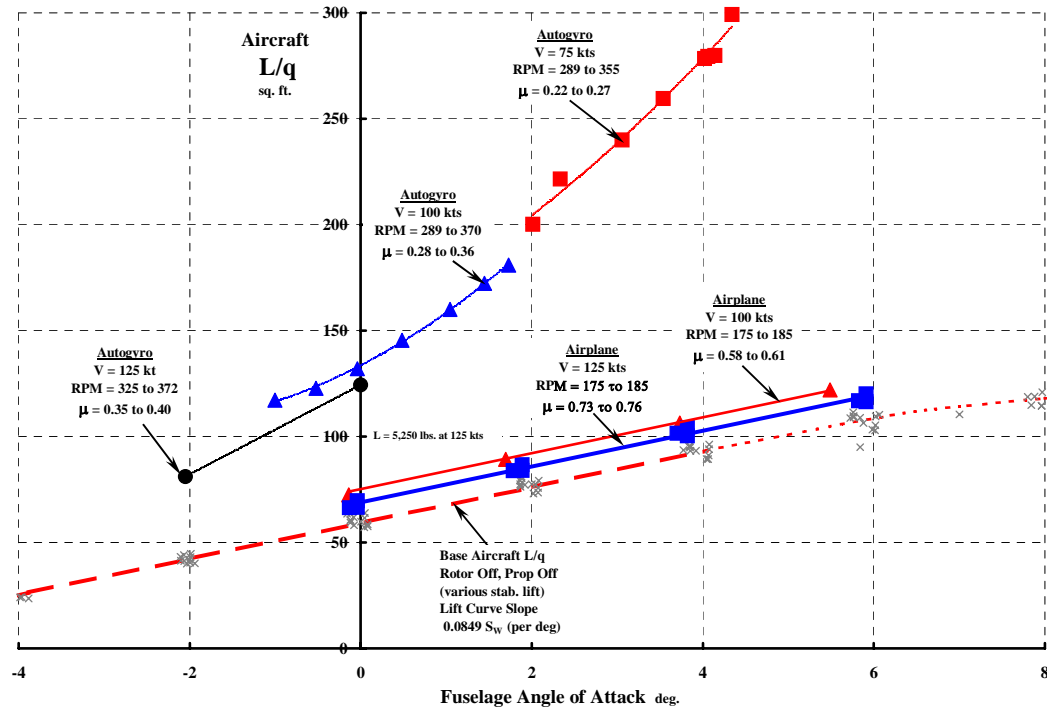
Figure 10. The XV–1 Lift Curve in Autogyro and Airplane Modes.
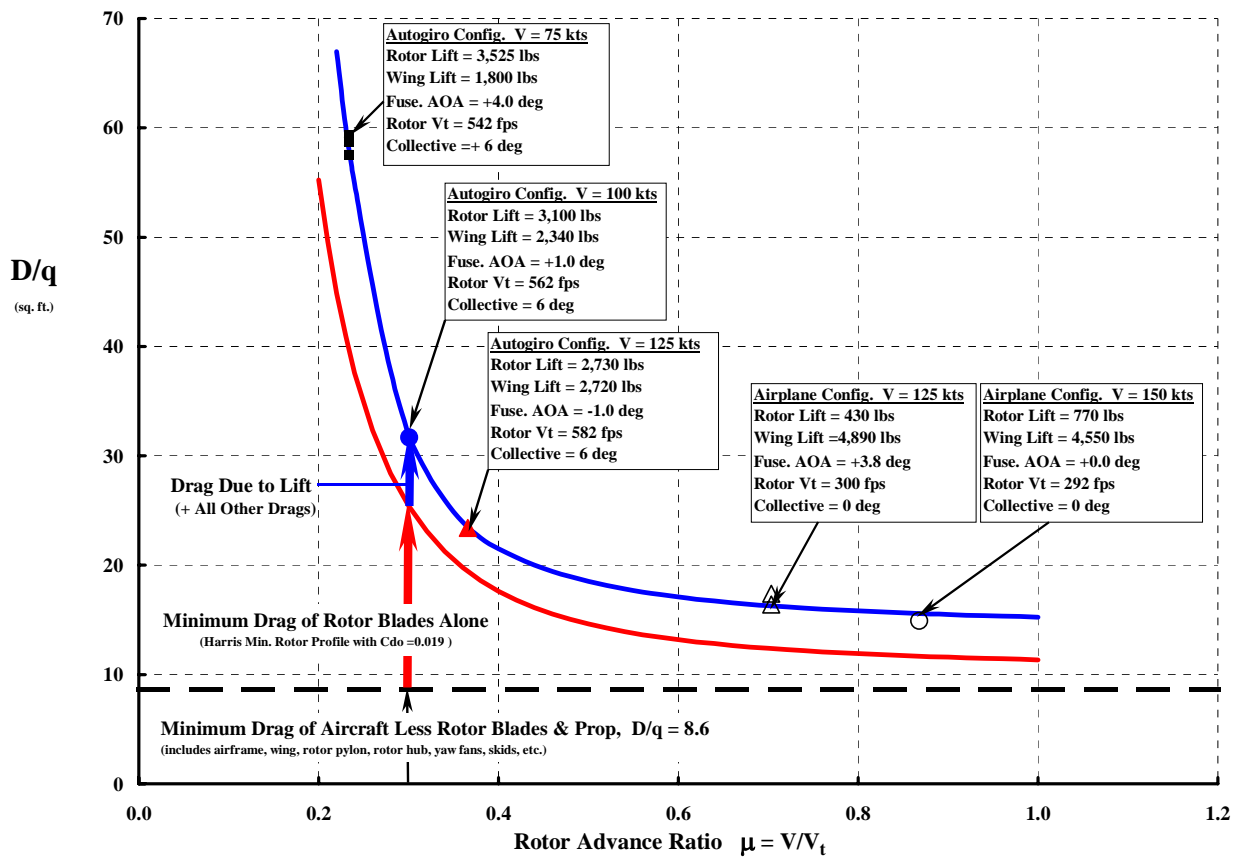
Figure 11. The XV–1's Total Parasite Drag Area versus Advance Ratio.

A considerable amount of discussion in both Hickey's NACA and Hohenemser's MAC reports deals with the aerodynamics of the floating horizontal tail (A–99). The tail, or elevator if you prefer, operated with much the same properties as the large elevator on a UH–60. However, the XV–1's tail was not hydraulic powered or computer controlled. Because the XV–1's tail flew principally in proportion to dynamic pressure, the prop wash "produced a very sizeable download." Hohenemser thoroughly designed for a flutter free elevator and checked for tail flutter. He found that the complete aircraft needed to be free in pitch to avoid coupling with the wind tunnel support system. A thorough stability and control data matrix was obtained during this second test that would be applicable to future convertiplanes.

The sheer number of other questions that Hohenemser got answers to from this test of the complete aircraft is very impressive. For example,

(a) the experimental propeller was stress surveyed and a resonance was found just below 2,000 engine rpm,

(b) engine cooling was found to be adequate for the experimental aircraft, but cooling drag was $D/q = 0.3$ ft^2 due to an excessive boundary layer in the inlet,

(c) the cooling fan itself appeared to be operating on the stall side of the power map,

(d) the best flight procedure for transition from autogyro to airplane mode was worked out. Maximum loads throughout the aircraft and rotor system as the rotor passed through its two resonance's were established,

(e) early problems with the rotor incidence, flyball governor system were solved,

(f) starting and stopping the rotor in a 42 knot wind showed that a rotor brake would not be needed on the experimental XV–1,

(g) the preferred way of flying the rotor in the autogyro mode was found to be a fixed collective and stem incidence fixed at $+3^o$ aft, using the elevator to adjust fuselage attitude,

(h) a mini–vibration survey was completed and stiffened tail booms were required,

(i) comparison of measured and design fatigue rotor loads showed that only during the transition from autogyro and airplane modes would there be a problem,

(j) four unsatisfactory subsystem characteristics were found that needed to be eliminated prior to extensive flight testing, and

(k) high drag caused by separated pylon flow at the intersection of the pylon and the hub was not solved despite a number of tries. A return to the 8 ft model was planned.

In summarizing his conclusions, Hohenemser says that "the information obtained from the wind tunnel tests is the equivalent of many months of flight testing and should help very much to expedite flight testing of the Model XV–1 convertiplane in the autogiro and airplane flight phases."

Rotor Stability In Forward Flight

The Helicopter Division of the McDonnell Aircraft Corporation began studies of the convertiplane in 1949. These studies, sponsored by the Office of Naval Research, included theory, model testing and preliminary design of what was to become the XV–1. At the 1952 AHS Forum, Kurt Hohenemser gave a paper[14] which included experimental data for a two bladed, teetering, 7.6 foot diameter rotor tested in the University of Washington wind tunnel in Seattle.[15] Hohenemser's paper devotes considerable attention to rotor performance before addressing the high advance ratio flapping stability issue. He includes, in Appendix B to his paper, his solution to the classical one degree of freedom flapping differential equation. His theoretical attack proved conclusively that the XV–1 type of rotor would be free of instabilities. But then he goes on to say that "this reassuring [theoretical] result is unfortunately not verified by tests. A large number of test runs within a wide range of Reynold's Number have definitely established the fact that for our specific case the flapping motion becomes unstable between an advance ratio of 1.5 and 1.6. The frequency of the unstable flapping motion is ½ per rev, which again disagrees with [theoretical results] ……"

In Hohenemser's next report to the rotorcraft community,[16] he takes up this blade flapping instability at high advance ratio problem again, opening the paragraph by saying "I first have to apologize for an erroneous conclusion I gave you three years ago with respect to this subject." [How often do you see a statement like that in the literature.] He apparently felt he had offered a useable approximation of the differential equation for high advance ratio, but his application of the "twin ripple" method of solution was ill advised.

Fortunately, using numerical integration of the flapping equation, he was able to present some evidence that the ½ per rev instability was analytically predictable. Furthermore, he included an experimentally measured waveform of the flapping motion in the vicinity of the stability limit. This waveform is reproduced here as Figure 12. The pitch–flap coupling is 2.2^o pitch down for 1° flap up. The Lock number is 5.0 and the record was obtained at an advance ratio $\mu = 1.55$.

Figure 12 illustrates the blade motion characteristic at the threshold of the ½ per rev flapping instability. Note that to see a ½ per rev, the waveform must be plotted over two revolutions before the repetition becomes clear. By the time full scale rotor and complete aircraft testing had begun, a sufficient number of model tests had produced a picture of the instability regions to be avoided. The ½ per rev flapping instability was drawn as a boundary independent of rotor speed and virtually as a limit to forward speed, which Figure 13 (also see page A–128) shows was about 225 knots.

It is not at all clear that this high advance ratio flapping instability has received a great deal of attention by the rotorcraft community. In fact, it is this author's opinion that a clear explanation

---

[14] Hohenemser, Kurt H., "Some Aerodynamic Problems of the Compound Rotary–Fixed Wing Aircraft", 8th AHS Forum, 1952

[15] Ray Prouty attended the Seminar. He told the group that he was a student at the University of Washington during the time that Kurt Hohenemser and Fred Doblhoff used the University wind tunnel for several tests. Ray became well acquainted with both men, Because of this experience, Ray wrote his Master's thesis on the subject "Wind Tunnel Wall Corrections for Rotors." Later, Ray told Kurt Hohenemser that because of Kurt and the tests, he embarked in a rotorcraft career. Hohenemser's reply was that Ray shouldn't blame him.

[16] Hohenemser, Kurt H., "Remarks on the Unloaded Rotor Type of Convertiplane" 11th AHS Forum, 1955.

has not been published detailing the physics of the ½ per rev instability and why it would be a speed limit independent of rotor speed.

Figure 13 also shows a flutter onset boundary which Hohenemser says[16] was at "about 2.3 per revolution and elastic blade bending and elastic blade torsion were predominant." The flutter instability is much better understood by rotorcraft engineers. The trend shown on Figure 13 follows the classical behavior where instability onset depends on advancing blade relative speed and dynamic pressure. That is, ½ ρ $(V+V_t)^2$ = constant so for the XV–1,

$$V_{knots} + 0.96 RPM = 560$$

which fits the locked hub, collective pitch = 0° data on Figure 13.

In 1962, at the 18th AHS Forum, C.H. Perisho (et al) presented "A Comparison of Detailed and Simplified Methods of Analysis of Rotor Stability in Forward Flight with Model Test Results." One of the analyses – the most successful one – was a 40 degrees of freedom model representing the motion of all three blades (at least to one node of bending) and the hub. The equations were programmed on an analog computer by R.H. MacNeal of Computer Engineering Associates Inc. A key conclusion was that for the XV–1 type of hub, inter–blade coupling was quite important to accurately predict instability boundaries over the full range of rotor speed.

Finally, Hohenemser[16] was quite satisfied with the dynamically similar, quarter scale (i.e. 8 foot diameter) rotor models that accompanied the XV–1's development. The one shortcoming he noted was that the cyclic control system "was not in all respects dynamically to scale and for this reason the oscillating cyclic control loads were underestimated from the model tests." He goes on to say that "with a little further refinement we would have had a model which would have given us without exception the right answers to all the complicated dynamic and loading problems of the rotor."
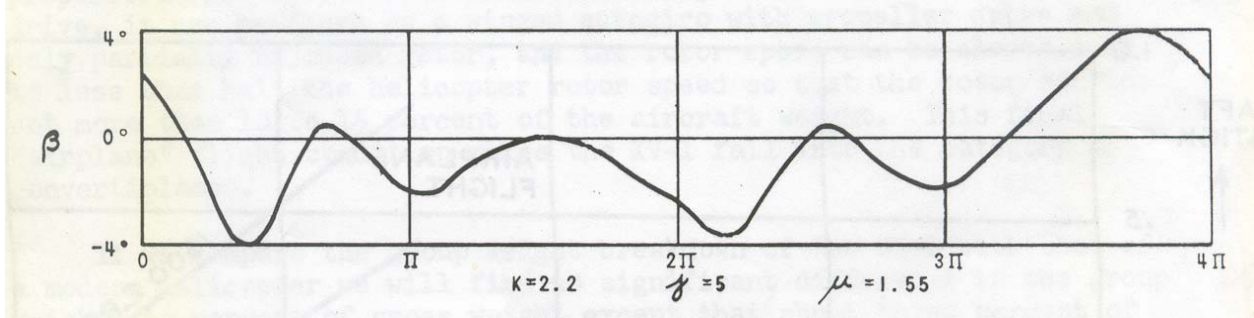
Figure 12. Hohenemser's Model Test Results of Flapping Motion "in the Vicinity of the Flapping Stability Limit."[16]
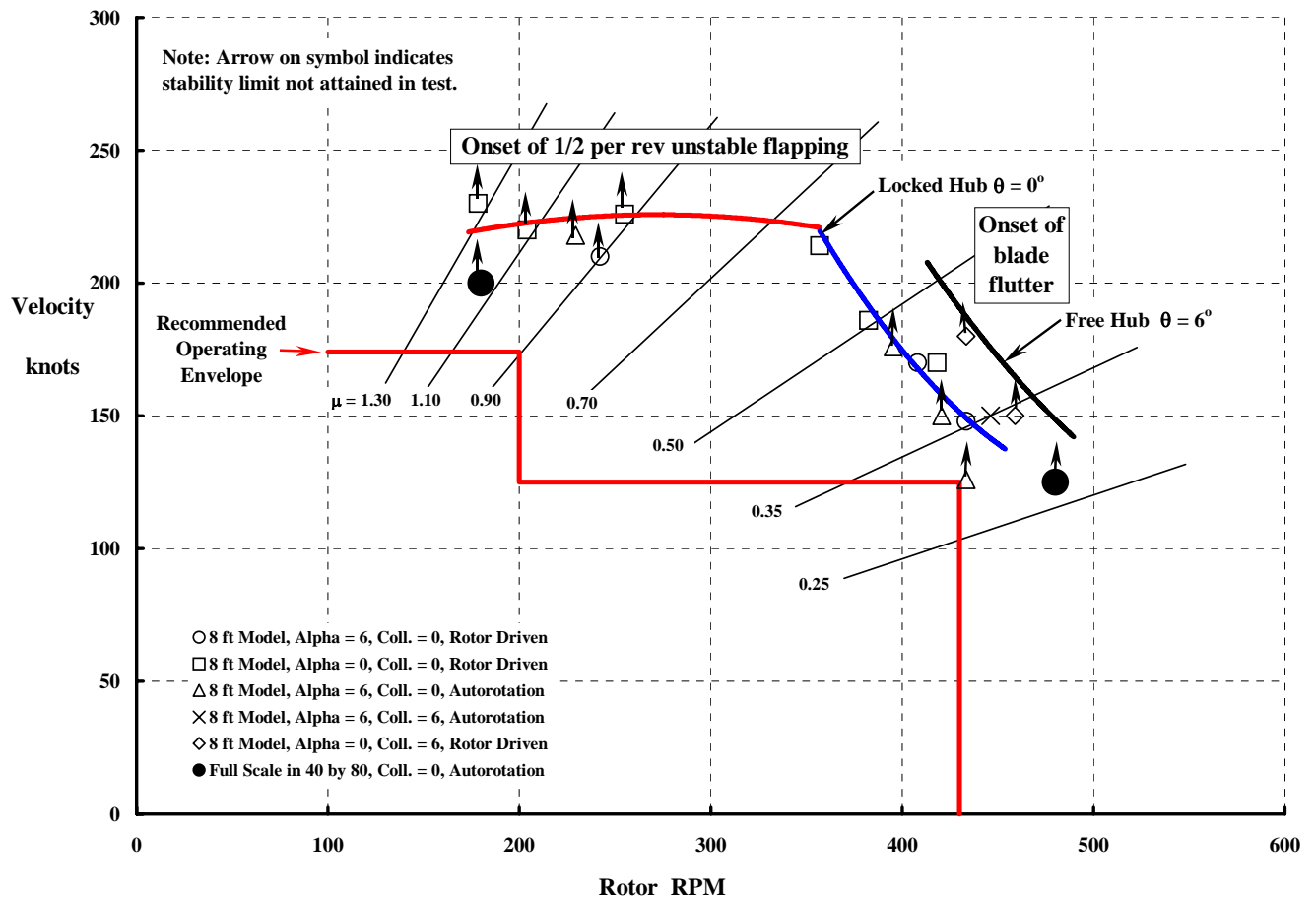
Figure 13. The XV–1 Recommended Operating Envelope Developed From Model and Full Scale Wind Tunnel Tests.

Phase II Flight Evaluation

The XV–1 (Ship No. 1 of two) rolled out in January 1954.[17] Its first lift off was accomplished one month later. The first conversion to airplane flight was performed in April 1955. One year later, the contractor, McDonnell Aircraft Corp., had completed their share of development flying and the Air Force began its formal flight evaluation on April 12, 1956.[18]

The problem of the XV–1's higher than expected drag (that the full scale wind tunnel testing brought to light and Hohenemser repeatedly mentioned) was still an obvious issue during McDonnell's one year of contractor flight testing. This point is illustrated by Figure 14. Tufts were used to survey airflow about the whole aircraft and pylon–hub interference drag apparently was attacked with a form of end plating as Figure 14 shows. It is not clear just how successful this aspect of development testing was. However, the fundamental problem, in one form or another, has continually plagued virtually every new helicopter as any number of authors have documented.[19]

Pylon–hub interference
drag reducing end plate.

Figure 14. Early XV–1 Flight Testing Was Devoted to Drag Reduction, the Major Problem Hohenemser Repeatedly Identified During the Full Scale Wind Tunnel Testing.

The Air Force conducted its formal flight from April 12, 1956 through May 2, 1956. Thirty-four flights were made, which yielded 9+ hours of flight time. The abstract to Putnam's and Eggert's Phase II Flight Evaluation report[18] reads as follows:

> "The unloaded rotor principle was found to be a satisfactory convertiplane
> from the standpoint of flying qualities and operation. The unloaded rotor
> does not appear to have any adverse effect on the flight characteristics at
> high speed in airplane flight and is beneficial in delaying wing stall at low
> speed. Transition from helicopter flight to airplane flight was not difficult

---

[17] Marks, Marvin D., "Flight Development of XV–1 Convertiplane" J. of the AHS Vol. 2 No. 1, 1957.

[18] Putnam, V.K. and Eggert, Wayne W., "Phase II Flight Evaluation of the XV–1" AFFTC–TR–56–35, Feb. 1957. Or see ASTIA Document No. AD–112423.

[19] See for example, Harris, F.D., "AHIP – The OH–58D From Conception to Production," AHS 42nd National Forum, June 1986

but could be simplified with development. The pitch–cone coupling in this rotor design provides outstanding stability and control characteristics in helicopter flight compared to current designs. With the exception of the extremely high fuel consumption and the high noise level, the pressure jet system presented no unusual operating problems. Reliability of the burners was marginal. Numerous deficiencies in performance and control were found, but were primarily attributed to this particular airframe configuration."

The report's recommendations were just as positive, reading as follows:

"It is recommended that the XV–1 be utilized to the fullest extent in the development of the unloaded rotor principle, the pressure jet system, and the pitch–cone coupled rotor system for application to future designs. A minimum of XV–1 flight time should be expended in solutions of problems associated with this particular airframe configuration."

The magnitude of the two concerns raised in the abstract (pressure jet system fuel consumption and noise) are quantified in Figures 15 and 16 (A–171 and A–165 respectively). In regards to fuel consumption, Figure 15, advocates of the pressure jet system frequently argue that when slow speed flying will only be a small portion of the mission, there will be a net weight empty reduction accompanied by considerable simplification in dynamic components. Unfortunately, no pressure jet, tip driven lifting rotor has reached production, so the claims have yet to be validated.
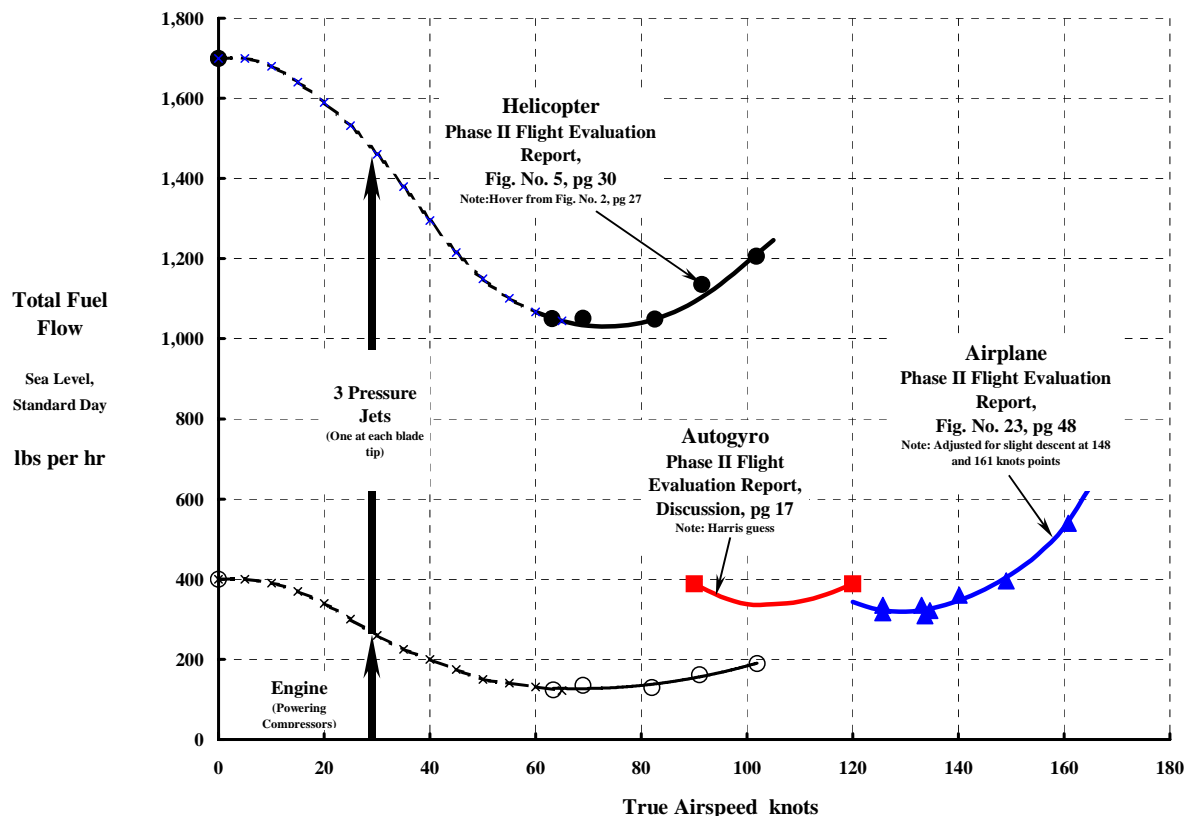
Figure 15. The Helicopter Mode Used 3 Times More Fuel per Hour than the Airplane Mode.

With respect to noise, Figure 16, the Flight Evaluation report was somewhat more candid in its detailed discussion stating that "personal exposed to the noise of the XV–1 have described it as intense, fluctuating and extremely irritating. A heavy repetitive beat is noted when the rotor tip burners are ignited during run up. Subjective comments made by several personnel exposed to this noise indicated that within a radius of 30 feet, one's reaction is to 'turn and run' even when protective devices for the ears are worn. Noise from the helicopter remained above 90 decibels at distances estimated to be as much as one-half mile away." It was somewhat quieter in the cockpit where a level of 116 db was recorded. It appears that this noise level must be reduced if the pressure jet system is to be given serious consideration.[20]
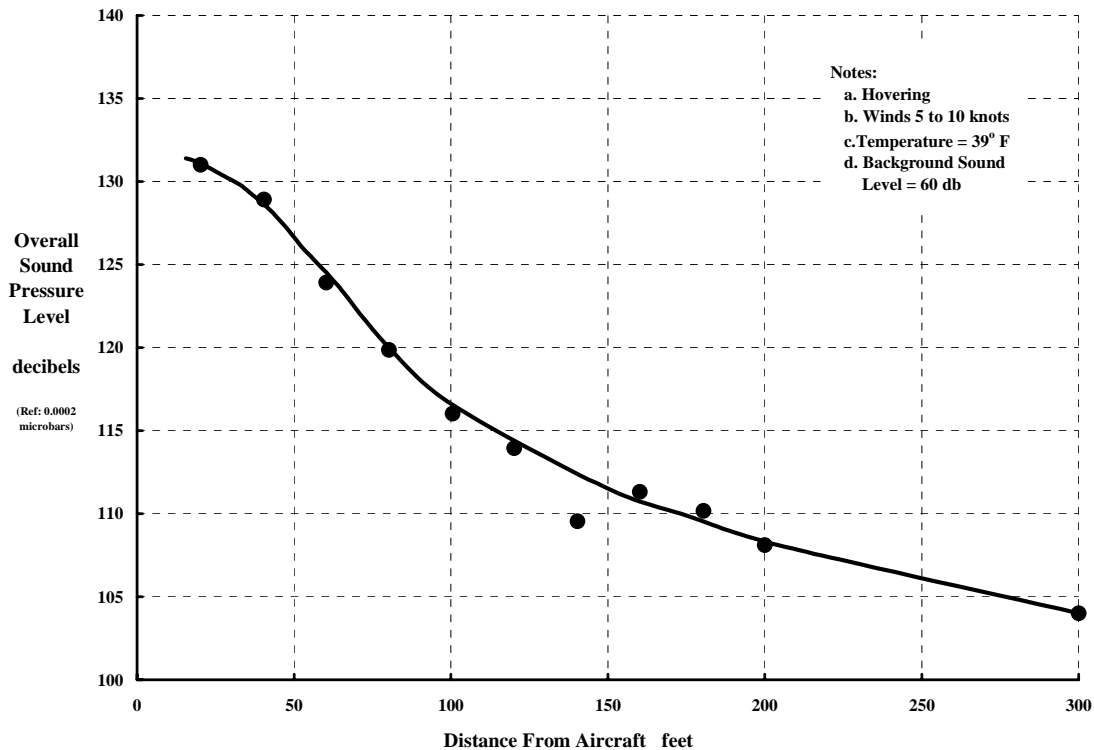
Figure 16. Pressure Jet Noise Was a Real Operational Concern.

While the XV–1's rotor system was clearly viewed favorably by the Air Force, a number of complaints about the aircraft were discussed. For example, the transition from helicopter to airplane flight was accompanied by significant vibration in the cockpit as the rotor passed through two resonances. At about 290 rpm, vibration of about 0.2 g became apparent. This predominately 3 per rev vibration reached a peak of 0.7 g at about 260 rpm and then dropped back to 0.2 g at 225 rpm (A–154). The Phase II report states that "vibration at this amplitude is of course unsatisfactory; however, since this is a transient condition lasting only from 5 to 10 seconds, it is considered tolerable." Vibration in helicopter and autogyro modes was deemed unsatisfactory above 80 knots, but in airplane flight, vibration was quite acceptable being below 0.1 g (A–160, A–161 & A–162).

---

[20] G.S. Hislop in his paper, "The Fairey Rotodyne," (Journal of the Helicopter Association of Great Britain, Vol. 13, No.1, Feb. 1959) notes that "the noise emission appears to be proportional to the jet exit velocity raised to the 6th or 7th power." The Fairey Aviation Company explored several silencers in full scale testing. They achieved some 14 db attenuation.

Another example dealt with handling qualities. The stability and control in airplane flight was considered "good", but an investigation into "the pitch roll coupling experienced during all dynamic longitudinal stability tests" was recommended (A–158 & A–159).

Overall, the Air Force's report took a positive outlook about the XV–1's unloaded rotor concept. The pitch–coning coupling approach that Hohenemser created was particularly single out for praise. The pressure jet tip drive system that Fred Doblhoff pioneered was worthy of further development. And last but not least, the Phase II's conclusions and recommendations (A–173 and A–174) down played the performance shortcomings of the basic airframe caused by excessive drag, excessive weight empty, an under powered reciprocating engine and an under sized propeller.

But in the end, it was the tilt rotor concept that went forward.

CLOSING REMARKS

Juan de la Cierva's invention and development of the autogyro began in 1919. He progressed from failure (with his Model C–1 in 1920) to production (with his Model C.19) in ten years. His aircraft and his engineering, marketing and business skills attracted Harold Pitcairn, the Kellett brothers and others to the autogyro field. Together, these pioneers laid the foundation to today's rotorcraft industry.

The basic aerodynamic technology of the autogyro and its many derivatives (aka compound helicopters, convertiplanes, airplane with a rotor, etc.) is captured with a few simple equations. These equations show that the drag of the rotor blades alone is of minor importance to the successfully performing convertiplane. A much more serious concern is the drag of hubs and their pylon support to say nothing about fuselages and un-retracted landing gear. Controlling rotor speed at high advance ratio is a very difficult task for a pilot and some form of autopilot appears mandatory. The conventional rotor experiences, around unity advance ratio, a reversal in the change of thrust with collective pitch. Stability of the flapping motion is a serious question when the advance ratio approaches 1.5. Instabilities in both sub harmonic and higher harmonic blade motions are quite real high speed limitations. Fortunately, today's comprehensive rotorcraft theory and wind tunnel model technology are capable of discovering these rotor system instabilities before detailed design is completed.

The McDonnell XV–1 Convertiplane was created by Kurt Hohenemser and Fred Doblhoff. It was the first aircraft to demonstrate the unloaded rotor principle. The rotor system contained a unique hub configuration that was a very successful precursor of today's bearingless rotor. In fact, because it had no lead–lag damper, it should be viewed as better than what the helicopter industry is producing today. Furthermore, pitch–cone coupling of 2.2^{o} nose down for 1° cone up (but negligible pitch–flap coupling) was demonstrated to give outstanding aircraft longitudinal stability when the XV–1 was in its helicopter mode. In the cruise mode, as an airplane with rotor unloaded and at idle

rpm, the use of 2.2^o nose down pitch for 1° flap up coupling made the rotor tip path plane follow the mast. In essence, the aircraft behaved as if the rotor system was transparent. The use of a simple fly ball governor actuating direct control of the hub plane (i.e. the plane of no feathering) to control rotor speed in the airplane mode was very successful. The Air Force recommended, in its Phase II Flight Evaluation report, "that the XV–1 be utilized to the fullest extent in the development of the unloaded rotor principle, the pressure jet system and the pitch–cone coupled rotor system for application to future designs."

The Air Force recommendation was followed, but only for a few years. A rotor system from one XV–1 was used on a mini-crane, the McDonnell Model 120 (A–176). Pitch–roll coupling was corrected and problems with the pressure jet tip drive system were corrected on this small aircraft. Then, with interest growing for a military heavy lift helicopter, a 75 foot diameter rotor with pressure jet system was built and whirl tested. Unfortunately, military interest dissolved, little additional progress was made and the Air Force's other recommendations (such as the benefits of pitch–cone coupling) began to take their place in rotorcraft history.

LET'S REVISIT AUTOGYROS

First Some History

Cierva, Pitcairn, and Kellett Era (1919 to 1941)
Selection of the Helicopter (1942)
Legacy

Some Technology Aspects

What's in a Name?
Fuselages, Wings, Propellers, Rotors and Trim
Rotor Thrust and Flapping Behavior at High Advance Ratio
Limits to Rotor Lift and Propulsion
To Review Then

XV–1 Re–examined

Full Scale Wind Tunnel Tests in 40 by 80
    Rotor (With & Without Wing)
    Complete Aircraft
Rotor Stability In Forward Flight
Phase II Flight Evaluation

Concluding Remarks

Table of Contents

Cierva, Pitcairn, Kellett & Others Developed 129 Autogyros.

HP per Ton of Gross Weight (y-axis, ranging from 1 to 10,000)

Speed (mph) (x-axis, ranging from 1 to 10,000)

Labels within chart:
- Airplane Up To 1950s
- Concorde
- 129 Autogyros
- Westland Lynx ●
- Boeing 360 ●
- Tiltrotors
- Helicopters
- Russian Tu-142
- Lockheed Electra
- What Price Speed by Gabrielli and Von Karman Oct, 1950
- Train
- Car
- Truck
- 4 Min. Mile ✕
- Ship
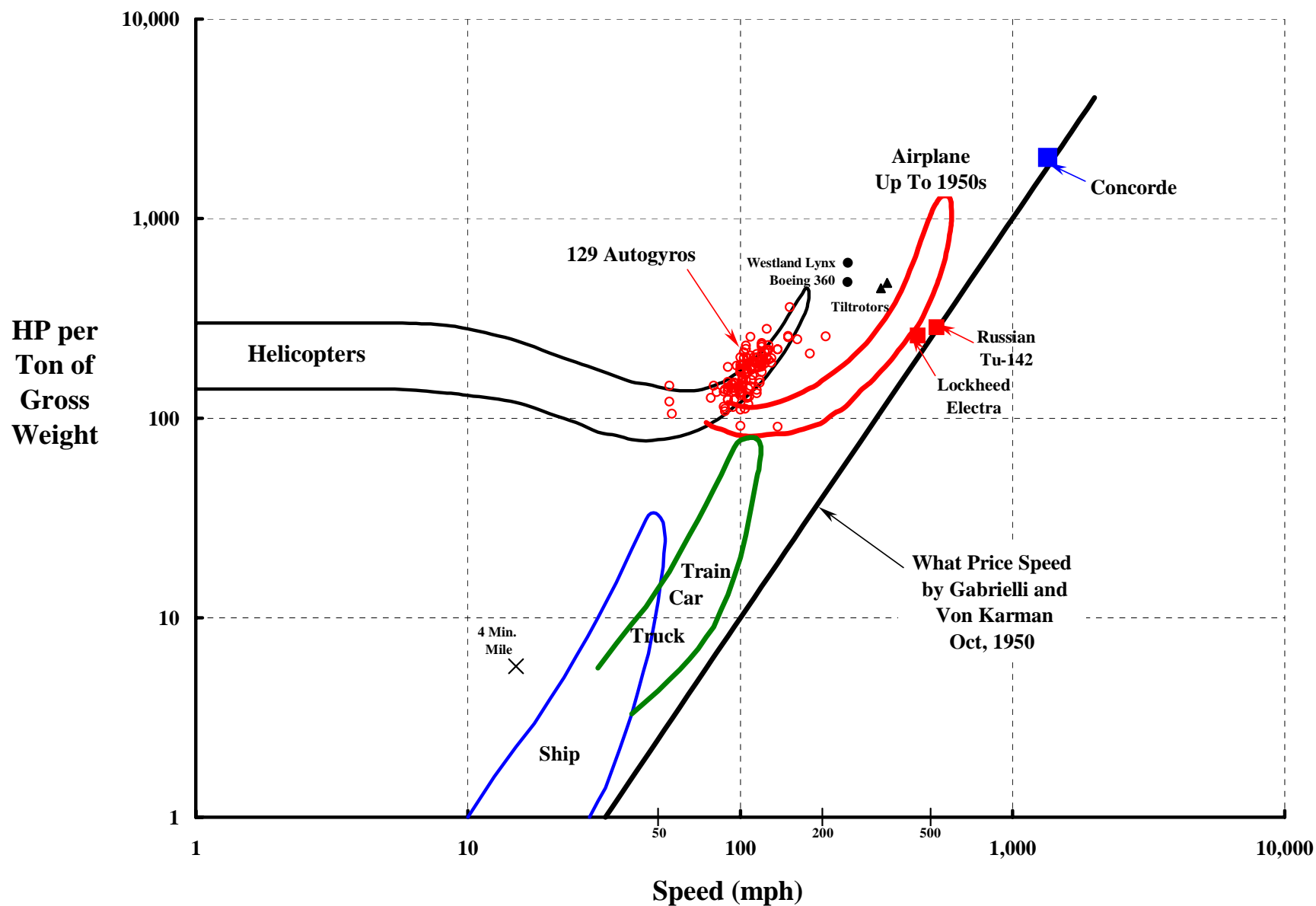
Ref. Gabrielle, G. and von Karman, T., "What Price Speed," Mechanical Engineering, Vol. 72, Oct. 1950

Cierva Went From Failure To Production In 10 Years.

Cierva C–1 Oct. 1920

Type	No of Configurations	Notes
C.1	1	Failure
C.2	4	Limited Success
C.3	9	Failure (Tried Cyclic)
C.4	15+4 lesser mods	Success Jan.17,1923 (Had Flapping Hinge)
C.5	1	Flew, but blade fatigued in torsion
C.6	2	First flight Feb. 1924. Great improvement.
		Taken to Britain for Demo in Oct. 1925

Cierva C–6 Farnborough Oct. 1925

Cierva C.19 Mk.IV June 1931
First Production Autogiro

Ref. Brooks, Peter W., "Cierva Autogiros-The Development of Rotary–Wing Flight, Smithsonian Inst. Press, Washington D.C. 1988

Cierva's Marketing Brought Pitcairn & The Kellett Brothers Aboard.
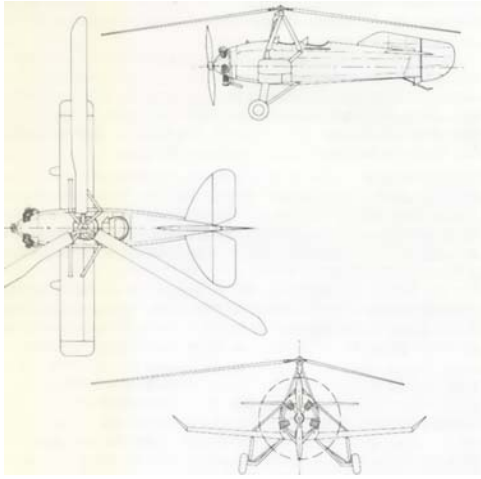
Cierva C.19 Mk.IV June 1931

Cierva C.30 1934 Production + World Wide Licenses

Pitcairn PCA-2 Certified April 2, 1931(ATC No. 410)
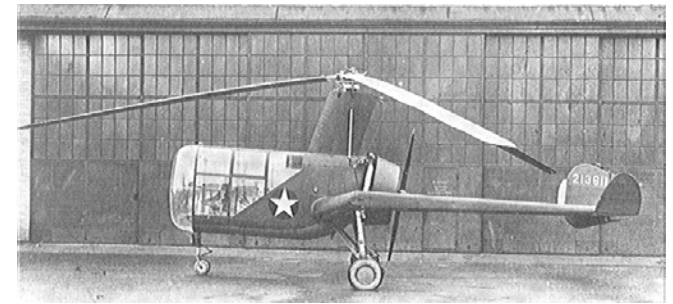
Pitcairn XO-61 for 1941 Air Force Competition

Kellett KD-1 1935 Production (Direct Control)

Ref. Photos Brooks, Artist Rendition Apostolo

NACA Purchased The Pitcairn PCA-2 In ???, 1931. The First Flight Test Report Was Published As Technical Report No. 434 on May 2, 1932.

PCA-2 Dimensions

GW ≈ 2,940 lbs   **Rotor**

WE ≈ 2,050 lbs   D ≈ 45 ft   c ≈ 22 in

ESHP ≈ 300 hp $\sigma \approx 0.0976$ $V_t \approx 340$ fps

Fuel ≈ 52 US gal   Airfoil : Gött. 429

Propeller (?)

  D ≈ 10.5 ft   c ≈ 6 in

  $\sigma \approx 0.061$ $V_t \approx 700$ fps

Wing

  Span ≈ 30.3 ft

  Area ≈ 101 sq. ft

  Airfoil : Mod of NACA M3

PCA-2 Performance

Speed Range ≈ 20 to 118 mph

Rate of Climb ≈ 800 fpm

Service Ceiling ≈ 15,000 ft

Range ≈ 290 statute miles
          at 87-98 mph

PCA-2 Price

$15,000

© FDH Fig. 1-17 Ref. : Brooks

The Force, Velocity And Angle Trim Diagram For The PCA-2 Gliding Flight Test That Wheatley Did.

Lift

Resultant Of Lift And Drag

Drag

Horizontal Velocity

Glide Angle

Rate of Descent Velocity

Airspeed

Glide Path

Weight
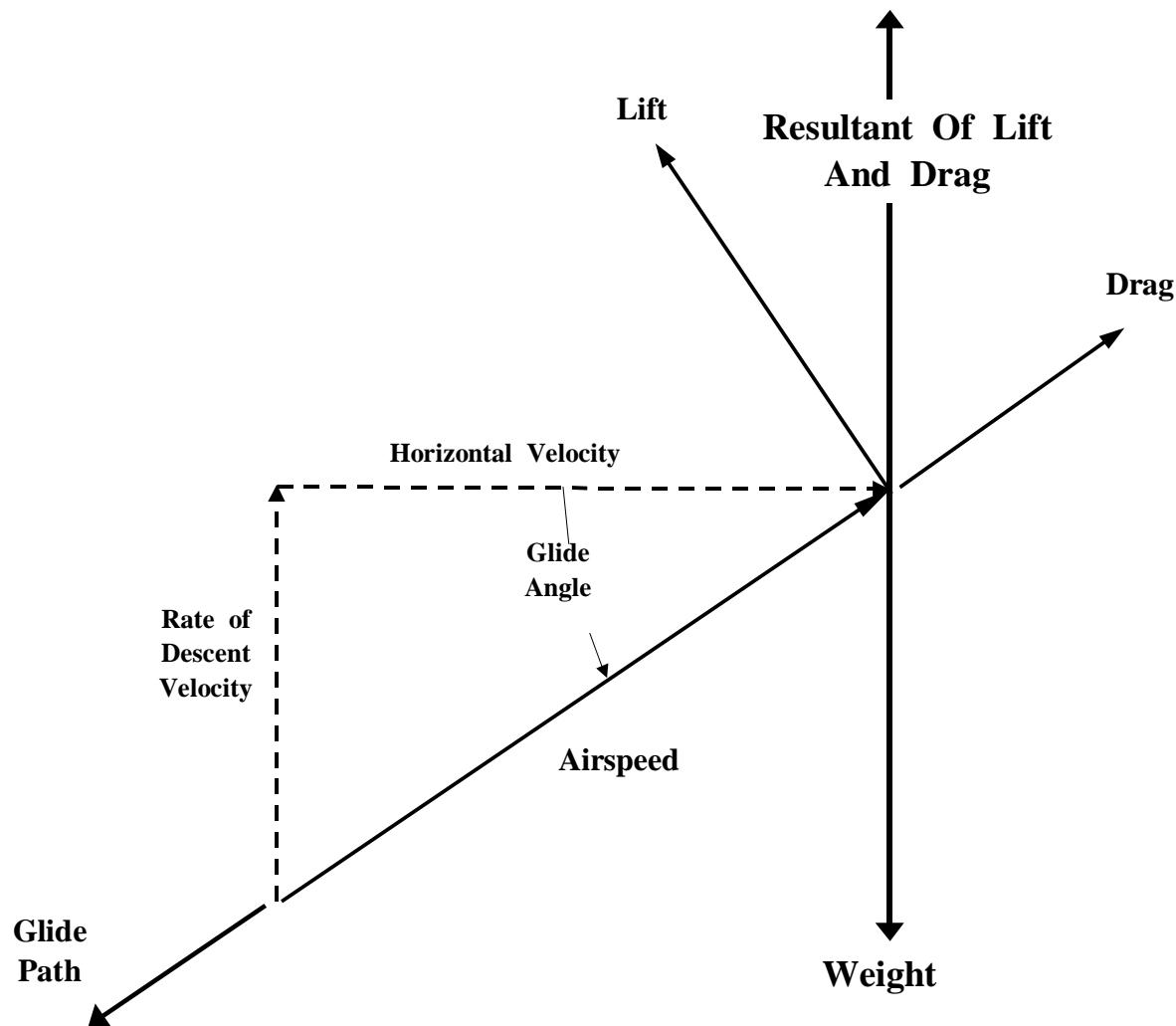
© FDH Fig. 1-18

Wheatley's Data Measurement And Reduction Was Simple, Accurate And Thorough. He Provided The First Really Good Results To The Industry.

From A Trailing Bomb Suspended 80 feet Below The Aircraft, He Obtained Dynamic Pressure [q] And Flight Path Angle [γ]. At Times He Also Used A Sensitive Altimeter And A Battery Of Stop Watches To Get Vertical Velocity. The Attitude [θ] Of The Autogiro Was Recorded By A Pendulum-type Inclinometer Fixed In The Fuselage. He Calculated Density [ρ] From Observations Of A Liquid-in-glass Type Thermometer Placed In The Airstream And A Aneroid-type Recording Altimeter. He Corrected Takeoff Gross Weight For Fuel Burned.

It Was Simple

$$Airspeed = V = \sqrt{\frac{2q}{\rho}} = \sqrt{V_H^2 + V_{RD}^2}$$

$$V_H = V\cos\gamma \quad and \quad V_{RD} = V\sin\gamma \quad and \quad \alpha_{hp} \approx \gamma + \theta$$

$$L = W\cos\gamma \quad and \quad D = W\sin\gamma$$

$$C_L = \frac{L}{q(A + S_W)} \quad and \quad C_D = \frac{D}{q(A + S_W)}$$

$$Rotorcraft \quad \frac{L}{D} = \frac{W\cos\gamma}{W\sin\gamma} = \frac{1}{\tan\gamma} = \frac{C_L}{C_D}$$

Lift And Drag Coefficients Were Obtained Through 90 Degrees In Gliding Tests With The PCA-2.
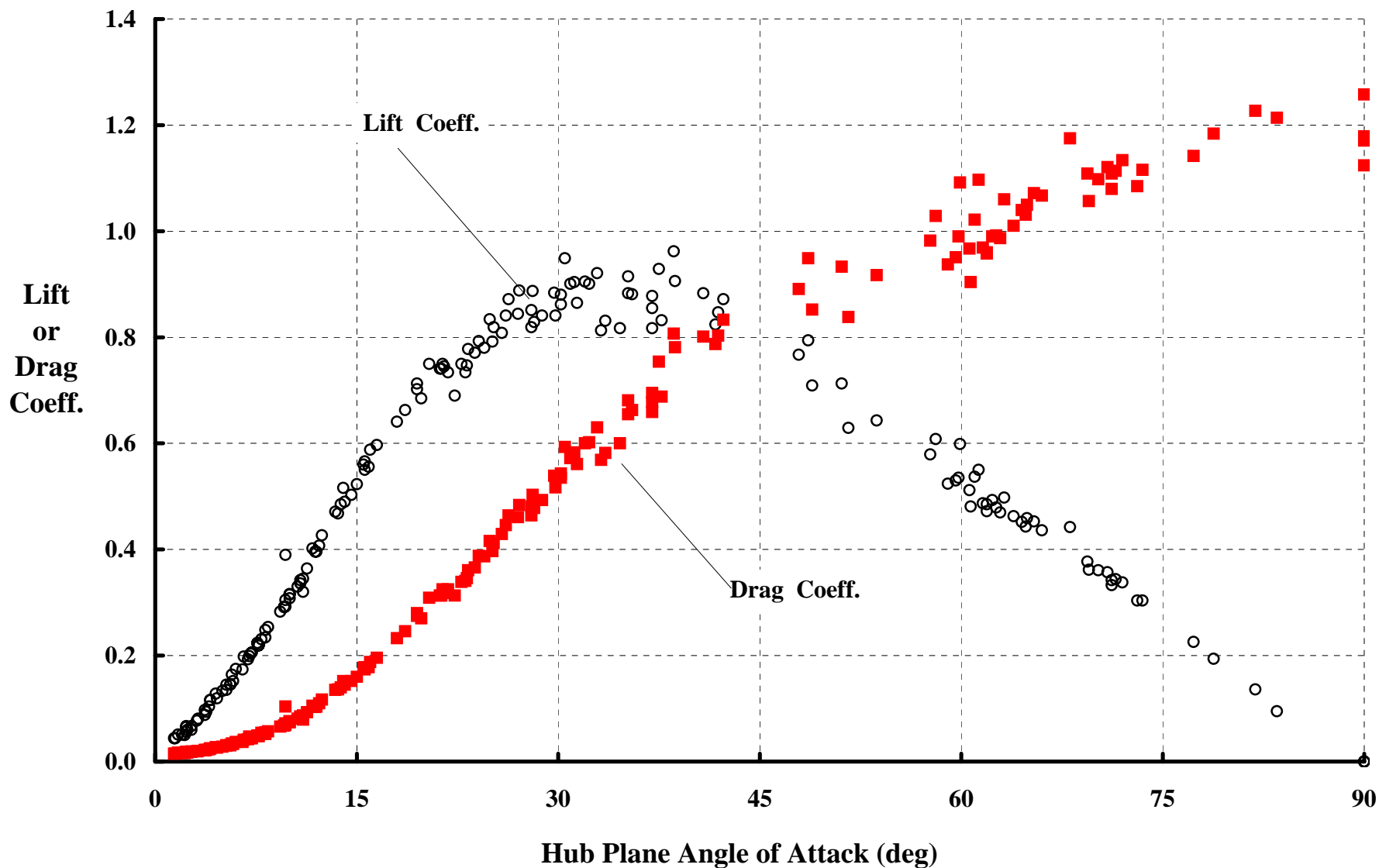
The PCA-2's Aerodynamic Efficiency Left A Lot To Be Desired As Wheatley Found Out In The Mid 1930s.

Rotor Blades Alone L/D
(NACA TR 515)

Total Rotorcraft L/D
(NACA TR 434)

Lift to Drag Ratio

Rotor Advance Ratio
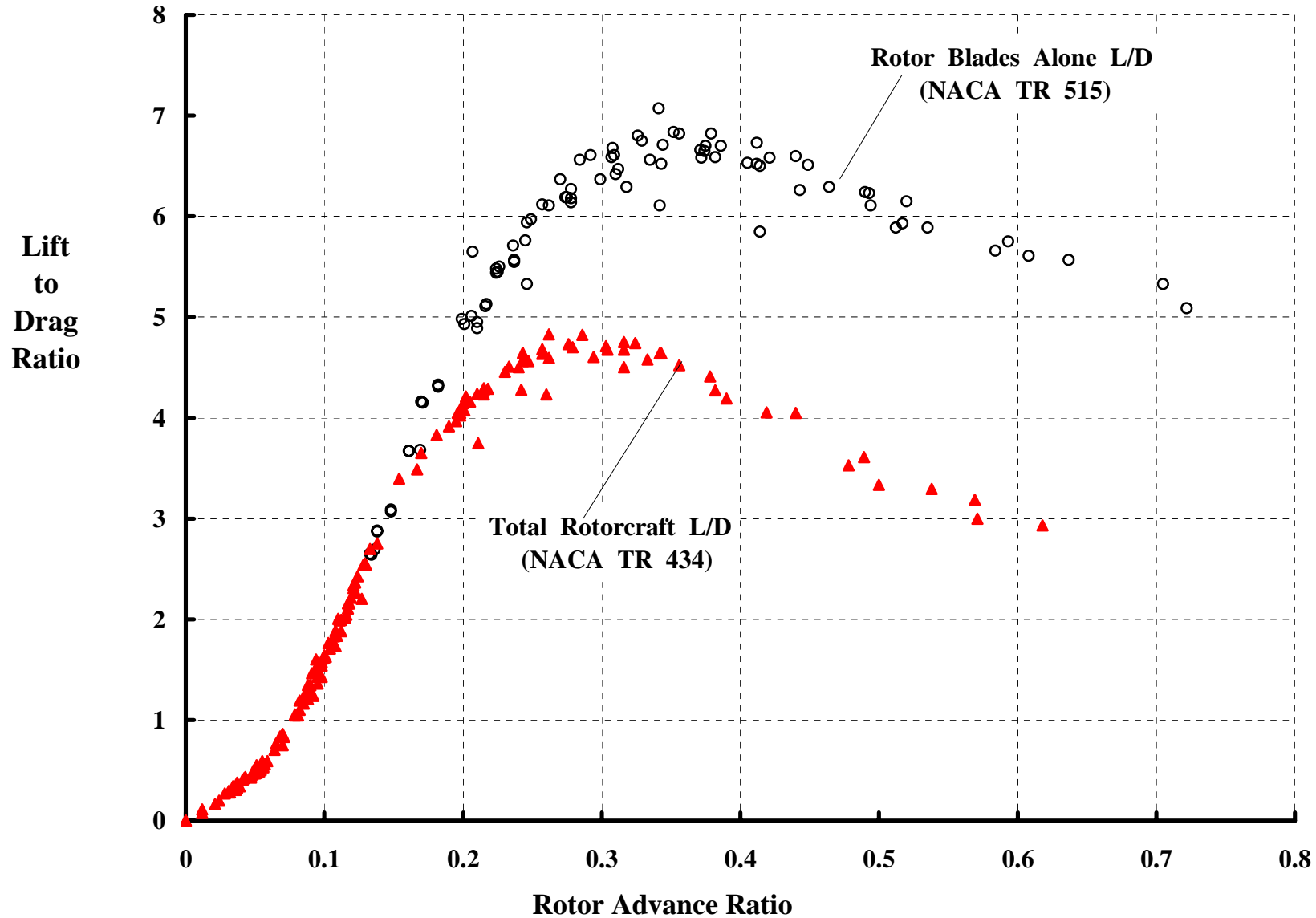
The PCA-2's Gliding Performance Provided
A Safe Envelope In The Power Off Situation.

Horizontal Velocity   (knots)

Rate Of Descent (ft / sec)

10 deg. Glide Angle
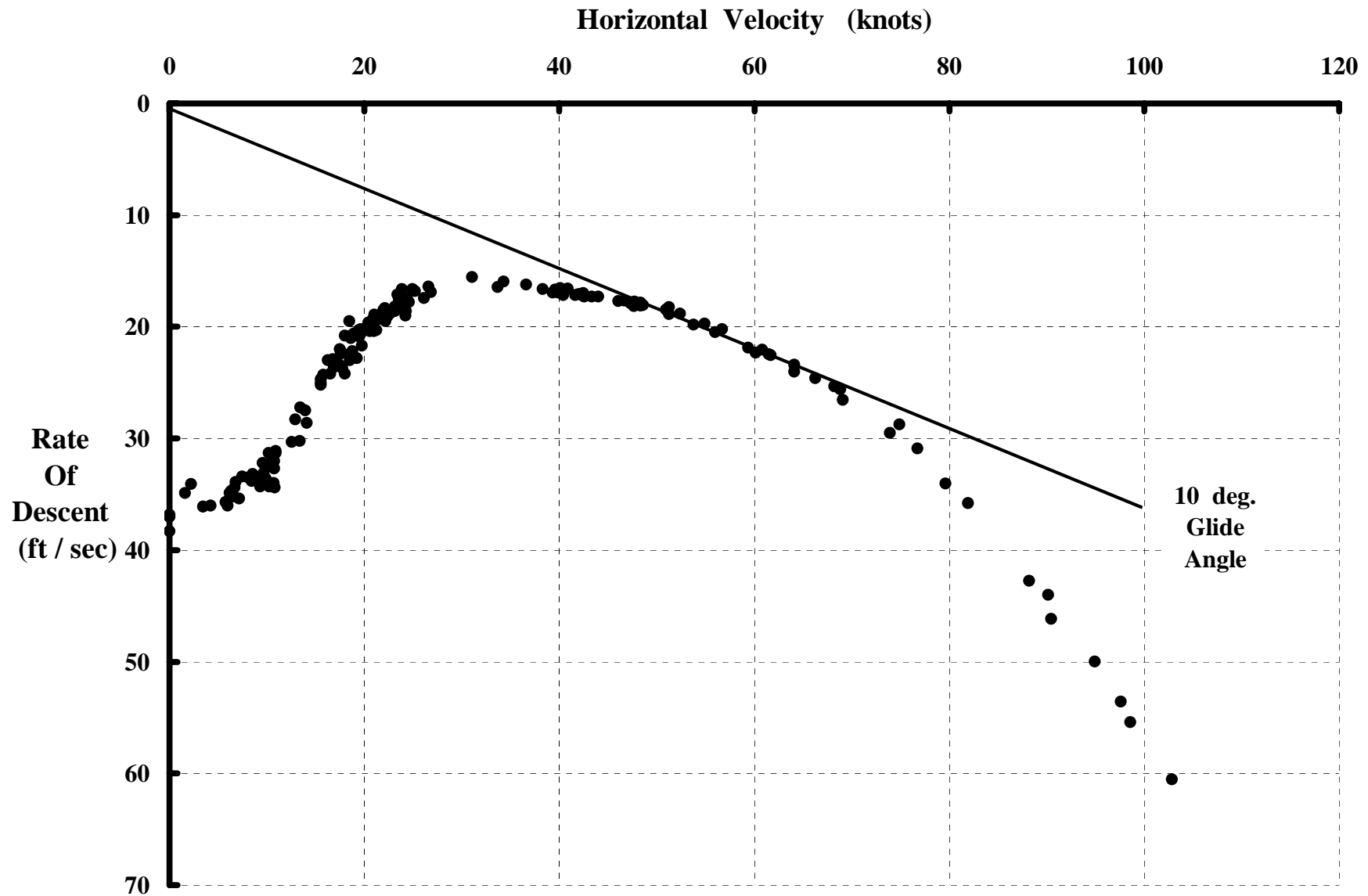
The PCA-2's Equivalent Flat Plate Area At Zero Lift
Was 17.6 sq. ft.— Over 4 Times That Of A P–51B.

$$D/q = 17.56 + 0.08904 \, (L/q) + 0.00022248 \, (L/q)^2$$

Drag/q
sq. ft

Lift/q   sq. ft
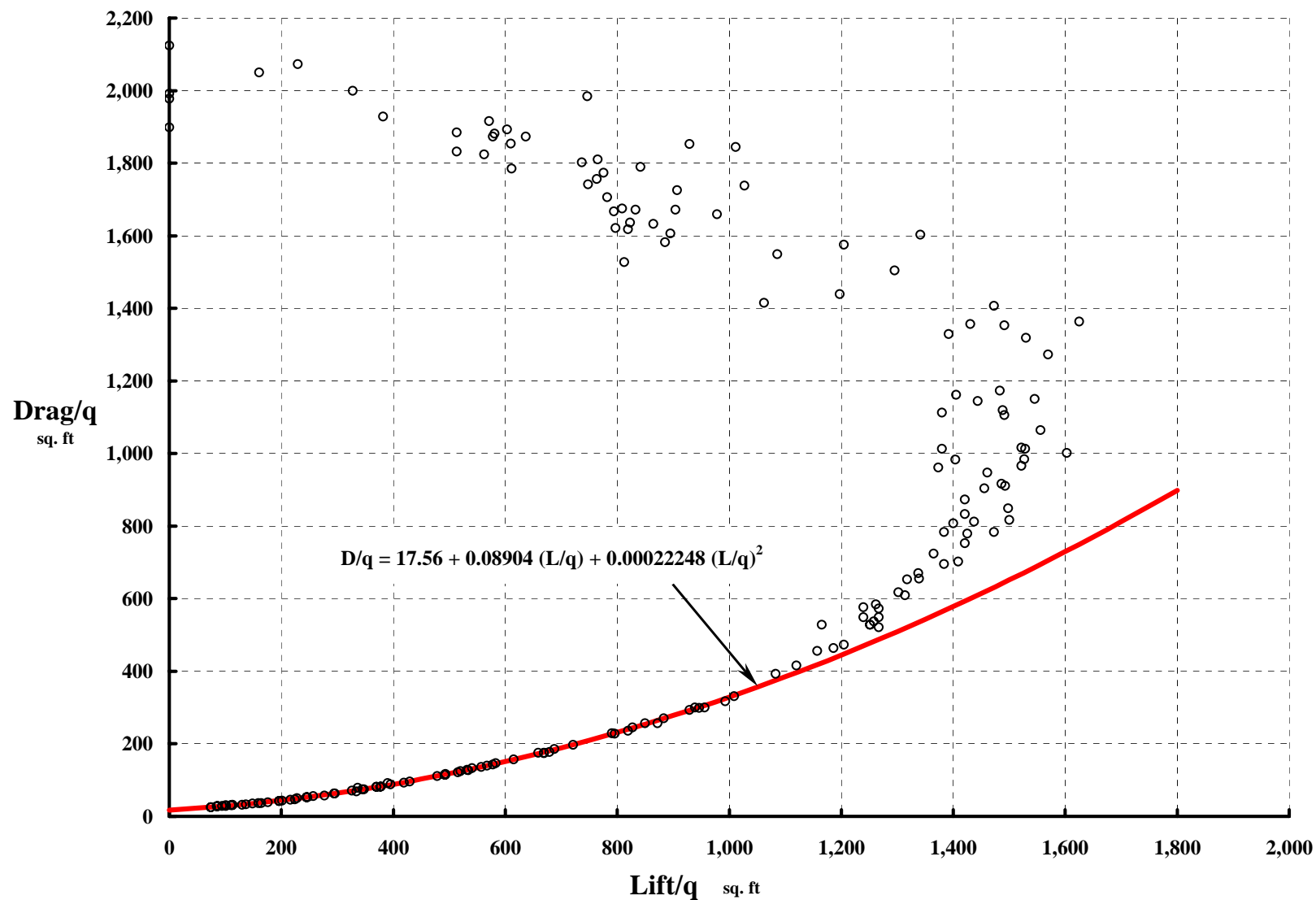
The PCA-2's Maximum Lift–Drag Ratio Occurred At Low Lift.

$$\frac{L}{D} = \frac{L/q}{17.56 + 0.08904\,(L/q) + 0.00022248\,(L/q)^2}$$

Lift to Drag Ratio (y-axis)

Lift/q sq. ft (x-axis)
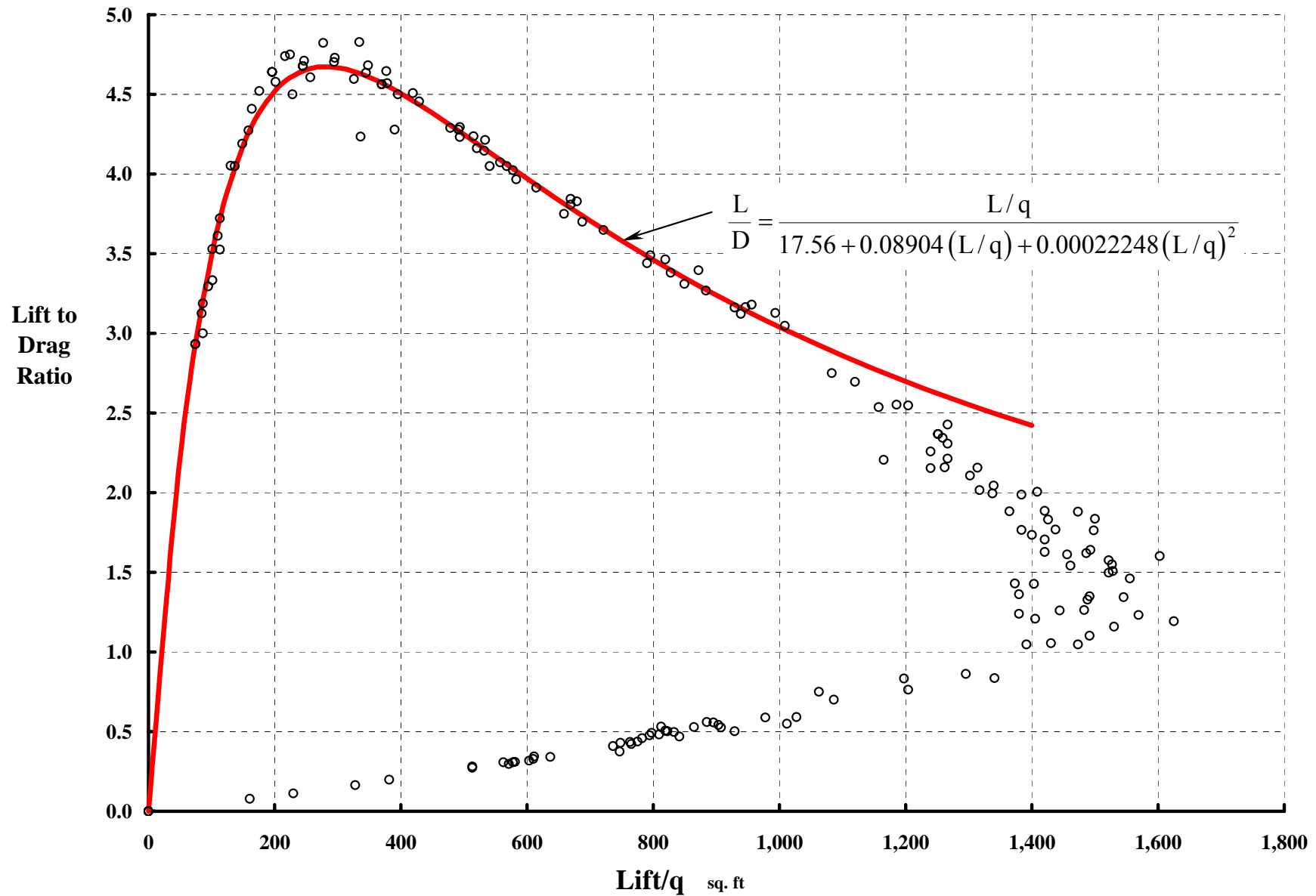
Sikorsky's VS–300 Convinced The Air Corp To Buy The Sikorsky R–4.

Kellett YO-60, First Flight Feb. 1942
(Collective + Cyclic + Jump Takeoff)

Sikorsky R–4, First Flight Jan. 1942
(Collective + Cyclic + VTOL)

Ref. Apostolo, Giorgio, "The Illustrated Encyclopedia of Helicopters" Bonanza Books, New York, 1984

Configuration Comparison

Parameter	YO–60	YR–4B
Gross Weight	2,800 lbs	2,540
Weight Empty		2,011
ESHP	300 hp	190
Fuel	36 US gal	30
Disc Loading	1.91 lbs/ft^2	2.26
Rotor		
Diameter	43.2 ft	38.0
Chord	12.92 in	14.33
Solidity	0.0476	0.060
Tip Speed	370 fps	450
Airfoil (root)	23016	0012
Airfoil (tip)	23010	0012
Prop/Tail Rotor	Fixed Pitch	Collective
Diameter	8.50 ft	7.92
Chord	6 in	5
Solidity	0.075	0.10
Tip Speed	957 fps	665
Performance		
Speed	26 to 134 mph	0 to 80
Rate of Climb	1,020 fpm	725
Service Ceiling	13,750 ft	8,000
Range	210 st. miles	200
Cruise Speed	70 to 102 mph	60 to 70
Price	$25K to $30K	

The Kellett YO-60 Achieved An L/D Max. Of 5.5.
It Was About The Best Autogyros Would Do.

Rotor Blades Alone

Total Rotorcraft

Lift to Drag Ratio

Wiesner, W., "Performance Analysis of U. S. Army Air Force Model XO-60 Rotor Aircraft Equipped with a Jacobs I - 6MB - A Engine Rated at 300 H. P. and a Hamilton Constant Speed Propeller", Kellett Autogiro Corp. Report No. 130.8, May 1943. (Private letter of December 18, 1992)

Airspeed (mph)

© FDH Fig. 1-22a
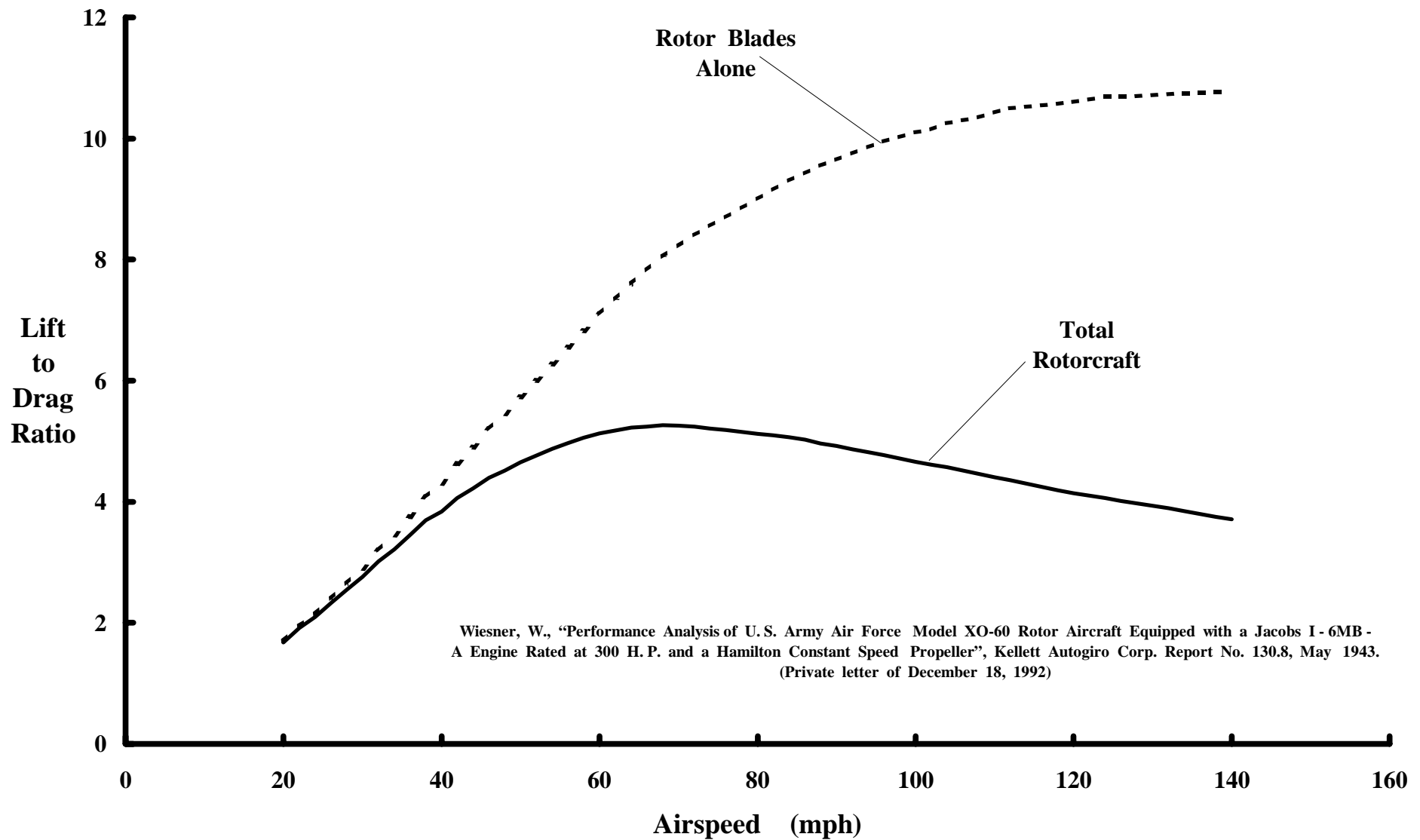
The Body Drag Of The YO–60 Was High.

Parasite
Drag
Area,
fe
(sq. ft.)

Cruise

Low Speed

Rotor Hub Plane Angle of Attack (deg)
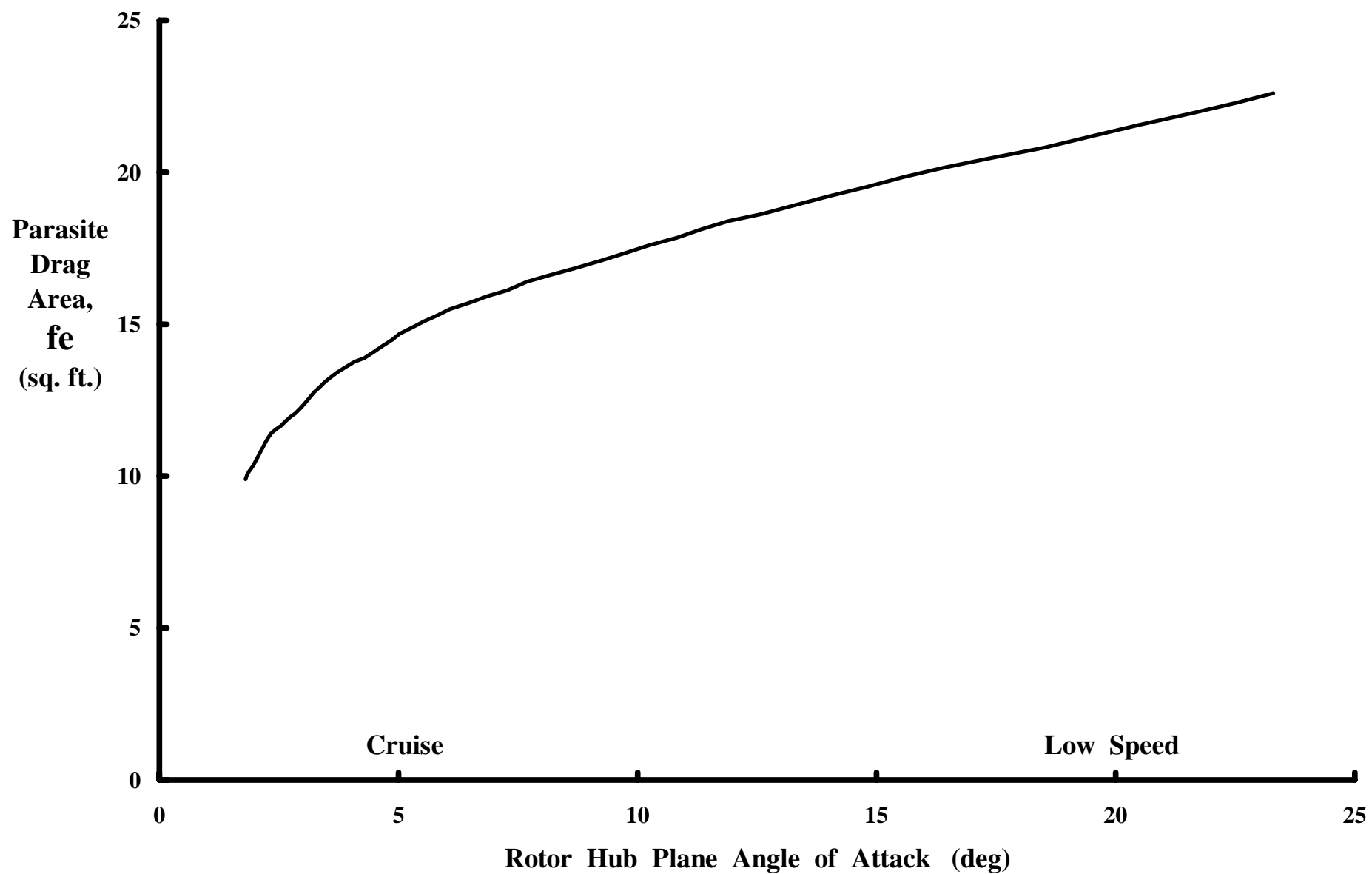
The XO-60 Propeller, A Fixed Pitch Type, Was Made By Hamilton Standard.

Propeller Efficiency (y-axis, 0 to 0.9)

Airspeed (mph) (x-axis, 0 to 160)

© FDH Fig. 1-22c
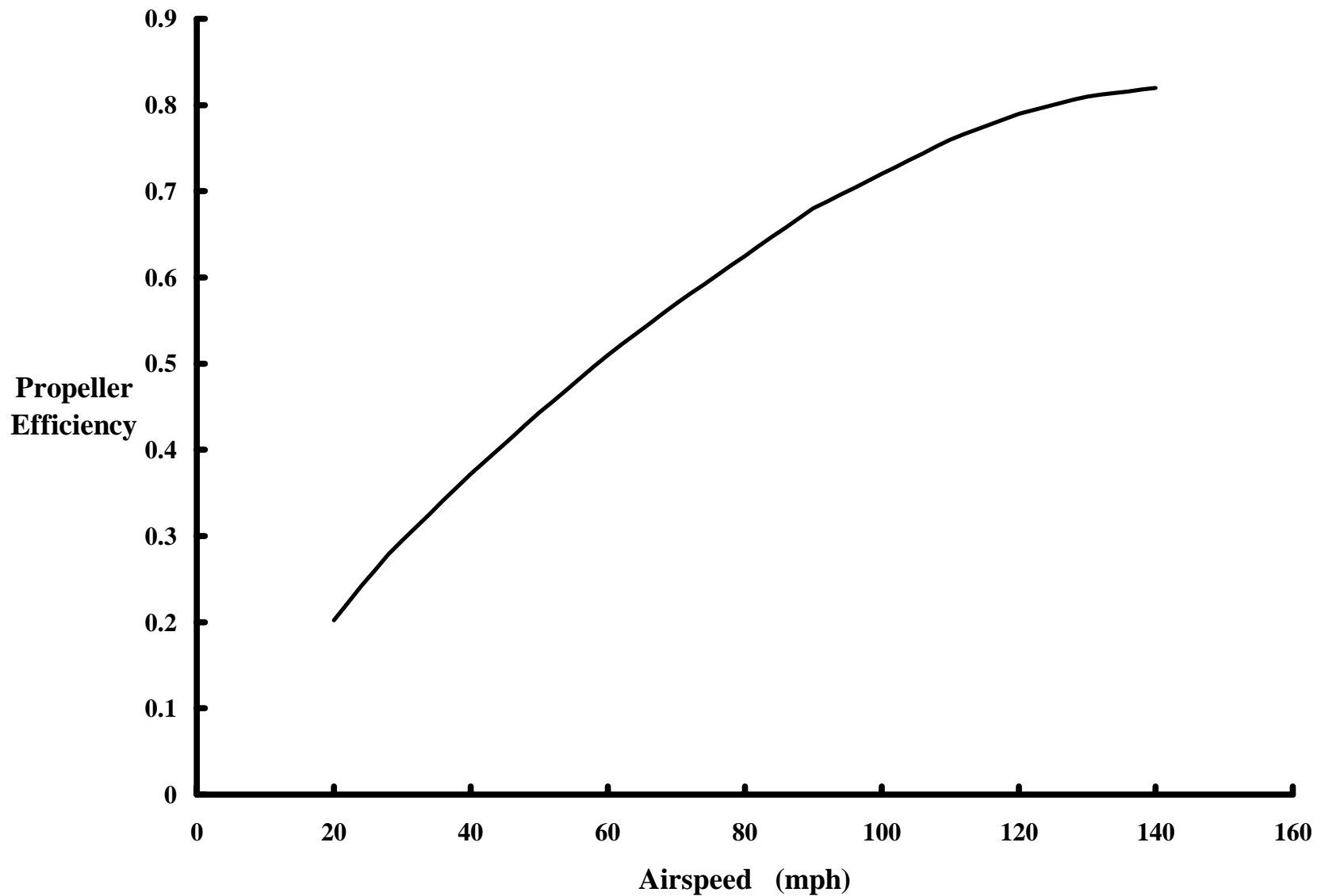
The XO-60 Did Not Have Great Performance When Compared To Airplanes Of The Early 1940s.

Horsepower

YO-60 Engine Power Available

YO-60 Engine Power Required

$$\frac{D \times V}{550\,\eta_P}$$

$$\frac{D \times V}{550}$$

Propeller Inefficiency

Airspeed (mph)

© FDH Fig. 1-22d
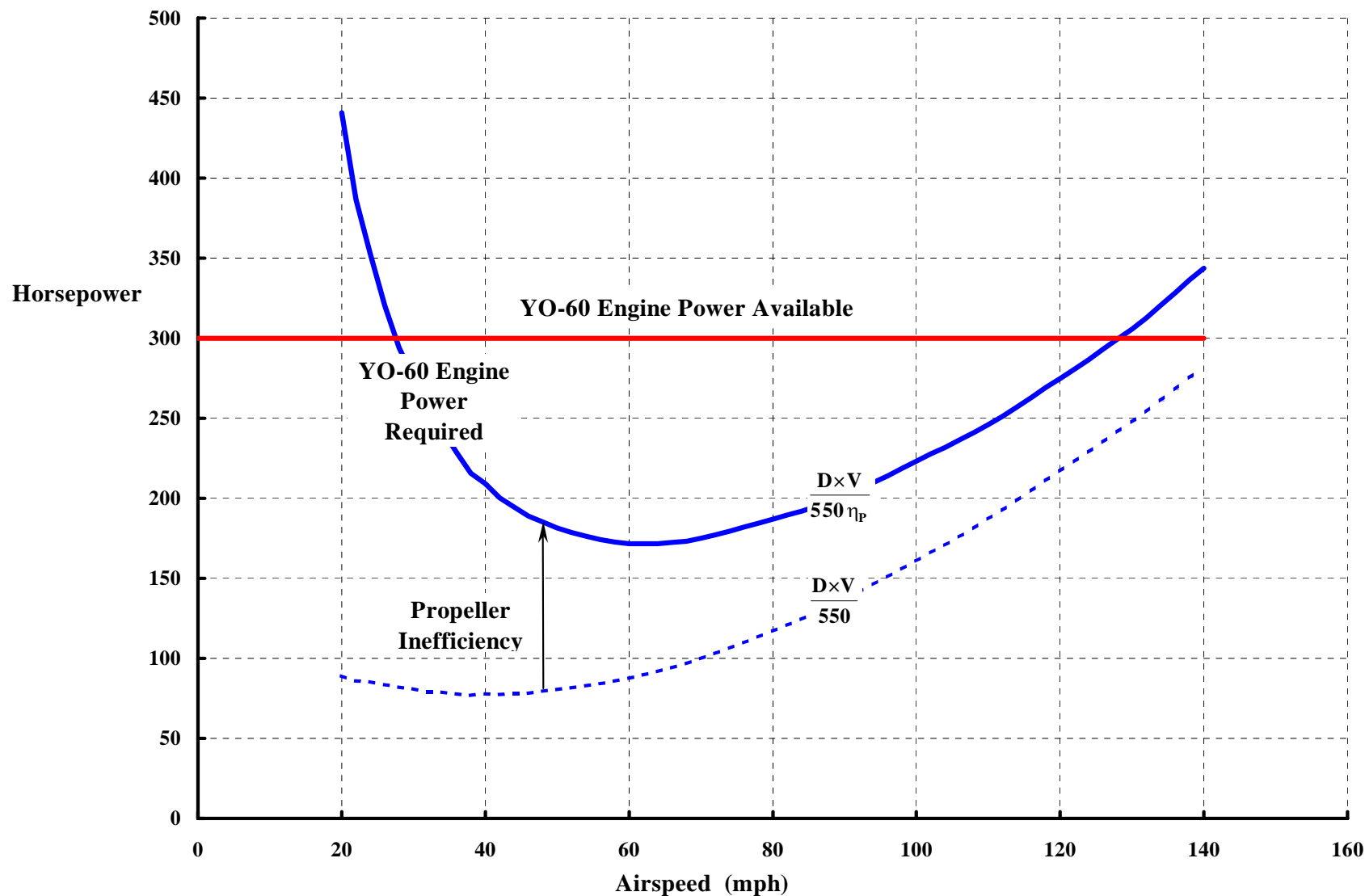
The YO-60 Was Faster, But The R-4 Could Hover. The Autogyro Era Was Over By 1943–As Far As The Military Was Concerned.

YO-60 Engine Power Available

YO-60 Engine
HP Required
GW = 2,800 lbs

$$\frac{D \times V}{550 \eta_P}$$

$$\frac{D \times V}{550}$$

YR-4B Engine Power Available

YR-4B Engine
HP Required
GW = 2550 lbs

Horsepower

Airspeed (mph)

Ref. YH-4B
1. NACA MR No. L5C10 or Wartime Report L-595
2. NACA MR No. L5D09a or Wartime Report L-596

© FDH Fig. 1-22d

A-19
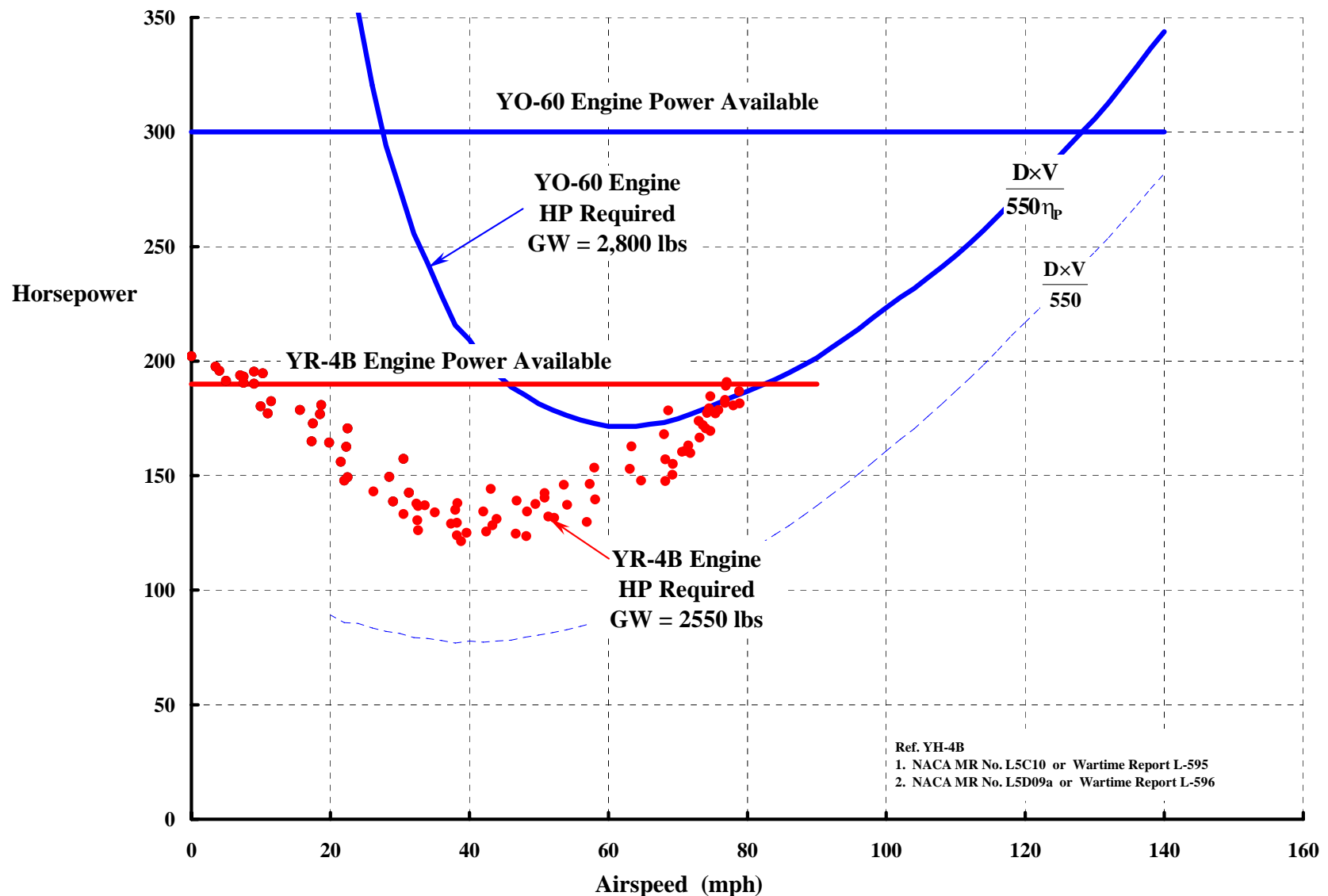
The Autogyro's Safety Record, Even Including Development, Was Excellent. However, The First Autogyro Fatality Finally Occurred Dec. 19, 1932.

By This Time :

- **120 Autogiros Built, Including 30 Prototypes**
- **30 To 40 Pilots Trained**
- **Over 100 Fixed Wing Pilots Had Flown Autogyros In The U. S. Alone**
- **About 35,000 Hours And Over 2 1/2 Million Miles Flown**

General Aviation In United Kingdom In 1974

General Aviation In United States In 1969

GA In US
1939

Autogyros World Wide In 1932

0   10,000   20,000   30,000   40,000   50,000

Flight Hours Between Fatalities
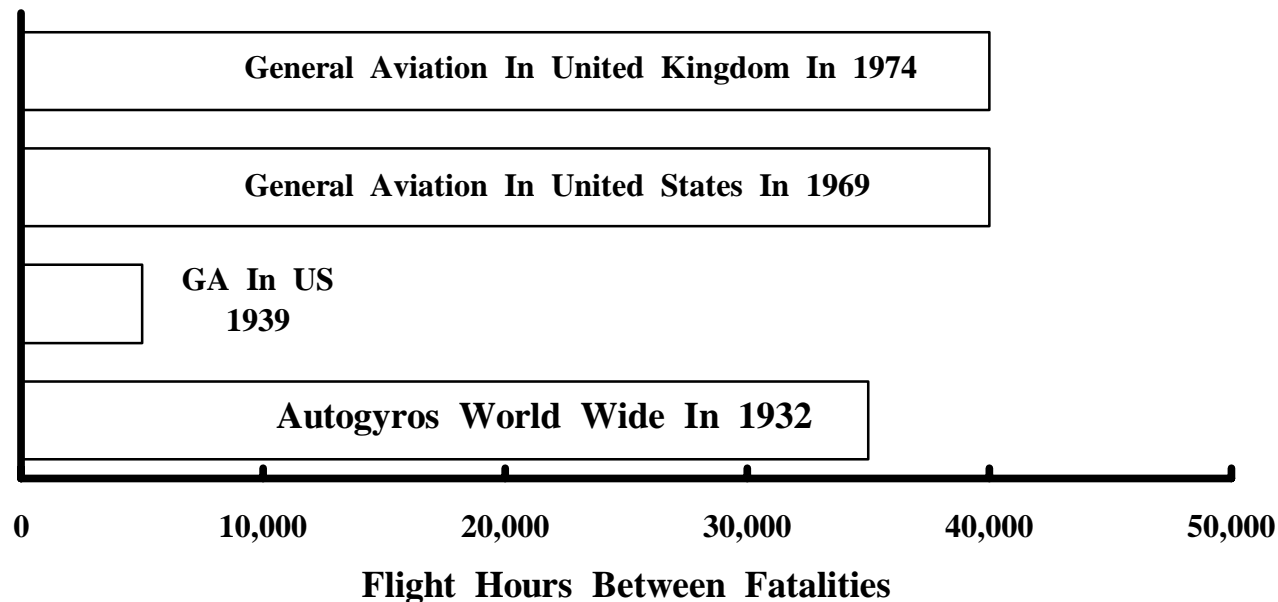
By The End Of WW II, The Autogyro Industry Had
(1) Created Some 46 Types
(2) Delivered About 450 Rotorcraft.

Ts AGI

Kayaba — Ka - 2 — Ka - 1A

Kellett — KD - 1 — K - 2/4

Pitcairn — PA - 18 — PAA - 1 — PCA - 2

Cierva Licensees — C. 30 — C. 19

Producton Run (0, 20, 40, 60, 80, 100, 120, 140, 160, 180, 200)
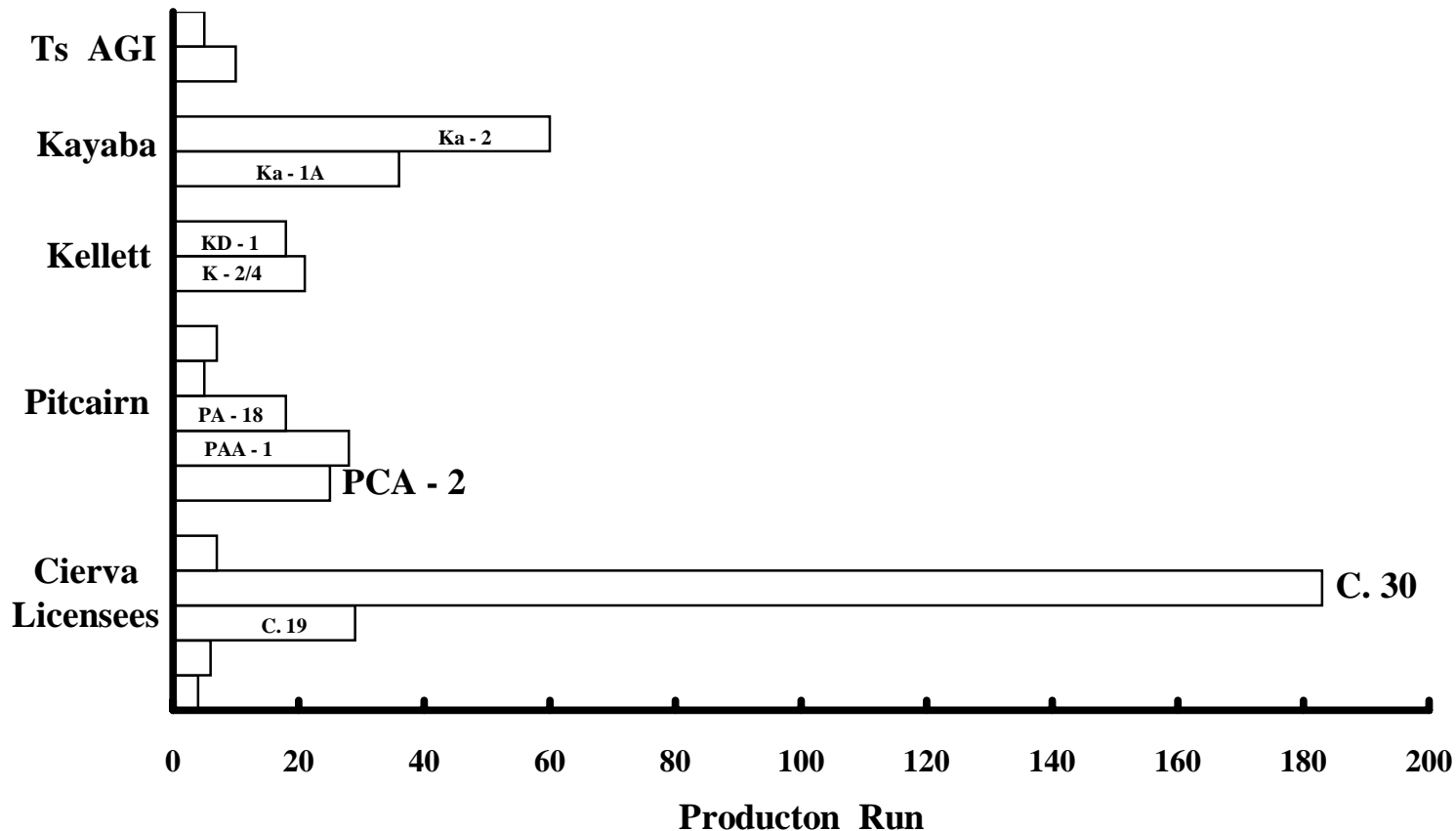
The Autogyro Industry Reduced The Weight Fraction From 0.81 To 0.58 In About 20 Years.
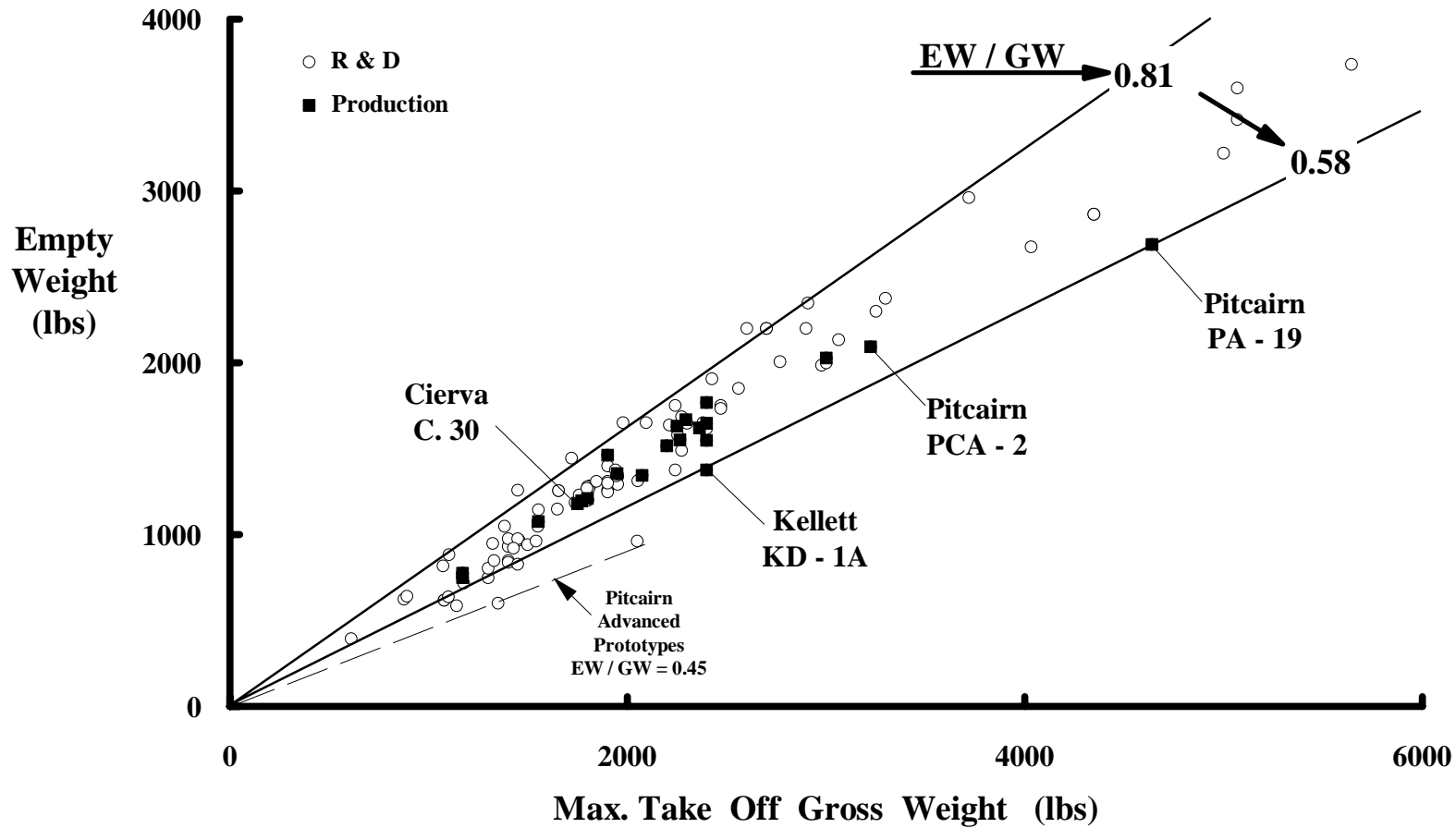
The Industry Demonstrated It Had A Product At Under $ 5.50 Per Pound Of Empty Weight.

$16,000

$5.50 / Lb

Pitcairn
PCA - 2
PA - 21

Pitcairn
PA - 19

"Back
Then"
Dollars

$8,000

$3.50 / Lb

Kellett
K - 3

Cierva
C. 30

0

0   1000   2000   3000

Empty Weight   (lbs)

© FDH Extra 48

A-23
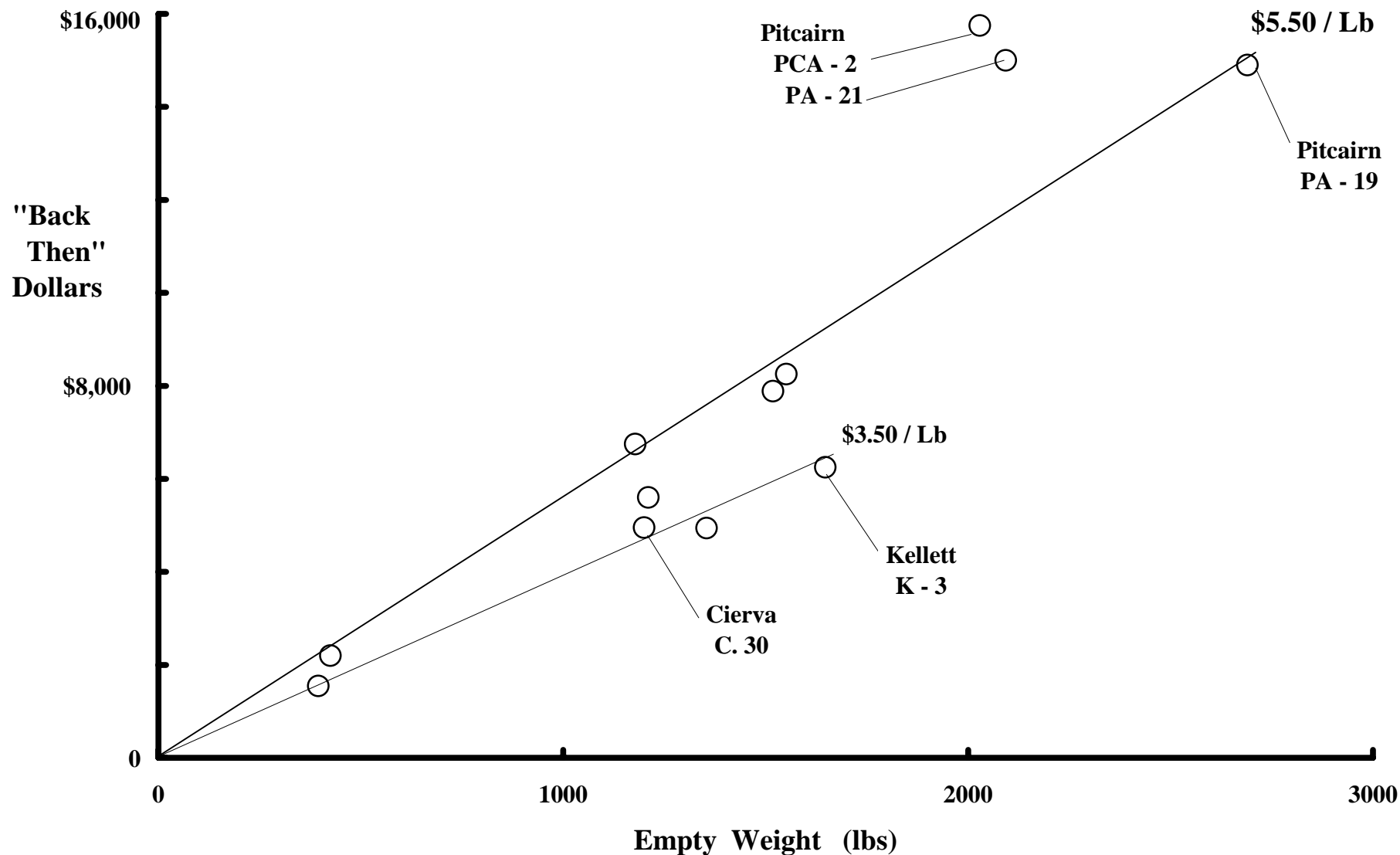
Just A Few Things The Autogyro Pioneers Accomplished In Starting Our Rotorcraft Industry:

- Created A "Flying Machine" Other Than An Airplane

- Acquainted The Public With The Aircraft

- Achieved An Enviable Safety Record

- Pursued A Vigorous Product Improvement Program

- Developed And Shared Technology
  1. Applied low flapping hinge offset concept
  2. Introduced the lag hinge
  3. Encountered and solved the ground resonance problem with lag dampers
  4. Achieved low solidity rotors
  5. Obtained direct control of the rotor tip path plane
     a. hub tilting
     b. swashplate, pitch links and blade feathering
  6. Demonstrated a soft inplane, hingeless rotor system
  7. Mechanized power take off and overriding clutch for jump takeoff
  8. Found first order solutions to aerodynamic, dynamics, flying quality, aeroelastic and structural equations
  9. Demonstrated–in flight–start up of a stopped rotor
  10. Related airfoil pitching moment to elastic twist and stick gradients

LET'S REVISIT AUTOGYROS

First Some History
Cierva, Pitcairn, and Kellett Era (1919 to 1941)
Selection of the Helicopter (1942)
Legacy

Some Technology Aspects

What's in a Name?
Fuselages, Wings, Propellers, Rotors and Trim
Rotor Thrust and Flapping Behavior at High Advance Ratio
Limits to Rotor Lift and Propulsion
To Review Then

XV–1 Re–examined

Full Scale Wind Tunnel Test in 40 by 80
Rotor (With & Without Wing)
Complete Aircraft
Rotor Stability In Forward Flight
Phase II Flight Evaluation

Concluding Remarks

A-25

In Oct. 1956 The McDonnell XV-1 Compound Was The 1st Rotorcraft To Reach 199 mph. It Flew In 3 Modes: Helicopter, Autogyro & Airplane.

Note: The 199 mph (174 knots true) was achieved in a slight descent, not ... **0.9.**
GW = 5,510 lbs, 550hp Continental R–975

3 Bladed. 31 ft Diameter, Tip Burning Pressure Jets
Gimbaled hub, flex strap blade retention, stiff inplane
**Note:2.2° feather down per 1° cone up BUT about
0.268° feather down per 1° flap up in Helicopter &
Autogyro flight. Then 2.2° feather down per 1° flap
or cone up in Airplane mode.**

Engine clutched to
compressor and to prop

Very Unique Free
floating elevator

Twin booms

2 Blade, 6 ft 5inch Diameter Prop

1 Pilot, 3 Passenger, WE = 4,280lbs

26 ft Wing Span, 100 ft² Area, 6.76 Aspect Ratio
Wing Incidence of 7 deg. Outboard span twisted –3 deg.
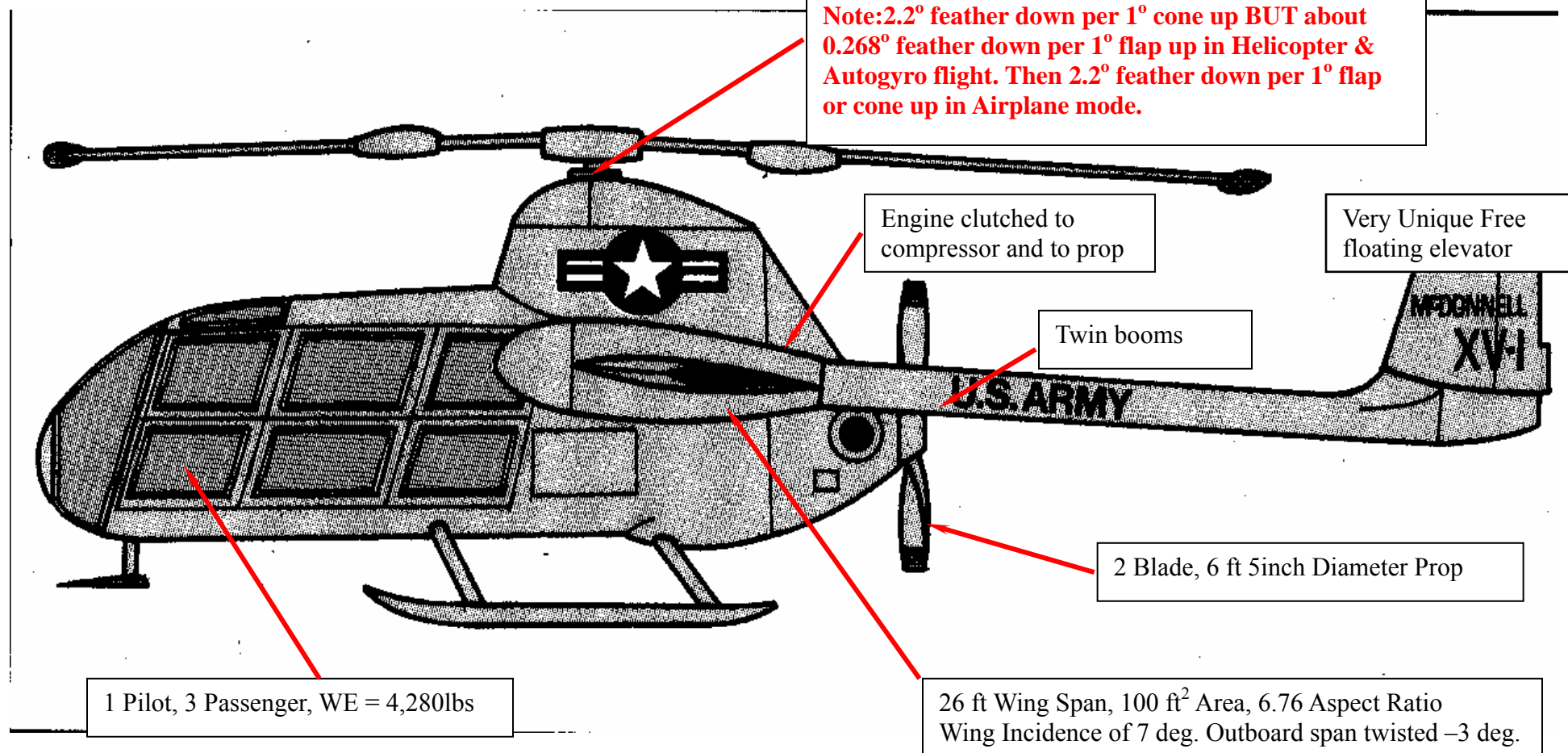
Now Then–What Would You Call This "Flying Machine"?

I Prefer The Total Aircraft Lift To Drag Ratio.

L/D From A Power Off Glide
Test Does Not Include
Propulsive Efficiency Of
Thruster
(Example Is YO-60)

YO-60
Aircraft L/D
(Includes Prop
Inefficiency)

YR-4B
Aircraft L/D

$$\left(\frac{\text{Lift}}{\text{Drag}}\right)_{\text{Aircraft}} = \frac{\text{Flight Weight (lbs)}}{\frac{550}{V_{fps}}\sum_{n=1}^{N}\left(\text{Engine Horsepower}\right)_n}$$

Flight Speed (mph)

Lift to Drag Ratio
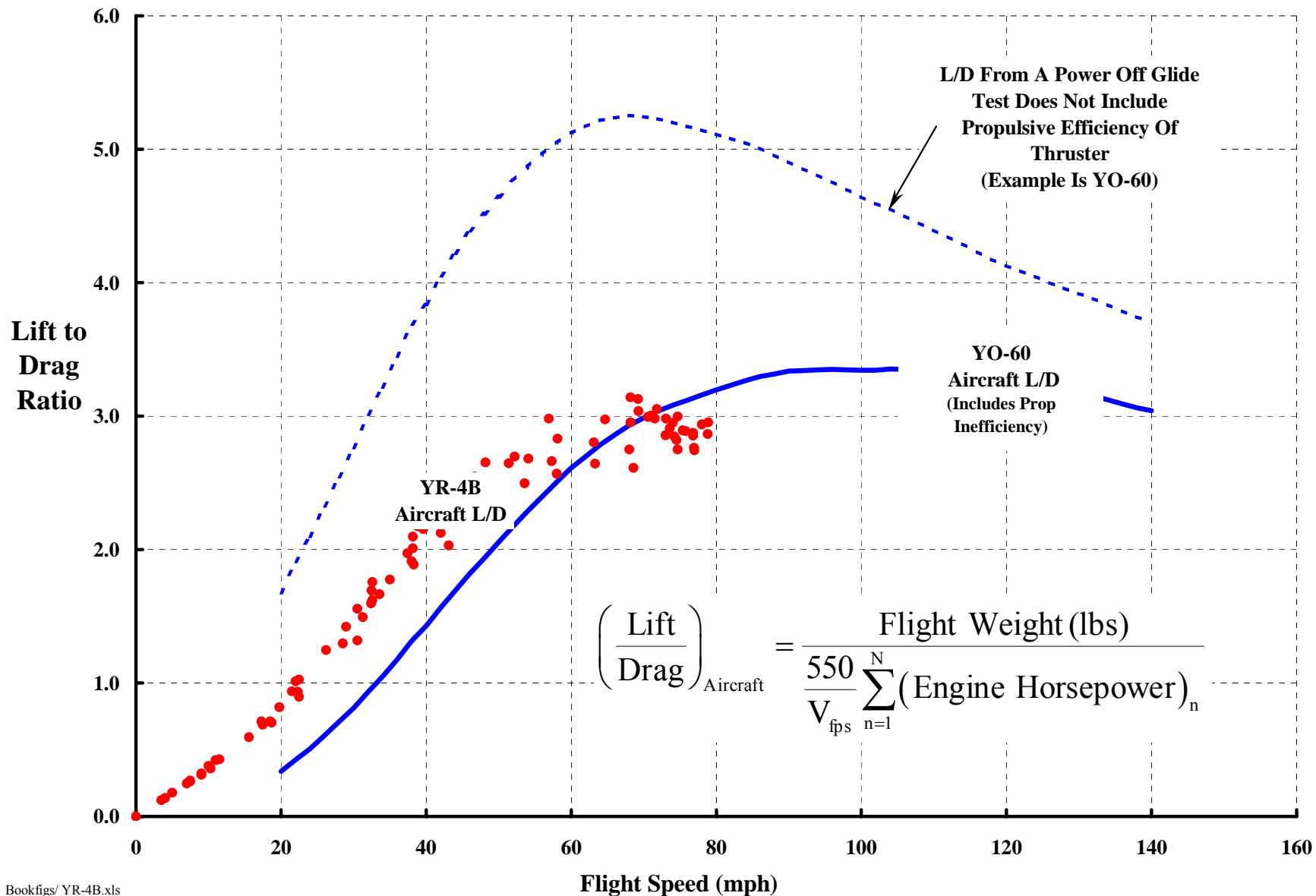
Bookfigs/ YR-4B.xls

The Component Lift And Drag Descriptions I Prefer Are:

Fuselage (Everything but wing and rotor blades. Fuselage lift assumed zero)

$$\frac{D_{Fuselage}}{q} = f_e + y(\alpha) \qquad \text{where } f_e \equiv \text{equivalent flat plate area } (ft^2)$$

Wing

$$\frac{D_{Wing}}{q} = S_w C_{do} + S_w \varepsilon (C_L - Design\,C_L)^2 + \frac{1}{\pi}\left(\frac{L_w}{q\,b_w}\right)^2 (1+\delta) \qquad \left\{ From\ C_{Dw} = C_{Do} + \frac{C_{Lw}^2}{\pi\,AR} \right\}$$

Propeller (Lift assumed zero)

$$P_{Prop} = Profile\,(P_0) + Induced\,(Tv_i) + Propulsive\,(TV)$$

where

$$P_o = b\left(\tfrac{1}{2}\rho V_t^3\ R\right)\left[\int_{x_c}^{1}(c_x)(C_d)\left(x^2+\lambda^2\right)^{3/2}dx\right] \approx \frac{\rho\left(bc_{ave}R\right)V_t^3}{8}C_{d\,ave}F(\lambda, x_c) \qquad \text{where } \lambda = \frac{V}{V_t}$$

$$F(\lambda, x_c) = \left[\left(1+\lambda^2\right)^{3/2} - x_c\left(x_c^2+\lambda^2\right)^{3/2}\right] + \frac{3}{2}\lambda^2\left[\left(1+\lambda^2\right)^{1/2} - x_c\left(x_c^2+\lambda^2\right)^{1/2}\right] + \frac{3}{2}\lambda^4\left\{\ln\left[\frac{1+\sqrt{1+\lambda^2}}{x_c+\sqrt{x_c^2+\lambda^2}}\right]\right\}$$

$$v_i = \frac{V}{2}\left[\sqrt{1+\frac{4}{\pi}\left(\frac{T}{qD^2}\right)} - 1\right]$$

Ref. 1. Perkins, C. D. & Hage, R.E. "Airplane Performance, Stability and Control", Wiley & Sons, New York, 4th Printing, 1954
Ref. 2. Harris, F.D., "Performance Analysis of Two Early NACA High Speed Propellers With Application to Civil Tiltrotor Configurations", NASA Contractor Report 196702, August 1996

And The Rotor Lift And Drag Descriptions I Prefer Are:

$$L_R = T_R \cos\alpha_{tpp} - H_R \sin\alpha_{tpp}$$

$$D_R = T_R \sin\alpha_{tpp} + H_R \cos\alpha_{tpp} \quad OR \quad D_R = -\frac{\text{Engine Power to Rotor}}{V} + \frac{\text{Induced Power}}{V} + \frac{\text{Profile Power}}{V}$$
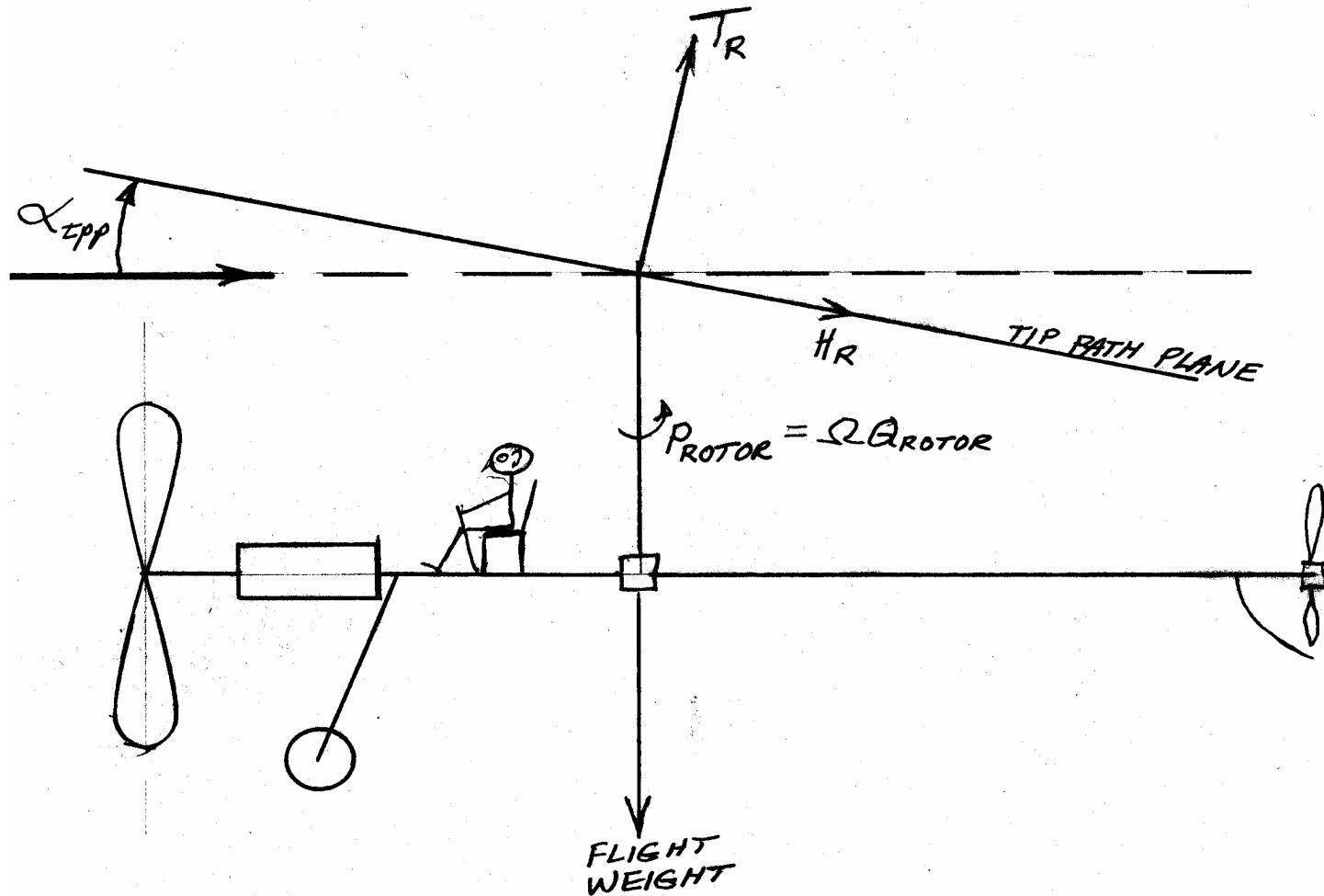
Where H–Force and Rotor Power Are Calculated As:

$$H_R = \rho A_R V_t^2 \sigma \left\{ \frac{\mu \lambda}{2} \left[\frac{C_T}{\sigma} - \frac{5.73}{4} \lambda \right] + C_{do} H(\mu) \right\}$$

where $H(\mu) = 0.25\mu + 0.0029470\mu^2 + 0.0893173\mu^3 + 0.0030383\mu^4 - 0.0009527\mu^5 + 0.0001083\mu^6$ for $\mu \le 3.0$

$$\lambda = \frac{V \sin \alpha_{tpp} - v_i}{V_t}, \quad \mu = \frac{V \cos \alpha_{tpp}}{V_t} \quad \text{and} \quad \frac{C_T}{\sigma} = \frac{T}{\rho (bcR) V_t^2}$$

$$P_R = \text{Induced}\,(T_R v_i) + \text{Propulsive}\,(-D_R V) + \text{Profile}\,(P_0)$$

where

$$P_o = b\left(\tfrac{1}{2}\rho V_t^3\ R\right) \left[\int_{x_c}^1 (c_x)(C_d)\left[(x + \mu \sin \psi)^2 + (\mu \cos \psi)^2 \right]^{3/2} dx \right] \approx \frac{\rho (bc_{ave}R) V_t^3}{8} C_{d\,ave} K(\mu)$$

$$K(\mu) = 1 + 4.65\mu^2 + 4.15\mu^4 - \mu^6 \qquad \text{for}\ \mu \le 1.0$$

or

$$K(\mu) = 1 + 5.2003\mu^2 + 2.8777\mu^4 - 0.1788\mu^6 - 0.0202844\mu^8 + 0.0052625\mu^{10} - 0.0002735\mu^{12} \quad \text{for}\ \mu \le 3.0$$

$$\text{Glauert's}\ v_i = \frac{T_R / 2\rho A}{\left[(V \sin \alpha_{tpp} - v_i)^2 + (V \cos \alpha_{tpp})\right]^{1/2}} \quad \text{and for}\ \mu > 0.15 \quad v_i = \frac{T_R / 2\rho A}{V}$$

Note: The K(μ) functions were first developed from numerical computations tabulated in my paper "Preliminary Study of Radial Flow Effects on Rotor Blades" Journal of the AHS, July 1966. See Table in Supplemental Data and Charts, Item 13. The adequacy of $K(\mu) = 1 + 4.65\mu^2 + 4.15\mu^4 - \mu^6$

was demonstrated by comparison to experiments in my paper "Rotary Wing Aerodynamics–Historical Perspective and Important Issues", given at the AHS Southwest Region Specialists' Meeting on Aerodynamics and Aeroacoustics, Feb. 25-27, 1987. Chairman Tom Wood of Bell Helicopter. See Supplemental Data and Charts, Item 11.

The Adequacy Of K(μ) Was Demonstrated By Comparison To Experiment.
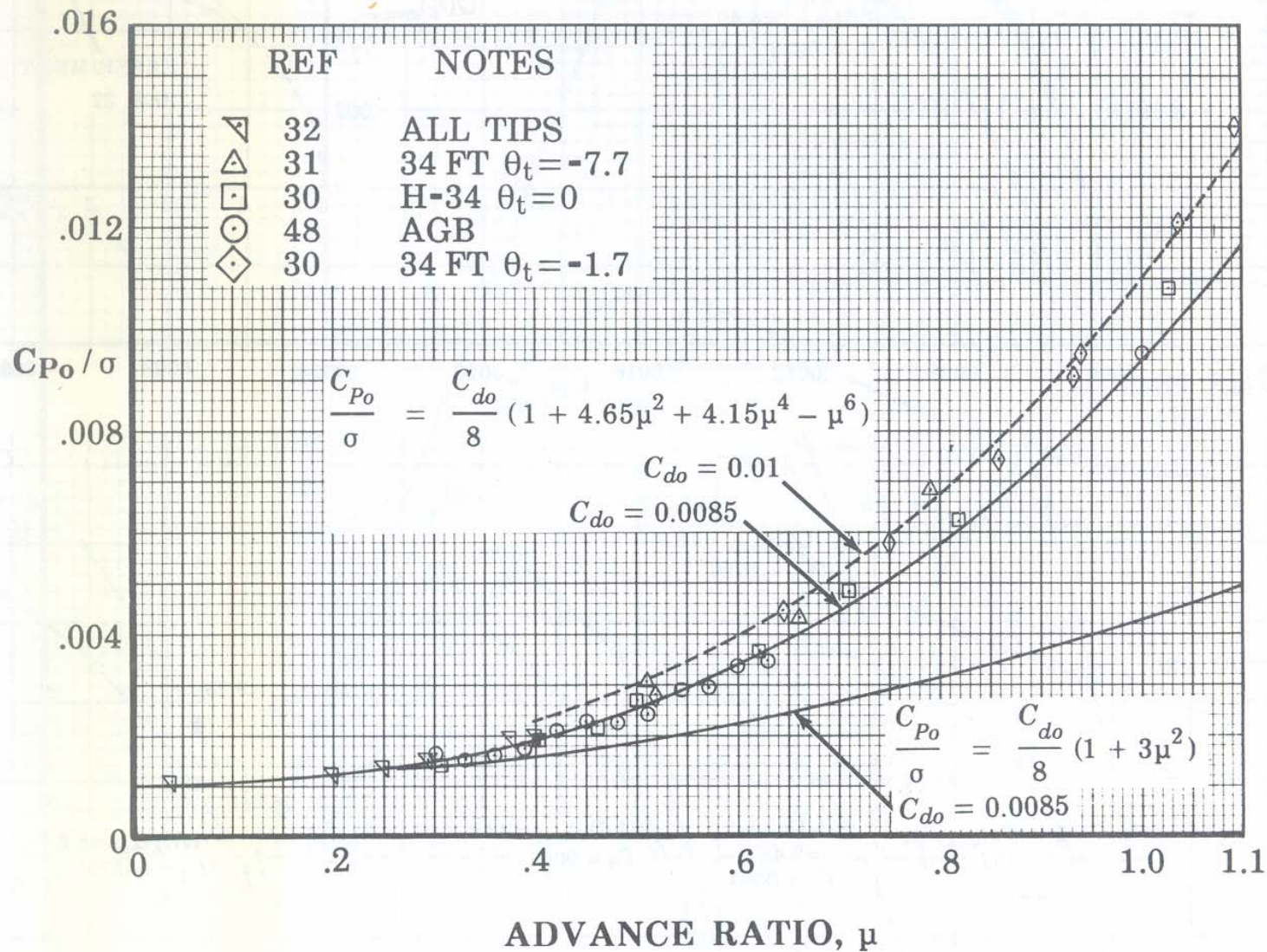
Ref.: Figure 26 of "Rotary Wing Aerodynamics–Historical Perspective and Important Issues", F.D. Harris Paper Given at AHS Southwest Region Specialists' Meeting on Aerodynamics and Aeroacoustics, Feb. 25-27, 1987. Chairman Tom Wood of Bell Helicopter

As An Aside, I Like Glauert's Quartic Roots Displayed This Way.

Note: See Supplemental Data and Charts, Item3 for quartic solution that is single valued for all values of V/vh

Glauert's Assumption

$$v = \frac{T/2\rho A}{\sqrt{\left(V \sin \alpha_{tpp} - v\right)^2 + \left(V \cos \alpha_{tpp}\right)^2}}$$

$$v_h = \sqrt{T/2\rho A}$$

$$\frac{v}{v_h} = \sqrt{\left(\frac{V}{2v_h}\right)^2 + 1} + \frac{V}{2v_h}$$

$$\frac{v}{v_h} = \frac{V}{2v_h} + \sqrt{\left(\frac{V}{2v_h}\right)^2 - 1}$$

$$\frac{v}{v_h} = \frac{V}{2v_h} - \sqrt{\left(\frac{V}{2v_h}\right)^2 - 1}$$

$$\frac{v}{v_h} = \left[\sqrt{\left(\frac{V^2}{2v_h^2}\right)^2 + 1} - \frac{V^2}{2v_h^2}\right]^{1/2}$$

$$\frac{v}{v_h} = \sqrt{\left(\frac{V}{2v_h}\right)^2 + 1} - \frac{V}{2v_h}$$

$\alpha_{tpp} = +90$

$\alpha_{tpp} = +90$

+80

+75

+70

+60

+45

+30

$\alpha_{tpp} = 0$

-30

-90

v / v_h

V / v_h

Some Background About Airplane & Rotorcraft fe.

Equivalent Flat Plate Drag Area (sq. ft.)

Gross Weight (lbs)

Propeller Driven Early WW II Technology
Fe = 3.0 (GW / 1000)^2/3

Propeller Driven Ending In 1980
Fe = 1.4 (GW / 1000)^2/3

Propeller Driven Starting From 1914
Fe = 11 (GW / 1000)^2/3

German Bomber Gotha G-V (1917)

Ford Trimotor

C-123
B-17G B-24J

B-29 C-130 KC-135 B-52H

Super Constellation

Jet Bombers, Transports And Attack Fighters
Fe = 0.75 (GW / 1000)^2/3

DC-3

Martin B-26F

727

B-47E

737

Martin B-57A

Spirit Of St. Louis (1927)

Sopwith Camel

Cessna RG-310-II

North American F-51D

Lockheed F-104G

Jet Fighters
Fe = 0.5 (GW /1000)^2/3

Curtiss R2C-1 (Racer Of 1923)

Some Background About Airplane & Rotorcraft fe. (Continued)

Helicopter
Koren War Technology
Fe = 8.5 (GW / 1000)^2/3

Helicopter
Viet Nam War Technology
Fe = 5.0 (GW / 1000)^2/3

Helicopter
1980 Technology
Fe = 2.5 (GW / 1000)^2/3

PCA-2

YO-60
Cruise

Cierva
C.30

XV-1

Propeller Driven
Early WW II Technology
Fe = 3.0 (GW / 1000)^2/3

Propeller Driven
Ending In 1980
Fe = 1.4 (GW / 1000)^2/3

Equivalent Flat Plate Drag Area   (sq. ft.)

Gross Weight   (lbs)

100

10

1

1,000

10,000

100,000

Some Background About Airplane & Rotorcraft fe. (Continued)

$$fe = K \, (\text{Gross Weight} / 1000)^{2/3}$$

Legend:
- □ Propeller Airplanes
- ■ Helicopters

K Constant For Drag Area Equation (y-axis, 0 to 12)

Era	Propeller Airplanes	Helicopters
WW I	11.0	
WW II	3.0	
Korean War	2.0	8.5
Viet Nam War	1.6	5.0 (Hub=1.2)
Modern Era	1.4	2.5 (Hub=0.85)

Some Background About Airplane & Rotorcraft fe. (Concluded)

Some Background About Wing Lift–Drag Polars.

Wing Drag Coefficient C_{Dw}

Wing Lift Coefficient C_L

All Data Referenced To An Aspect Ratio of 5

- AR = 7
- AR = 6
- AR = 5
- AR = 4
- AR = 3
- AR = 2
- AR = 1

Ref. Data from Figure 5 in "Theory of Wing Sections" by Abbott and von Doenhoff
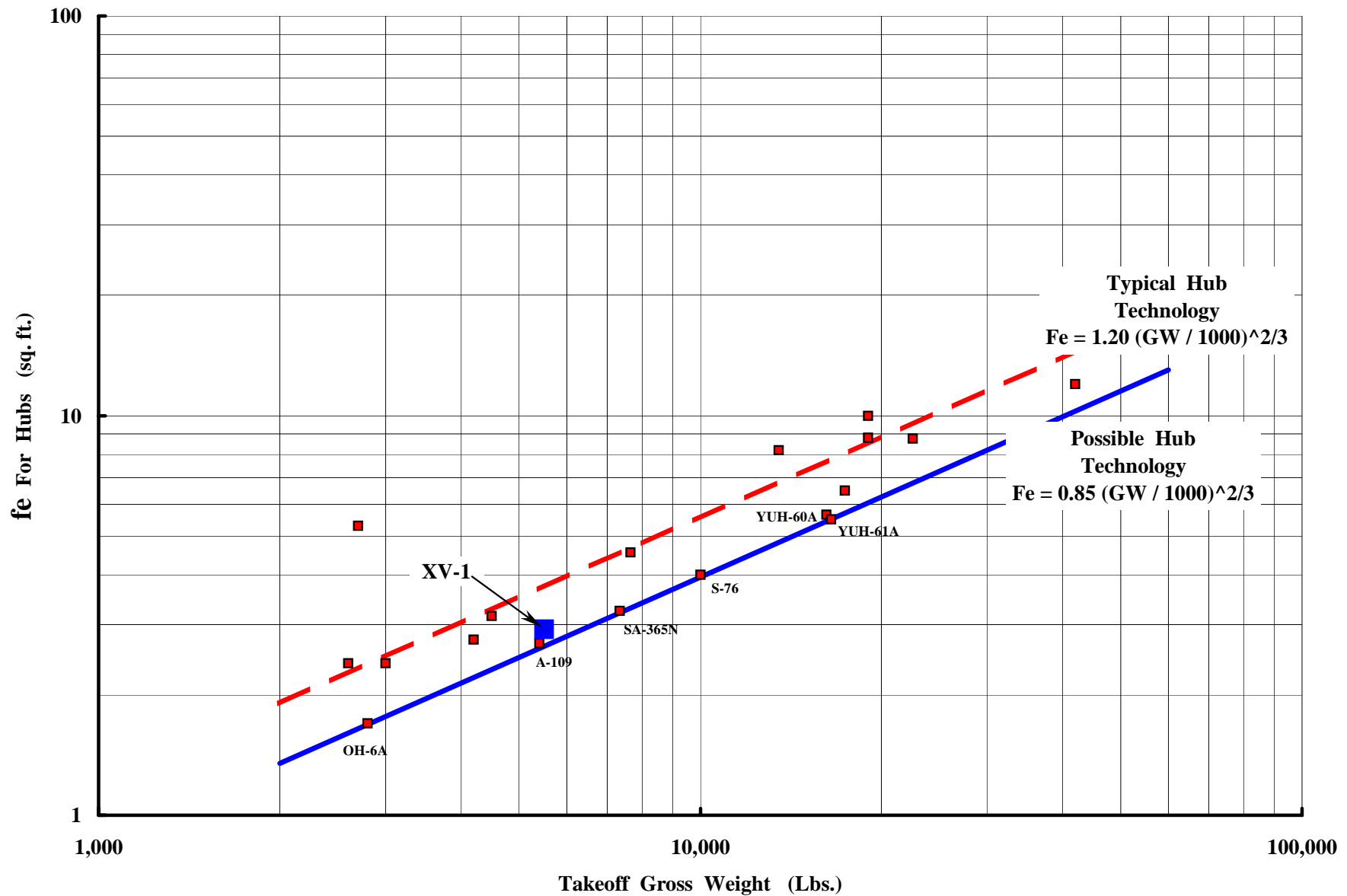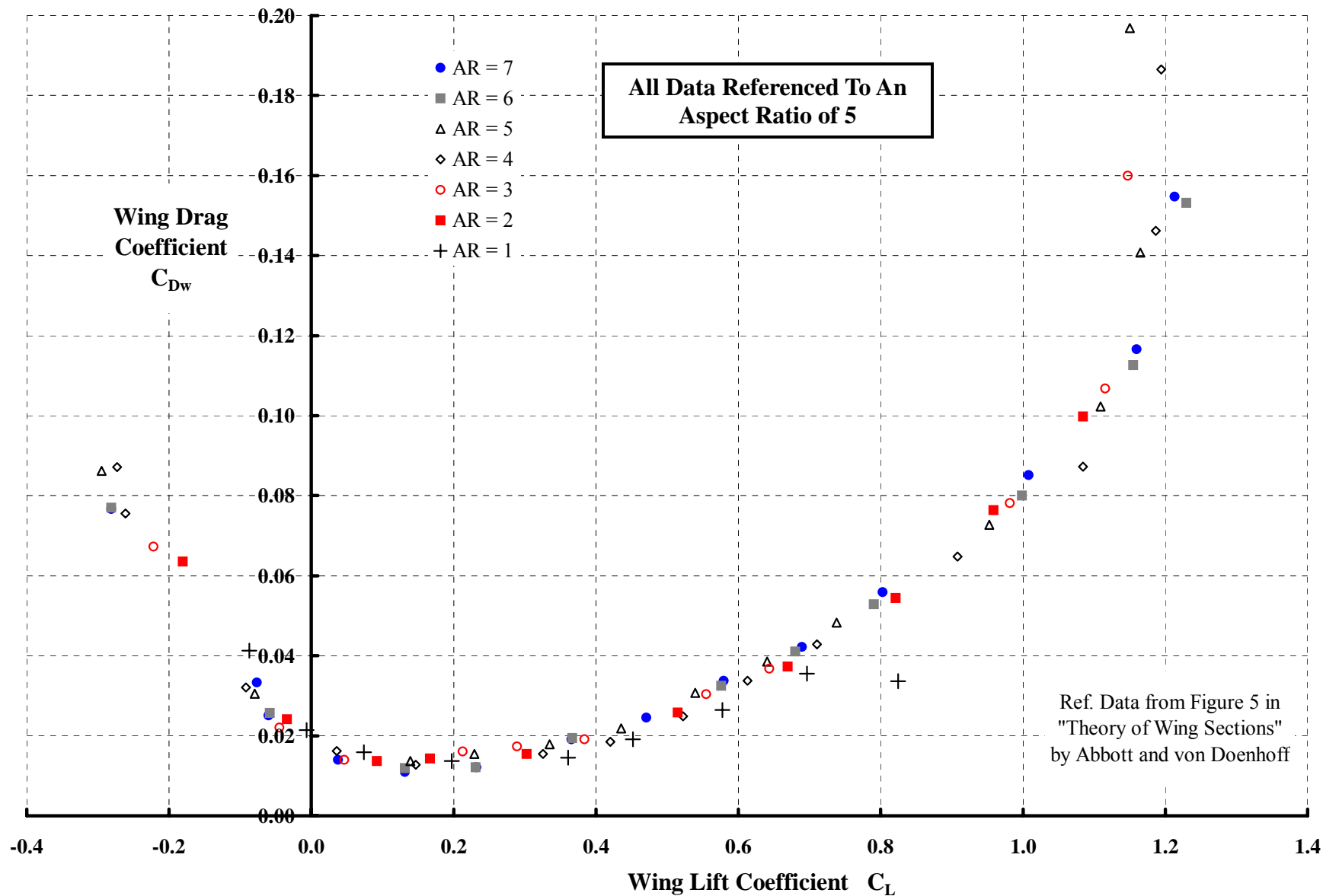
Ref: Prandtl, L., "Applications of Modern Hydrodynamics to Aeronautics." NACA Technical Report No. 116

Some Background About Wing Lift–Drag Polars (Concluded)

All Data Referenced To An Aspect Ratio of 5

Legend:
- ● AR = 7
- ■ AR = 6
- ▲ AR = 5
- ◆ AR = 4
- ○ AR = 3
- □ AR = 2
- + AR = 1

$$C_{Dw} = C_{Do} + \varepsilon\left(C_L - \mathrm{Design}\,C_L\right)^2 + \frac{C_L^2}{\pi\,AR}\left(1+\delta\right)$$

with $C_{D0} = 0.009$, $\varepsilon = 0.009$, $\mathrm{Design}\,C_L = 0.3$, $\delta = 0.055$

Ideal Induced Drag Alone

Wing Drag Coefficient C_{Dw}

Ideal Induced Drag Coefficient $(C_L^2/\pi AR)$
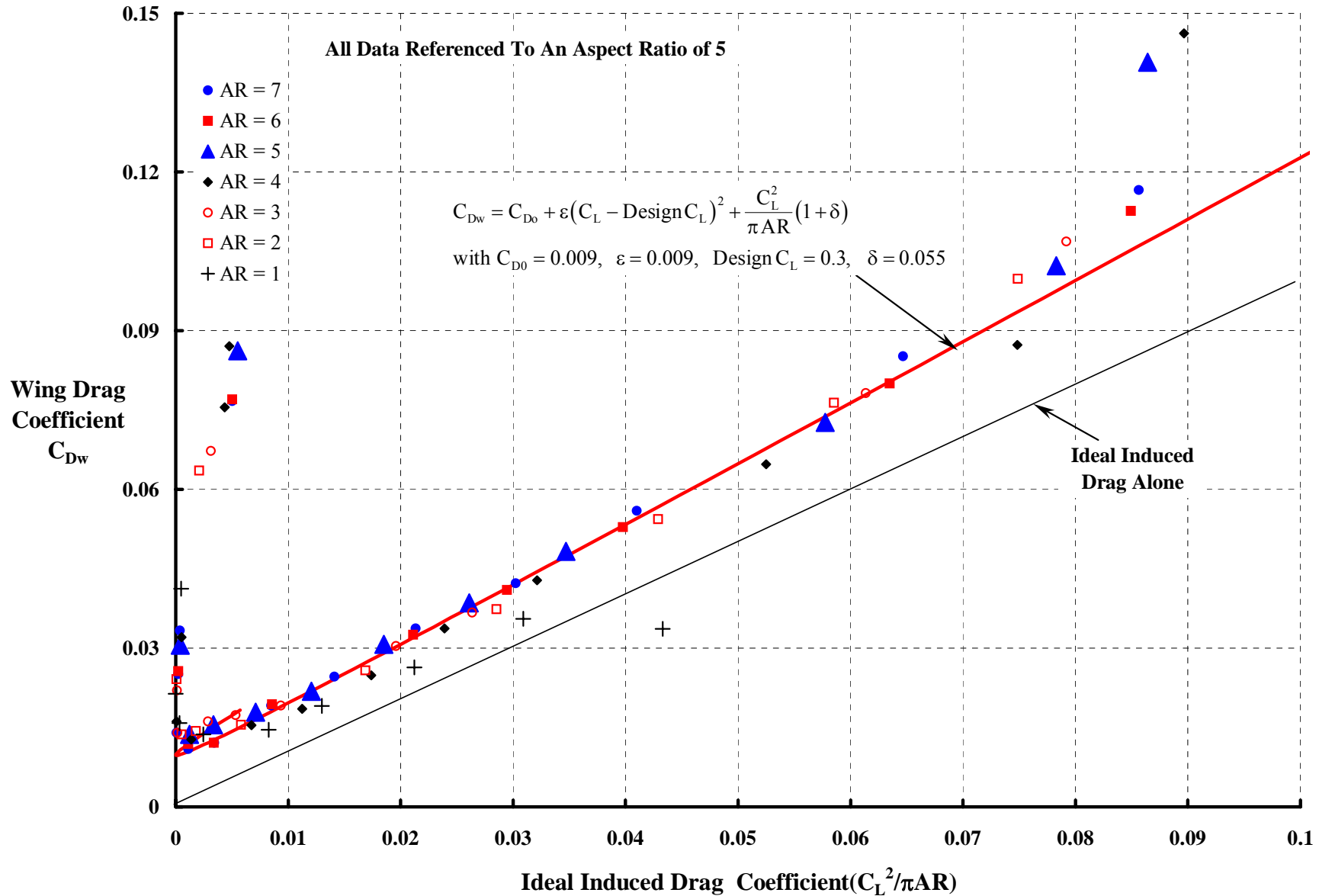
Some Background About Rotor Blade Lift–Drag Polars.
First Consider The Rotor In Autorotation With Zero Power In.

Autorotation occurs because the rotor's drag is balanced by the propulsion from some other thrusting force. Thus, if

$$0 = T_R v_i - D_R V + P_0$$

$$\text{then} \quad D_R = \frac{P_0}{V} + \frac{T_R v_i}{V} \quad \text{and} \quad \frac{D_R}{q} = \frac{P_0}{qV} + \frac{T_R v_i}{qV}$$

Now, think of the rotor blades as if they form an ideal fixed wing. For $0.15 < \mu < 1.0$ you have

$$\frac{D_R}{q} \simeq \frac{1}{qV}\left\{ \frac{\rho(b\,c_{ave}R)\,V_t^3}{8}C_{d\,ave}\left(1 + 4.65\mu^2 + 4.15\mu^4 - \mu^6\right) \right\} + \frac{T_R}{qV}\left\{ \frac{T_R/2\rho A}{V} \right\}(1+\delta)$$

which reduces to

$$\frac{D_R}{q} \simeq (b\,c_{ave}R)\,C_{d\,ave}\left(\frac{1 + 4.65\mu^2 + 4.15\mu^4 - \mu^6}{4\mu^3}\right) + \frac{1}{\pi}\left(\frac{T_R}{q\,D}\right)^2(1+\delta)$$

which compares to the fixed wing equation given earlier.

$$\frac{D_{Wing}}{q} = S_w C_{do} + S_w \varepsilon (C_L - \text{Design}\,C_L)^2 + \frac{1}{\pi}\left(\frac{L_w}{q\,b_w}\right)^2(1+\delta)$$

The Pitcairn PCA-2 Offers An Adequate Comparison Between Rotor And Wing Lift–Drag Polars.

PCA-2 Dimensions

Rotor
Diameter, 45 ft
Total Blade Area, 155 ft^2
Swept Disc Area, 1,590 ft^2
Chord, 22 in
Blade No. 4
Solidity, 0.0976
Tip Speed, 340 fps
Airfoil :Gott. 429

Wing
Span, 30.3 ft
Area, 101 sq. ft
Airfoil : Mod of NACA M3

Propeller (?)
D $\approx$ 10.5 ft   c $\approx$ 6 in
$\sigma \approx 0.061$ $V_t \approx 700$ fps

Additional Data
GW, 2,940 lbs
WE, 2,050 lbs
ESHP, 300 hp
Speed Range, 20 to 118 mph
Fuel, 52 US gal

PRODUCTION VERSION
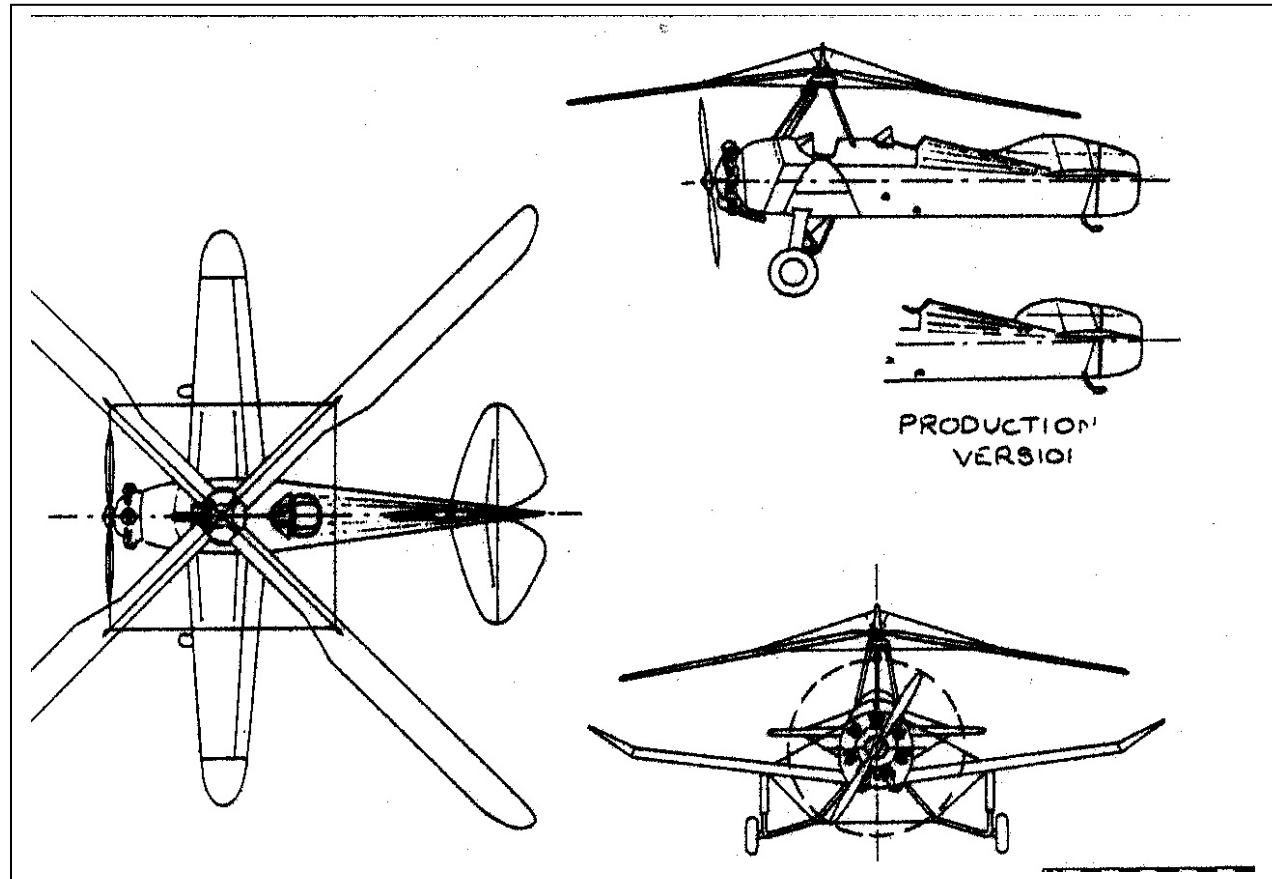
Rotor D_R/q At Zero Lift Decreases With Advance Ratio.
Wing and Fuselage D/q Do Not Depend On μ (PCA–2 Example).

Equivalent Parasite Drag Area at Zero Lift

$f_e = D/q$

sq. ft.

PCA-2 Fuselage (All but wing & blades) = 17.56 ft^2

$$\frac{D_R}{q} \simeq \left(b\, c_{ave}\, R\right) C_{dave} \left(\frac{1 + 4.65\,\mu^2 + 4.15\,\mu^4 - \mu^6}{4\,\mu^3}\right)$$

versus

$$\frac{D_W}{q} = S_w C_{do}$$

PCA-2 Rotor =2.9 ft^2 at μ = 1.0 (bcR = 155 ft^2, Cdo = 0.0085)

120 mph
@ 340 fps
q = 37 lbs/ft^2

PCA-2 Wing = 0.86 ft^2 (Sw = 101 ft^2, Cdo = 0.0085)

Advance Ratio V/Vt
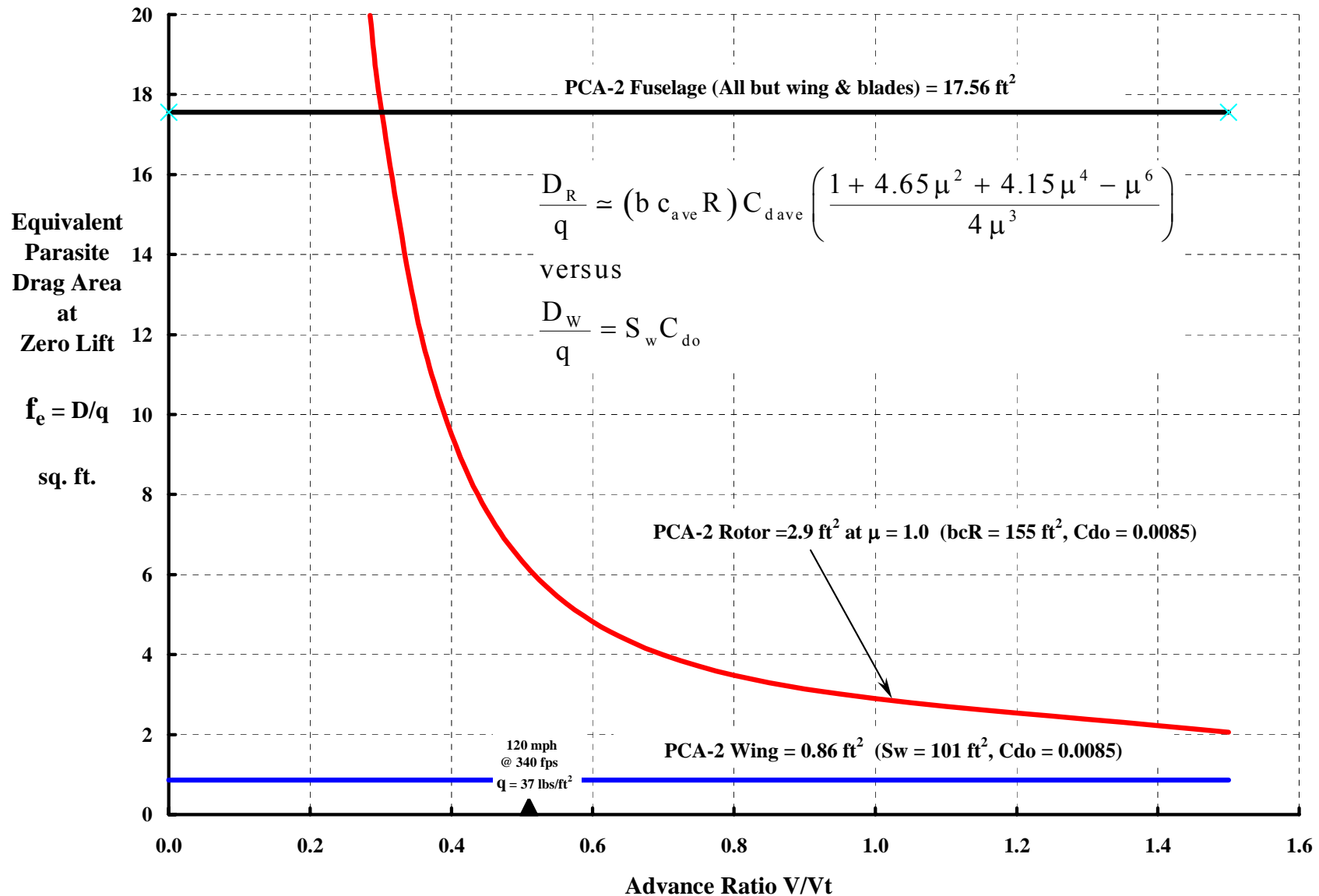
The Induced Drag Situation Looks Like This
IF The Span Loadings Are Elliptical.

Equivalent Parasite Drag Area Due To Lift

$(D/q)_{Induced}$

sq. ft.

PCA-2 Wing Carries All The Weight (2,940 lbs)
V = 120 mph
q = 37 lbs/ft^2
b$_w$ = 30.3 ft

PCA-2 Rotor Carries All The Weight (2,940 lbs)
V = 120 mph
Vt = 340 fps
μ = 0.51
q = 37 lbs/ft^2
D = 45 ft

$$\text{Ideal}\left(\frac{D}{q}\right)_{Induced} = \frac{1}{\pi}\left(\frac{\text{Span Loading}}{q}\right)^2 (1+0)$$

Span Loading/q   (L$_w$/q b$_w$ OR   T$_R$/q D)
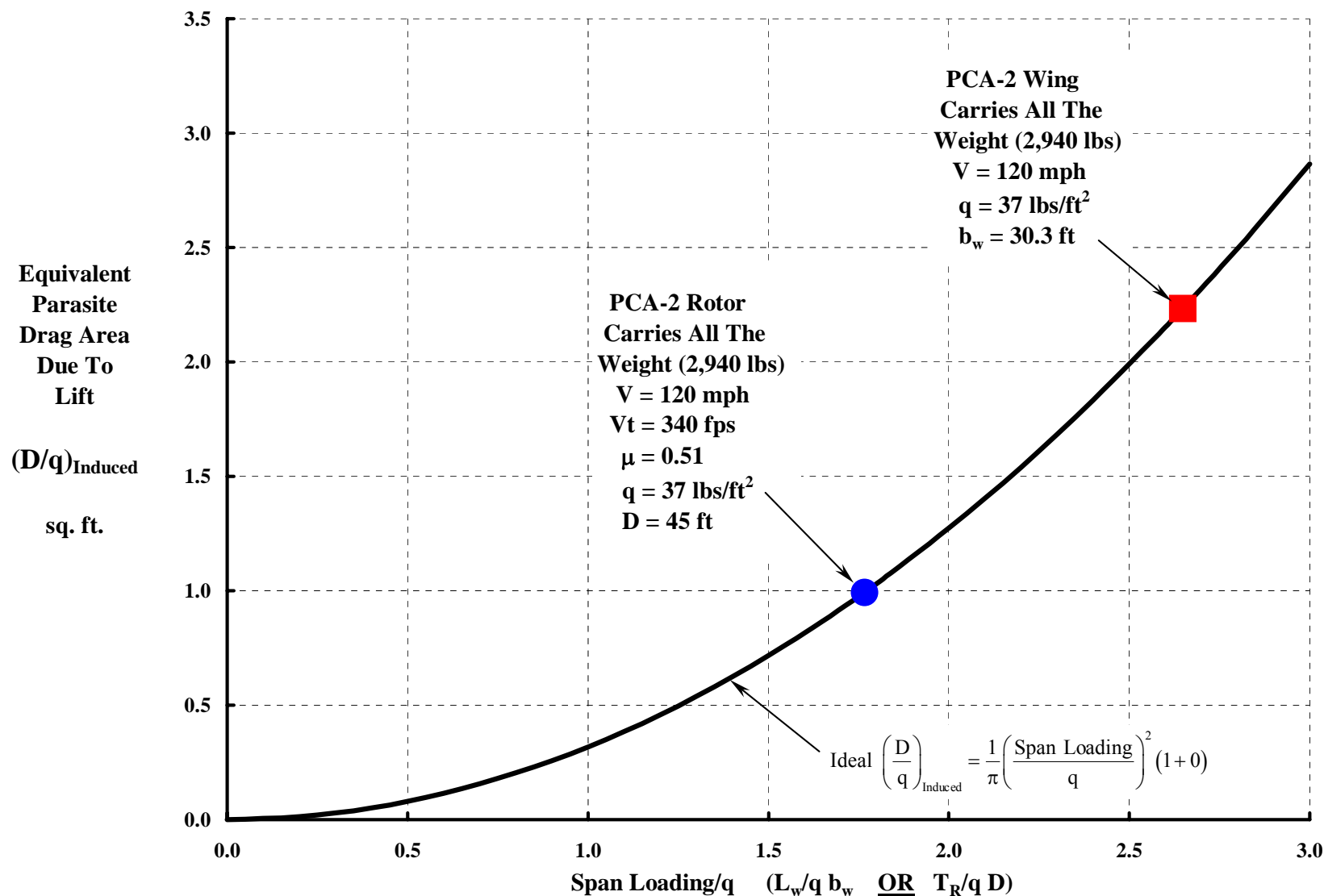
BUT–The Rotor's Span Loading Is Far From Elliptical (δ = 2 to 8), Versus Even A Terrible Wing, Which Has $\delta < 0.10$.

Rotor Non-elliptical Loading
Ref. 1. Prouty, R.W., "Helicopter Performance, Stability,
and Control" PWS Engineering, Boston, 1986 (Pgs. 125-129)
Ref. 2. Harris, F.D., "Rotary Wing Aerodynamics-Histoprical Perspective
and Important Issues, AHS Southwest Region, Feb. 1987 (Pgs. 51-53)

Equivalent Parasite Drag Area Due To Lift

$(D/q)_{Induced}$

sq. ft.

PCA-2 Rotor Carries All The Weight (2,940 lbs)
V = 120 mph
Vt = 340 fps
μ = 0.51
q = 37 lbs/ft^2
D = 45 ft

δ = 2.00
δ = 0.50
δ = 0.25

PCA-2 Wing Carries All The Weight (2,940 lbs)
V = 120 mph
q = 37 lbs/ft^2
b_w = 30.3 ft
δ = .075

Ideal $\left(\dfrac{D}{q}\right)_{Induced} = \dfrac{1}{\pi}\left(\dfrac{\text{Span Loading}}{q}\right)^2 (1+0)$

Span Loading/q ($L_w/q\, b_w$ **OR** $T_R/q\, D$)

Calculations With Free Wake Show Just How Poor Glauert's Ideal Wing Approximation Is For Induced Power At High Advance Ratio.

S-76 Rotor Geometry
Input To CAMRAD II
Diameter = 44 ft.
Blades = 4
Solidity = 0.07476
Twist = -10 deg
Analysis Run With:
  1.) Collect = 1 deg. at 3/4 R
  2.) Tip Path Plane Trimmed
     Normal To Shaft With Cyclic.
  3.) Shaft Angle Swept Nose Up From Zero.
  4.) Tip Speed = 670 fps
  5.) SL Std. Density & Temperature

Rotor Lift Coefficient C_L

Rotor Induced Power Coefficient C_{Pi}

Glauert
$C_L = 0.004$
$C_L = 0.002$

$$C_L = \frac{\text{Rotor Lift}}{\rho\,\pi R^2 V_t^2}$$

$$C_{Pi} = \frac{\text{Induced Power}}{\rho\,\pi R^2 V_t^3}$$

$$\text{Glauert's } P_i = Tv_i \approx T\frac{T}{2\rho\pi R^2 V}$$

$$\text{Or } C_{Pi} \approx \frac{C_L^2}{2\mu}$$

Advance Ratio, V/V_t

Rotors With Twisted Blades Have Significant Induced Power Even At Low Thrust.

Ref.: 1987 Result, Figure 39 of "Rotary Wing Aerodynamics–Historical Perspective and Important Issues", F.D. Harris Paper Given at AHS Southwest Region Specialists' Meeting on Aerodynamics and Aeroacoustics, Feb. 25-27, 1987. (Chairman: Tom Wood of Bell Helicopter)
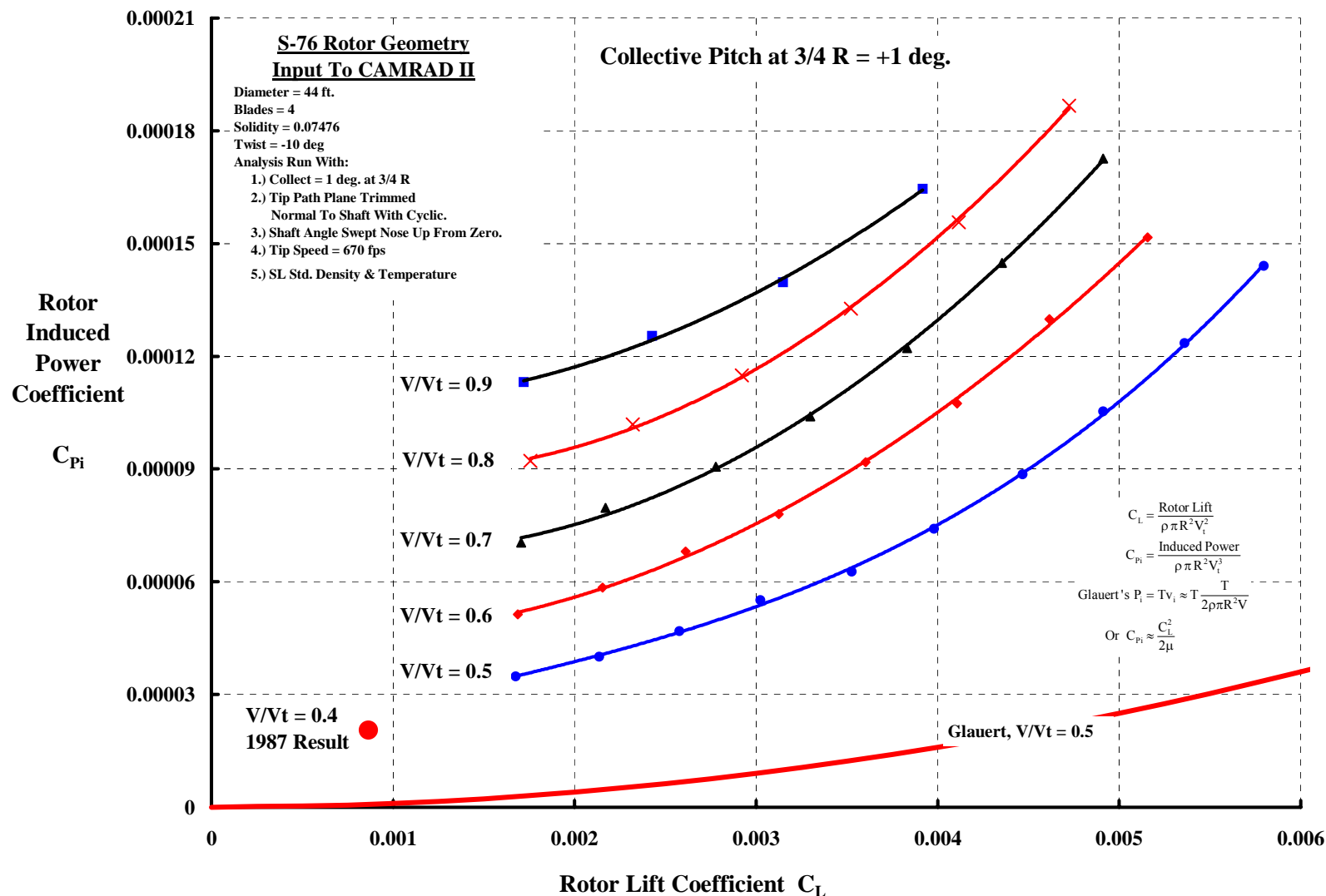
Twisted Blades, Operating At Low Thrust And Zero Tip Path Plane Angle Of Attack, Have Significant Induced Power Losses On The Advancing Side Of The Disc–Even At Low Thrust.

Ref.: 1987 Results, Figure 39. $\mu = 0.4$, $C_T = 0.000865$ S–76 Rotor
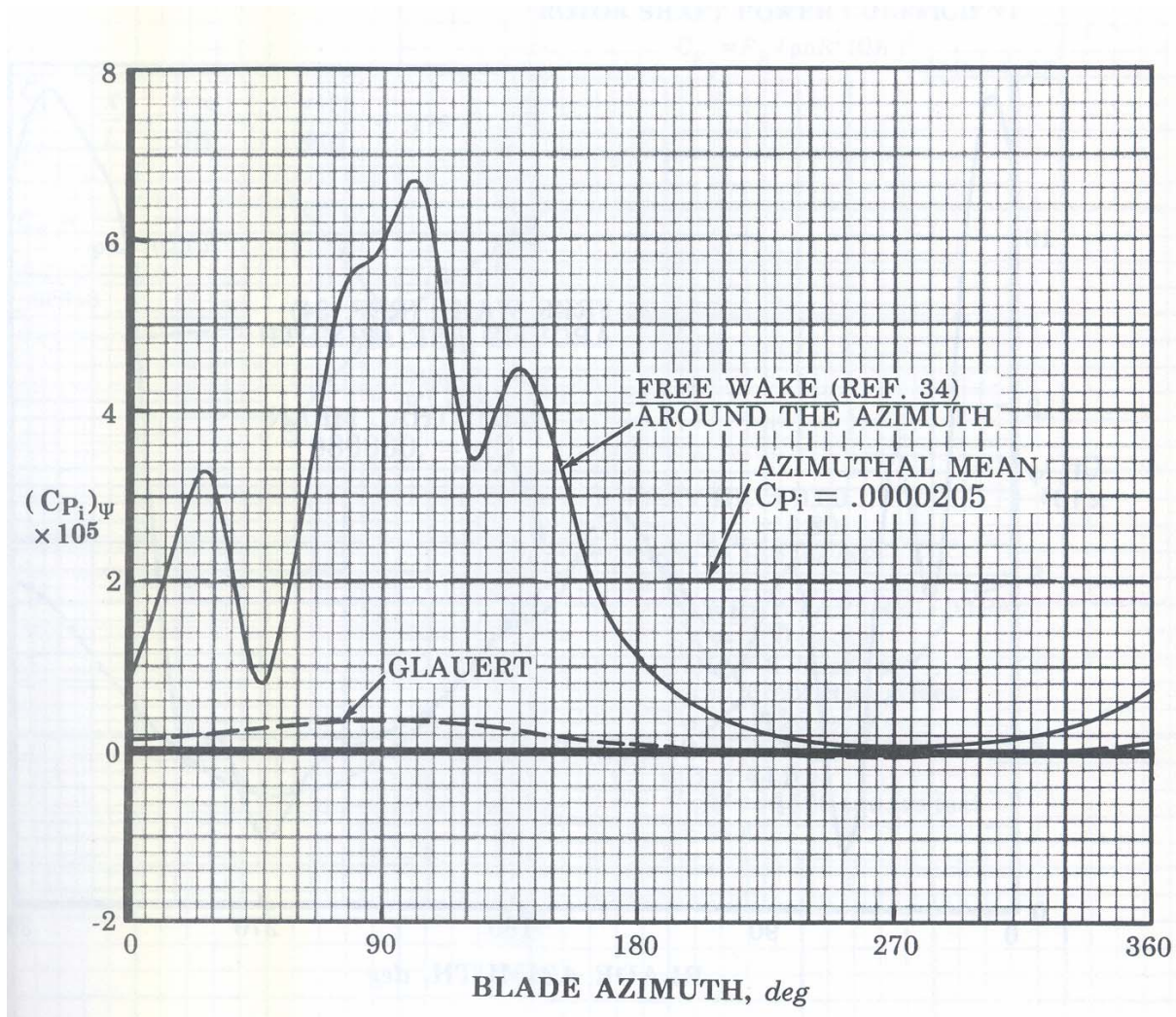
At High C_T And $\alpha_{tpp} = 0$, The Aft Portion Of The Disc Contributes Enormous Induced Power Losses.

Ref.: 1987 Results, Figure 40 $\mu = 0.4$, $C_T = 0.006$. S–76 Rotor
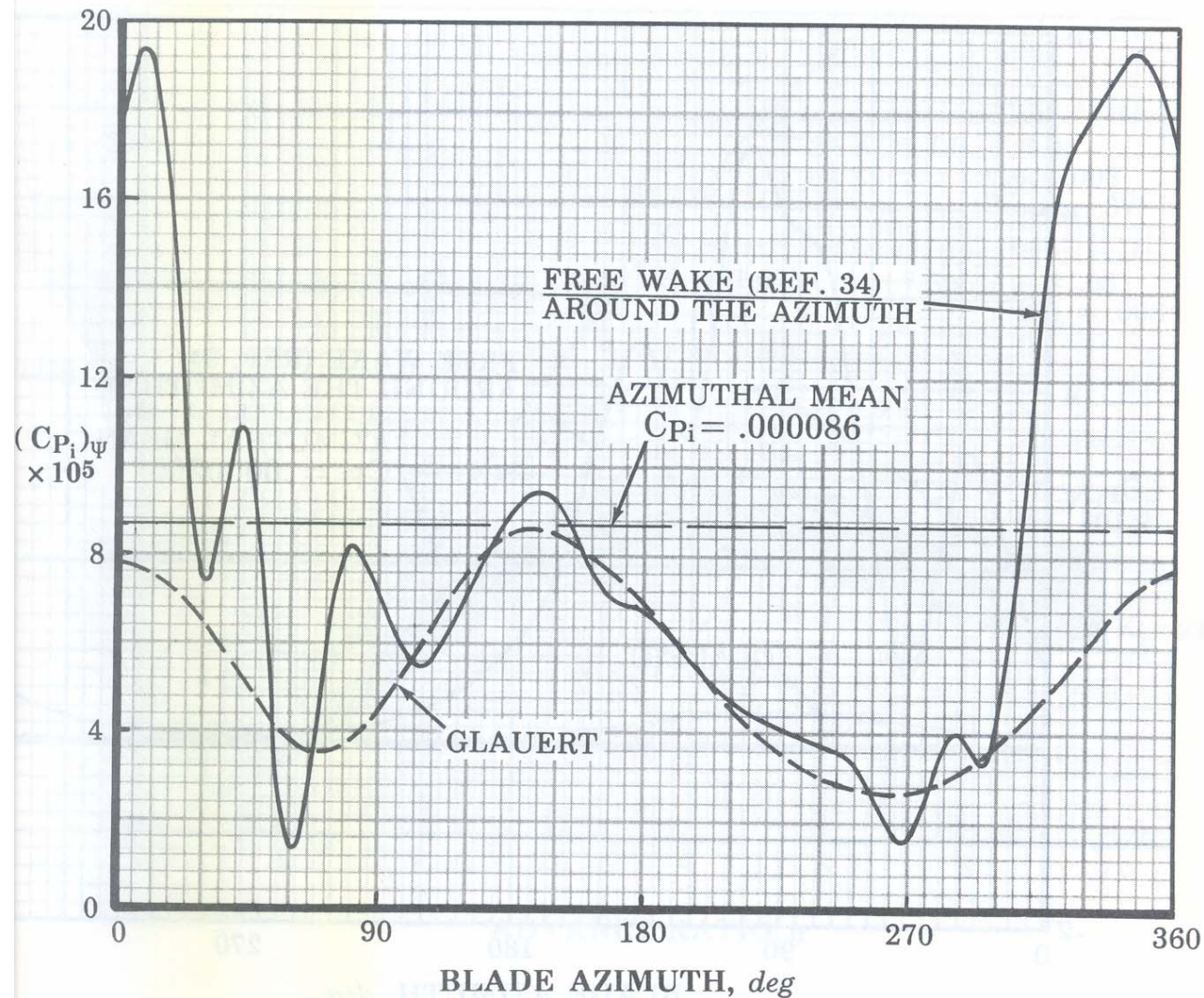
Twisted Rotary Wings Have Induced Drag At Zero Lift And A "Sorta" Parabolic Drag Polar.

S-76 Rotor Geometry Input To CAMRAD II

Diameter = 44 ft.
Blades = 4
Solidity = 0.07476
Twist = -10 deg
Analysis Run With:
1.) Collective = 1 deg. at 3/4 R
2.) Tip Path Plane Trimmed Normal To Shaft With Cyclic.
3.) Shaft Angle Swept Nose Up From Zero.
4.) Tip Speed = 670 fps
5.) SL Std. Density & Temperature

Collective Pitch at 3/4 R = +1 deg.
Blade Twist = -10 deg.

$$\frac{D_{Rotor}}{q} = \left(\frac{D}{q}\right)_{Min} + \frac{1}{\pi}\left(\frac{L_{Rotor}}{qD}\right)^2(1+2.5)$$

$$\frac{D_{Rotor}}{q} = \frac{1}{\pi}\left(\frac{L_{Rotor}}{qD}\right)^2$$

Rotor Induced Drag D/q sq. ft.

Rotor Span Loading, L/qD sq. ft. per foot

Reducing Twist From –10⁰ To 0⁰ Saves Roughly 0.5 sq. ft. Of Drag.

S-76 Rotor Geometry
Input To CAMRAD II

Diameter = 44 ft.
Blades = 4
Solidity = 0.07476
Twist = 0 deg
Analysis Run With:
  1.) Collective = 2 deg. at 3/4 R
  2.) Tip Path Plane Trimmed
     Normal To Shaft With Cyclic.
  3.) Shaft Angle Swept Nose Up From Zero.
  4.) Tip Speed = 670 fps
  5.) SL Std. Density & Temperature

Collective Pitch at 3/4 R = +2 deg.
Blade Twist = 0 deg.

Rotor
Induced
Drag

D/q

sq. ft.

V/Vt = 0.5

V/Vt = 0.6

V/Vt = 0.7

V/Vt = 0.8

V/Vt = 0.9

V/Vt =
1.0, 1.1, 1.2

$$\frac{D_{Rotor}}{q} = \frac{1}{\pi}\left(\frac{L_{Rotor}}{q\,D}\right)^2$$

Rotor Span Loading, **L/qD**   sq. ft. per foot

0   0.2   0.4   0.6   0.8   1   1.2   1.4   1.6

2   1.5   1   0.5   0

Both Wing And Rotor Have Maximum Practical Lift Limits.

For The Rotor

$$\text{Operating } C_T = \frac{D\mu^2}{2A}\left(\frac{T_R}{qD}\right)$$

$$\left(\frac{C_T}{\sigma}\right)_{\substack{\text{Blade}\\\text{Stall}\\\text{Onset}}} = \frac{C\ell_{max}}{6}\left[\frac{1-\mu^2+9\mu^4/4}{1+8\mu/3+3\mu^2/2}\right] + \frac{\alpha_{tpp}^{deg}}{120}\left[\frac{\mu+\mu^2-2\mu^3-3\mu^4}{1+5\mu/3+\mu^2/3}\right]$$

$$\text{Therefore } \left(\frac{T_R}{qD}\right)_{\substack{\text{Blade}\\\text{Stall}\\\text{Onset}}} = \frac{2A\sigma}{D\mu^2}\left(\frac{C_T}{\sigma}\right)_{\substack{\text{Blade}\\\text{Stall}\\\text{Onset}}}$$

For The Wing

$$\text{Operating } C_L = \frac{b_w}{S_w}\left(\frac{L_w}{qb_w}\right)$$

$$\left(C_L\right)_{\substack{\text{Stall}\\\text{Onset}}} = f(\alpha, RN, M, \text{etc.})$$

$$\text{Therefore } \left(\frac{L_w}{qb_w}\right)_{\substack{\text{Stall}\\\text{Onset}}} = \frac{S_w}{b_w}\left(C_L\right)_{\substack{\text{Stall}\\\text{Onset}}}$$

In The PCA-2 Example At 120 mph, If The Rotor Carries All The Weight, $C_T/\sigma = 0.0666$ (at $V_t = 340$ fps) And If The Wing Carries All The Weight, $C_L = 0.795$ (at SL, Std.)

Now, Some Background About Propellers.

(1) Any Power Above $(T{\times}V + T{\times}v_{ideal})$ Is A Loss – Period!
(2) I Do Not Like Using Propeller Efficiency (η_P) At All.
(3) I Much Prefer George Schairer's Non–dimensional Form.

$$P_{Prop} = Profile\,(P_0) + Induced\,(T_P v_i) + Propulsive\,(T_P V)$$

Schairer's Form

$$\frac{P_{Prop}}{qV\,D^2} = \frac{P_0}{qV\,D^2} + \frac{T_P}{q\,D^2}\frac{v_i}{V} + \frac{T_P}{q\,D^2}$$

$$\text{where}\quad \frac{v_i}{V} = \frac{1}{2}\left[\sqrt{1 + \frac{4}{\pi}\left(\frac{T}{qD^2}\right)} - 1\right] \approx \frac{1}{\pi}\left(\frac{T_P}{q\,D^2}\right) - \frac{1}{\pi^2}\left(\frac{T_P}{q\,D^2}\right)^2 + \frac{2}{\pi^3}\left(\frac{T_P}{q\,D^2}\right)^3 \cdots \text{ for } \frac{T_P}{q\,D^2} < \frac{\pi}{4}$$

Therefore

$$\frac{P_{Prop}}{qV\,D^2} \simeq \frac{P_0}{qV\,D^2} + \frac{T_P}{q\,D^2}\left[1 + \frac{1}{\pi}\left(\frac{T_P}{q\,D^2}\right)\right] \qquad\qquad \text{for } \frac{T_P}{q\,D^2} \ll \frac{\pi}{4}$$

Ref. 2. Harris, F.D., "Performance Analysis of Two Early NACA High Speed Propellers With Application to Civil Tiltrotor Configurations", NASA Contractor Report 196702, August 1996

Here's A Darn Good Low Speed Propeller.

Tunnel Speed 152 knots

**Propeller
Efficiency**

$$\eta_P = \frac{TV}{P_{actual}}$$

Ref. NACA TR 999
NACA 4-(5)(08)-03
2 Blades of Duralumin
NACA 16 Series Cambered Airfoils
Diameter = 4.00 ft
Variable Chord
Nominal Solidity = 0.07
Variable t/c = 0.137 to 0.0114
Twist = -32.8 deg (Non linear)

Legend:
- Beta @ 3/4R = 20 deg.
- Beta @ 3/4R = 25 deg.
- Beta @ 3/4R = 30 deg.
- Beta @ 3/4R = 35 deg.
- Beta @ 3/4R = 45 deg.

X-axis: **Propeller Tip Speed (fps)** — 0, 200, 400, 600, 800, 1,000, 1,200, 1,400

Y-axis: 0.60, 0.65, 0.70, 0.75, 0.80, 0.85, 0.90, 0.95, 1.00

Here's A Very Good Variable Pitch Propeller Designed For High Speed.

Propeller Efficiency

$$\eta_P = \frac{TV}{P_{actual}}$$

Legend:
- Beta @ 3/4R = 50.8 deg
- Beta @ 3/4R = 54.7 deg
- Beta @ 3/4R = 60.2 deg

Tunnel Speed 397 kts

Tunnel Speed 588 kts

Ref. NACA TR 1375
Curtiss-Wright Corp. No. 109622
3 Blades of Solid 6415 Steel
NACA 16 Series Symmetrical Airfoils
Diameter = 9.75 ft
Constant Chord = 1.17 ft
Solidity = 0.2292
t/c = 0.06 to 0.02
Twist = -31 deg (Non linear)

Tip Speed   (fps)
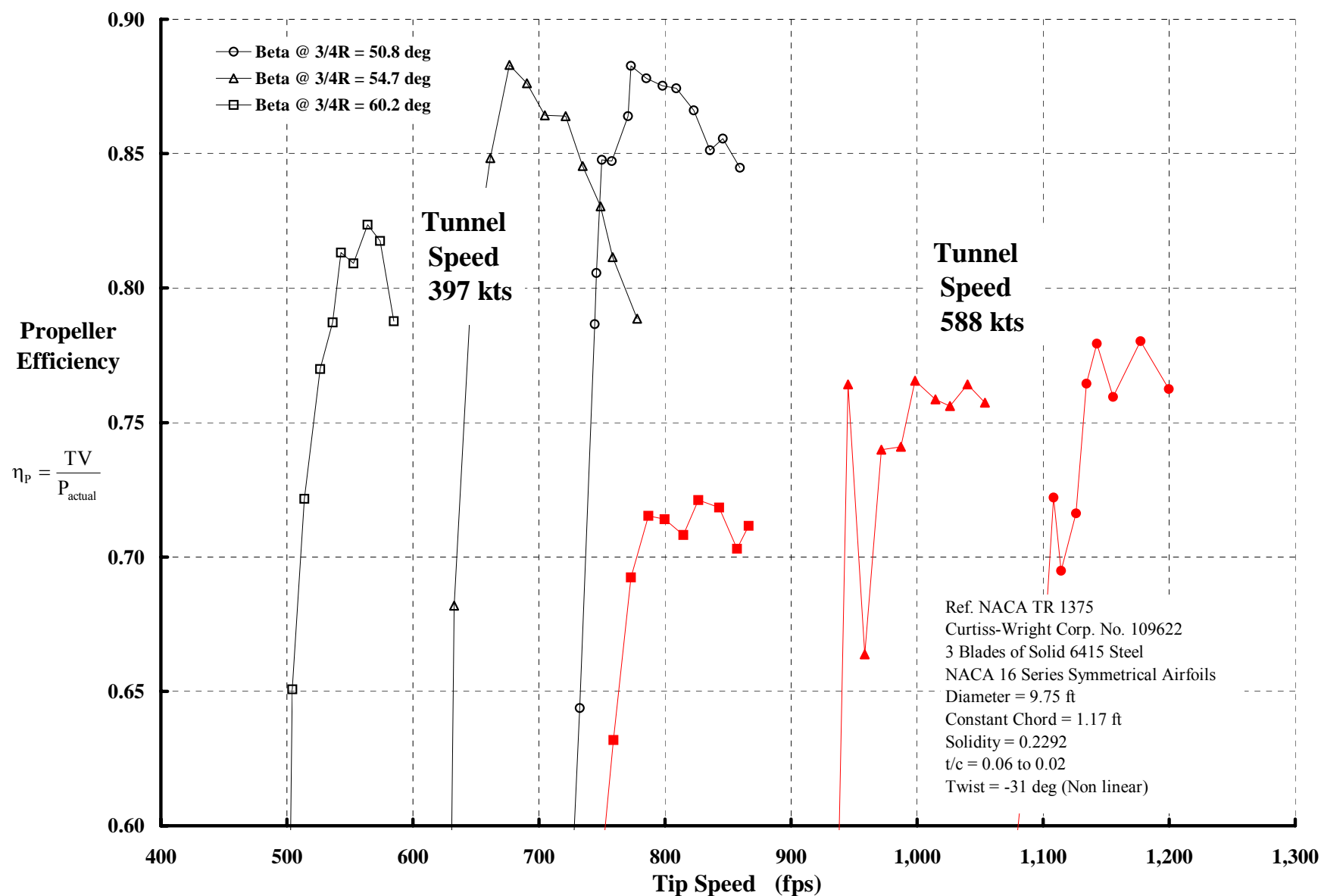
And It Performs Well Over A Wide Speed Range.

Tip Speed 811 fps

- Beta @ 3/4R = 20.2 deg
- Beta @ 3/4R = 25.2 deg
- Beta @ 3/4R = 30.2 deg
- Beta @ 3/4R = 35.2 deg
- Beta @ 3/4R = 40.2 deg
- Beta @ 3/4R = 45.4 deg
- Beta @ 3/4R = 50.8 deg

Propeller
Efficiency

$$\eta_P = \frac{TV}{P_{actual}}$$

Ref. NACA TR 1375
Curtiss-Wright Corp. No. 109622
3 Blades of Solid 6415 Steel
NACA 16 Series Symmetrical Airfoils
Diameter = 9.75 ft
Constant Chord = 1.17 ft
Solidity = 0.2292
t/c = 0.06 to 0.02
Twist = -31 deg (Non linear)

Tunnel Speed   (knots)

Max. Efficiency Points In Schairer's Non–dimensional Form.

A Simple, Empirical Equation That Captures
A Variable Pitch Propeller's Performance.
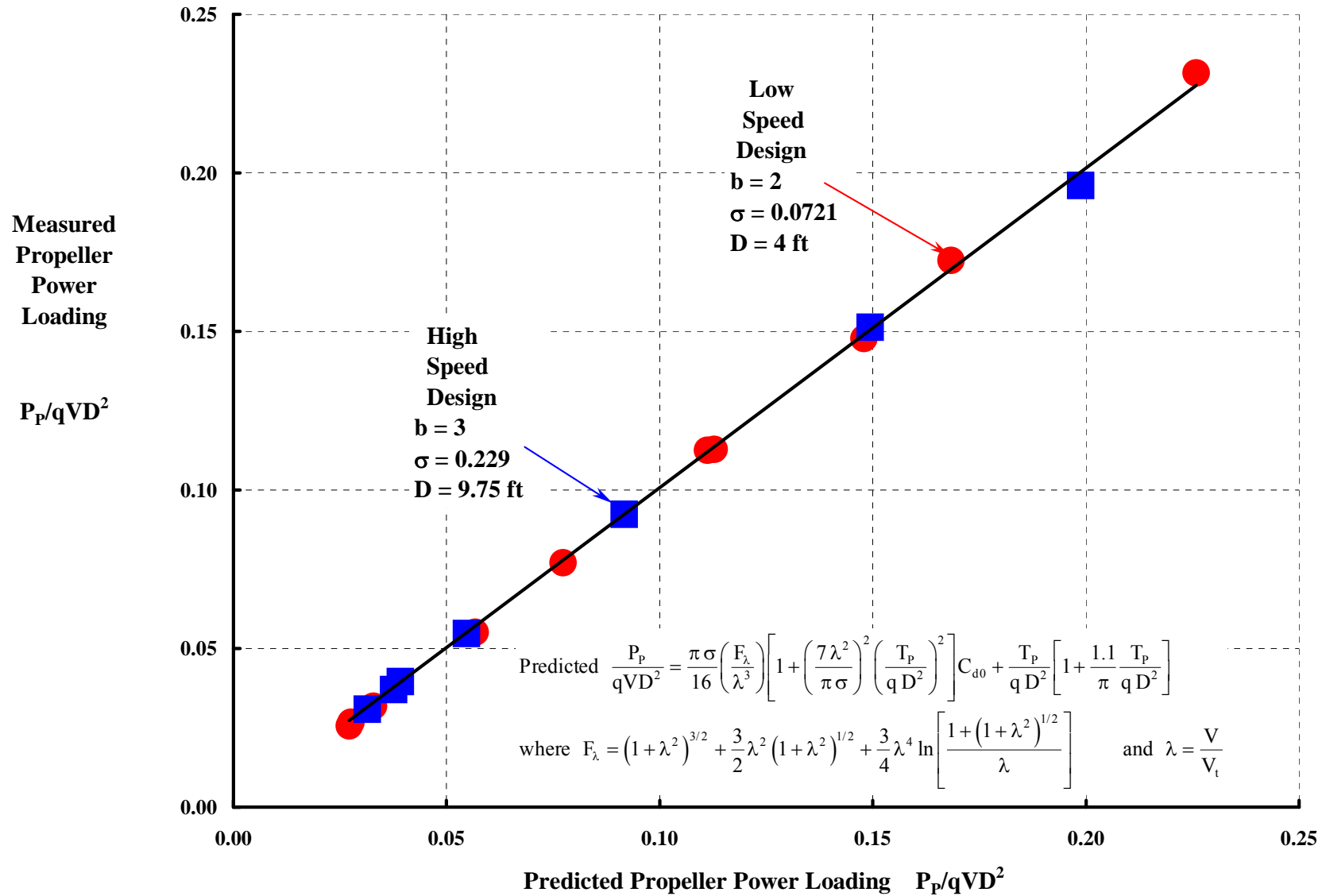
Measured Propeller Power Loading

P_P/qVD^2

Low Speed Design
b = 2
σ = 0.0721
D = 4 ft

High Speed Design
b = 3
σ = 0.229
D = 9.75 ft

Predicted $\dfrac{P_P}{qVD^2} = \dfrac{\pi\,\sigma}{16}\left(\dfrac{F_\lambda}{\lambda^3}\right)\left[1+\left(\dfrac{7\lambda^2}{\pi\,\sigma}\right)^2\left(\dfrac{T_P}{q\,D^2}\right)^2\right]C_{d0}+\dfrac{T_P}{q\,D^2}\left[1+\dfrac{1.1}{\pi}\dfrac{T_P}{q\,D^2}\right]$

where $F_\lambda = \left(1+\lambda^2\right)^{3/2}+\dfrac{3}{2}\lambda^2\left(1+\lambda^2\right)^{1/2}+\dfrac{3}{4}\lambda^4\ln\left[\dfrac{1+\left(1+\lambda^2\right)^{1/2}}{\lambda}\right]$ and $\lambda = \dfrac{V}{V_t}$

Predicted Propeller Power Loading P_P/qVD^2

LET'S REVISIT AUTOGYROS

First Some History

Cierva, Pitcairn, and Kellett Era (1919 to 1941)
Selection of the Helicopter (1942)
Legacy

Some Technology Aspects

What's in a Name?
Fuselages, Wings, Propellers, Rotors and Trim
→ Rotor Thrust and Flapping Behavior at High Advance Ratio
Limits to Rotor Lift and Propulsion
To Review Then

XV–1 Re–examined

Full Scale Wind Tunnel Test in 40 by 80
Rotor (With & Without Wing)
Complete Aircraft
Rotor Stability In Forward Flight
Phase II Flight Evaluation

Concluding Remarks

Larry Jenkins Uncovered The Rotor's Unique Behavior At μ's Up To 1.45 With A 2–Bladed, 15.25–ft Diameter, Teetering Rotor In 1964.
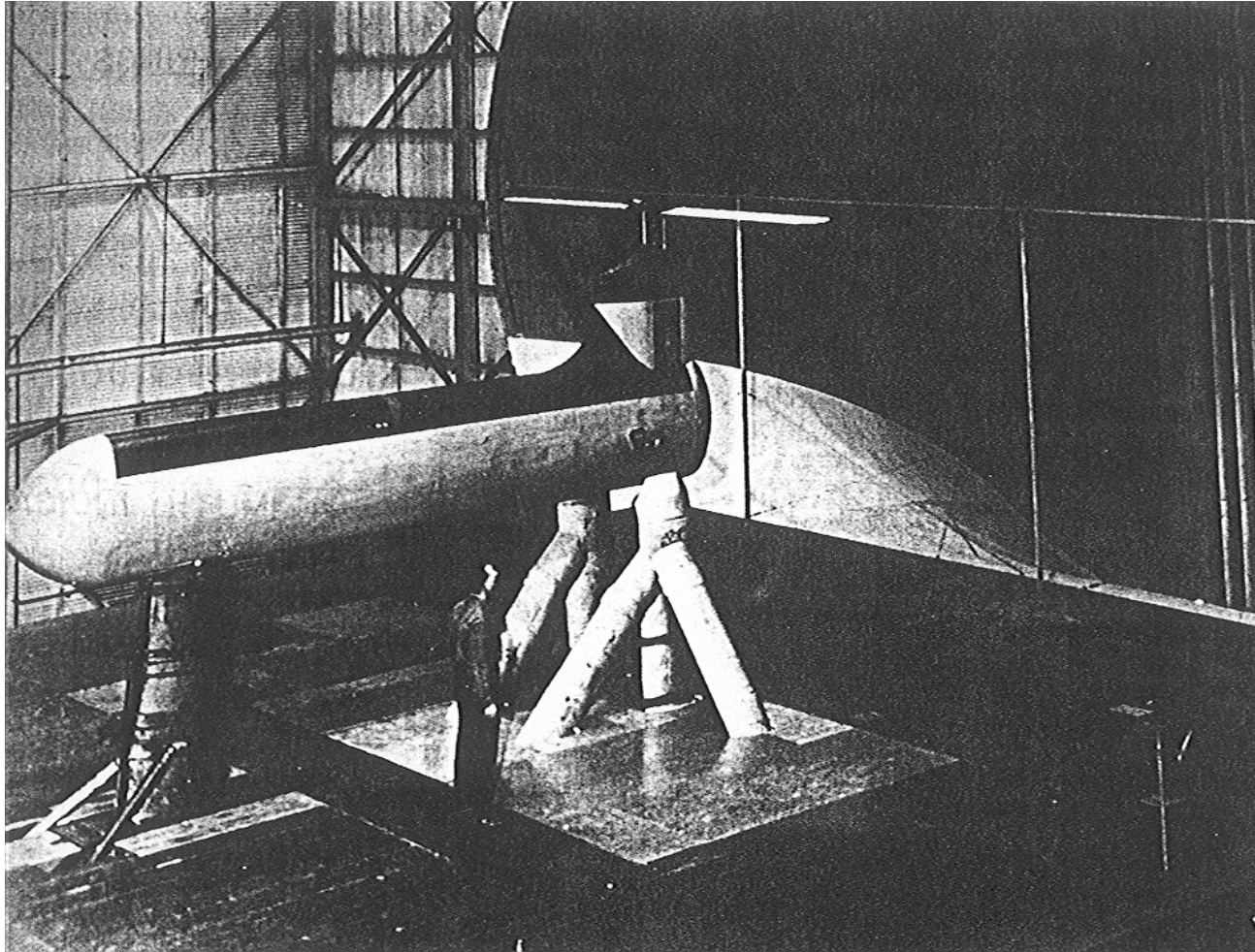
D = 15.25 ft
b = 2
c = 1.16 ft
σ = 0.097
γ = 5.05
rc = 0.16R
Zero twist
NACA 0012
Vt = 110 fps
Rotor trimmed
normal to shaft

Ref. Jenkins, J.L., "Wind Tunnel Investigation of a Lifting Rotor Operating at Tip–Speed Ratios from 0.65 to 1.45," NASA TN D–2628, Feb. 1965. (See also NASA TN D–2462 and NASA TN D–2655 by Jenkins)

Ref. McCloud, J.L., Biggers, J.C. and Stroub, R.H. "An Investigation of Full–Scale Helicopter Rotors at High Advance Ratios and Advancing Tip Mach Numbers." NASA TN D–4632, July 1968

Jenkins Found That Thrust Diminished With Collective Increase For $\mu > 1$.

He Was, However, Always Able To Trim The Rotor To A Specific α_{tpp}
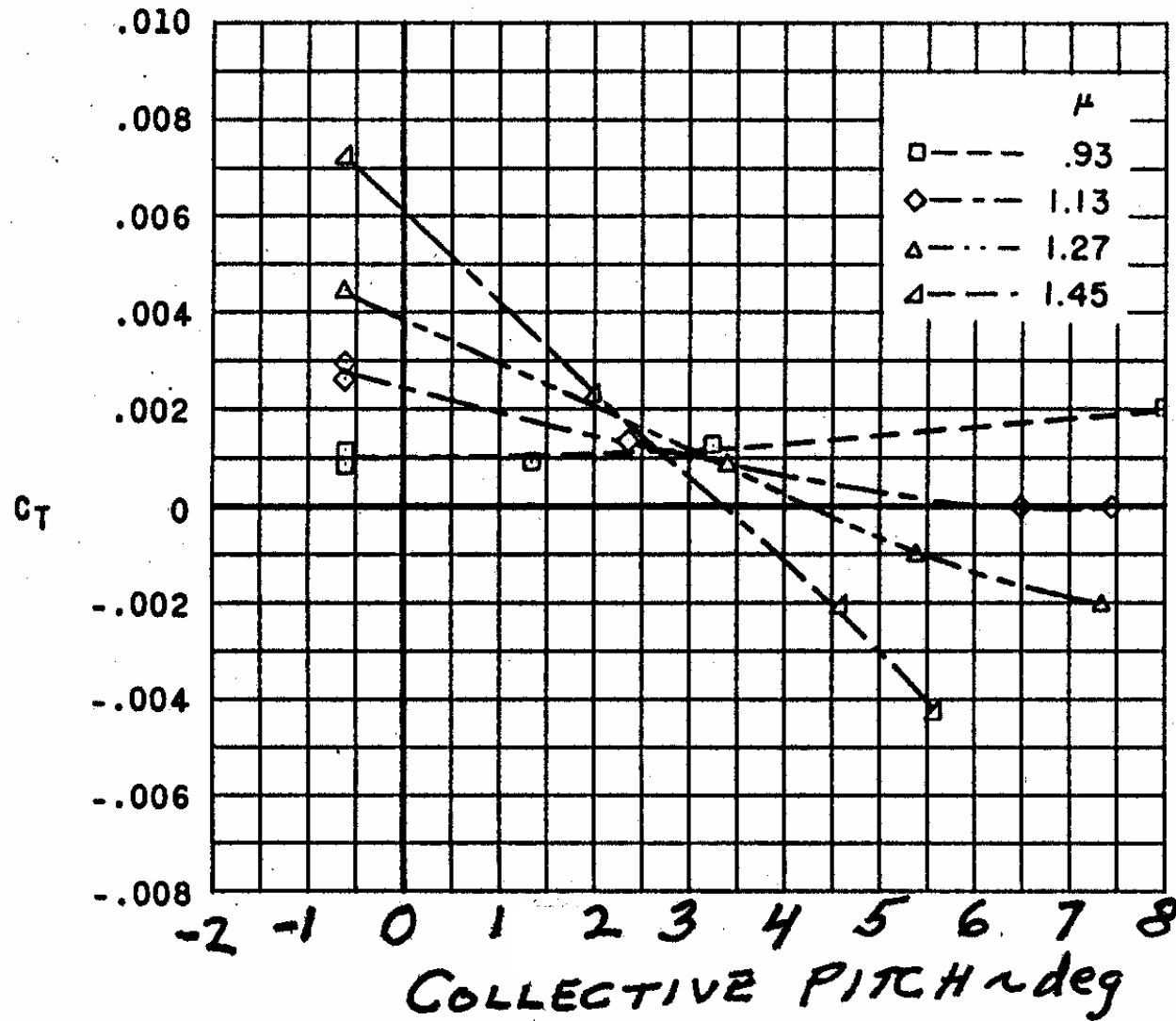
Ref. Jenkins, NASA TN D–2628, Figure 4, page 13.

$\alpha_{tpp} = 0.5$ deg

This Rotor Behavior At High μ Depends On Only Two Equations.

$$\frac{2C_T}{\sigma a} = \frac{1}{2\pi}\int_0^{2\pi}\int_{x_c}^1 \left(\alpha\, U_T^2\right)dx\, d\psi = \theta_0\left(T_{\theta o}\right) + \theta_t\left(T_{\theta t}\right) + \lambda_{tpp}\left(T_{\lambda tpp}\right) - \left(B_{1C} + a_{1S}\right)\left(T_{B1C}\right)$$

$$\frac{2C_{Roll}}{\sigma a} = \frac{-1}{2\pi}\int_0^{2\pi}\int_{x_c}^1 \left(\alpha\, U_T^2\right)\left(x\sin\psi\right)dx\, d\psi = -\theta_0\left(RM_{\theta o}\right) - \theta_t\left(RM_{\theta t}\right) - \lambda_{tpp}\left(RM_{\lambda tpp}\right) + \left(B_{1C} + a_{1S}\right)\left(RM_{B1C}\right)$$

where $\theta_{x,\psi} = \theta_0 + x\theta_t - B_{1C}\sin\psi - A_{1C}\cos\psi$ $\beta_\psi = \beta_0 - a_{1S}\cos\psi - b_{1S}\sin\psi$

Feathering and/or Flapping Change With αtpp To Make Roll Moment = 0.

$$\theta_{x,\psi} = \theta_0 + x\,\theta_t - B_{1C}\sin\psi - A_{1C}\cos\psi$$

$$\beta_\psi = \beta_0 - a_{1S}\cos\psi - b_{1S}\sin\psi$$

$$\frac{\partial(B_{1C} + a_1)}{\partial\alpha_{tpp}}$$

degree
per
degree

□ Rotor A
△ Rotor B
✕ Rotor C
■ Rotor D
● Rotor E
▲ Rotor F
◇ Rotor G
◆ Rotor H (Jenkins) Solidity = 0.097, Xc = 0.16
- - - Uniform Inflow Theory for Rotor H
—— Harris Empirical Non-uniform Inflow Theory for Rotor H
—— CAMRAD II (Prescribed Wake) for Rotor H

Advance Ratio V/V$_t$

Feathering and/or Flapping Change With θ₀ To Make Roll Moment = 0.

$$\theta_{x,\psi} = \theta_0 + x\,\theta_t - B_{1C}\sin\psi - A_{1C}\cos\psi$$

$$\beta_\psi = \beta_0 - a_{1S}\cos\psi - b_{1S}\sin\psi$$

$$\frac{\partial(B_{1C} + a_1)}{\partial\theta_0}$$

degree
per
degree

- □ Rotor A
- △ Rotor B
- ✕ Rotor C
- ▪ Rotor D
- ● Rotor E
- ▲ Rotor F
- ◇ Rotor G
- ◆ Rotor H (Jenkins) Solidity = 0.097, Xc = 0.16
- --- Uniform Inflow Theory for Rotor H
- —— Harris Empirical Non-uniform Inflow Theory for Rotor H
- —— CAMRAD II (Prescribed Wake) for Rotor H

Advance Ratio V/V$_t$

Thrust Sensitivity To Tip Path Plane α_{tpp} Holding Zero Roll Moment.

$$\frac{\partial C_T / \sigma}{\partial \alpha_{tpp}}$$

per radian

Legend:
- □ Rotor A
- △ Rotor B
- × Rotor C
- ■ Rotor D
- ● Rotor E
- ▲ Rotor F
- ◇ Rotor G
- ◆ Rotor H (Jenkins) Solidity = 0.097, Xc = 0.16
- – – Uniform Inflow Theory for Rotor H
- —— Harris Empirical Non-uniform Inflow Theory for Rotor H
- —— CAMRAD II (Prescribed Wake) for Rotor H

Advance Ratio V/V_t

Thrust Sensitivity To Collective Pitch Holding Zero Roll Moment.
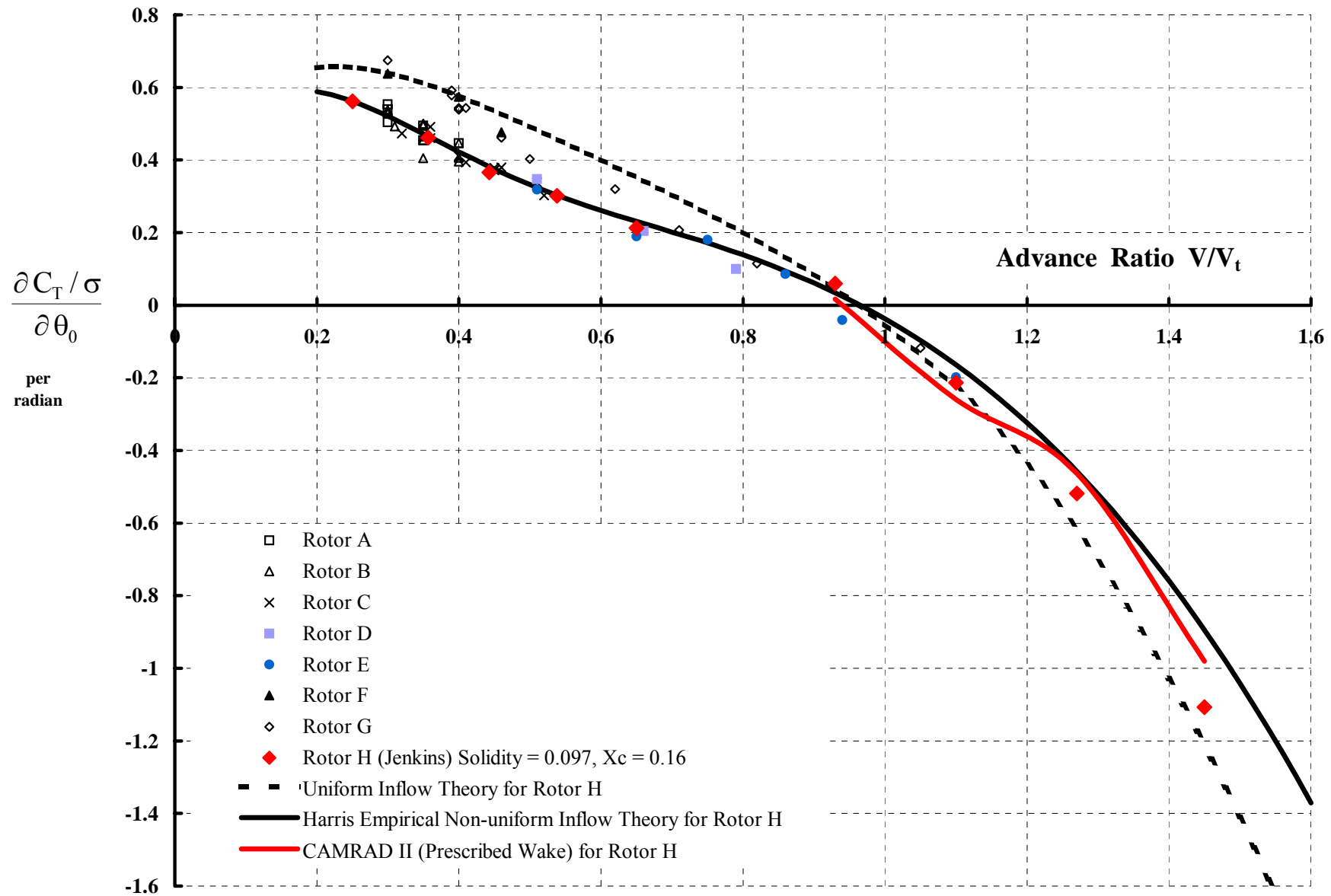
The Inplane Velocity Distribution Around μ = 1 Creates Thrust Insensitivity To Collective Pitch Changes WHEN Zero Roll Moment Is Imposed.

Ref.: Page 22 of "Rotary Wing Aerodynamics–Historical Perspective and Important Issues", F.D. Harris
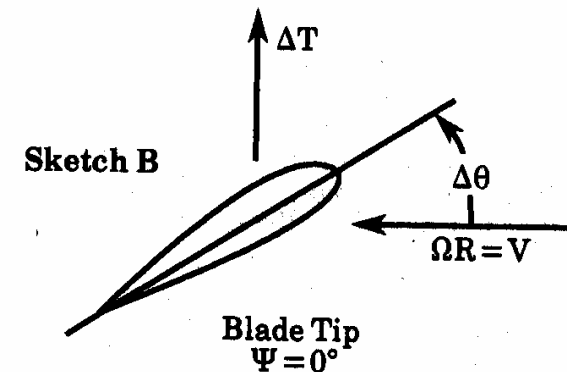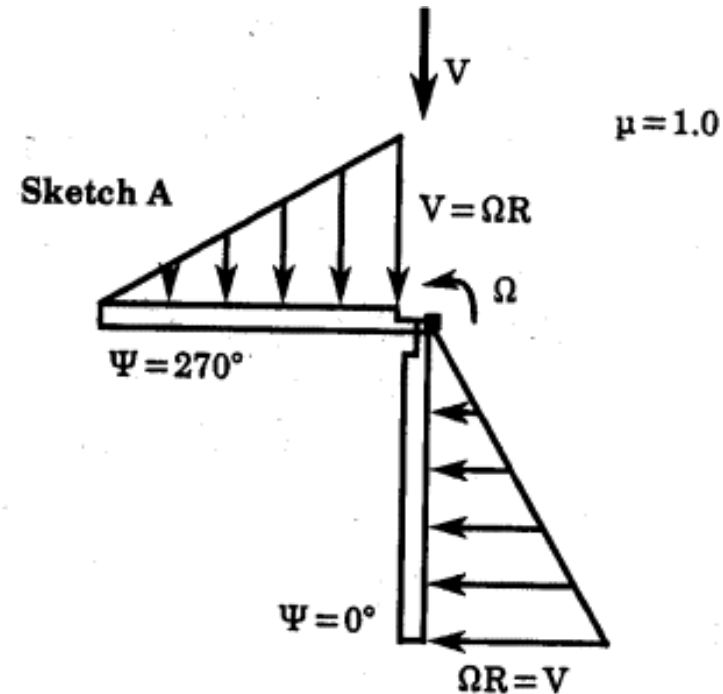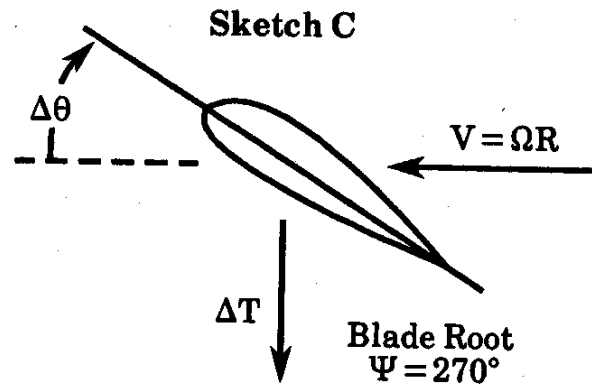
In December 1959, Peter Arcidiacono (UAC) Experimentally Found An Upper μ Limit To Flapping Stability For Rotors Having Articulated Blades. The Potential Instability Was Traced To 2nd Harmonic Flapping. This Work, Along With A Clear Explanation Of The Problem, Was Presented To The 19th AHS Forum In 1963.
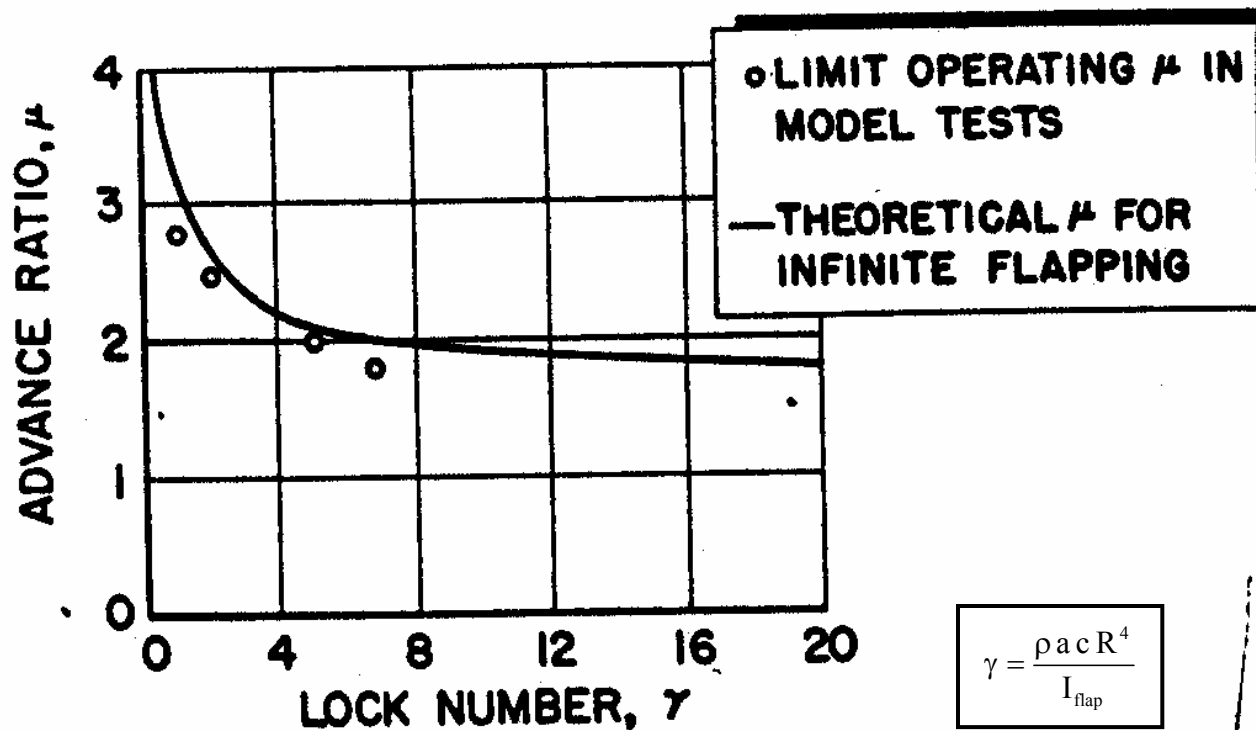
Ref. Arcidiacono, P.J. "Aerodynamic Characteristics of a Model Helicopter Rotor Operating at Advance Ratios as High as 2.5. UAC Research Laboratories Report R–0324–1, December 1959. Note: Dean Borgman and his Secretary resurrected a copy of this report for me.

Ref. Jenny, D.S., Arcidiacono, P.J. & Smith, A.F. " A Linearized Theory for the Estimation of Helicopter Rotor Characteristics at Advance Ratio Above 1.0." 19th AHS Forum, 1963

Jenny (et al) Predicted Rotor Response To A 20 fps Gust.

Load Factor

Longitudinal Flapping

a_{1S}

degrees

Legend:
— ARTICULATED
--- TEETERING

$\gamma = 10.0$ 2.3

ADVANCE RATIO, μ
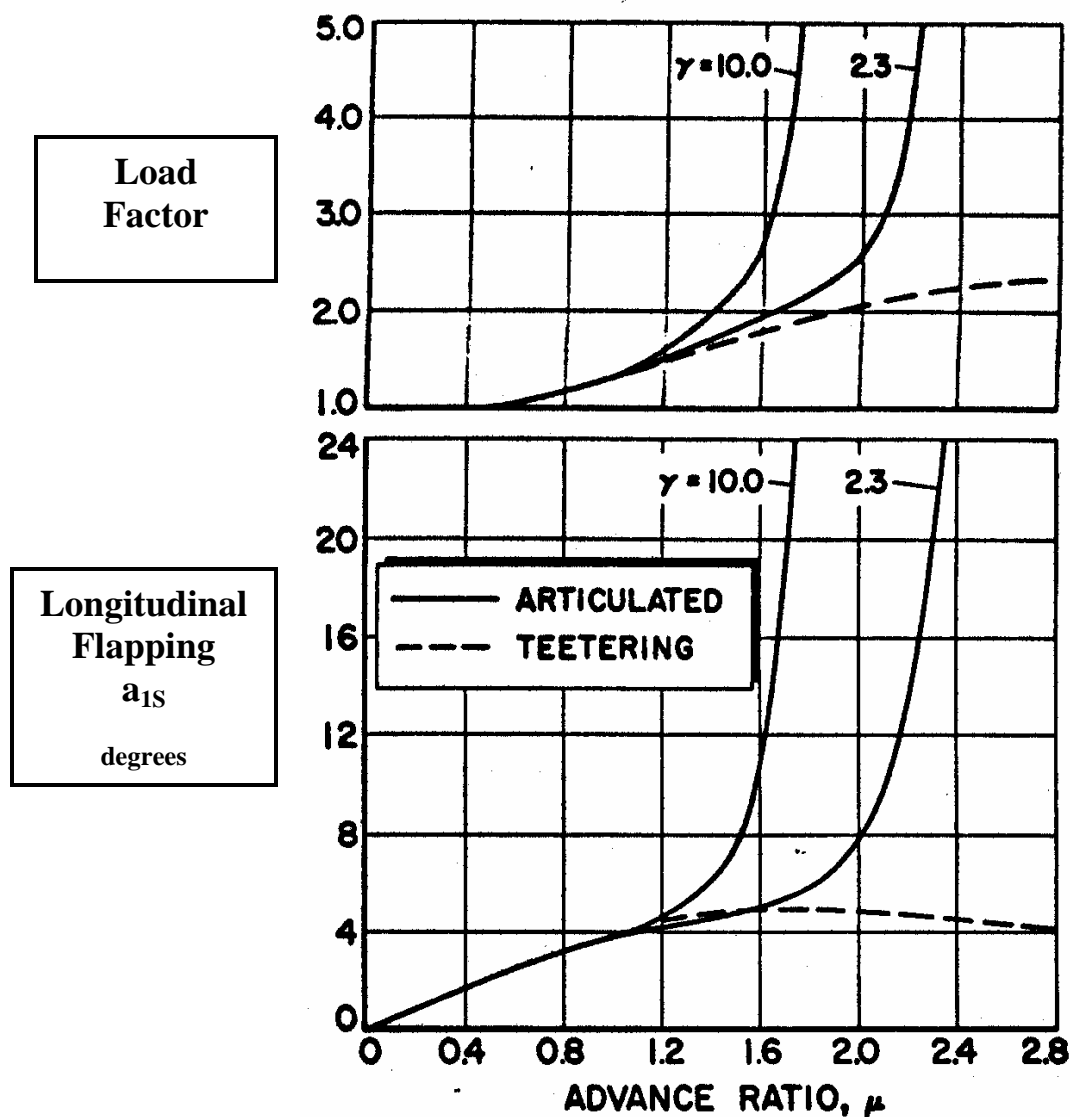
Linearized Theory Assumptions
1. Small angles
2. Flap hinge at rotor centerline
3. $Cl = a\alpha$ $Cd = Cdo$
4. Rigid, untapered, linear twisted blades
5. Lead lag and torsion ignored
6. Uniform inflow
7. Tip loss by B= 0.97
8. Zero root cut out
9. No cyclic
10. Coning, 1st and 2nd harmonic flapping for articulated rotor
11. Pre–cone and 1st harmonic flapping for teetering rotor
12. Lock Number = $\gamma = \dfrac{\rho\, a\, c\, R^4}{I_{flap}}$

Ref. Jenny, D.S., Arcidiacono, P.J. & Smith, A.F. " A Linearized Theory for the Estimation of Helicopter Rotor Characteristics at Advance Ratio Above 1.0." 19th AHS Forum, 1963

Pitch–Flap Coupling To Reduce Rotor Sensitivity Recommended

Note: XV–1 used about 2.2° feather down for 1° flap up in its Airplane mode. This is 65.56° of δ_3 and tan 65.56 = 2.2.
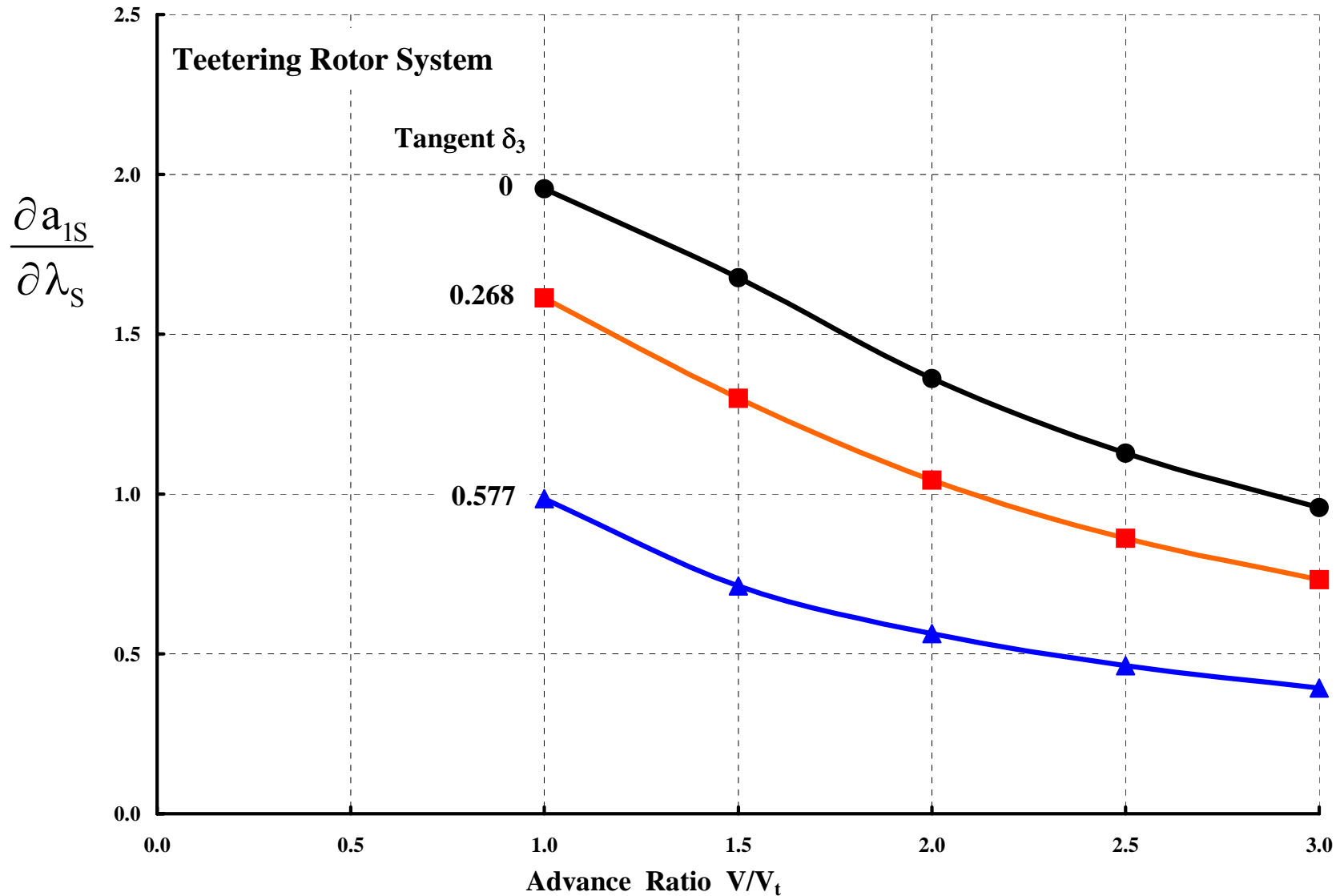
Teetering Rotor System

$\dfrac{\partial a_{1S}}{\partial \lambda_S}$

Tangent δ_3

0

0.268

0.577

Advance Ratio V/V_t

Ref. Jenny, D.S., Arcidiacono, P.J. & Smith, A.F. " A Linearized Theory for the Estimation of Helicopter Rotor Characteristics at Advance Ratio
Above 1.0." 19th AHS Forum, 1963

LET'S REVISIT AUTOGYROS

First Some History

Cierva, Pitcairn, and Kellett Era (1919 to 1941)
Selection of the Helicopter (1942)
Legacy

Some Technology Aspects

What's in a Name?
Fuselages, Wings, Propellers, Rotors and Trim
Rotor Thrust and Flapping Behavior at High Advance Ratio
➤ Limits to Rotor Lift and Propulsion
To Review Then

XV–1 Re–examined

Full Scale Wind Tunnel Test in 40 by 80
Rotor (With & Without Wing)
Complete Aircraft
Rotor Stability In Forward Flight
Phase II Flight Evaluation

Concluding Remarks

CAMRAD II's Opinion Of S–76 Rotor Lift & Propulsive Capability.

198 knots. Lines of Constant Power

V/V_t = 0.5, V = 198.5 kts, Vt = 670 fps,
q = 133.7 psf, M_{1,90} = 0.900

Cp = 0
Cp = 0.0004
Cp = 0.0008
Cp = 0.0012
Trim for Fe = 13 sq ft, GW = 10,000 lbs

$$C_L = \frac{L}{\rho \, A V_t^2}$$

$$C_X = \frac{(-D)}{\rho \, A V_t^2}$$

$$C_P = \frac{P}{\rho \, A V_t^3}$$

α_{tpp} = +5°
α_{tpp} = 0°
α_{tpp} = -10°
α_{tpp} = -20°

HP for trim 2,370

Dimensions
D = 44 ft.
σ = 0.07476
πR² = 1520 sq. ft.
b = 4
ρ = 0.002378 slug/cubic foot
HP = 1976.6 x 10³ x C_P
L = 1622.6 x 10³ x C_L lbs.

Propelling   Dragging

Propulsive Force Coeff. C_X (Blades alone)

S–76 Rotor Propulsive Efficiency At 198 kts & L = 10,000lbs.

CAMRAD II Opinion

**V/V$_t$ = 0.5, V = 198.5 kts, Vt = 670 fps,
q = 133.7 psf, M$_{1,90}$ = 0.900**

Dimensions
D = 44 ft.
σ = 0.07476
πR^2 = 1520 sq. ft.
b = 4
ρ = 0.002378 slug/cubic foot
HP = 1976.6 x 10^3 x C$_P$
L = 1622.6 x 10^3 x C$_L$ lbs.

L = 10,000 lbs.

$$C_L = \frac{L}{\rho A V_t^2} = 0.006$$

$$\frac{C_L}{\sigma} = 0.08$$

$$C_P = \frac{P}{\rho A V_t^3}$$

$$\Delta C_P = \frac{\Delta C_X \left(V/V_t\right)}{0.764}$$

**Power
IF
Prop. Eff.
Were 100%**

$$C_X = \frac{(-D)}{\rho A V_t^2}$$

Dragging

Propelling

0.0012

0.0008

0.0004

0

-0.0012   -0.0008   -0.0004   0   0.0004   0.0008   0.0012

CAMRAD II's Opinion Of S–76 Rotor Lift & Propulsive Capability.

238 knots. Lines of Constant Power

$$C_L = \frac{L}{\rho A V_t^2}$$

$$C_X = \frac{(-D)}{\rho A V_t^2}$$

$$C_P = \frac{P}{\rho A V_t^3}$$

Propulsive Force Coeff. C_X (Blades alone)
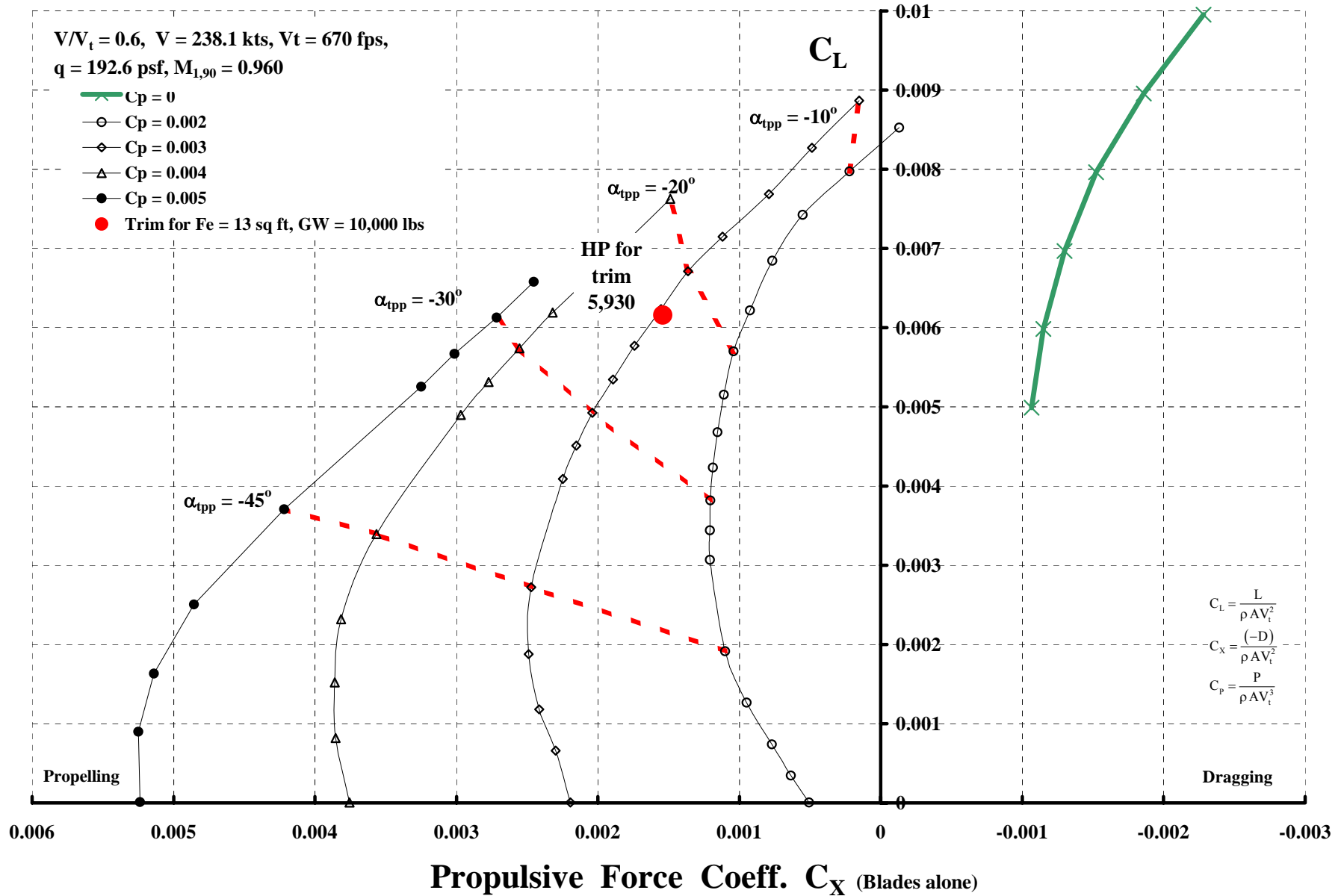
CAMRAD II's Opinion Of S−76 Rotor Lift & Propulsive Capability.

278 knots. Lines of Constant Power

Propulsive Force Coeff. C_X (Blades alone)

V/Vt = 0.7, V = 277.8 kts, Vt = 670 fps,
q = 262.1psf, M1,90 = 1.02

Cp = 0
Cp = 0.002
Cp = 0.003
Cp = 0.004
Cp = 0.005
Trim for Fe = 13 sq ft, GW = 10,000 lbs

C_L

$\alpha_{tpp} = -10^o$
$\alpha_{tpp} = -20^o$
$\alpha_{tpp} = -30^o$
$\alpha_{tpp} = -45^o$

HP for trim 9,490

Propelling

Dragging

$C_L = \dfrac{L}{\rho A V_t^2}$

$C_X = \dfrac{(-D)}{\rho A V_t^2}$

$C_P = \dfrac{P}{\rho A V_t^3}$
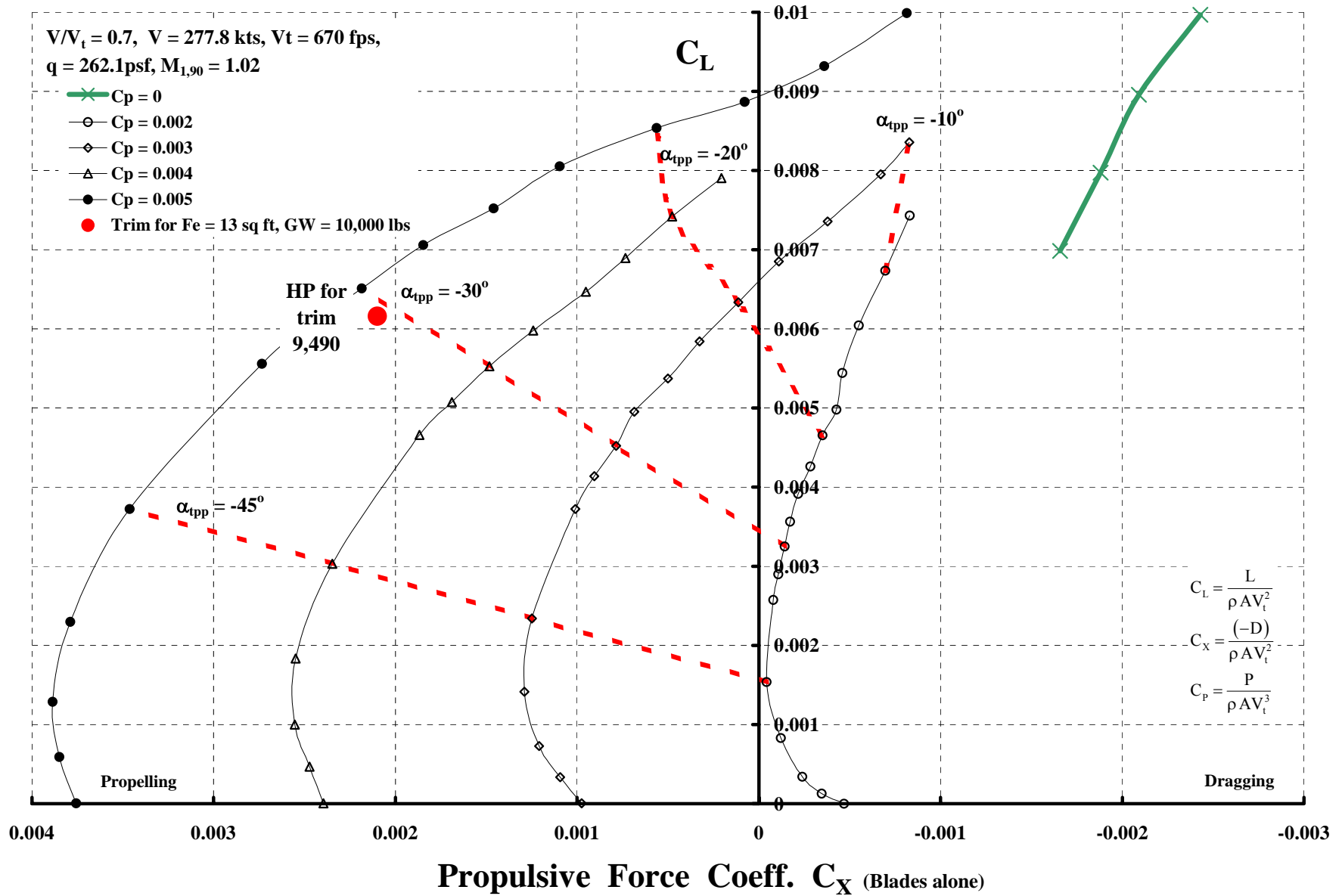
CAMRAD II's Opinion Of S–76 Rotor Lift & Propulsive Capability.

318 knots. Lines of Constant Power

V/Vt = 0.8, V = 317.5 kts, Vt = 670 fps,
q = 342.3 psf, $M_{1,90}$ = 1.08

Legend:
- ✕ Cp = 0
- ○ Cp = 0.002
- ◇ Cp = 0.003
- △ Cp = 0.004
- ● Cp = 0.005
- ■ Cp = 0.006
- ▲ Cp = 0.007
- ● Trim for Fe = 13 sq ft, GW = 10,000 lbs

C_L

α_{tpp} = -20°

α_{tpp} = -30°

α_{tpp} = -35°

HP for trim 14,820

α_{tpp} = -45°

Propelling

Dragging

$$C_L = \frac{L}{\rho A V_t^2}$$

$$C_X = \frac{(-D)}{\rho A V_t^2}$$

$$C_P = \frac{P}{\rho A V_t^3}$$

Propulsive Force Coeff. C_X (Blades alone)
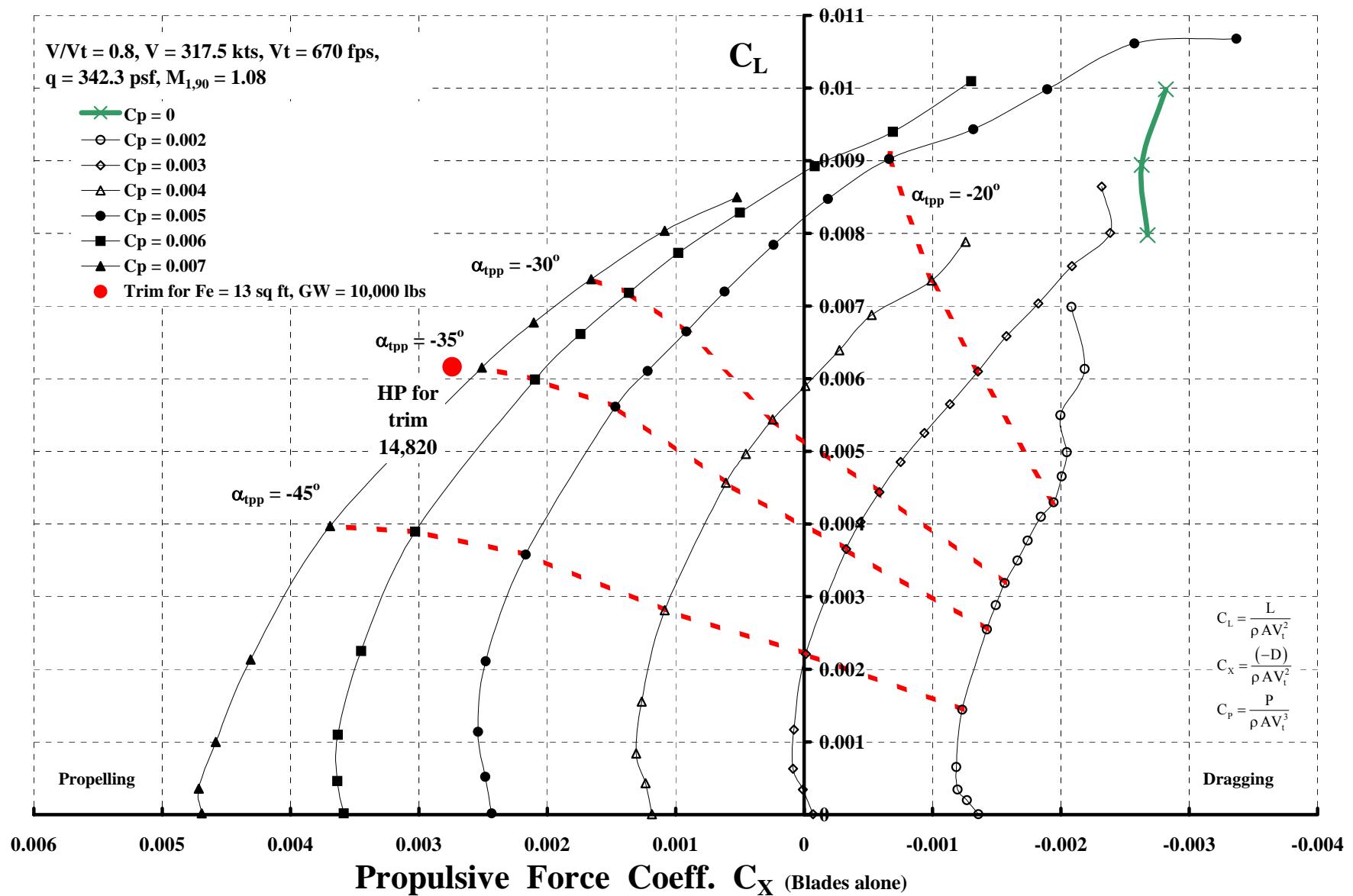
CAMRAD II's Opinion Of S–76 Rotor Lift & Propulsive Capability.

358 knots. Lines of Constant Power

V/Vt = 0.9, V = 357.2 kts, Vt = 670 fps,
q = 433.3 psf, M$_{1,90}$ = 1.14

- ✕ Cp = 0
- ◇ Cp = 0.003
- △ Cp = 0.004
- ● Cp = 0.005
- ■ Cp = 0.006
- ▲ Cp = 0.008
- ✕ Cp = 0.010
- ● Trim for Fe = 13 sq ft, GW = 10,000 lbs

Trim Not Possible. Need More Solidity.

$\alpha_{tpp} = -20^o$

$\alpha_{tpp} = -30^o$

$\alpha_{tpp} = -45^o$

C$_L$

0.011
0.01
0.009
0.008
0.007
0.006
0.005
0.004
0.003
0.002
0.001
0

Propelling

Dragging

$C_L = \dfrac{L}{\rho\,A V_t^2}$

$C_X = \dfrac{(-D)}{\rho\,A V_t^2}$

$C_P = \dfrac{P}{\rho\,A V_t^3}$

0.006   0.004   0.002   0   -0.002   -0.004   -0.006

Propulsive Force Coeff. C$_X$ (Blades alone)
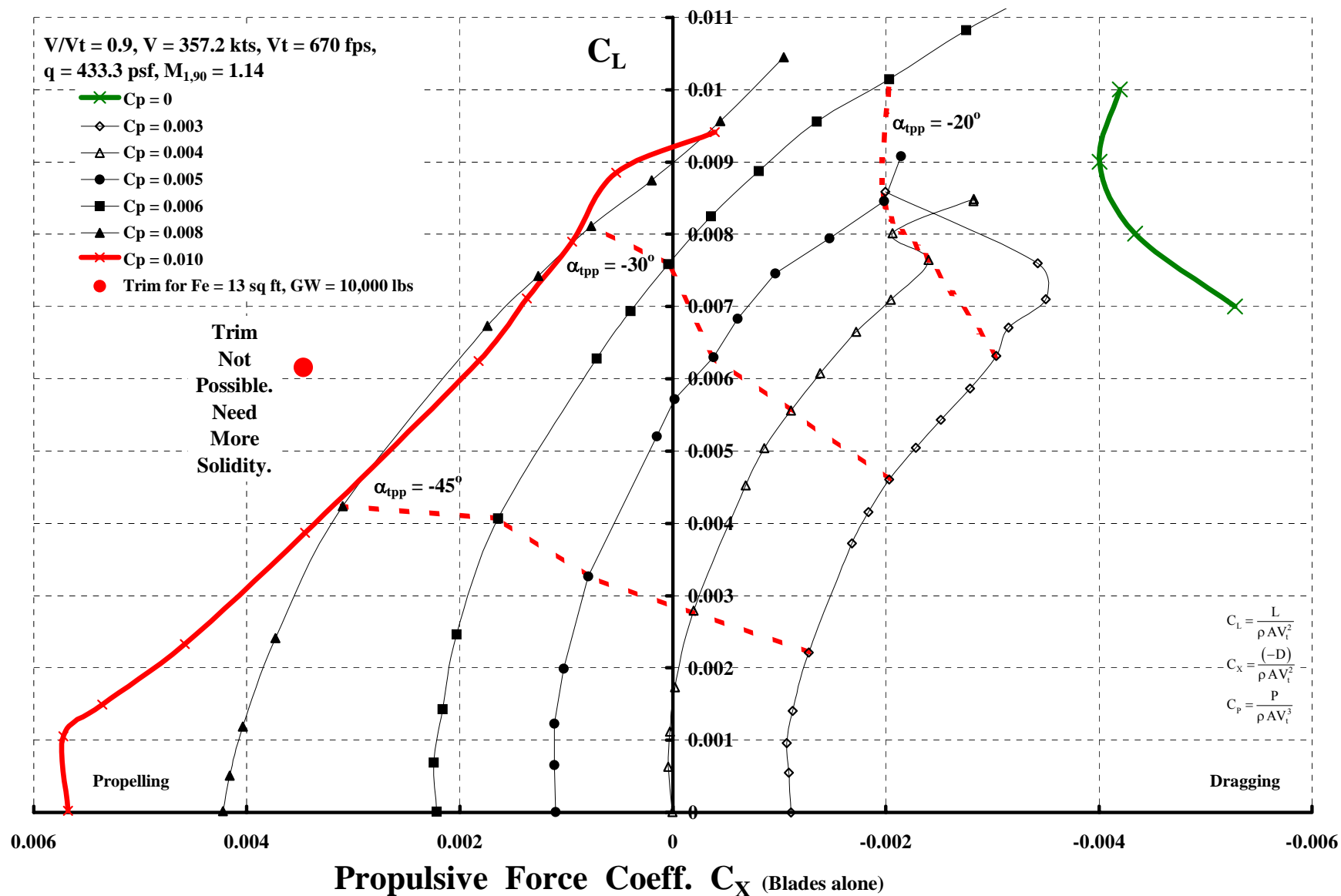
To Review Then.

Our autogyro pioneers build a solid foundation for us.

Many of the VTOL aircraft that have been studied aren't easy to describe simply.

Elementary aerodynamics captures the performance of fuselages, wings, props and rotors.

We have a wealth of experimental data in the old NACA TRs, TNs, TMs RMs etc.

Theoretically, a conventional rotor can both lift and propel at speeds above 300 kts. Its just that inordinately large forward shaft tilts and enormous power is required, to say nothing about loads and vibration.

Around $\mu = 1$ conventional rotors experience a collective pitch control reversal if rolling moment equilibrium is maintained.

Rotor flapping instability caused by 2nd harmonic blade motion is a show stopper to very high μ operation (i.e. $\mu = 1.5$ to 2.0 depending on configuration). Other potential instability problems are too numerous to list.

LET'S REVISIT AUTOGYROS

First Some History

Cierva, Pitcairn, and Kellett Era (1919 to 1941)
Selection of the Helicopter (1942)
Legacy

Some Technology Aspects

What's in a Name?
Fuselages, Wings, Propellers, Rotors and Trim
Rotor Thrust and Flapping Behavior at High Advance Ratio
Limits to Rotor Lift and Propulsion
To Review Then

XV–1 Re–examination

Full Scale Wind Tunnel Tests in 40 by 80
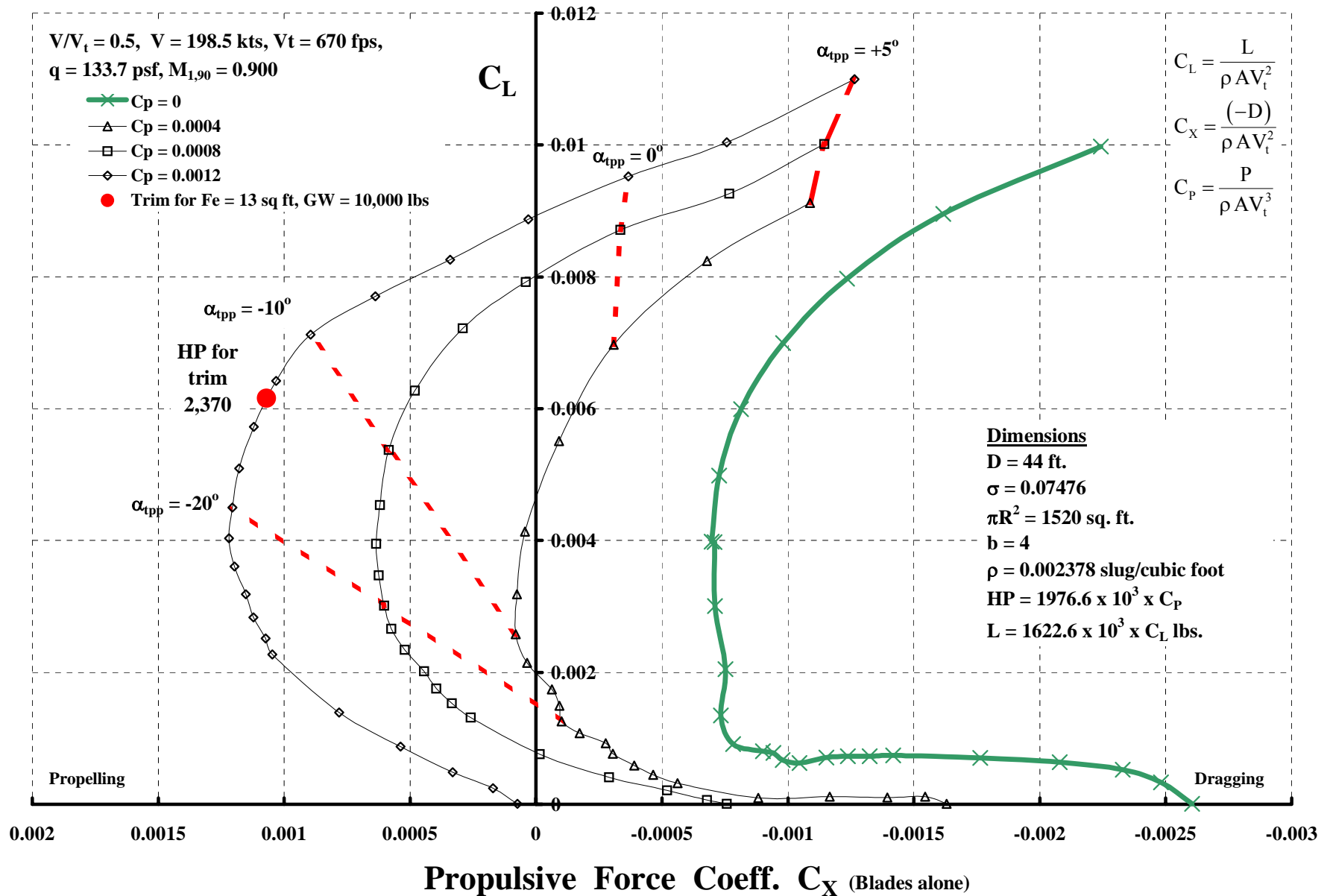Rotor (With & Without Wing)
Complete Aircraft
Rotor Stability In Forward Flight
Phase II Flight Evaluation
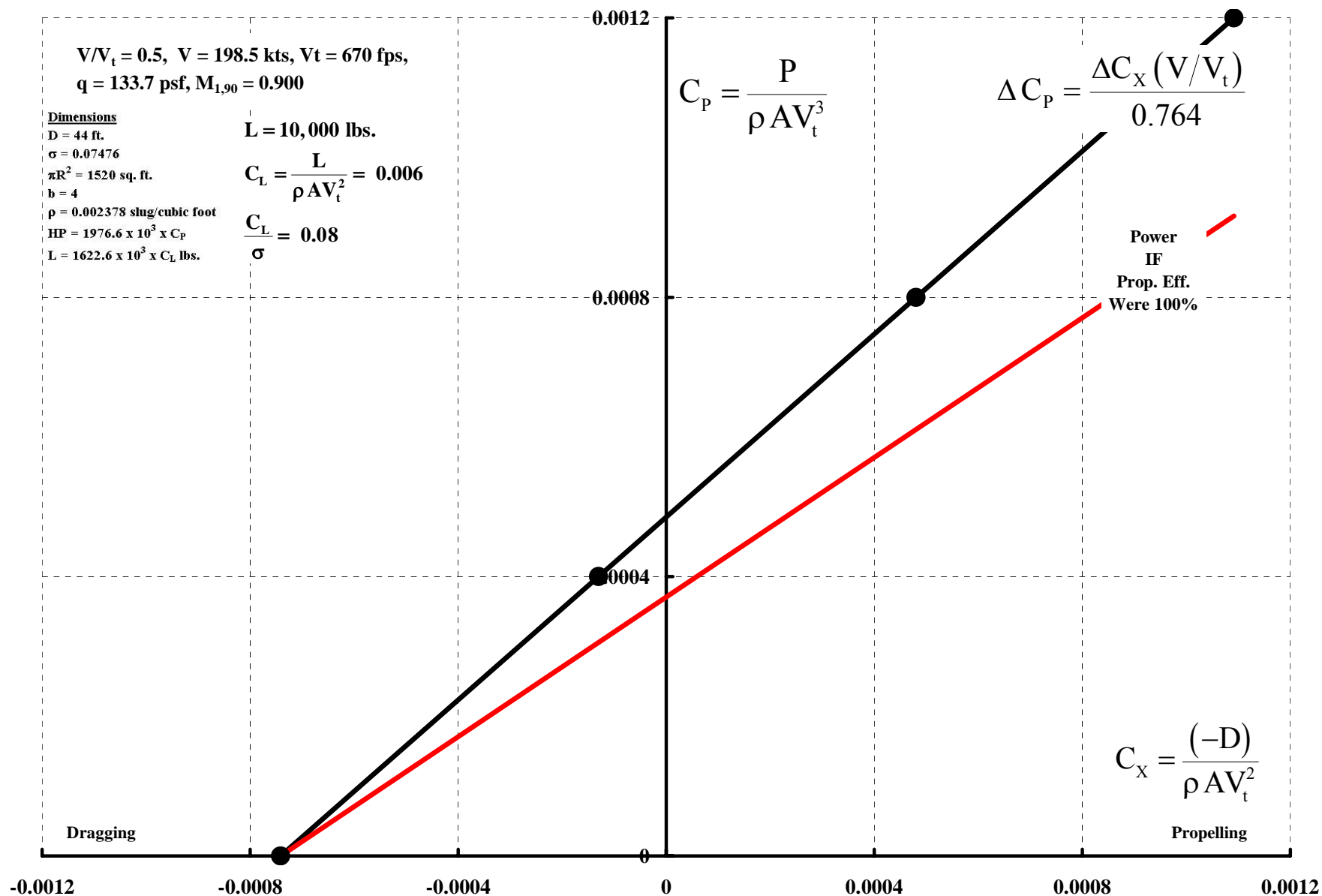
Concluding Remarks

Kurt Hohenemser* Presented "A Type of Lifting Rotor with Inherent Stability" at the Rotating Wing Aircraft Session, 18th Annual I.A.S. Meeting in NYC Jan. 1950. This Idea Became The Basis Of The XV–1's Main Rotor System

Note: Paper published in the Journal of the Aeronautical Sciences, Vol. 17, pg. 555 Sept. 1950. This is a "must read paper" in my opinion! See Supplemental Data And Charts, Item 16 for a copy of this paper.
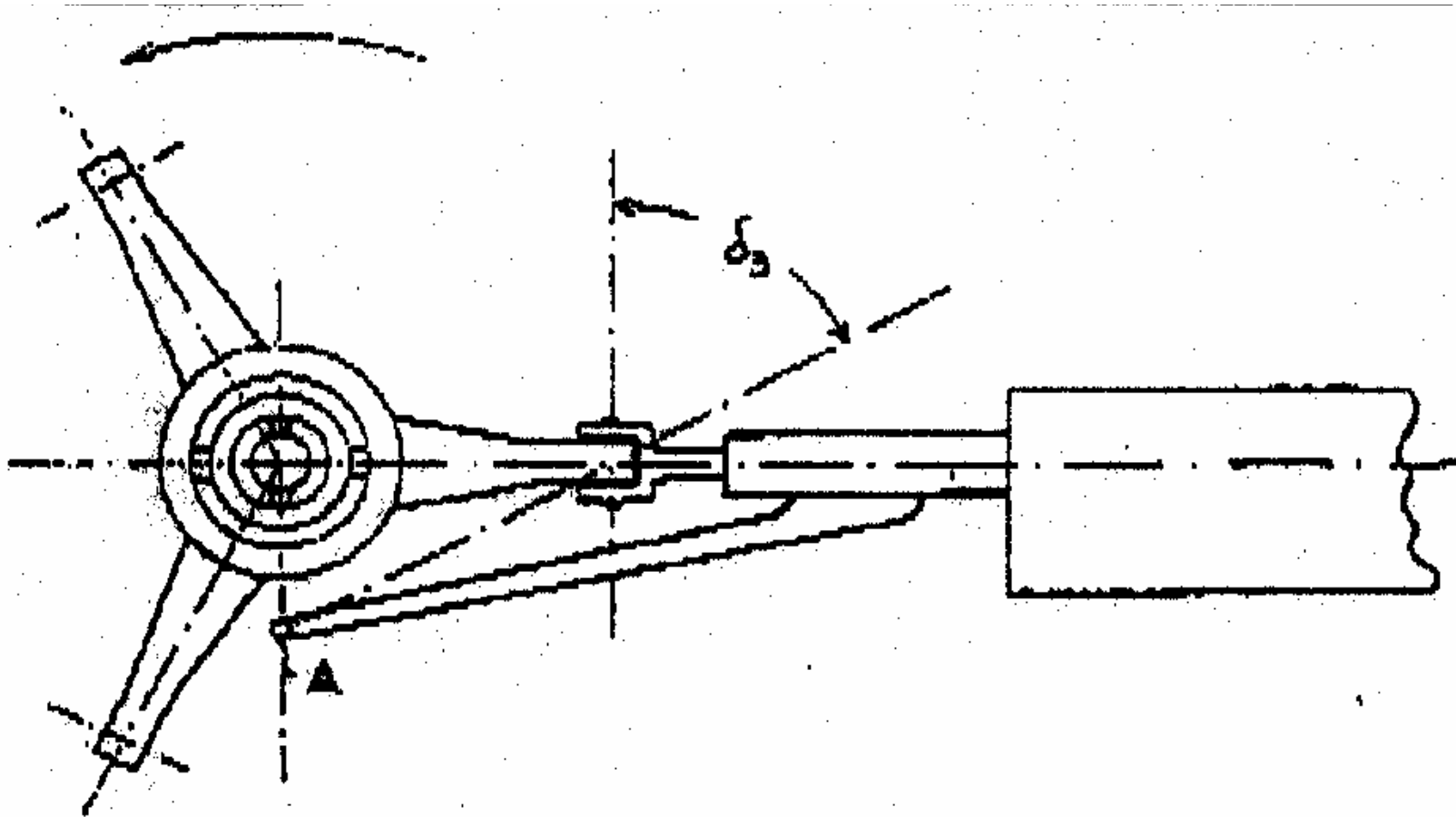
FIG. 2. Plan view of rotor hub with pitch-cone change.

*Chief of Aerodynamics, Helicopter Division, McDonnell Aircraft Corporation

The XV–1's Rotor Blades, Hub and Pylon (With & Without A Wing) Were Tested In The NASA 40 by 80 ft WT In July/August 1953.

The rotor was mounted on a rotor adapter of which the upper portion had the geometric shape of the prototype pylon and which carried a fixed wing of rectangular planform, constant thickness and zero washout in order to keep its manufacturing costs down. The fixed wing had the same area as the prototype wing and was located at the same distance from the rotor center. During the test, collective pitch and longitudinal cyclic pitch were controlled from the control room. However, lateral cyclic was fixed at zero degrees throughout the test. [Note non-representative fuselage. Also, blades not installed.]

Ref: Table's 1 & 2 of Hohenemser's MAC Report No. 3379

Rotor Parameter	Dimension
Diameter	31.0 feet
Blade Chord	17.5 inches
Solidity Ratio	0.09
Blade Airfoil	NACA 63_2 A(1.5)15
Blade Twist	– 8 degrees
Coning Hinge Offset, a	11.5 inches
Pitch Arm Offset, d	6.00 inches
Control Advance Ratio, A	$15° 49'$
Pitch Cone Ratio, PCR = a/d + tan A	2.20
Strap Length	45.90 inches
Strap Spacing Inboard	11.25 in. at Sta. 8.85
Strap Spacing Outboard	7.15 in, at Sta. 54.75
Hub Diameter (Faired)	35 inches
Blade Pitch Axis	0.23 c
Blade Moment of Inertia (pitch axis)	5.4 lb. in. sec.^{2}
Blade Moment of Inertia (cone hinge)	3,180 lb. in. sec.^{2}
Blade Inplane Bending Freq. (20 straps)	452 CPM
Blade Inplane Bending Freq. (30 straps)	484 CPM
Blade Vertical Bending Freq.	545 CPM
Blade Torsional Freq.	1,980 CPM
Blade Weight*	122.5 lbs.
Chordwise c.g.	0.265 c

* Weight and balance does not include retention strap assembly or any attachments on inboard end of torque tube

Two Laminated, Metal, Flex Strap "Bundles" Retained The Blade To The Hub. A Torque Tube Transmitted Pitch Arm Motion To The Blade. The Cuff Fairing Rotated With The Blade And Torque Tube.

Note: An elliptical fairing (not shown) was placed around the hollow torque tube, but the straps were external.

HUB

$\delta_3 = 2.2°$ PITCH DOWN FOR 1° CONE OR FLAP

LAMINATED STEEL FLEX STRAP

FAIRING

HOLLOW TORQUE TUBE

AIR DUCT

D SPAR (STEEL)

AIR

SPHERICAL BEARING

LAMINATED STEEL FLEX STRAP

AIR DUCT

FAIRING

PITCH HORN

+15°

> **Kurt Hohenemser attributes the pressure jet features of the design approach to Fred Dobloff and his development activities during WW II in Germany.**
> Ref: Hohenemser, "Aerodynamic Aspects of the Unloaded Rotor Convertible Helicopter" J. of AHS, Jan. 1957

Ref: Harris sketch from conversations with Bob Head.

Kurt Hohenemser's MAC Report No. 3379 Contained This Schematic Of A Very, Very Unique Rotor System.

FIGURE 1
SCHEMATIC
MODEL 82 (XV-1)
GIMBAL ASSEMBLY
SCALE: NONE

Elliptical Fairing Around Torque Tube

SPIDER

STRAP ATTACH POINT
SPIDER LINK PIVOT

GIMBAL

SPHERICAL BEARING

CONING HINGE
PITCH ARM

SEAL RING FLANGE

SUPPORT CONE

SUPPORT BEARING

COLLECTIVE PITCH CONTROL CYLINDER

ROTOR STEM
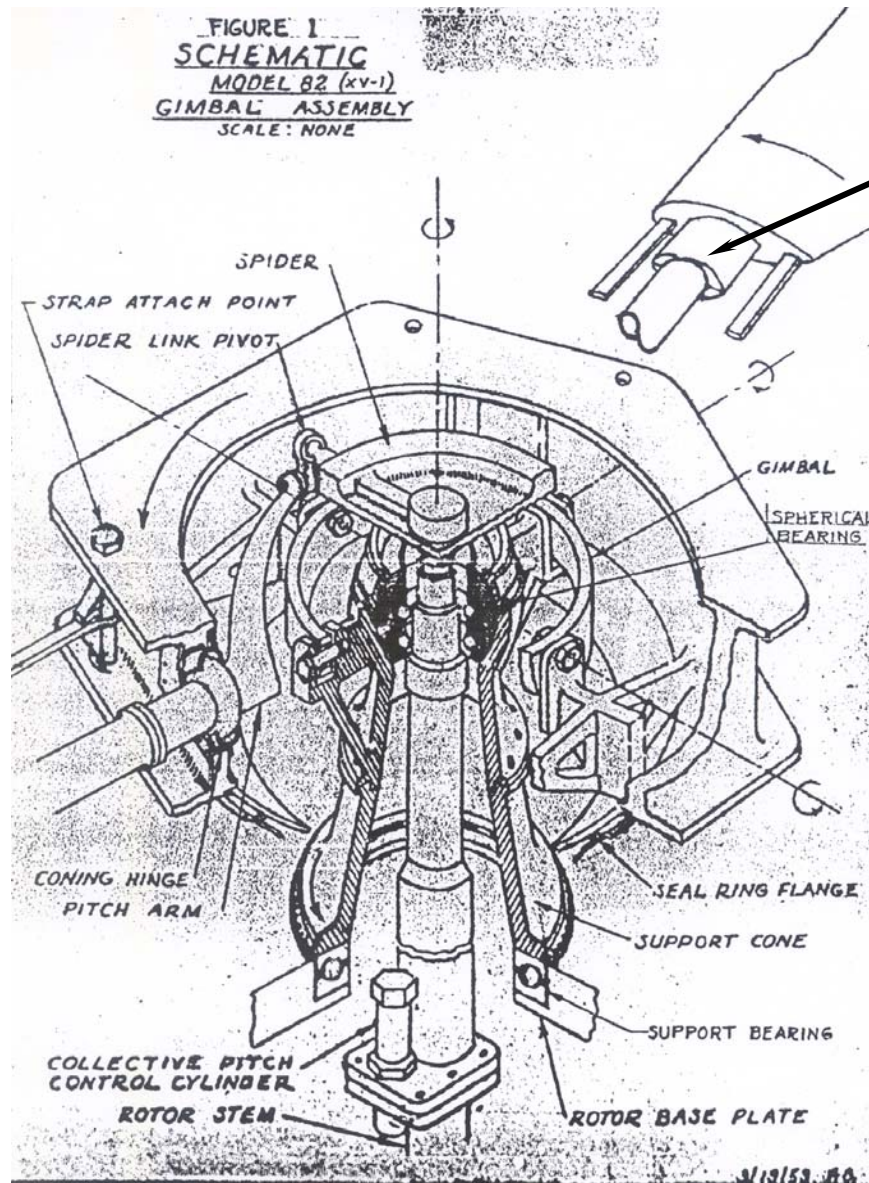
ROTOR BASE PLATE

The Control System Of The Model 82 (XV–1) Was Just As Unique.

Pivot Point For Control Stem At The Center Of The Gimbal

Control Stem Tilted Fore & Aft and Left & Right For Cyclic
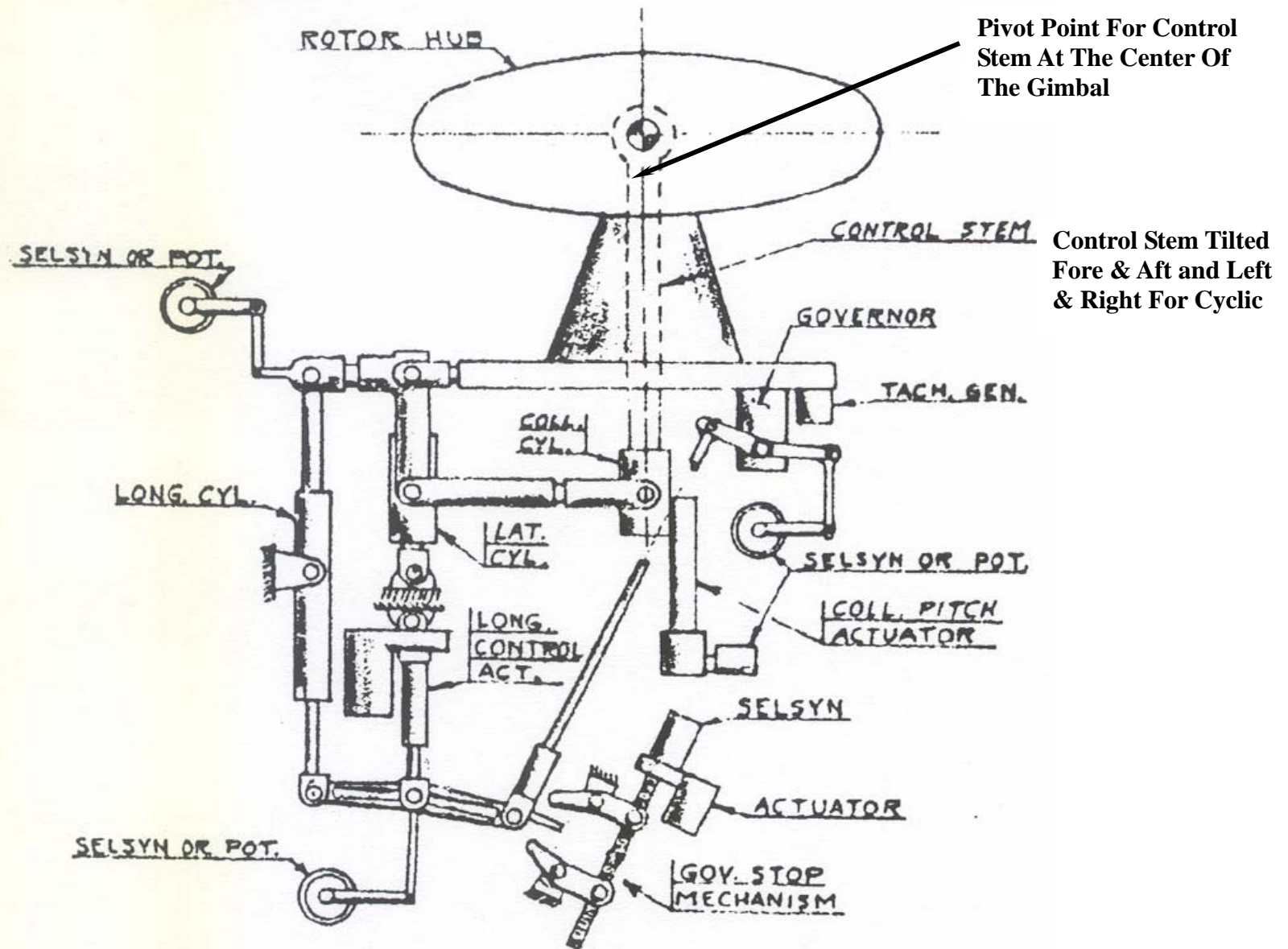
Ref: Figure 2 in MAC 3379

Whirl Testing Prior To Tunnel Entry Gave An Indication Of Pressure Jet Tip Thrust Required To Spin The Rotor In Flat Pitch.

Note: An average airfoil drag coefficient, C_{do}, of 0.0124 appears to match simple theory with test.

- Fig. 12, MAC Report No. 3379
- Simple Theory, Cdo = 0.0124

$$\text{Tip Thrust (per blade)} = \frac{\rho \, A \, V_t^2}{8} \left(\frac{1 \, c}{\pi \, R} \right) C_{do}$$

$$\text{where } C_{do} = 0.0124, \quad c = 17.5 \, \text{inch},$$

$$R = 15.5 \, \text{ft}, \quad \rho = 0.002378 \, \text{slug/ft}^3$$

Tip Pressure Jet Thrust per Blade

(lbs)

Tip Speed (ft/sec)
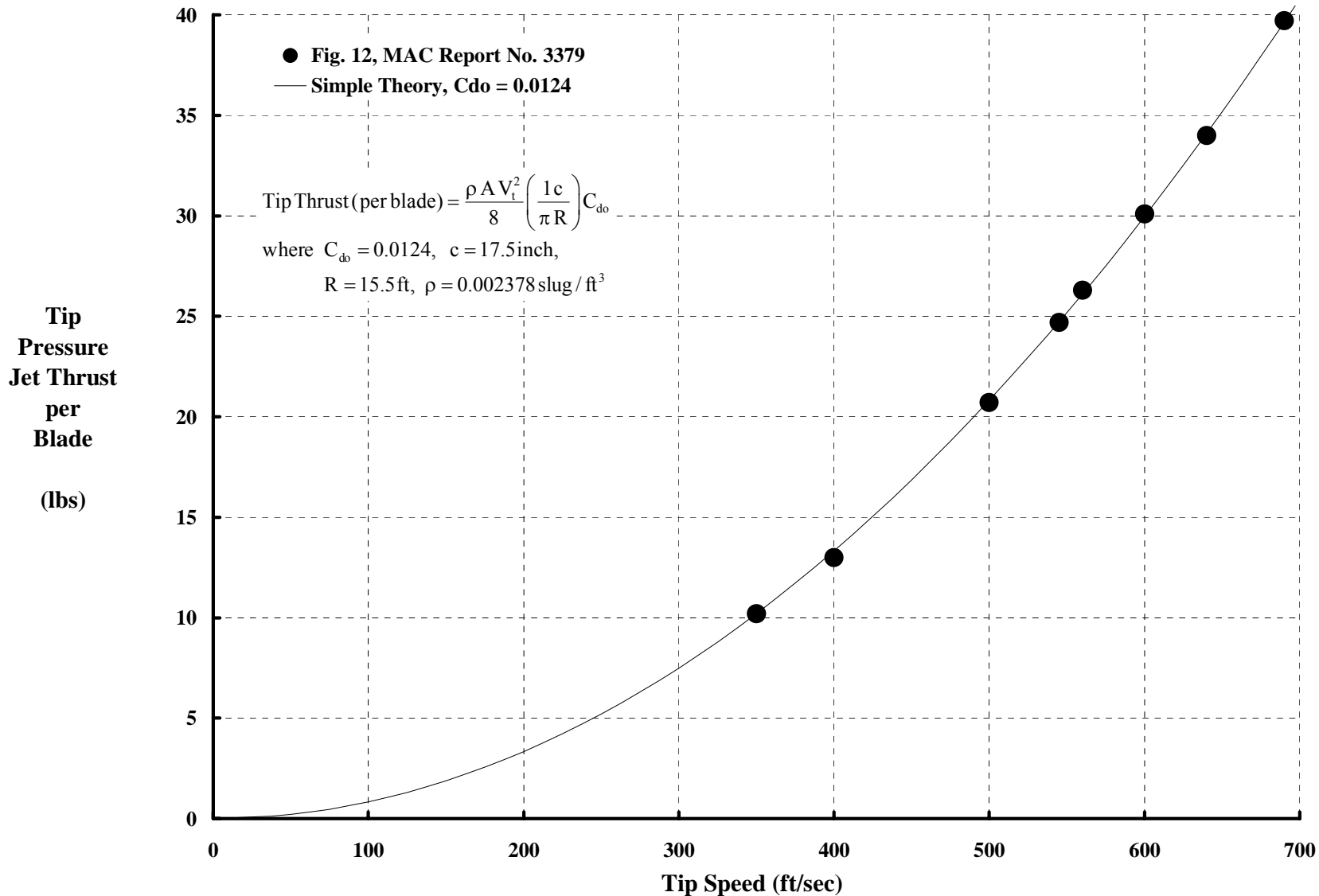
Prior 8 foot Diameter Dynamically Representative Model Rotor Data Established The Instability Boundaries For The Full Scale Test.

Note: No instabilities were encountered in the full scale wind tunnel tests.

Note: Arrow on symbol indicates
stability limit not attained in test.

Onset of 1/2 per rev unstable flapping

Locked Hub $\theta = 0^o$

Onset of blade flutter

Free Hub $\theta = 6^o$

Velocity

knots

Recommended Operating Envelope

$\mu = 1.30$ 1.10   0.90   0.70

0.50

0.35

0.25

○ 8 ft Model, Alpha = 6, Coll. = 0, Rotor Driven
□ 8 ft Model, Alpha = 0, Coll. = 0, Rotor Driven
△ 8 ft Model, Alpha = 6, Coll. = 0, Autorotation
✕ 8 ft Model, Alpha = 6, Coll. = 6, Autorotation
◇ 8 ft Model, Alpha = 0, Coll. = 6, Rotor Driven
● Full Scale in 40 by 80, Coll. = 0, Autorotation

Rotor RPM

At A Given Speed And Collective Pitch, The Angle Of Attack Of The Plane Of No Feathering Controlled Rotor RPM.

Note: Plane of no feathering angle of attack = fuselage angle of attack + control stem incidence.

Autogyro Mode, Wing Off
Collective = 6 deg.

$y = 0.00200x^2 - 0.04631x + 0.46024$
$R^2 = 0.99089$

Advance Ratio

V/V_t

Note: RPM increases (and μ decreases) as angle of attack increases.

■ V = 75 kts, RPM = 280 to 400, Mu = 0.20 to 0.28, q = 19.10 psf (Fig. 71)
▲ V = 100 kts, RPM = 302 to 400, Mu = 0.26 to 0.34, q = 34.0 psf (Fig. 71)
● V = 125 kts, RPM = 325 to 385, Mu = 0.34 to 0.40, q = 53.0 psf (Fig. 71)

Plane of No Feathering Angle of Attack deg
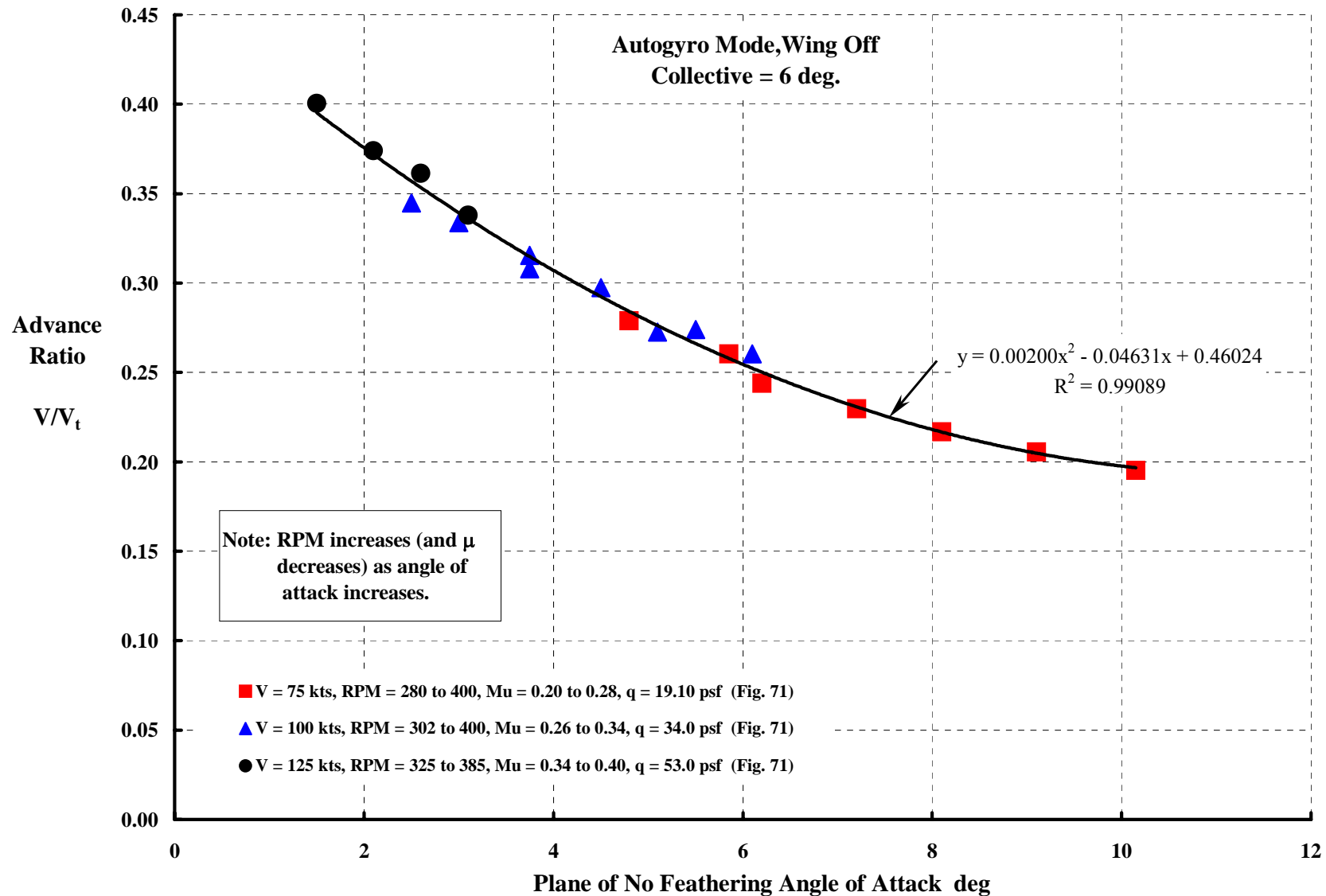
The PNF Angle Of Attack + RPM Determined Rotor Lift, For The Given Speed And Collective Pitch.

Note: The rotor's lift curve slope is not linear because advance ratio is changing.

Autogyro Mode, Wing Off
Collective = 6 deg.

■ V = 75 kts, RPM = 280 to 400, Mu = 0.20 to 0.28, q = 19.10 psf (Fig. 70 &71)

▲ V = 100 kts, RPM = 302 to 400, Mu = 0.26 to 0.34, q = 34.0 psf (Figs. 70 &71)

● V = 125 kts, RPM = 325 to 385, Mu = 0.34 to 0.40, q = 53.0 psf (Figs. 70 & 71)

Lift Divided By Dynamic Pressure L/q

sq. ft.

$y = 1.3112x^2 + 13.051x + 46.864$

$R^2 = 0.9957$

Plane of No Feathering Angle of Attack deg
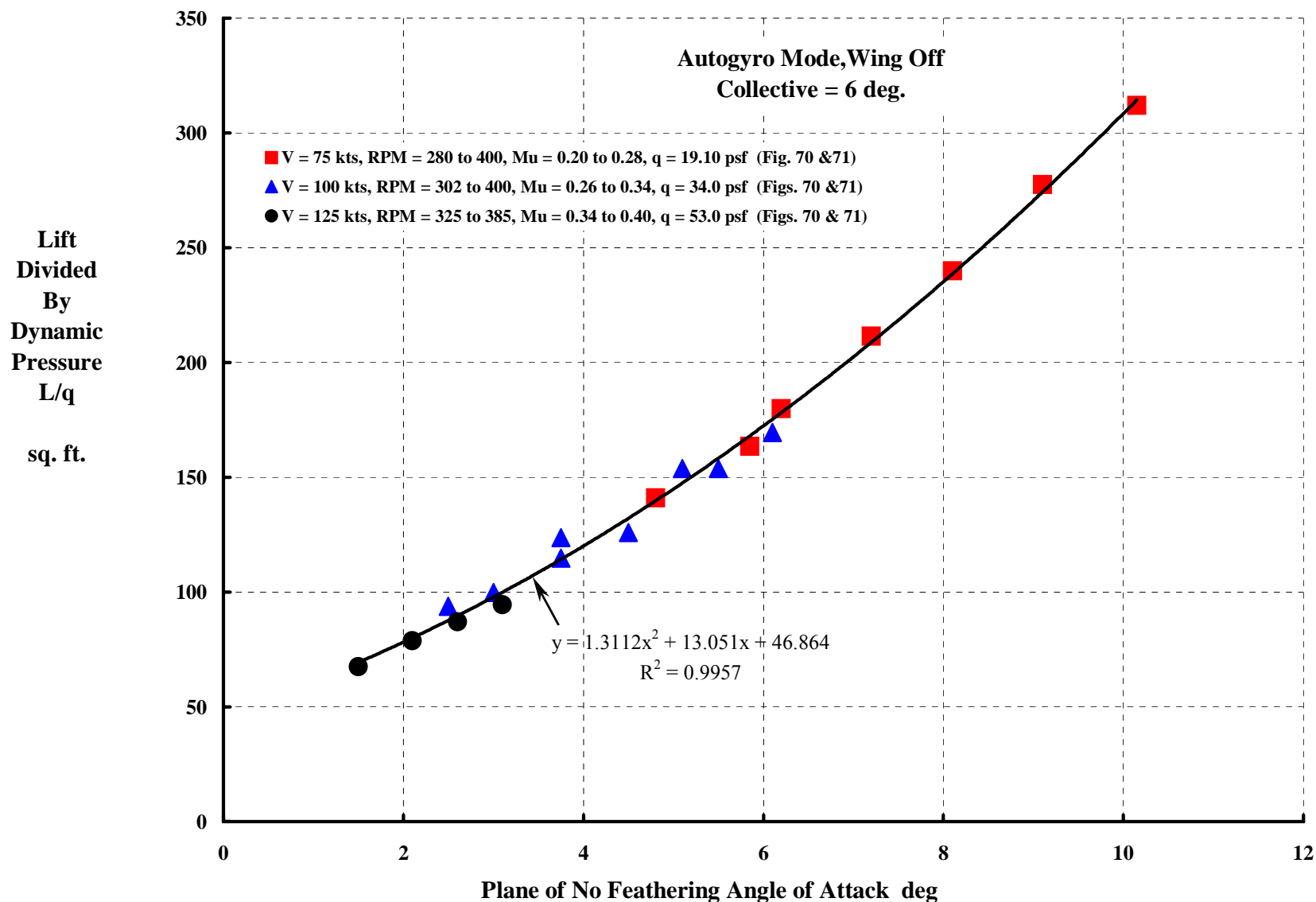
The Rotor System + Pylon Maximum L/D Was About 4.

Note: Drag of hub and pylon was adversely effected by the rotor blades. Increased regions of separated flow were suspected.

Autogyro Mode, Wing Off
Collective = 6 deg.

Harris Simple Theory
For Blades Alone

Lift Divided By Dynamic Pressure L/q

sq. ft.

Hub + Pylon + Struts Drag Tare
Measured Blades Off = 9 ft^2
Probable Blades On = 10 to 11 ft^2

■ V = 75 kts, RPM = 280 to 400, Mu = 0.20 to 0.28, q = 19.10 psf (Fig. 70)
▲ V = 100 kts, RPM = 302 to 400, Mu = 0.26 to 0.34, q = 34.0 psf (Fig. 70)
● V = 125 kts, RPM = 325 to 385, Mu = 0.34 to 0.40, q = 53.0 psf (Fig. 70)

Harris Simple Theory

$$\frac{D_R}{q} = \frac{K_i}{\pi}\left(\frac{L_R}{q\,D}\right)^2 + \frac{(b\,c\,R)\,C_{do}}{4}\left(\frac{1 + 4.65\mu^2 + 4.15\mu^4 - \mu^6}{\mu^3}\right)$$

$$K_i = 1.075\text{Cosh}\left(6.76\mu^2\right) \quad \text{for } \mu \le 0.5$$

$$K_i = 1 - 29.332\mu + 92.439\mu^2 - 51.746\mu^3 \quad \text{for } 0.5 \le \mu \le 1.0$$

$$b = 3, \ c = 17.5 \text{ inch}, \ R = 15.5 \text{ ft}, \ C_{do} = 0.01568$$

Drag Divided By Dynamic Pressure   D/q   sq. ft.

Blade Drag Diminishes Rapidly With Increasing Advance Ratio.

Drag Divided By Dynamic Pressure

D/q

sq. ft.

■ V = 75 kts, RPM = 280 to 400, Mu = 0.20 to 0.28, q = 19.10 psf (Fig. 70)
▲ V = 100 kts, RPM = 302 to 400, Mu = 0.26 to 0.34, q = 34.0 psf (Fig. 70)
● V = 125 kts, RPM = 325 to 385, Mu = 0.34 to 0.40, q = 53.0 psf (Fig. 70)

Autogyro Mode, Wing Off
Collective = 6 deg.

Blades + Hub + Pylon + Struts

Blades Alone

Harris Simple Theory

Induced Drag

Profile Drag

Advance Ratio V/V$_t$
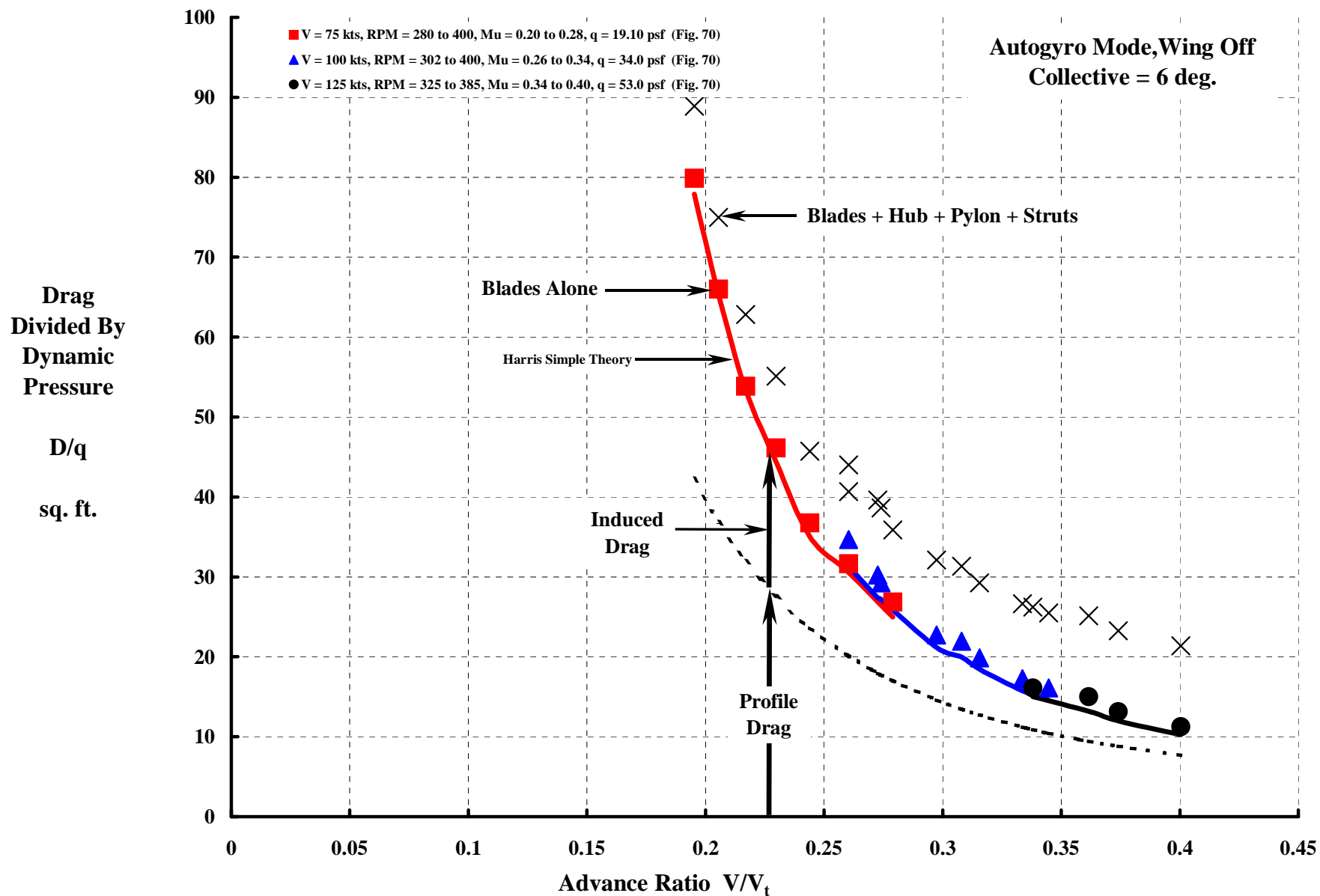
In The Airplane Mode, Rotor RPM Became Very, Very Sensitive To Angle Of Attack Of The Plane Of No Feathering.

Note: The fly ball governor controlled RPM very much better than a human could.

Airplane Mode vs. Autogyro Mode
Wing Off

Airplane Mode
(Hub & Gimbal Locked)
Collective = 0 deg.

Autogyro Mode
(Hub & Gimbal Free)
Collective = 6 deg.

Note: RPM increases (and μ decreases) as angle of attack increases.

Advance Ratio

V/V$_t$

Plane of No Feathering Angle of Attack deg
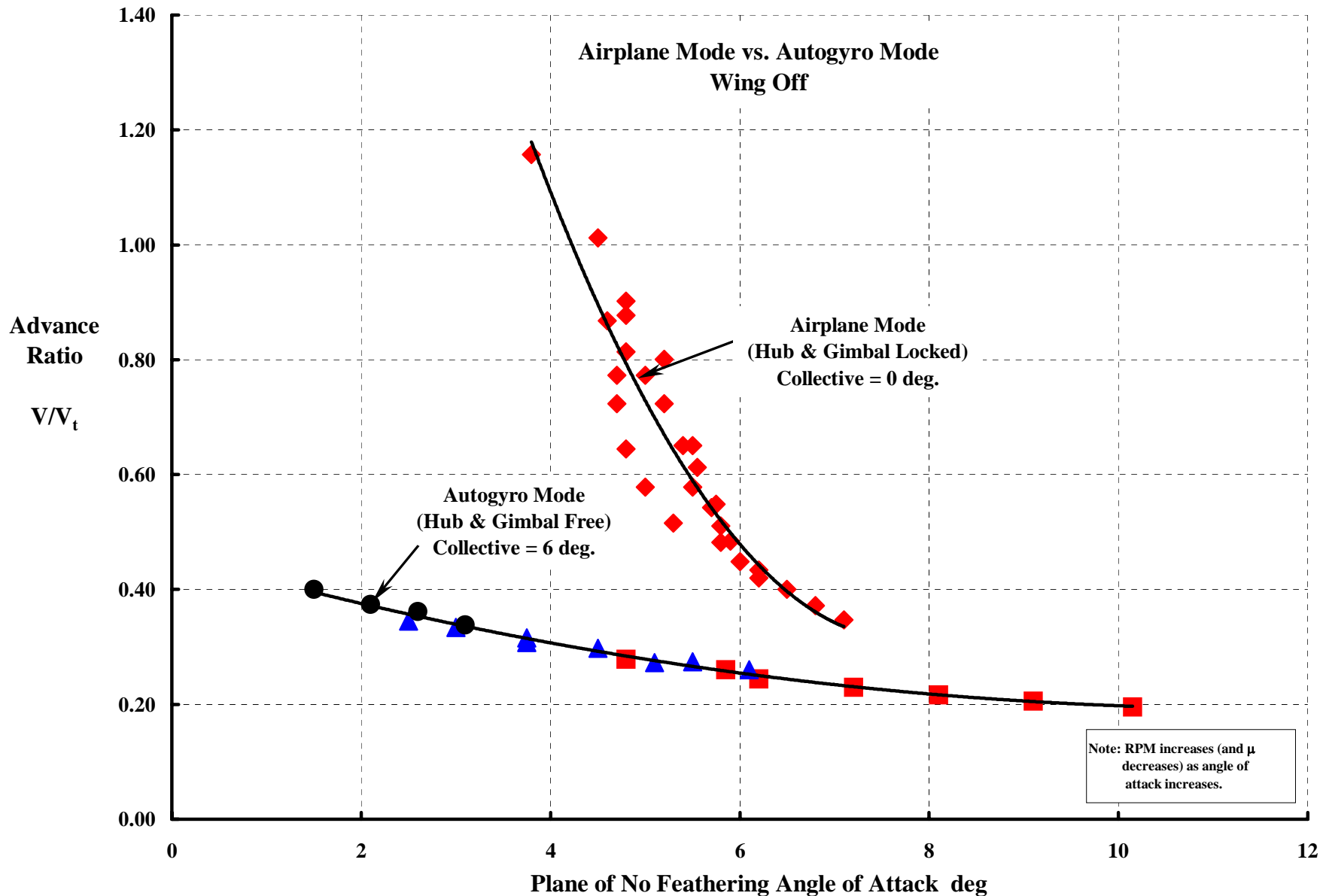
In The Airplane Mode, The Rotor Idled At 180 RPM With $\theta_{0.75} = 0^o$ And Very Little Lift Was Produced.

Airplane Mode vs. Autogyro Mode
Wing Off

Autogyro Mode
(Hub & Gimbal Free)
Collective = 6 deg.

$y = 1.3112x^2 + 13.051x + 46.864$
$R^2 = 0.9957$

$y = 1.799x^2 - 5.610x$
$R^2 = 0.906$

Airplane Mode
(Hub & Gimbal Locked
To Stem)
Collective = 0 deg.

Lift Divided By Dynamic Pressure L/q

sq. ft.

Plane of No Feathering Angle of Attack deg
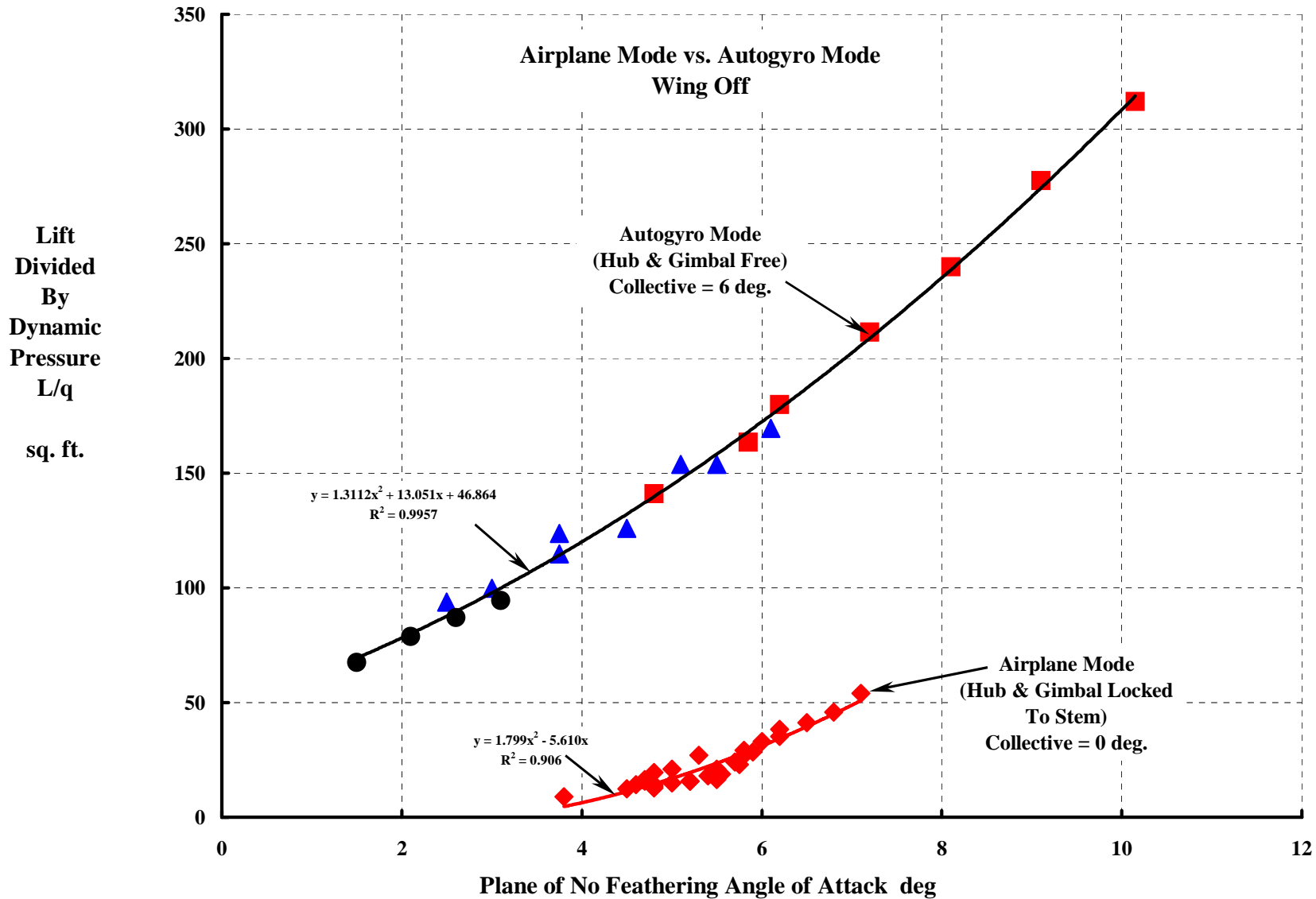
Apparently, Pylon/Hub Interference Drag Was Reduced By Operating The Rotor At Low Lift In The Airplane Mode.
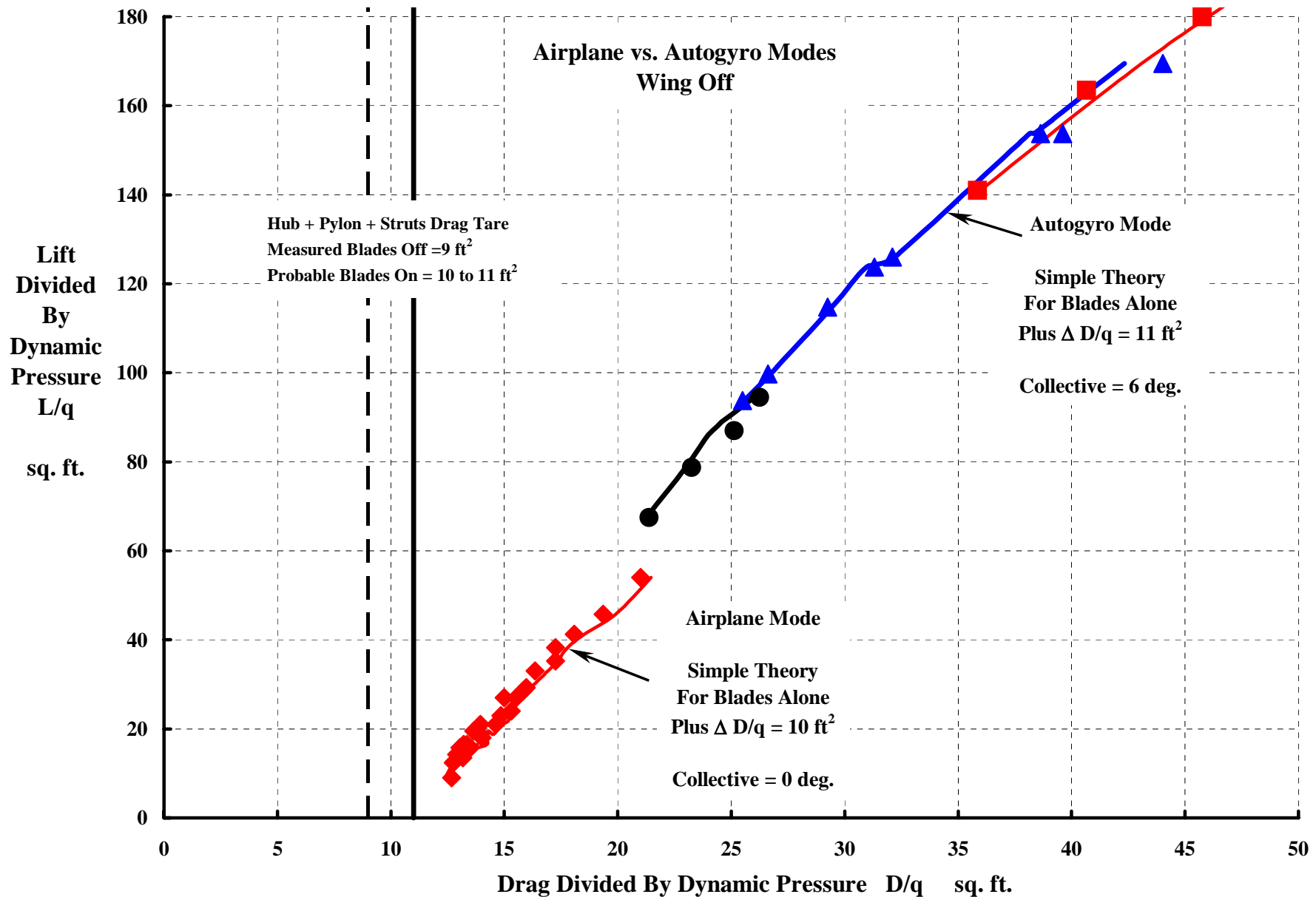
Airplane vs. Autogyro Modes
Wing Off

Lift Divided By Dynamic Pressure L/q sq. ft.

Hub + Pylon + Struts Drag Tare
Measured Blades Off =9 ft^2
Probable Blades On = 10 to 11 ft^2

Autogyro Mode

Simple Theory
For Blades Alone
Plus Δ D/q = 11 ft^2

Collective = 6 deg.

Airplane Mode

Simple Theory
For Blades Alone
Plus Δ D/q = 10 ft^2

Collective = 0 deg.

Drag Divided By Dynamic Pressure   D/q   sq. ft.

"Actually in a compound aircraft the drag of pylon and hub is of more importance than the drag of the rotating blades."
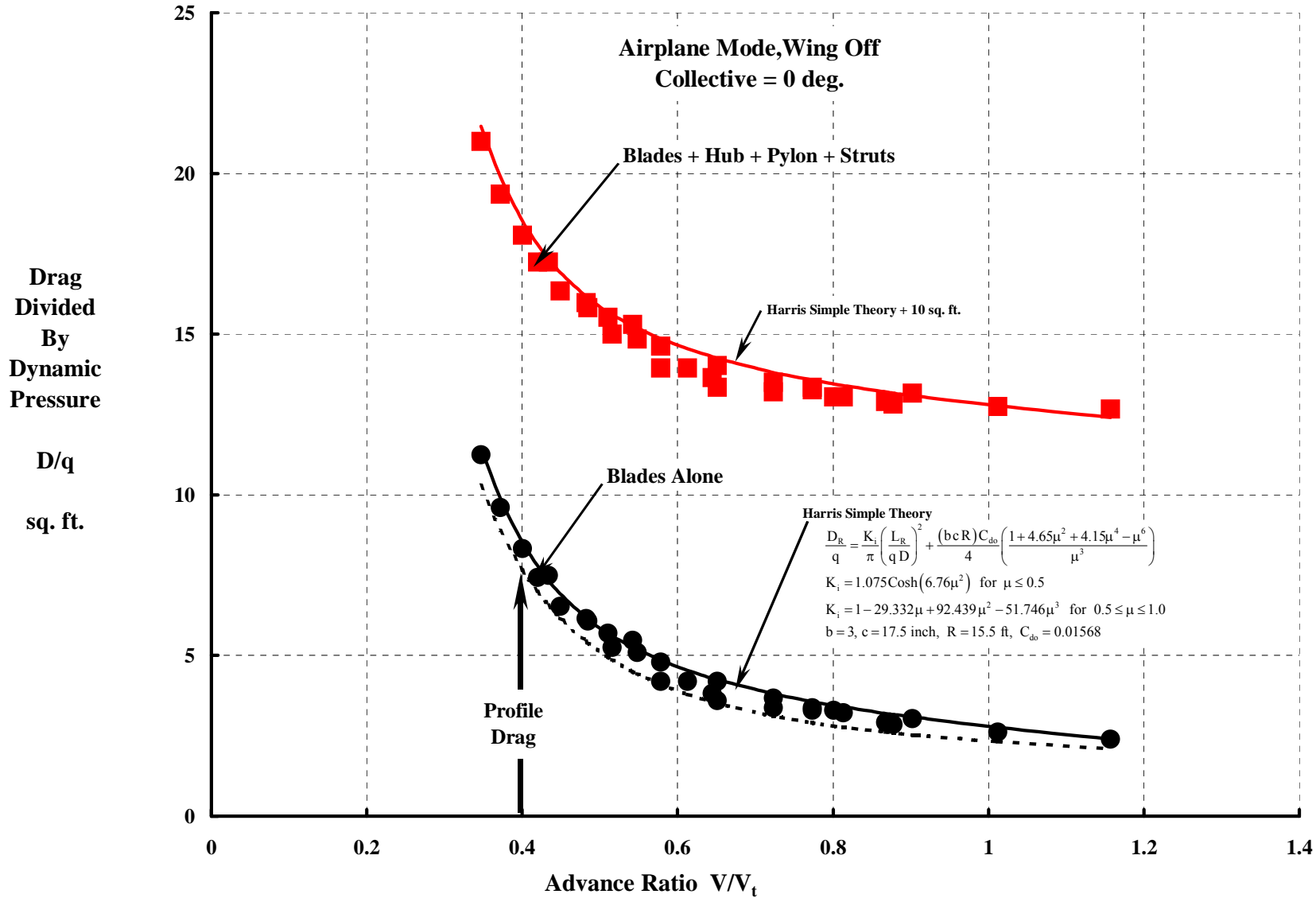
Even In The Autogyro Mode, There Was A Substantial Performance Benefit When The Wing Carried Some Of The Gross Weight

Note: The wing in this test had the area and span of the XV–1's wing, but was rectangular with no washout. Incidence about 7 deg.
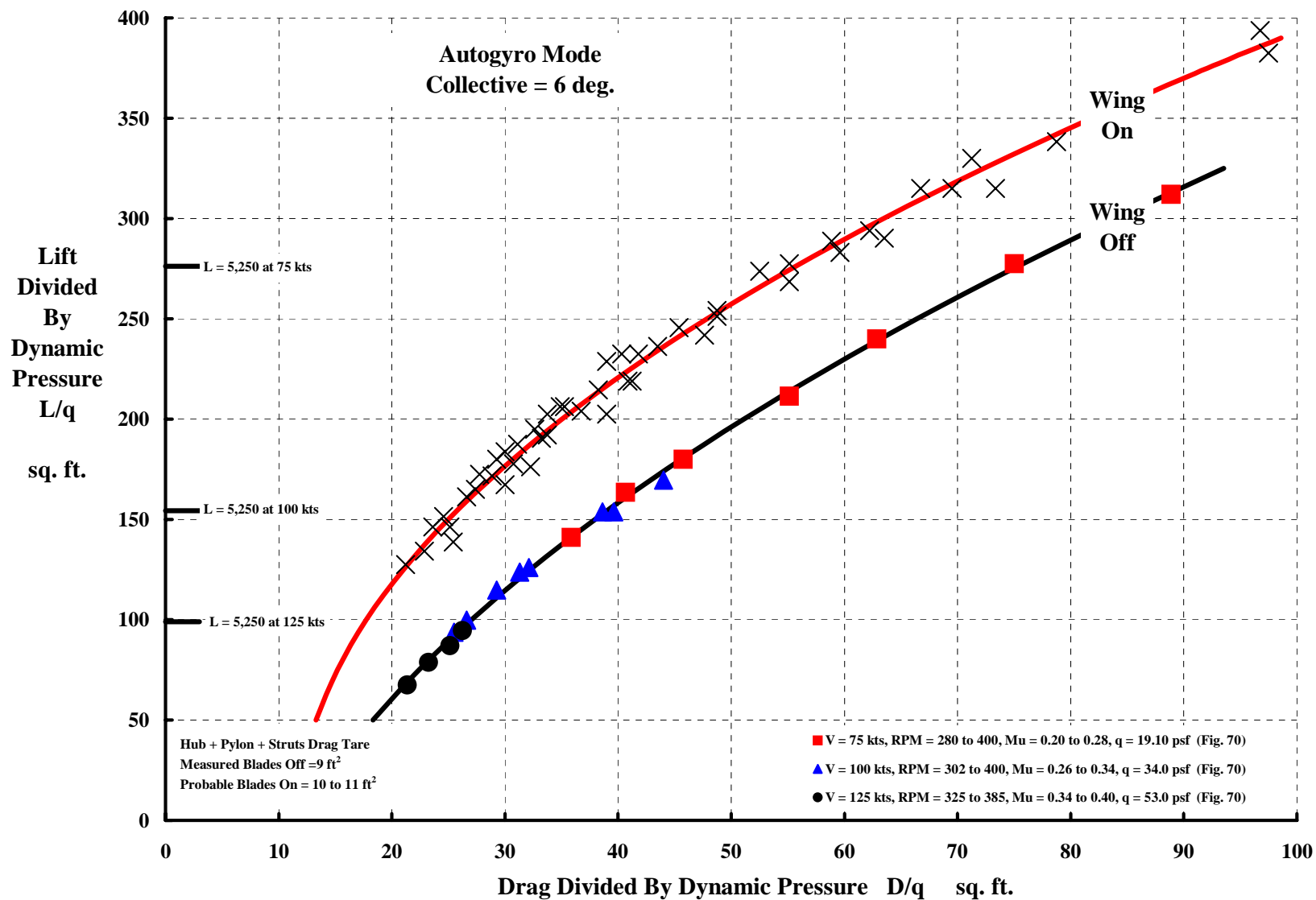

Autogyro Mode
Collective = 6 deg.

Wing On

Wing Off

Lift Divided By Dynamic Pressure L/q sq. ft.

L = 5,250 at 75 kts

L = 5,250 at 100 kts

L = 5,250 at 125 kts

Hub + Pylon + Struts Drag Tare
Measured Blades Off = 9 ft^2
Probable Blades On = 10 to 11 ft^2

Drag Divided By Dynamic Pressure   D/q   sq. ft.

■ V = 75 kts, RPM = 280 to 400, Mu = 0.20 to 0.28, q = 19.10 psf (Fig. 70)

▲ V = 100 kts, RPM = 302 to 400, Mu = 0.26 to 0.34, q = 34.0 psf (Fig. 70)

● V = 125 kts, RPM = 325 to 385, Mu = 0.34 to 0.40, q = 53.0 psf (Fig. 70)

The Transition From Autogyro (325 RPM) To Airplane (180 RPM) Could Easily Be Performed At Any Speed From 110 to 125 knots.

Note: The wing in this test had the area and span of the XV–1's wing, but was rectangular with no washout. Incidence about 7 deg.

Airplane Mode
Collective = 0 deg.

Rotor
RPM = 180

Autogyro
Wing On
Rotor
RPM = 325

L = 5,250 at 110 kts

Airplane
Wing On

Wing Angle of Attack
Approximately

13 deg.
10 deg.
7 deg.

L = 5,250 at 150 kts

Lift Divided By Dynamic Pressure L/q

sq. ft.

L = 5,250 at 175 kts

Airplane
Wing Off

Hub + Pylon + Struts Drag Tare
Measured Blades Off =9 ft^2
Probable Blades On = 10 to 11 ft^2

Drag Divided By Dynamic Pressure   D/q   sq. ft.

LET'S REVISIT AUTOGYROS

First Some History

Cierva, Pitcairn, and Kellett Era (1919 to 1941)
Selection of the Helicopter (1942)
Legacy

Some Technology Aspects

What's in a Name?
Fuselages, Wings, Propellers, Rotors and Trim
Rotor Thrust and Flapping Behavior at High Advance Ratio
Limits to Rotor Lift and Propulsion
To Review Then

XV–1 Re–examination

Full Scale Wind Tunnel Tests in 40 by 80
   Rotor (With & Without Wing)
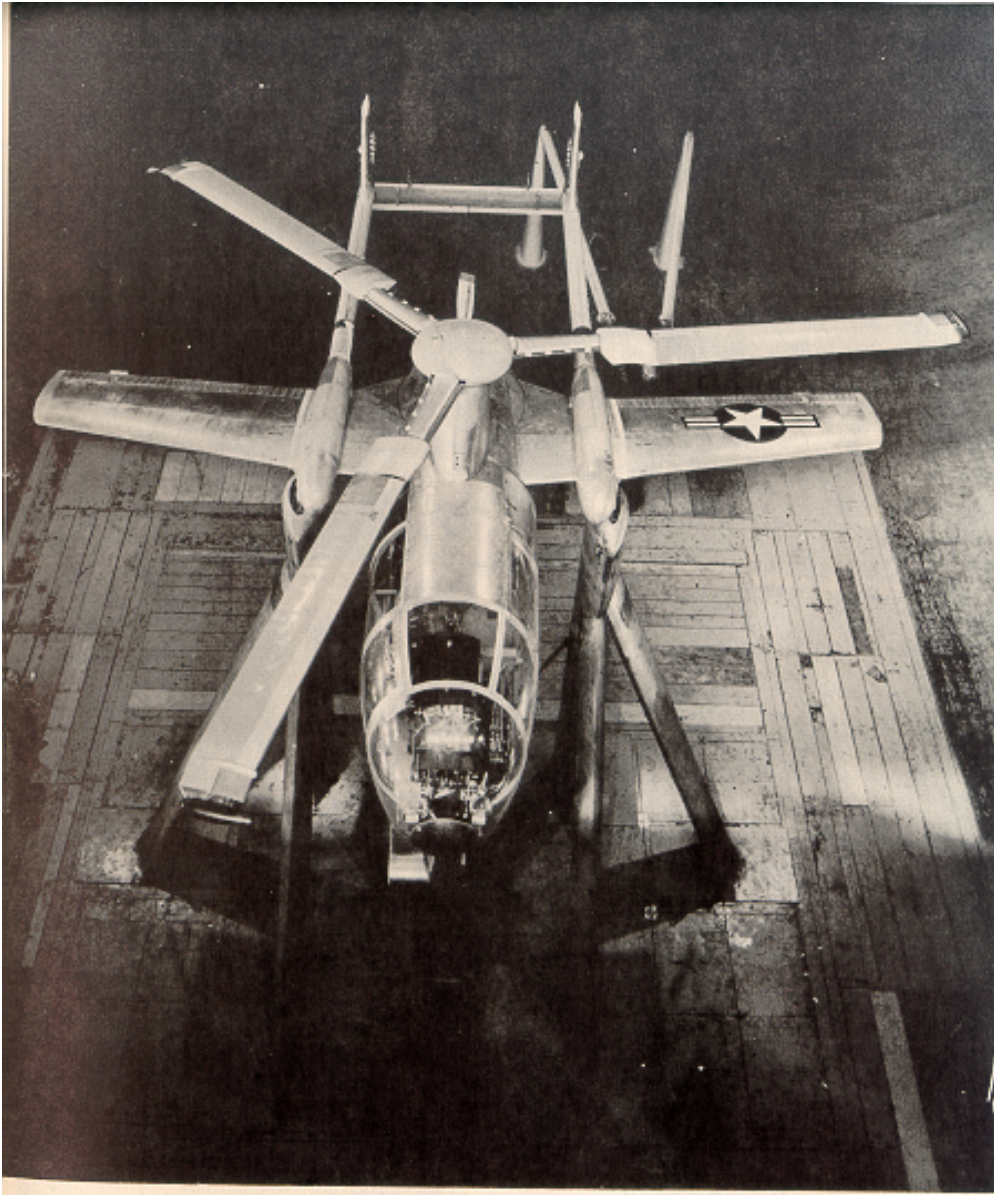   Complete Aircraft
Rotor Stability In Forward Flight
Phase II Flight Evaluation

Concluding Remarks

The XV–1 Was Tested In The NASA 40 by 80 ft WT In April/May 1954.

Configuration Comparison

Parameter	YO–60	XV–1
Gross Weight	2,800 lbs	5,505
Weight Empty	TBD	4,280
ESHP	300 hp	550+Tip Jets
Fuel	36 US gal	80
Disc Loading	1.91 lbs/ft^2	7.34
Rotor	3–Bladed	3–Bladed
Diameter	43.2 ft	31.0
Chord	12.92 in	17.5
Solidity	0.0476	0.090
Tip Speed	370 fps	280 to 665
Wing	No	Yes
Span	na	26 ft
Area	na	100 ft^2
Aspect Ratio	na	6.76
Prop	Fixed Pitch	Fixed Pitch
Diameter	8.50 ft	6.417
Chord	6.0 in	6.5
Solidity	0.075	0.11
Tip Speed	957 fps	665
Performance		
Speed	26 to 134 mph	0 to 160 (dive)
Rate of Climb	1,020 fpm	1,100
Service Ceiling	13,750 ft	na
Range	210 st. miles	na
Cruise Speed	70 to 102 mph	135 to 140

Data Was Acquired At 75, 100, 113, 125 And 150 knots.

Test Matrix
Rotor Off, Prop Off
Rotor On, Prop Off
Rotor On, Prop On
**Note:Tip Burners Never Run**
In Wind Tunnel

Dual Tail Yaw Fans
Fixed Pitch
Hydraulic Motor Power
Reversible RPM
4 Blades per Fan
Diameter = 15 in
Hub diameter = 4.4 in
Blade
   Root chord = 1.84 in
   Tip Chord = 1.54 in

Free Floating Elevator
Spring Loaded Servo Tab
Spring Loaded Trim Tab
Span = 8.12 ft
Chord = 25.0 in
Area = 17.0 ft^2
Dual Vertical Surfaces
Total area = 20.8 ft^2
Rudder area = 3.98 ft^2
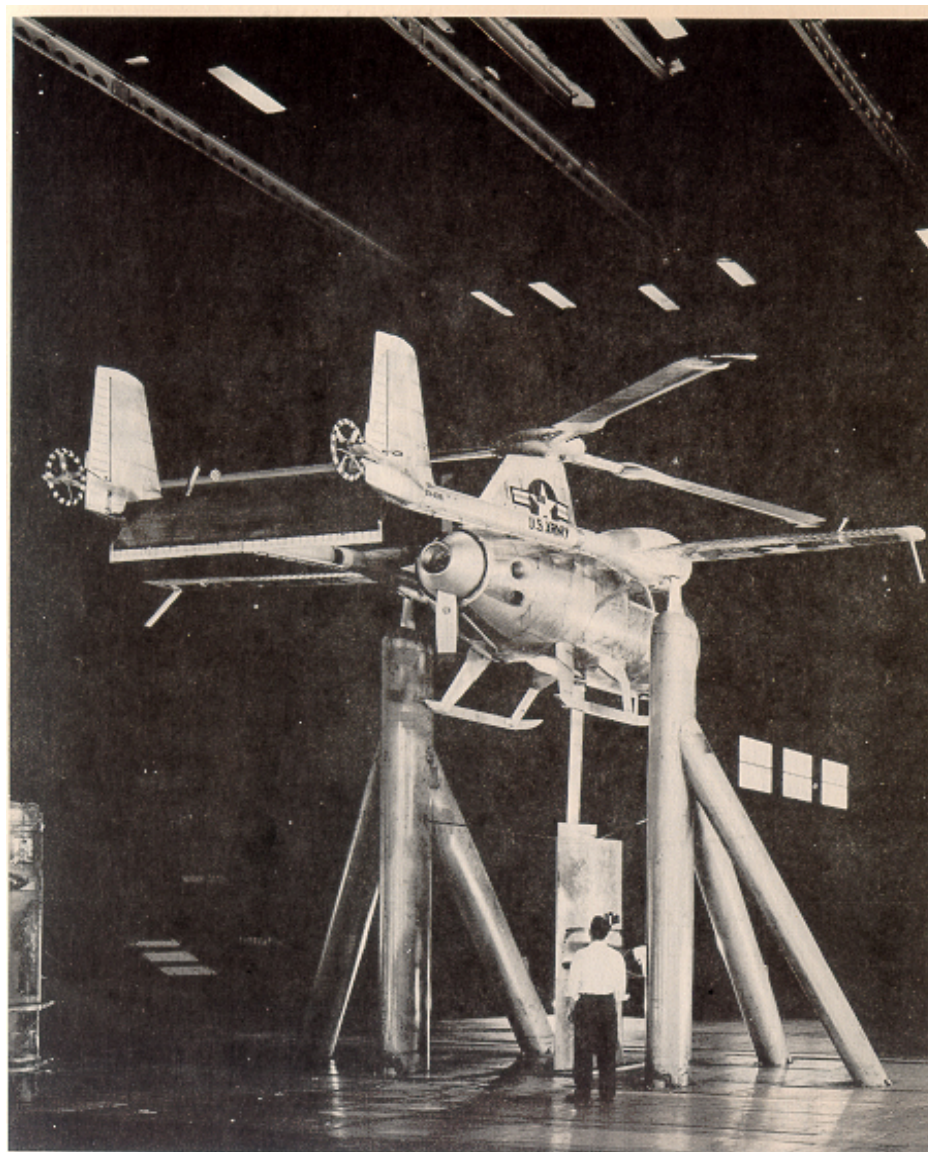
Pressure Jet Tip Drive
1. Air from 2 centrifigal compressors driven by engine.
2. Hub fairing used as plenum.
3. Air ducted up to hub and out blades through pitch change torque tube to tip burners.
3.Fuel ducted out blades to tip burners.

Mostly Estimated Prop Geometry
   McCauley Model 1A500/RHP-77-B
   Fixed Pitch
   Number of blades = 2
   Diameter = 77 in.
   Chord = 6.8 in.
   Solidity = 0.11
   Root cutout = 0.35(r/R)
   Twist Distribution = 0.35/(r/R) rad.
   3/4 Radius Pitch Angle= 33 deg.
   Airfoil lift curve slope = 5.73 per rad.
(Note: Prop RPM = Engine RPM /1.143)

Other Notes
"Flown" from control room
Fixed skid gear
Cockpit door closed
Pitch–Cone coupl. = 2.2^o per 1°
In Helicopter & Autgyro modes.
Pitch–Flap coupl. = 2.2^o per 1°
In Airplane mode.

Ref.: Hickey, David H. "Full–scale Wind Tunnel Tests of the Longitudinal Stability and Control Characteristics of the XV–1 Convertiplane in the Autorotating Flight Range." NACA Research Memorandum No. A55K21a, May 17, 1956

The Free Floating Elevator Was A Master – Piece Of Engineering.

(I really can't tell you how it worked–but it did. Read NACA RM A55K21a for details.)
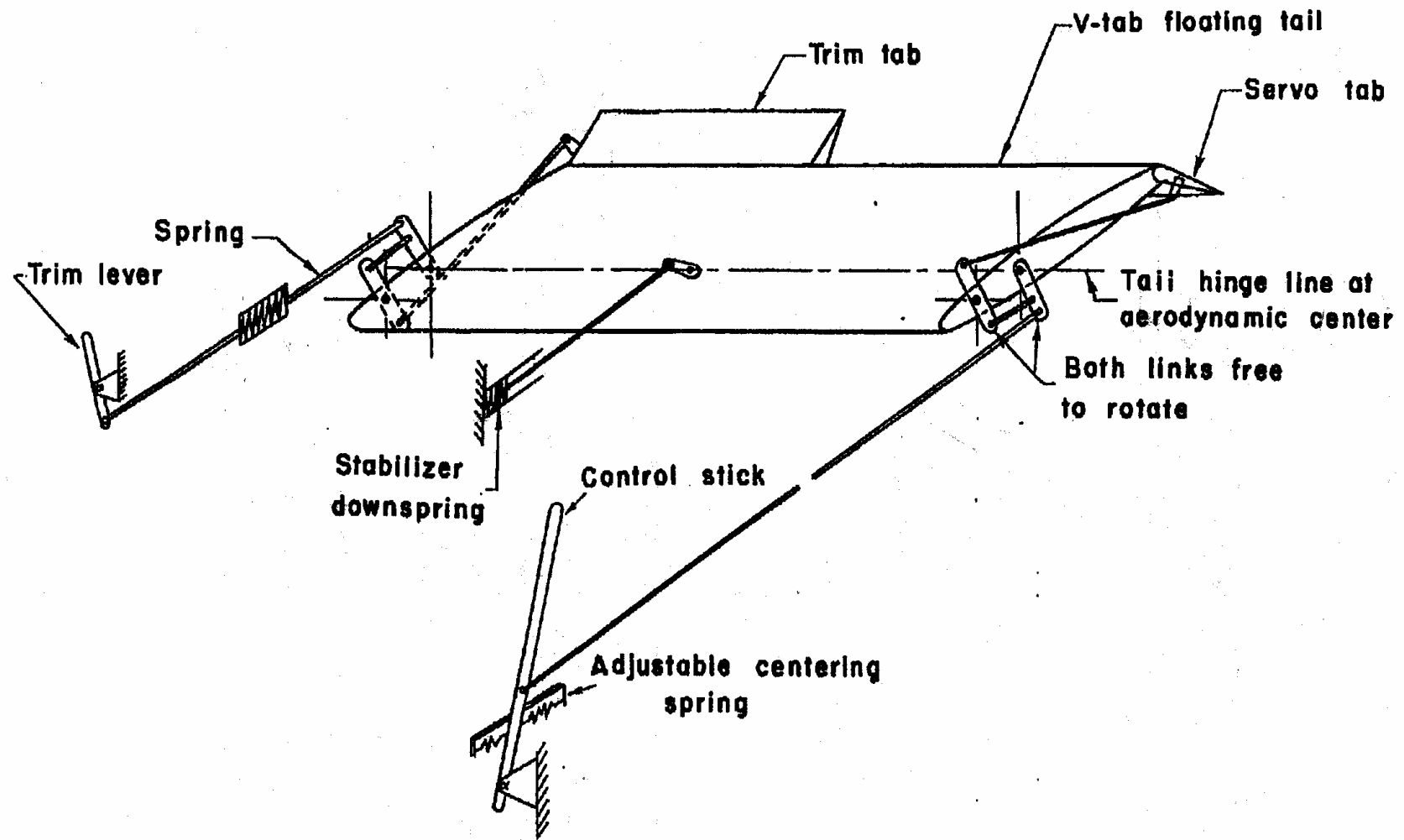
Figure 3.- Sketch of the V-tab horizontal tail and linkages.

The Min. Parasite Drag Area Was About 8.6 ft^2 & GW/fe ≈ 640.

Note: 8.6 ft^2 Is Rotor Blades Off, Prop Off, and Does Not Include Any Drag Due To Lift.

Maximum Lift to Drag Ratios–Prop Off

Base Configuration
Rotor Blades Off
L/D = 7.5 at L/q = 105

Autogiro Configuration
Rotor Blades On, Collective = +6 deg
Nominal Vt = 560 fps
L/D = 5.0 at L/q = 160

Airplane Configuration
Rotor Blades On, Collective = 0 deg
Governor Operating
Nominal Vt = 300 fps
L/D = 6.4 at L/q = 140

All dimensions in feet
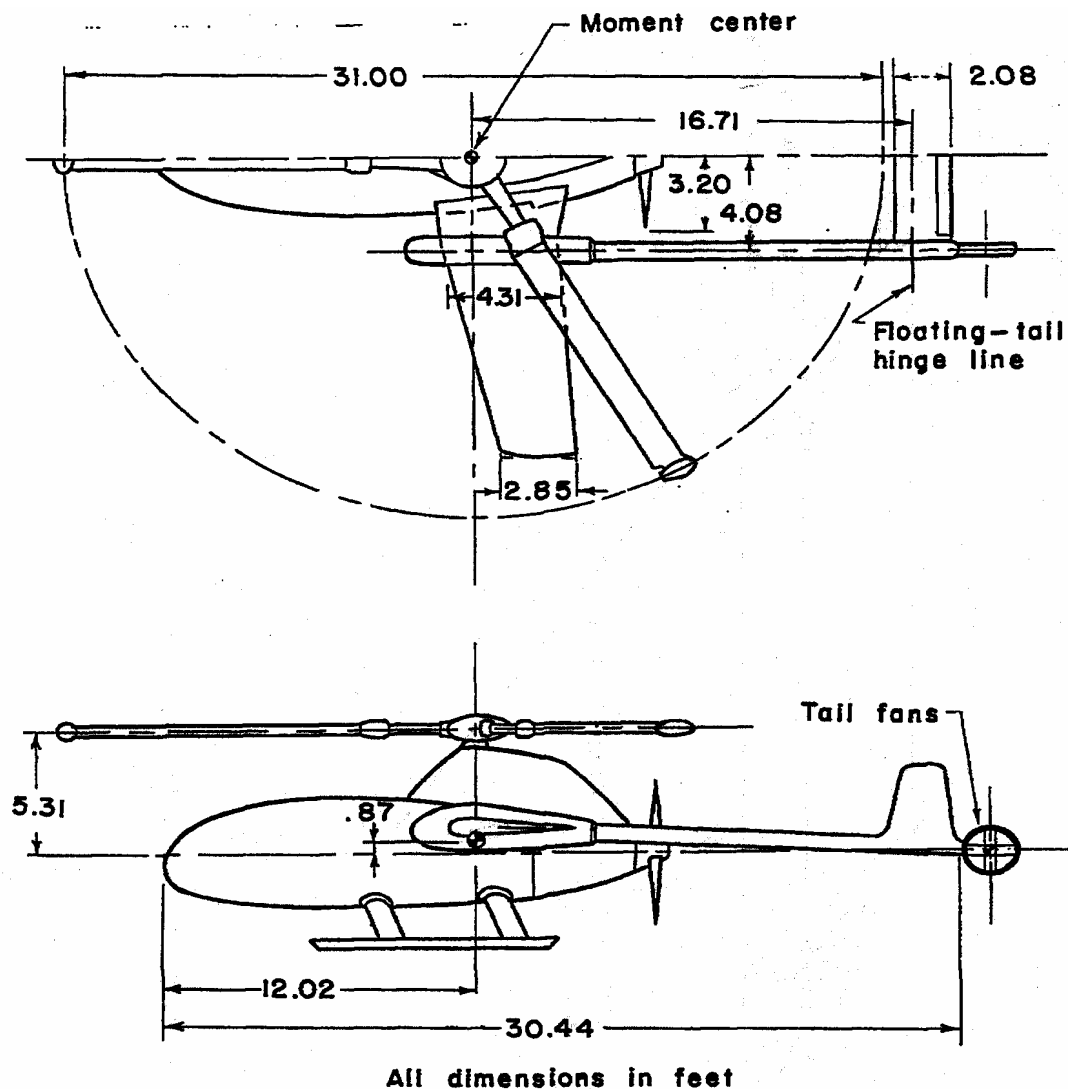
Figure 2.- General arrangement of the XV-1 convertiplane.

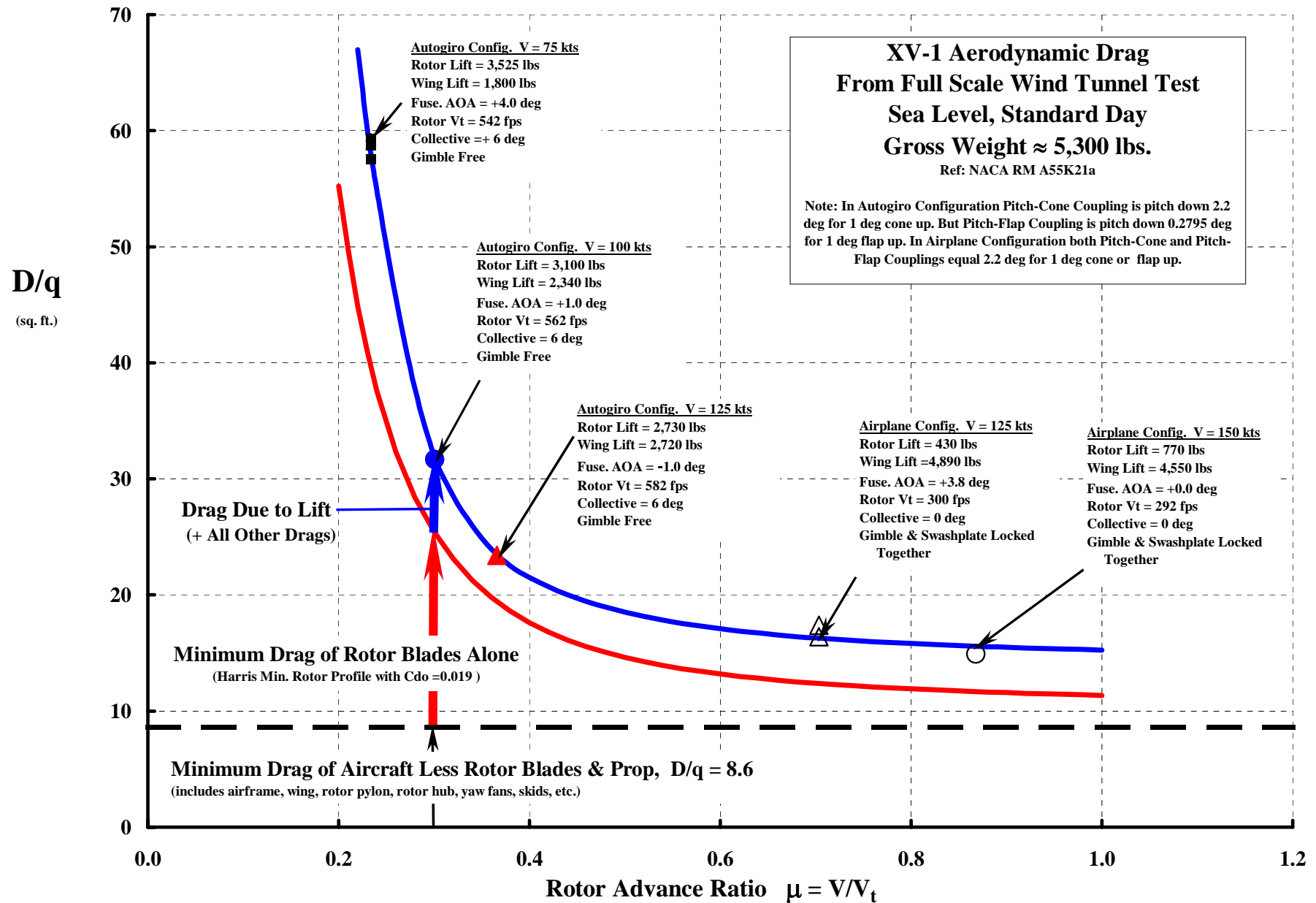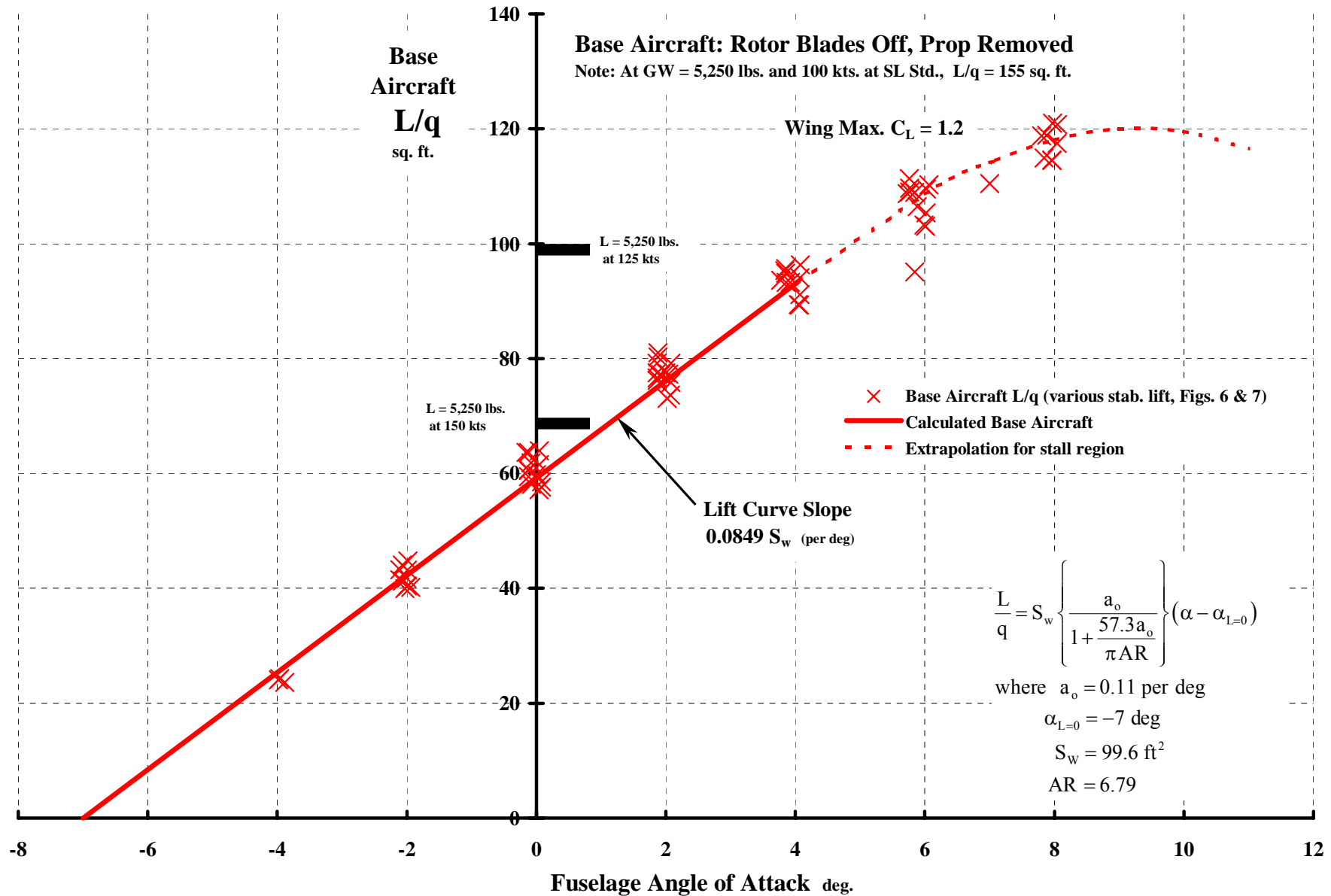# XV–1 D/q At High μ Was Dominated By Skin Friction & Form Drag.

Autogiro Config. V = 75 kts
Rotor Lift = 3,525 lbs
Wing Lift = 1,800 lbs
Fuse. AOA = +4.0 deg
Rotor Vt = 542 fps
Collective =+ 6 deg
Gimble Free

XV-1 Aerodynamic Drag
From Full Scale Wind Tunnel Test
Sea Level, Standard Day
Gross Weight ≈ 5,300 lbs.
Ref: NACA RM A55K21a

Note: In Autogiro Configuration Pitch-Cone Coupling is pitch down 2.2
deg for 1 deg cone up. But Pitch-Flap Coupling is pitch down 0.2795 deg
for 1 deg flap up. In Airplane Configuration both Pitch-Cone and Pitch-
Flap Couplings equal 2.2 deg for 1 deg cone or flap up.

Autogiro Config. V = 100 kts
Rotor Lift = 3,100 lbs
Wing Lift = 2,340 lbs
Fuse. AOA = +1.0 deg
Rotor Vt = 562 fps
Collective = 6 deg
Gimble Free

Autogiro Config. V = 125 kts
Rotor Lift = 2,730 lbs
Wing Lift = 2,720 lbs
Fuse. AOA = -1.0 deg
Rotor Vt = 582 fps
Collective = 6 deg
Gimble Free

Airplane Config. V = 125 kts
Rotor Lift = 430 lbs
Wing Lift =4,890 lbs
Fuse. AOA = +3.8 deg
Rotor Vt = 300 fps
Collective = 0 deg
Gimble & Swashplate Locked
Together

Airplane Config. V = 150 kts
Rotor Lift = 770 lbs
Wing Lift = 4,550 lbs
Fuse. AOA = +0.0 deg
Rotor Vt = 292 fps
Collective = 0 deg
Gimble & Swashplate Locked
Together

Drag Due to Lift
(+ All Other Drags)

Minimum Drag of Rotor Blades Alone
(Harris Min. Rotor Profile with Cdo =0.019)

Minimum Drag of Aircraft Less Rotor Blades & Prop, D/q = 8.6
(includes airframe, wing, rotor pylon, rotor hub, yaw fans, skids, etc.)
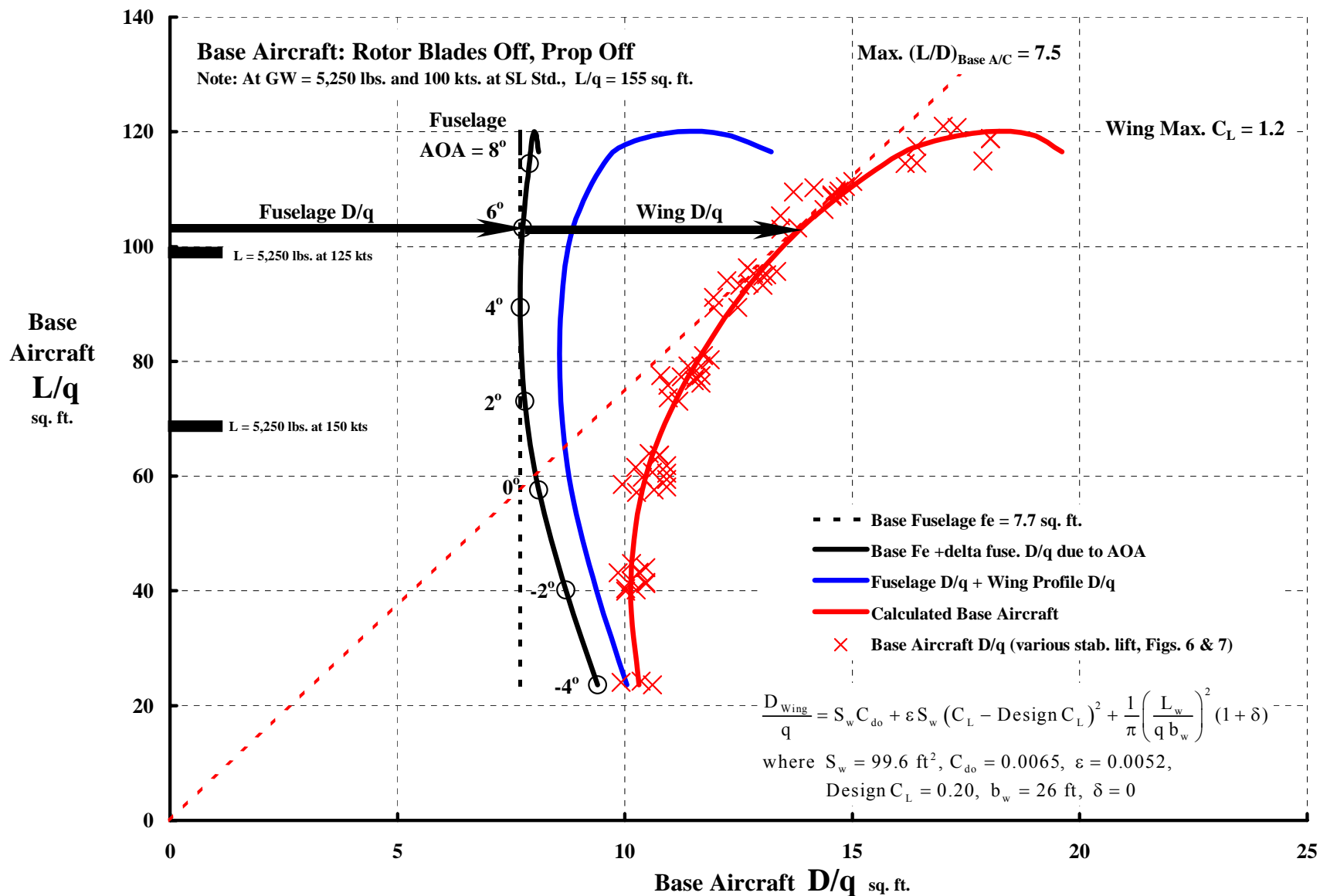
D/q
(sq. ft.)

Rotor Advance Ratio   μ = V/Vt

Without Rotor Blades & Prop, The XV–1 Behaved As A Simple Airplane.

Note: Wing incidence was about 7 degrees.

Base Aircraft L/q sq. ft.

Base Aircraft: Rotor Blades Off, Prop Removed

Note: At GW = 5,250 lbs. and 100 kts. at SL Std., L/q = 155 sq. ft.

Wing Max. C_L = 1.2

L = 5,250 lbs. at 125 kts

L = 5,250 lbs. at 150 kts

Lift Curve Slope 0.0849 S_w (per deg)

$\times$ Base Aircraft L/q (various stab. lift, Figs. 6 & 7)

— Calculated Base Aircraft

- - - Extrapolation for stall region

$$\frac{L}{q} = S_w \left\{ \frac{a_o}{1 + \dfrac{57.3 a_o}{\pi AR}} \right\} (\alpha - \alpha_{L=0})$$

where $a_o = 0.11$ per deg

$\alpha_{L=0} = -7$ deg

$S_W = 99.6$ ft^2

$AR = 6.79$

Fuselage Angle of Attack deg.

The Base Aircraft Lift–Drag Polar Was Quite Typical Of A Small Airplane.

Base Aircraft: Rotor Blades Off, Prop Off

Note: At GW = 5,250 lbs. and 100 kts. at SL Std., L/q = 155 sq. ft.

Max. (L/D)$_{Base A/C}$ = 7.5

Wing Max. C$_L$ = 1.2

Fuselage AOA = 8°

Fuselage D/q

Wing D/q

L = 5,250 lbs. at 125 kts

L = 5,250 lbs. at 150 kts

Base Aircraft L/q sq. ft.

Base Aircraft D/q sq. ft.

- - - Base Fuselage fe = 7.7 sq. ft.
Base Fe +delta fuse. D/q due to AOA
Fuselage D/q + Wing Profile D/q
Calculated Base Aircraft
✕ Base Aircraft D/q (various stab. lift, Figs. 6 & 7)

$$\frac{D_{Wing}}{q} = S_w C_{do} + \varepsilon S_w \left(C_L - \text{Design} C_L\right)^2 + \frac{1}{\pi}\left(\frac{L_w}{q\, b_w}\right)^2 (1 + \delta)$$

where $S_w = 99.6$ ft^2, $C_{do} = 0.0065$, $\varepsilon = 0.0052$,
Design $C_L = 0.20$, $b_w = 26$ ft, $\delta = 0$

There Was Plenty Of Room For Drag Reduction On The XV–1.

Adding The Prop Shifted The Lift–Drag Polar Into The Propulsive Regime.

Note change from lift vs. drag to lift vs. Fx, where Fx = –D. Also, there is little evidence of interference of the prop on the base aircraft.

Base Aircraft: Rotor Blades Off,
Prop Off & On, V = 125 kts,
Engine RPMs of 1,500 & 2,400

Maximums:
$(L/D)_{Base A/C} = 7.5$
Wing CL = 1.2

Aircraft
L/q
sq. ft.

L = 5,250 lbs. at 125 kts

Prop T/q = 15.5 ft^2
Engine RPM = 2,400

Base
Aircraft,
Rotor Off
Prop Off

Calculated
Base Aircraft
+
Prop T/q = 15.5
Engine RPM = 2,400

Calculated
Base Aircraft
+
Prop T/q = 1.5
Engine RPM = 1,500

× Base Aircraft, Prop Off (various stab. lift, Figs. 6 & 7)
— Calculated Base Aircraft, Prop Off
● Base Aircraft, Engine RPM = 1500 (Various stab. lift, Table II)
■ Base Aircraft, Engine RPM = 2,400 (Various stab. lift, Table

Propelling

Dragging

Aircraft **F$_X$/q** sq. ft.

The Rotor Blades Substantially Changed The Aircraft Lift Curve Slope.

Autogyro Configuration. Collective fixed at +6°. Gimbal free. Pitch–cone coupling 2.2° per 1° coning. Pitch–flap coupling 0.2679° per 1° flapping. No governor.

Note: There was substantial interference of rotor downwash on wing. On the order of 2 to 5 degrees angle of attack.

Aircraft L/q sq. ft.

Autogiro Config.: Rotor Blades On, Nominal RPM = 325, Prop Off

L = 5,250 lbs. at 75 kts

× Base Aircraft L/q (various stab. lift, Figs. 6 & 7)

Calculated Base Aircraft

Extrapolation for stall region

■ V = 75 kts, RPM = 289 to 355, Mu = 0.22 to 0.27, q = 19.10 psf (Fig. 8)

▲ V = 100 kts, RPM = 289 to 372, Mu = 0.28 to 0.36, q = 33.96 psf (Fig.8)

● V = 125 kts, RPM = 325 to 372, Mu = 0.35 to 0.40, q = 53.06 psf (Fig.8)

L = 5,250 lbs. at 100 kts

Note: RPM increases (and μ decreases) as angle of attack increases.

L = 5,250 lbs. at 125 kts

Base Aircraft L/q (various stab. lift, Figs. 6 & 7) Lift Curve Slope 0.0849 S_W (per deg)

Fuselage Angle of Attack deg.

Blades Also Substantially Changed The Aircraft Lift–Drag Polar.

Autogyro Configuration. Collective fixed at +6°. Gimbal free. Pitch–cone coupling 2.2° per 1° coning. Pitch–flap coupling 0.2679° per 1° flapping. No governor.

Autogiro Config.: Rotor Blades On, Nominal RPM = 325, Prop Off

Maximum $(L/D)_{Autogiro} = 5.0$

—— Calculated For All Configurations
× Base Aircraft D/q (various stab. lift, Figs. 6 & 7)
■ V = 75 kts, RPM = 289 to 355, Mu = 0.22 to 0.27, q = 19.10 psf (Fig.8)
▲ V = 100 kts, RPM = 289 to 372, Mu = 0.28 to 0.36, q = 33.96 psf (Fig.8)
● V = 125 kts, RPM = 325 to 372, Mu = 0.35 to 0.40, q = 53.06 psf (Fig.8)

L = 5,250 lbs. at 75 kts

L = 5,250 lbs. at 100 kts

Max. $(L/D)_{Base A/C} = 7.5$

L = 5,250 lbs. at 125 kts

Base Aircraft

Note: RPM increases (and μ decreases) as L/q increases.

Base Aircraft + Autorotating Rotor At High Lift and Low μ

L/q sq. ft.

Base Aircraft + Autorotating Rotor At High Lift and Low μ **D/q** sq. ft.

At 75 kts & Eng. RPM = 2,300, The Prop Nearly Got Fx/q To Zero.

Prop RPM = Engine RPM/1.143.
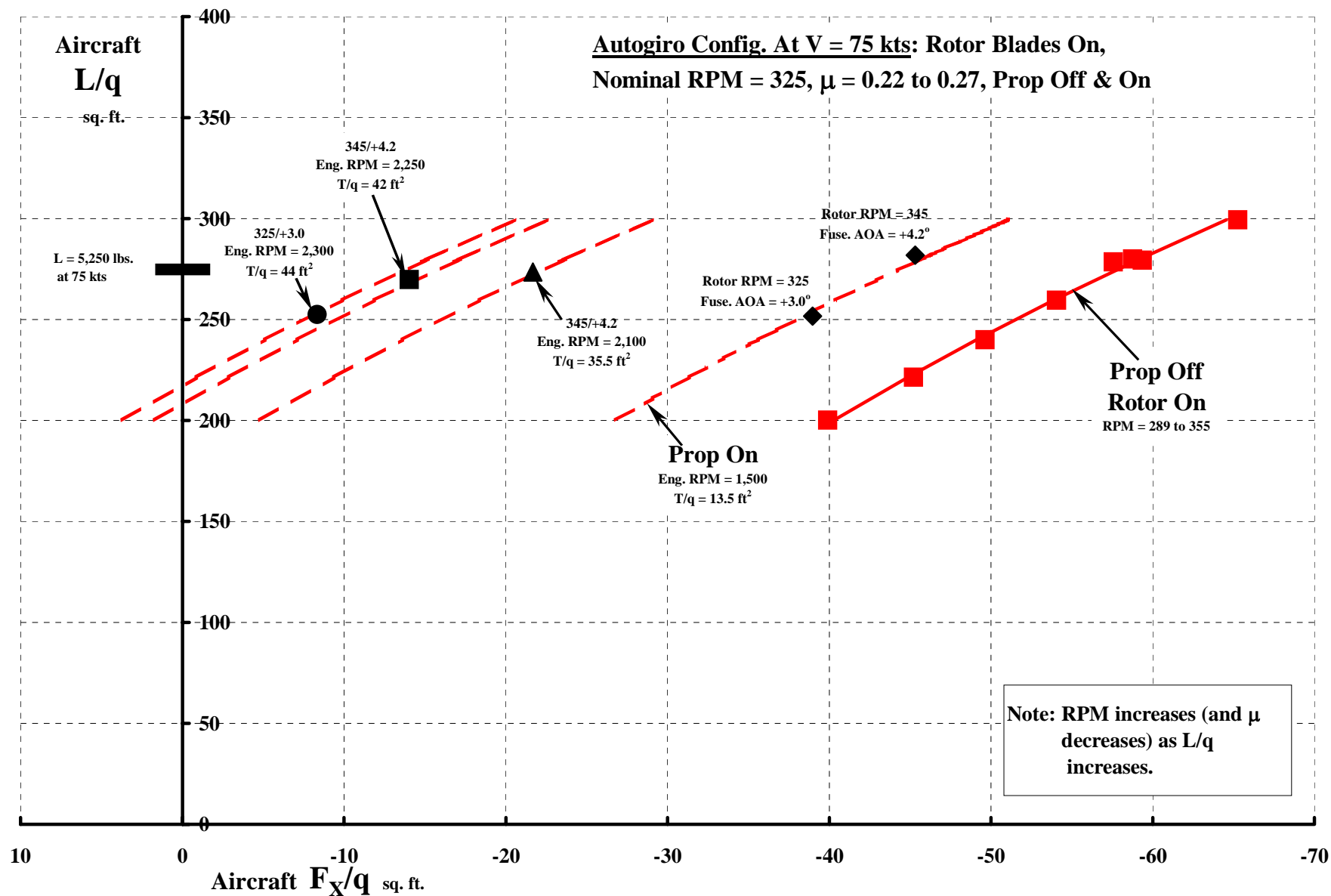
At 100 kts & Eng. RPM = 2,300, Prop Thrust Didn't Quite Overcome Autogiro Configuration Drag At 5,250 lbs Lift.
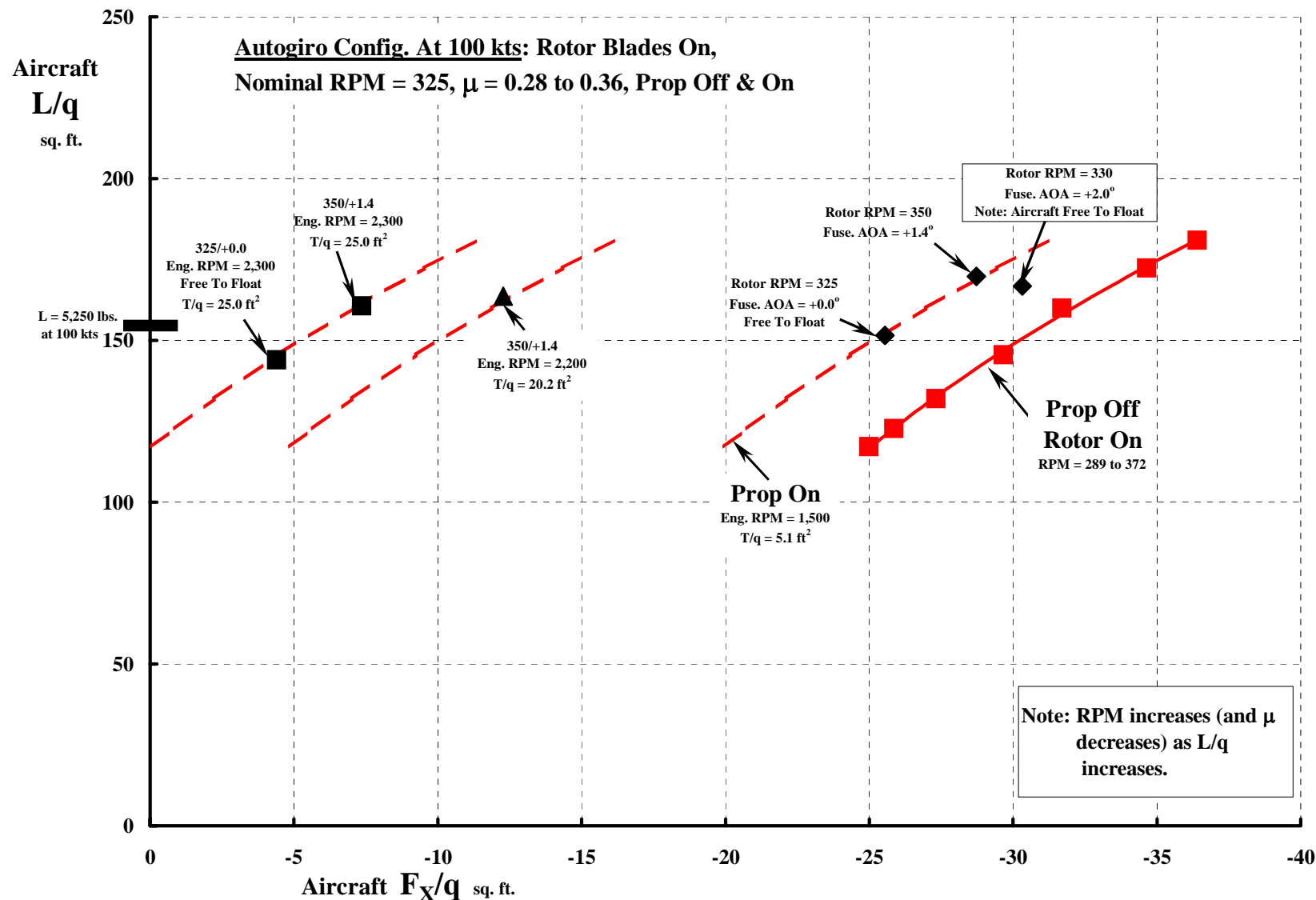
At 125 kts & Eng. RPM = 2,450, Wind Tunnel Data Was Still Showing An Underpowered/Under–Prop'ed XV–1 Autogiro.

Aircraft L/q sq. ft.

Autogiro Config. At 125 kts: Rotor Blades On, Nominal RPM = 325, μ = 0.35 to 0.40, Prop Off & On

330/+0.0
Eng. RPM = 1,500
Free To Float
$T/q = 1.3 \text{ ft}^2$

310/-2.0
Eng. RPM = 2,450
Free To Float
$T/q = 14.8 \text{ ft}^2$

325/-2.0
Eng. RPM = 1,500
Free To Float
$T/q = 1.3 \text{ ft}^2$

L = 5,250 lbs.
at 125 kts

Prop Off Rotor On
RPM = 325 to 372

Note: RPM increases (and μ decreases) as L/q increases.

Aircraft F_X/q sq. ft.
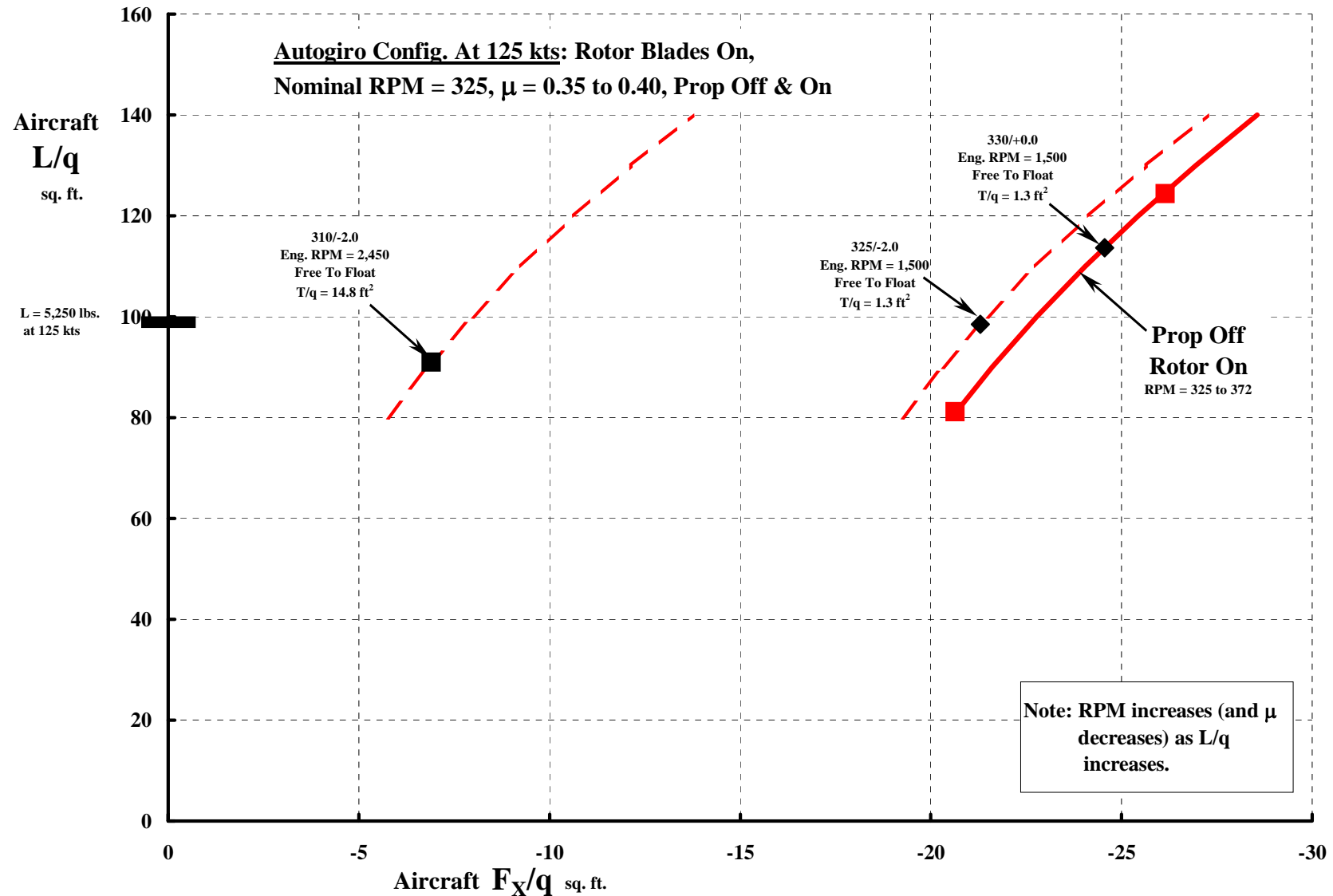
The XV–1 Airplane Configuration Used Pitch–Flap Coupling To Make The Rotor Insensitive to Angle of Attack.

Collective pitch = 0°. Pitch–flap & pitch–cone coupling were both pitch down 2.2° for 1° flap/cone up. Hub & gimbal locked to control stem.

By 125 kts, Wind Tunnel Data Showed The XV–1 Could Be Fully Converted Into Its Lower Drag, High μ Airplane Configuration.

Collective pitch = 0°. Pitch–flap & pitch–cone coupling were both pitch down 2.2° for 1° flap/cone up. Hub & gimbal locked to control stem.

Plot axes and labels:

Y-axis: **Base Aircraft + Autorotating Rotor At Low Lift and High μ   L/q   sq. ft.**

X-axis: **Base Aircraft + Autorotating Rotor At Low Lift and High μ   D/q   sq. ft.**

Maximum $(L/D)_{Base\ A/C} = 7.5$

Airplane Config.: Rotor Blades On, Nominal RPM = 185, Prop Off
Note: At GW = 5,250 lbs. and 100 kts. at SL Std., L/q = 155 sq. ft.

L = 5,250 lbs. at 125 kts

L = 5,250 lbs. at 150 kts

V = 75 kts (Calculated) Rotor Blades On μ = 0.422

V = 125 kts Rotor Blades On μ = 0.73 to 0.76

V = 100 kts Rotor Blades On μ = 0.58 to 0.61

Base Aircraft Rotor Blades Off

Note: RPM increases (and μ decreases) as L/q increases.

At 75 kts, The Aircraft Lift Was Inadequate, But Prop Thrust Was O.K.

Aircraft L/q sq. ft.

Airplane Config. At 75 kts: Rotor Blades On, Nominal RPM = 175, Prop Off & On

L = 5,250 lbs. at 75 kts

Prop Off Rotor On RPM = 289 to 355

Prop On (RPM = 2,450) Rotor On (RPM = 175)

Prop Off Rotor On RPM = 175 (Calc. Only)

● Prop Off, Rotor RPM = 325
— Cal. Prop Off, Rotor RPM = 325
— Cal. Prop Off, Rotor RPM = 175
▲ Prop On, Engine RPM = 2,250
— Cal. + T/q = 46.0 (Engine RPM = 2,250)

Aircraft F_X/q sq. ft.
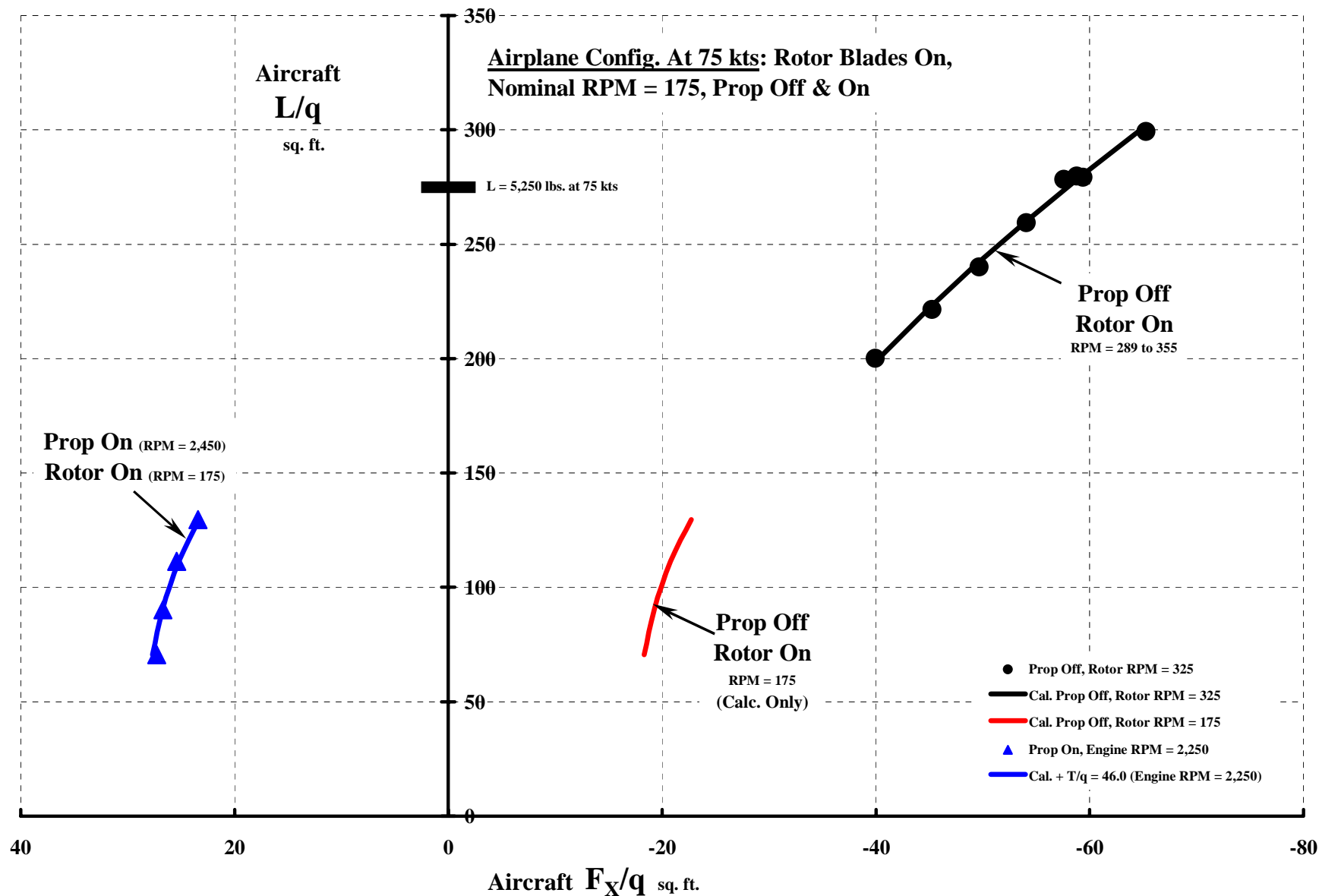
At 100 kts, The Lift Was Still Inadequate, But Prop Thrust Was Still O.K.

Aircraft L/q sq. ft.

Airplane Config. At 100 kts: Rotor Blades On, Nominal RPM = 175, Prop Off & On

L = 5,250 lbs. at 100 kts

Prop Off Rotor On RPM = 175

Prop On (RPM = 2,450) **Rotor On** (RPM = 175)

Prop Off Rotor On RPM = 289 to 372

Increments of Eng. RPM = 50

Prop On Engine RPM 1,500

Prop On Eng. RPM = 0 Stopped Prop D/q = 3.18 ft²

● Prop Off, Rotor RPM = 325
── Cal. Rotor RPM = 325
■ Prop Off, Rotor RPM = 175
── Cal. Rotor RPM = 175
▲ Prop On, Engine RPM = 2,450
── Cal. + T/q = 27.3 (Engine RPM = 2,450)
✕ Prop On, Engine RPM = Varies

Aircraft F_X/q sq. ft.

At 125 kts, XV−1 Lift Was Satisfactory, But Prop Thrust Was Marginal.

At 150 kts, XV–1 Lift Was Satisfactory, But Prop Thrust Was Marginal.
A Drag "Clean–up" Program Was Conducted, Which Found a 20% Reduction Was Possible.
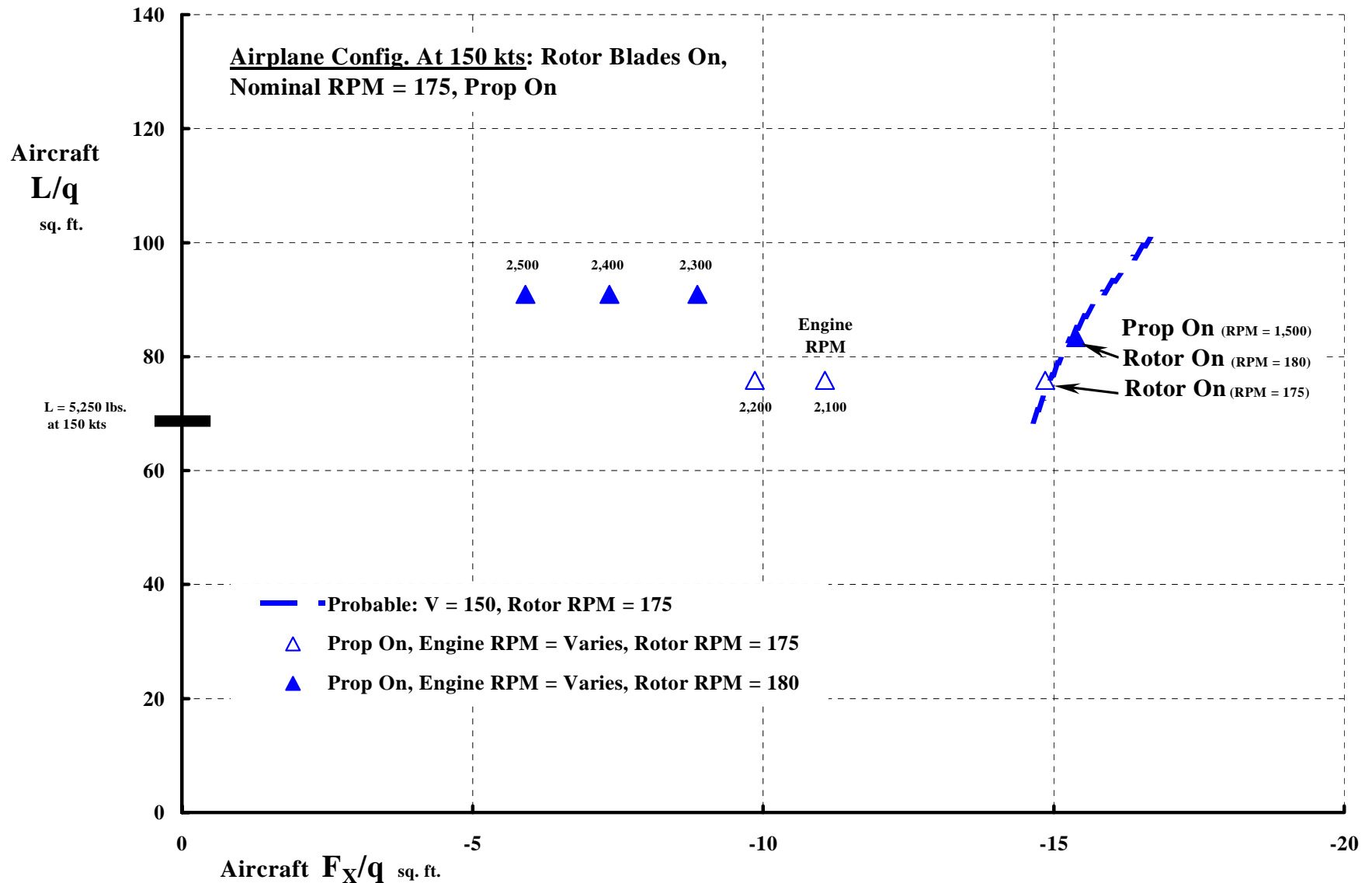
A Possible Approximation Of XV–1 Prop
Thrust Performance Using Estimated Geometry.

Harris Prop Theory
$C_T = 0.050911 - 0.11262\ \lambda$
NASA Contractor Rept 196702
    Eqs. A-77 through A-79
Mostly Estimated Prop Geometry:
    Fixed Pitch
    Number of blades = 2
    Diameter = 77 in.
    Chord = 6.8 in.
    Solidity = 0.11
    Root cutout = 0.35(r/R)
    Twist Distribution = 0.35/(r/R) rad.
    3/4 Radius Pitch Angle= 33 deg.
    Airfoil lift curve slope = 5.73 per rad.
(Note: Prop RPM = Engine RPM /1.143)

Propeller Thrust Coefficient

$$C_T = \frac{T_P}{\rho\,\pi\,R^2 V_t^2}$$

Legend:
- ○ Autogyro V = 75 kts, Fuselage AOA = 4.2 deg
- ■ (magenta) Autogyro V = 75 kts, Fuselage AOA = 3.0 deg
- △ Autogyro V = 100 kts, Fuselage AOA = 1.4 deg
- ✕ Autogyro V = 100 kts, Fuselage AOA = 0.0 deg
- ✳ Autogyro V = 100 kts, Fuselage AOA = 2.0 deg
- ● Autogyro V = 125 kts, Fuselage AOA = -2.0 deg
- + Airplane V = 75 kts, Fuselage AOA = 4.0 deg
- ▲ (red) Airplane V = 100 kts, Fuselage AOA = -1.0 deg
- ▲ (blue) Airplane V = 100 kts, Fuselage AOA = 2.0 deg
- ■ (red) Airplane V = 125 kts, Fuselage AOA = 2.0 deg
- ● (red) Airplane V = 150 kts, Fuselage AOA = 0.0 deg
- ○ (red) Airplane V = 150 kts, Fuselage AOA = 2.0 deg
- ◆ Derived From THP Available
- —— Harris Prop Theory

Prop Inflow Ratio, $\lambda = V/V_t$

Unfortunately, Both The Prop Shaft Strain Gage & The Engine Torque Meter Broke. Prop Power Was Estimated Per Engine Chart.

Note: Engine chart horsepower minus 9 percent for cooling and gearing losses. Viewed as crude by Hohenemser.
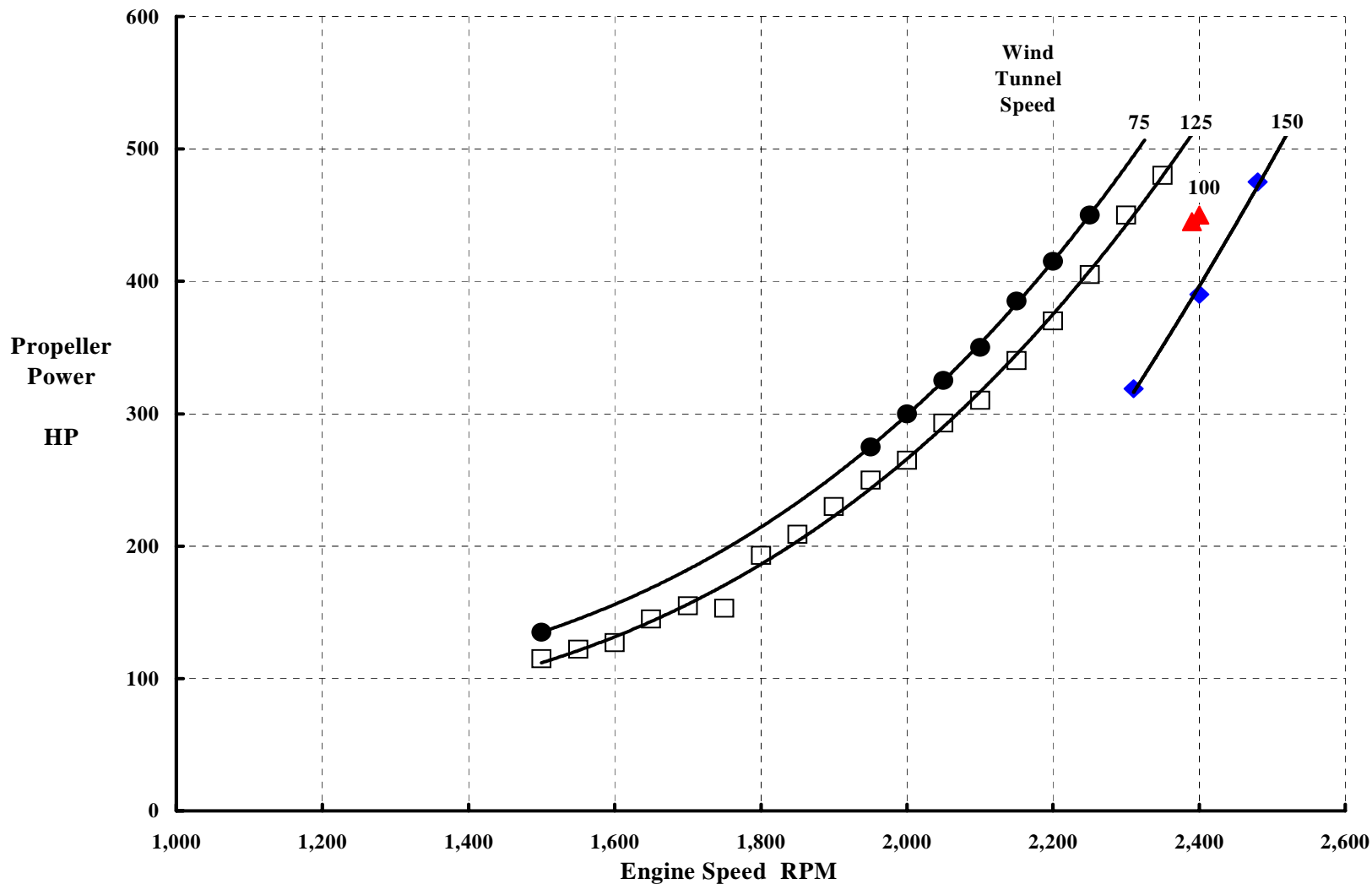
Ref: Figure 30 of Hohenemser's MAC Report No. 3599

This "Ballparks" The XV–1 Propeller Power Required.

$$C_{PProp} = \frac{550(0.91\,BHP)}{\rho\,\pi\,R^2\,V_t^3} = 0.01496 + 0.004202\lambda - 0.3129\lambda^2 + 1.2204\lambda^3 - 1.5175\lambda^4$$

Propeller Power Coefficient

C_{PProp}

Profile Power

Induced Power

Propulsive Power

Engine Chart Horsepower Minus 9%
For Cooling and Gear Losses
Ref: Fig. 30, MAC Report 3599

Harris Prop Theory
C_T = 0.50911 - 0.11262 λ
NASA Contractor Rept 196702
    Eqs. A-77 through A-79
Mostly Estimated Prop Geometry:
    Fixed Pitch
    Number of blades = 2
    Diameter = 77 in.
    Chord = 6.8 in.
    Solidity = 0.11
    Root cutout = 0.35(r/R)
    Twist Distribution = 0.35/(r/R) rad.
    3/4 Radius Pitch Angle= 33 deg.
    Airfoil lift curve slope = 5.73 per rad.
    (Note: Prop RPM = Engine RPM /1.143)

Prop Inflow Ratio, λ = V/Vt

XV–1 Prop Efficiency Was Not Very Promising As Viewed By NACA RM A55K21a Or Engine Chart Data Or Theory.

Propeller Efficiency

η_P

Derived From Fig. 22 of NACA RM A55K21a

V, kts	Vt. fps	THP	BHP
75	704	280	500
100	704	330	500
125	704	320	500
150	704	310	500

Engine Chart Horsepower Minus 9% For Cooling and Gear Losses Ref: Fig. 30, MAC Report 3599

Harris Prop Theory

$$\eta_P = \frac{\lambda C_T}{C_{PProp}} = \frac{\lambda(0.050911 - 0.11262\lambda)}{0.01496 + 0.004202\lambda - 0.3129\lambda^2 + 1.2204\lambda^3 - 1.5175\lambda^4}$$

Prop Inflow Ratio, $\lambda = V/Vt$
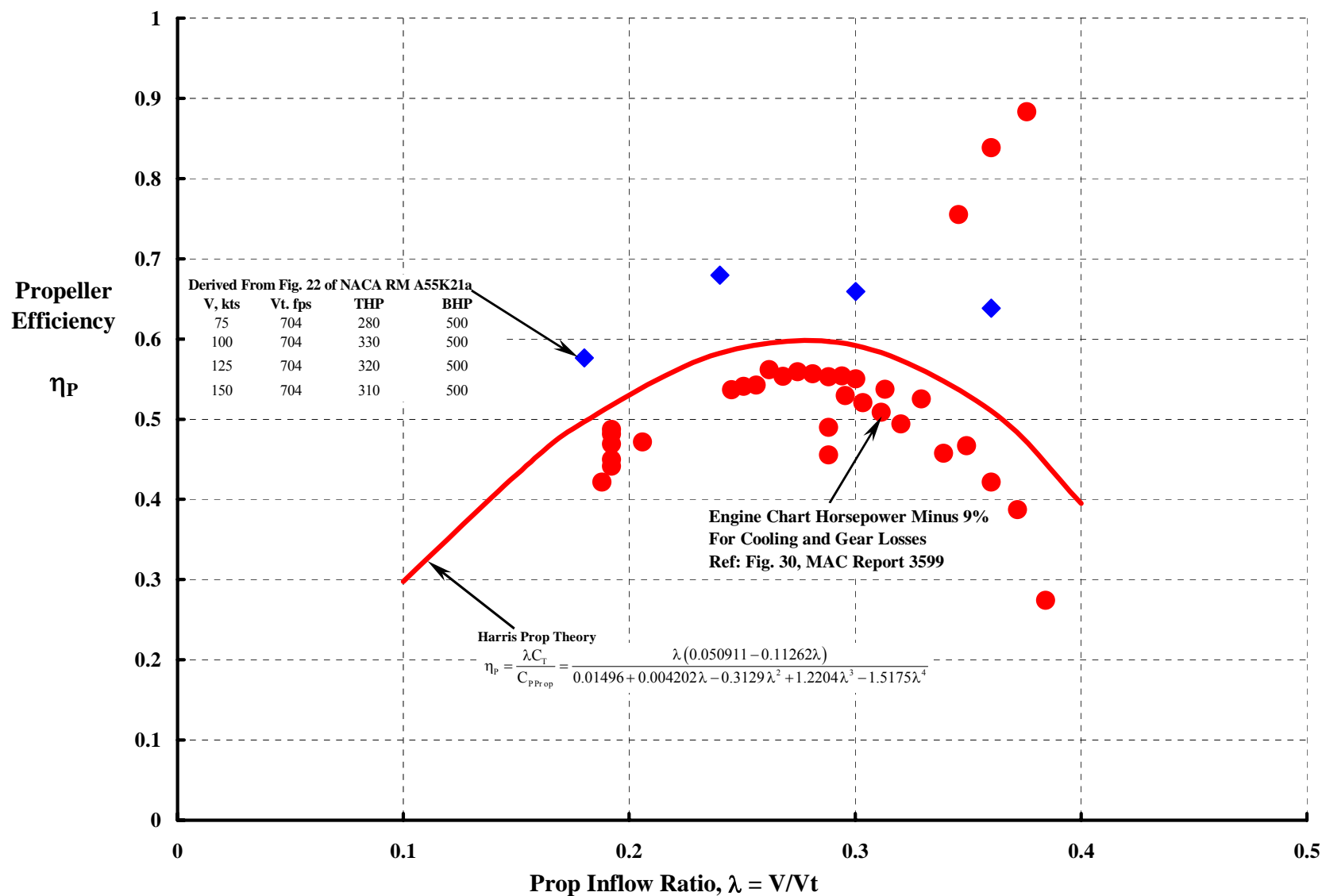
Some Thoughts So Far.

1. Kurt Hohenemser 1949 AHS Forum: "The characteristics of the combined rotary wing and fixed wing system are attractive enough to warrant serious consideration of this type of aircraft."

2. Fred Doblhoff 1950 AHS Forum: Advocates his long held belief that a pressure jet tip drive for the rotor of the compound rotary–fixed wing transport aircraft. This view was shared by J. Bennett at the Fairey Aviation Company, Ltd. In England and Mr. G Lepére in France.

3. Hohenemser 1950 IAS Annual Meeting: Convincingly shows that pitch–cone coupling alone (no pitch–flap coupling) offers significant improvements for rotorcraft stability.

4. Helicopter Division, McDonnell Aircraft Corp 1951: One of three winners of the Air Force convertible aircraft competition. The Bell XV–3 was another winner. (Sikorsky's 1 bladed, stowed rotor was to be the XV–2.)

5. Hohenemser 1952 AHS Forum (After 9 Model Rotor and 6 Model XV–1 Tests):

    a. "Actually in a compound aircraft the drag of pylon and hub is of more importance than the drag of the rotating blades."

    b. "Operation at higher advance ratios requires either an automatic and very sensitive rotor angle of attack control or a torque control where the rotor speed is kept more or less constant by transmitting torque to the rotor."

    c. "A large number of test runs within a wide range of Reynold's Number have definitely established the fact that for our specific case [Lock No. = 5, pitch–flap ratio of 2.25] the flapping motion becomes unstable between an advance ratio of 1.5 and 1.6."

    d. "The problems mentioned here [his paper] are only a few out of a much larger number of aerodynamic and dynamic problems which have to be solved for a successful development of a compound rotary–fixed wing aircraft."

6. Hohenemser 1955 AHS Forum (After 12 More Wind Tunnel Tests–Both Model and Full Scale):

    a. "The total weight increase of the convertiplane over the helicopter is five percent. This estimate is in disagreement with statements made in two recent publications (References 2 and 3) according to which convertiplanes would weigh 20 to 30 percent more than comparable helicopters.."

    b. "In hovering we have to add a download of seven percent from the wing so that the hovering lift will have to be increased by 12 percent" [7% download + 5% weight growth]

<u>Some Thoughts So Far (Concluded).</u>

c. "In rotors without lag hinges……the only safe method of avoiding mechanical instability especially in helicopters or convertiplanes with a wide range of operational rotor speeds is to design the blades sufficiently stiff in chordwise bending so that the maximum obtainable rotor rpm will be below the first chordwise blade bending frequency."

d. "Efficient pressure jet rotors require tip speeds of 650 to 700 feet per second………"

e. "The dynamic design criterion [stiff inplane with high tip mass at 650 to 700 fps tip speed] is the main reason why the XV–1 rotor has a blade solidity of 0.09 and a rotor disc loading of seven pounds per square foot."

f. "Part of the weight increase of the XV–1 type rotor as compared to a conventional three or more bladed rotor of same diameter and blade area stems from……..obtaining the rotor control stiffness and blade torsional stiffness necessary for high speed unloaded rotor operation."

g. "We are quite proud that after considerable efforts we finally managed to obtain such favorable blade dynamic conditions….The reward for these efforts came when we found that measured blade fatigue stresses in airplane flight were, in spite of the high advance ratio, considerably lower than in helicopter flight."

h. "Another dynamic problem I want to discuss briefly is the blade flapping instability at high advance ratio. Here I first have to apologize for an erroneous conclusion I gave you three years ago with respect to this subject."

i. "As to the XV–1 characteristics with respect to blade flapping stability, I would like to mention that the full scale rotor was operated in the 40- by 80- foot NACA wind tunnel in Moffett Field up to maximum tunnel speed of 200 knots corresponding to 1.2 advance ratio without any signs of beginning blade flapping instability."

j. "At this occasion I might mention that the experience with our dynamic quarter scale wind tunnel model was gratifying. The full scale wind tunnel tests confirmed almost all the data previously obtained from the quarter scale model tests within very reasonable margins."

k. "In summary……….Nothing has come up so far which would reflect unfavorably on the principle of the unloaded rotor convertiplane with pressure jet drive and I am confident that the final evaluation of the XV–1 experience will confirm my belief in the basic soundness of this type of aircraft for the applications in many fields."

7. Helicopter Division, McDonnell Aircraft Corp July 1955: First official flight of XV–1, Ship 1. (This was some 2 years before the Nov. 1957 official 1st flight of the Rotodyne Demonstrator by The Fairey Aviation Co., Ltd.)

LET'S REVISIT AUTOGYROS

First Some History

Cierva, Pitcairn, and Kellett Era (1919 to 1941)
Selection of the Helicopter (1942)
Legacy

Some Technology Aspects

What's in a Name?
Fuselages, Wings, Propellers, Rotors and Trim
Rotor Thrust and Flapping Behavior at High Advance Ratio
Limits to Rotor Lift and Propulsion
To Review Then

XV–1 Re–examined

Full Scale Wind Tunnel Test in 40 by 80
Rotor (With & Without Wing)
Complete Aircraft
→ Rotor Stability In Forward Flight
Phase II Flight Evaluation

Concluding Remarks

Frequency Placement Of 1st Chordwise And 1st Flapwise Elastic Modes .

FIG. 4
Lowest horizontal and vertical bending frequency vs. rpm
for XV-1 rotor blades.
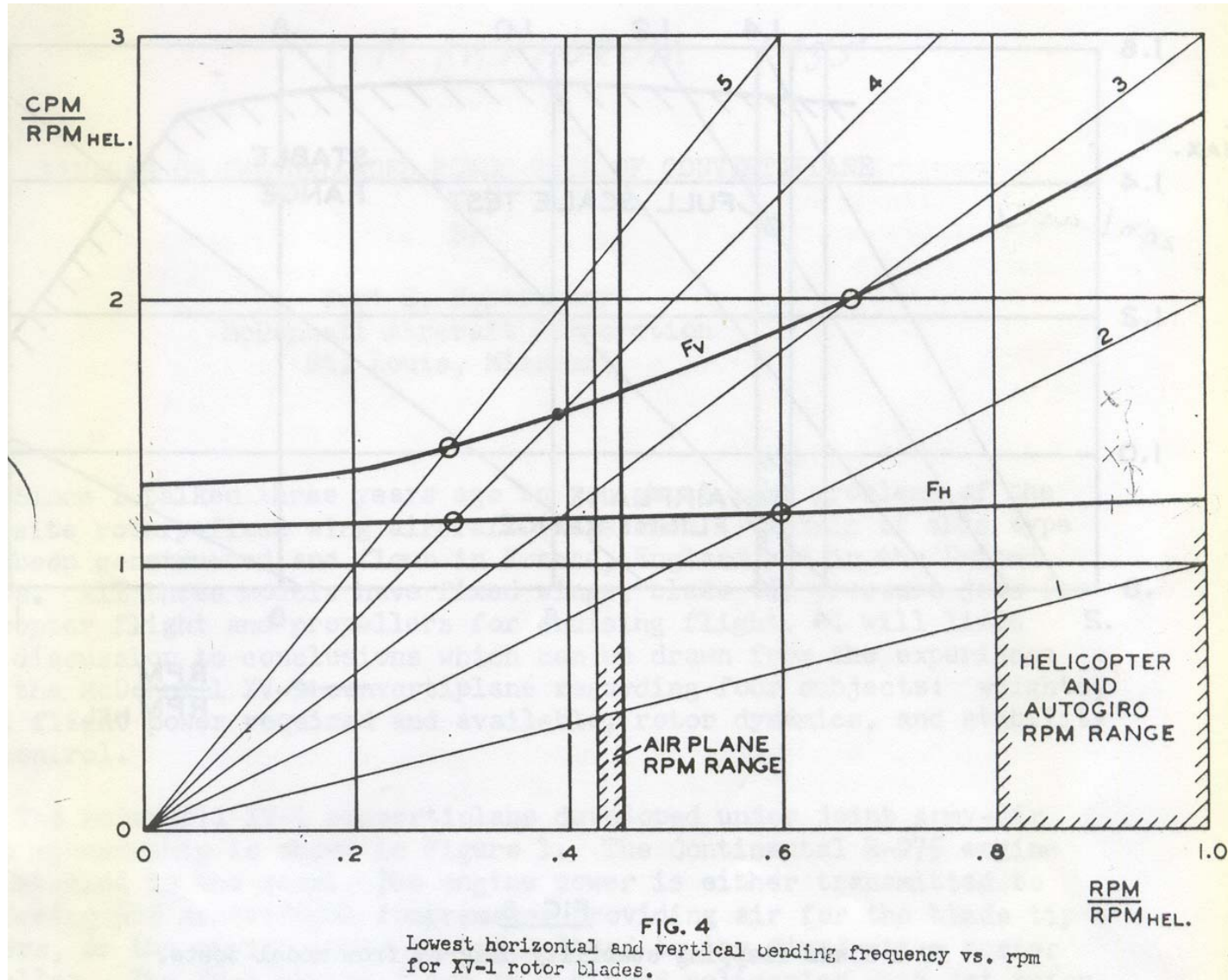
Nominal Rotor Tip Speeds & RPMs

Helicopter
Vt = 660 fps
RPM = 406

Autogiro
Vt = 520 fps
RPM = 320

Airplane
Vt = 280 fps
RPM = 172

Ref: K. Hohenemser "Remarks on the Unloaded Rotor Type Convertiplane" 11th AHS Forum, May 1955

One Of The 8 foot Diameter Models Of The XV–1 Rotor System.

Note: Pitch link azimuth point shown at advance angle A = +15 degrees, Model 2 test conducted with A = −15 degrees. Marks's referred to several 8/31 scale models of the XV–1. Full Scale, XV–1 R = 15.5 feet and c = 17.5 inch.
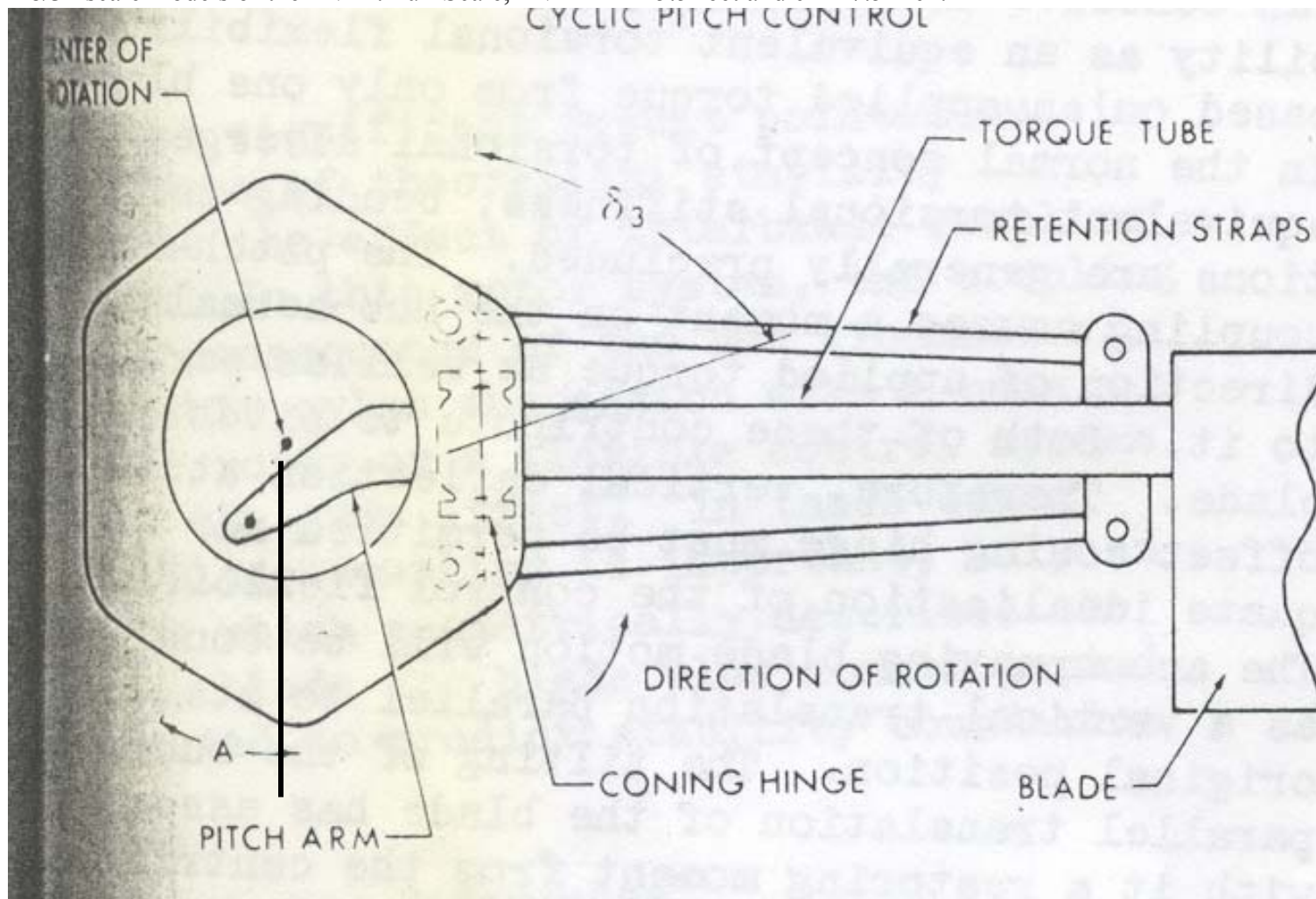
Parameter	Model 2
Lock Number	4.2
Pitch-cone ratio	1.7
Advance angle (A) deg.	-15
Coning hinge offset	0.061 R
Outer strap spacing	0.038 R
Inner strap spacing	0.060 R
Strap length	0.24 R
Blade feathering axis	0.23 c
First hinge–free vertical bending at zero rpm	1.42
First mode cantilever torsion at zero rpm	5.63
First inplane cantilever bending at zero rpm	1.30

Ref: Perisho, C.H. et al, "A comparison of Detailed and Simplified Methods of Analysis of Rotor Stability in Forward Flight with Model Test Results." 18th AHS Forum, 1962

Model 2 Of The XV–1 Rotor System Was A Dynamically Scaled Model.

Note: Dimensions are scaled by radius. Model radius R = 4 ft, Full scale XV–1 radius R = 15.5 ft.

DIRECTION OF ROTATION

FEATHERING, ELASTIC AXES

STRAP RETENTION FAIRING

OUTBOARD RETENTION FAIRING

HUB

1.0

.023

.0938

IDEALIZED BLADE PLANFORM
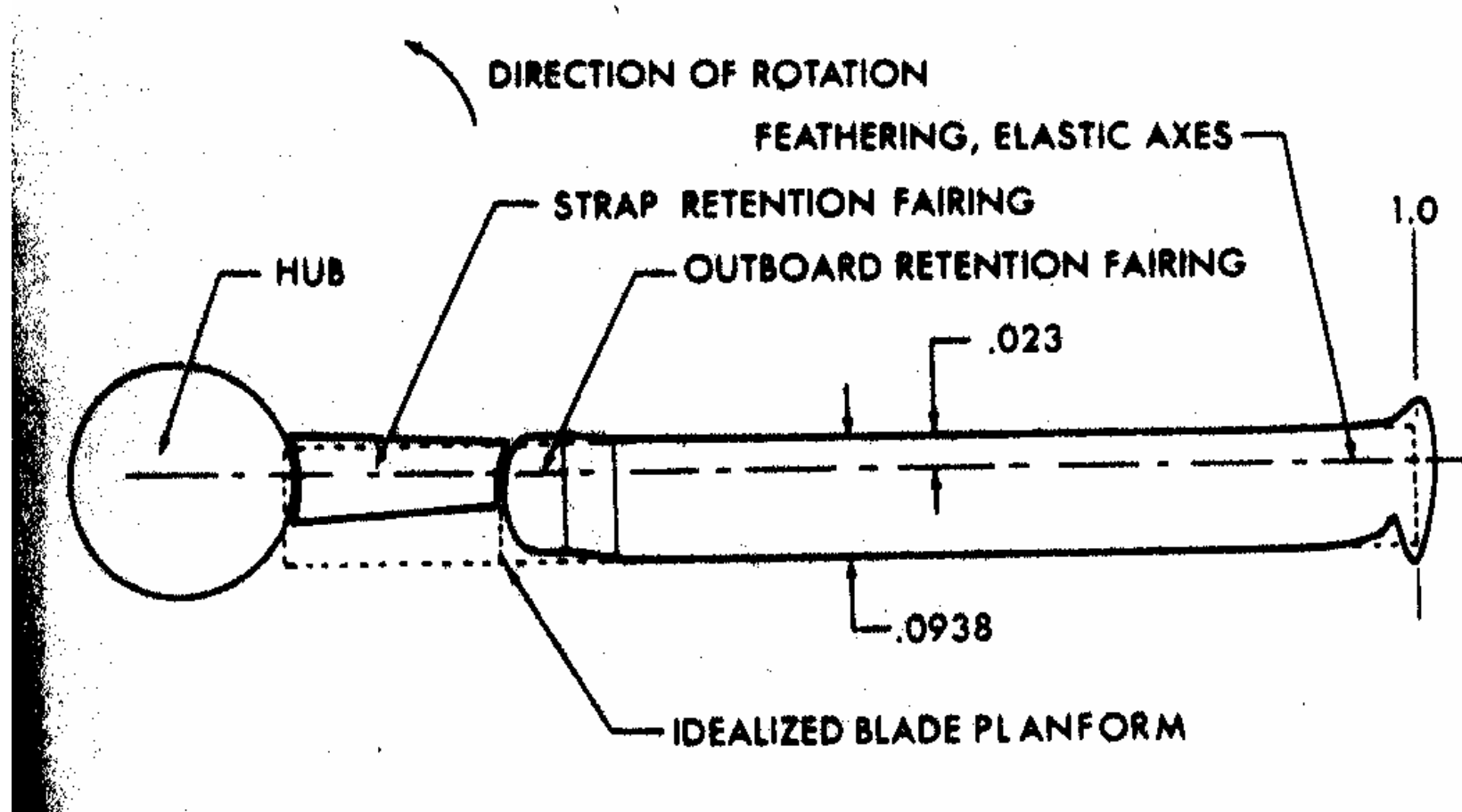
Ref: Perisho, C.H. et al,

C. H. Perisho's Sketch Of The 8 foot Model Rotor Hub Leaves Out A Lot Of Details About The Full Scale XV–1 "Hub."

Note: A more complete examination of the hub follows in Phase II Flight Evaluation discussion.
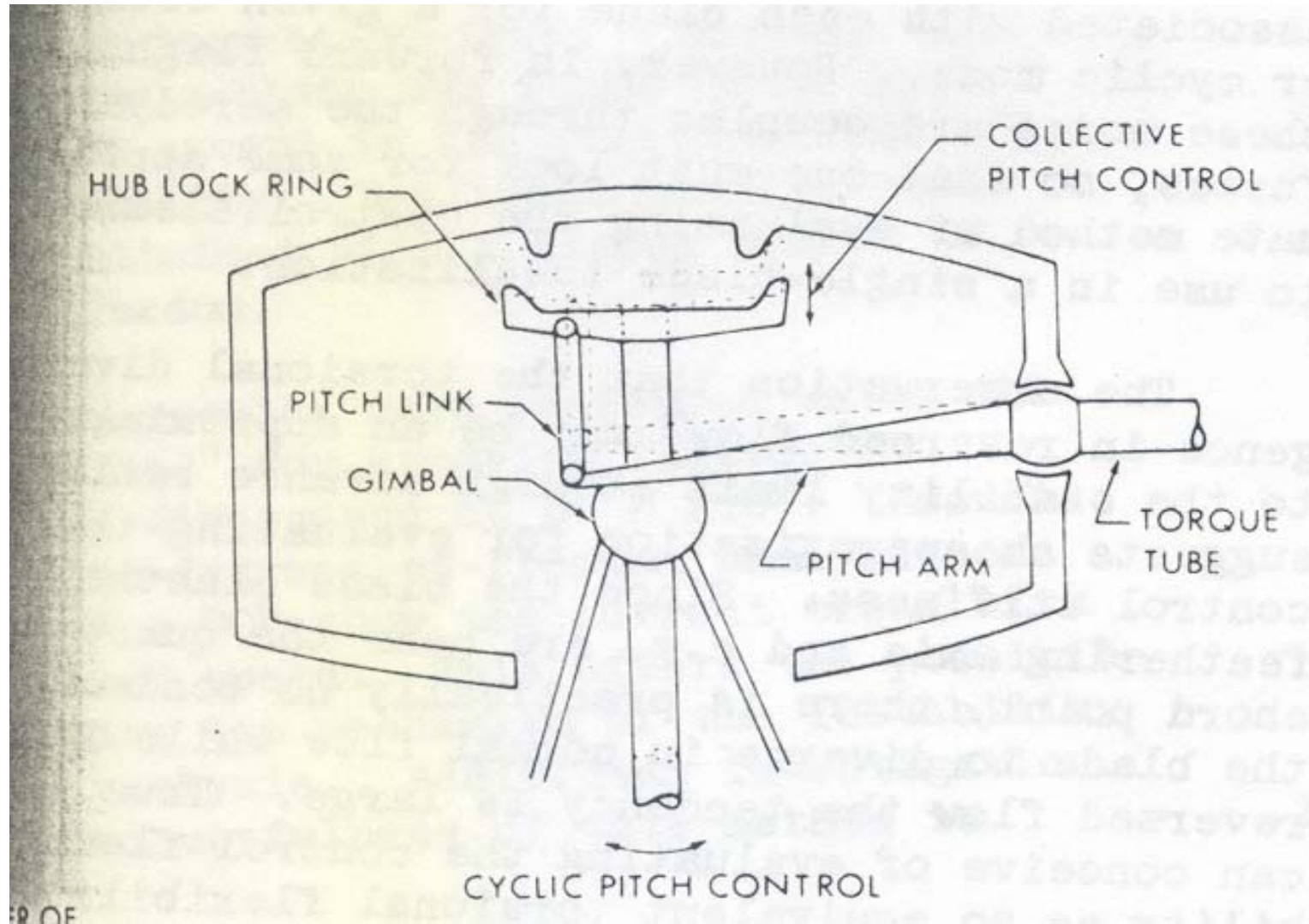
Ref: Perisho, C.H. et al,

C. H. Perisho's Fig. 3 Experimental Results From Model 2 Uncovered Two Different Rotor Instabilities.

Note: Reference Figure 3 dimensionalized to helicopter Vt = 660 fps by Harris.
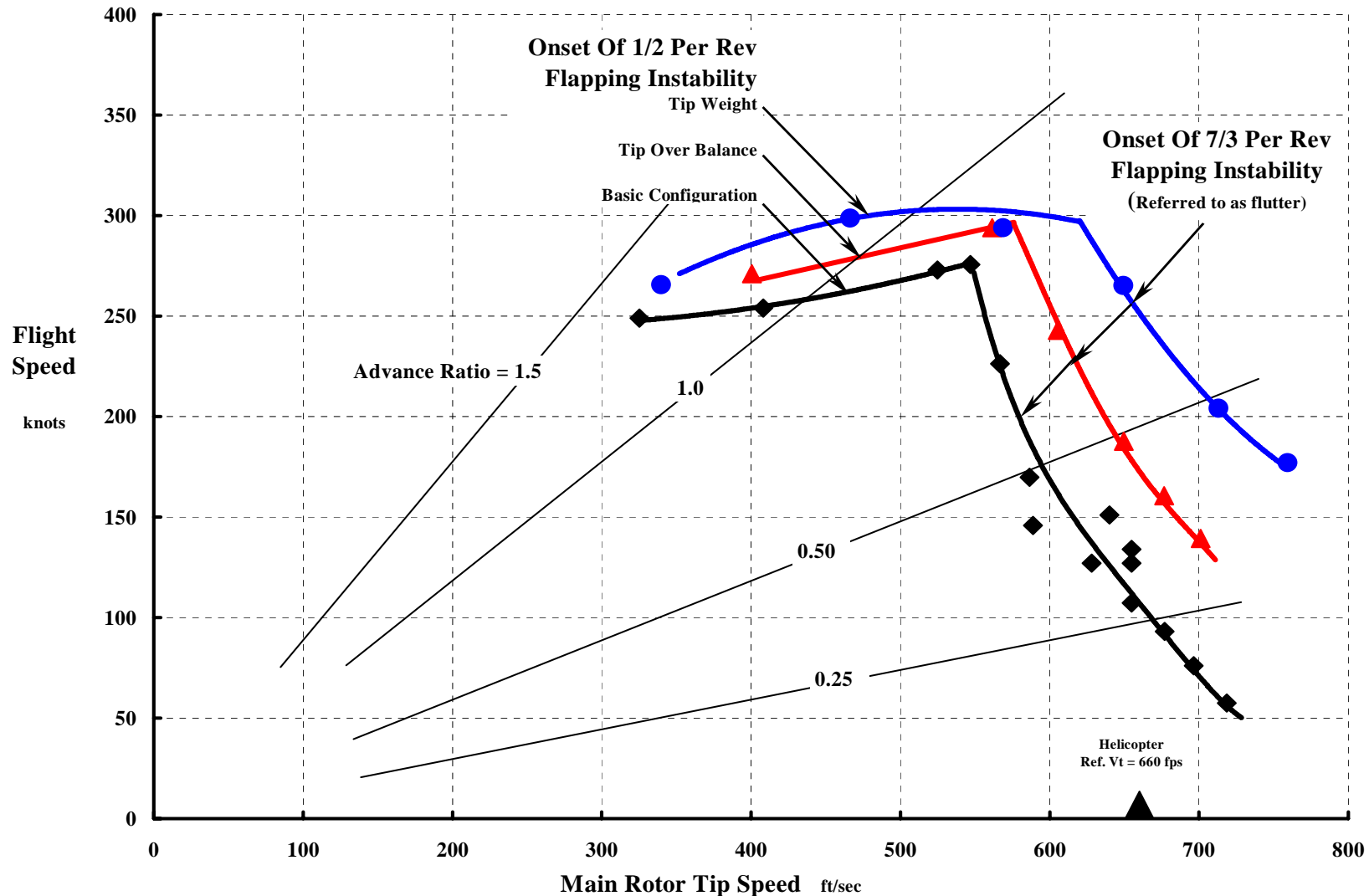
Ref: Perisho, C.H. et al,

Note: Dimensions are scaled by radius. Model radius R = 4 ft, Full scale XHCH–XHRH radius R = 32.5 ft. (I think, but needs checking)

Solidity = 0.095

HUB FAIRING
STRAP FAIRING
RETENTION FAIRING
FEATHERING.
ELASTIC AXES

.270
.170
.08
.023
.880
1.0

.057
.0995
.134

$\delta_3 = \tan^{-1} 1.9$

$A = \tan^{-1} .0875$

STRAP ATTACHMENT	—INBOARD	.0468
	—OUTBOARD	.223
STRAP SPACING	—INBOARD	.0656
	—OUTBOARD	.0520
GIMBAL OFFSET		.0074
CONING HINGE		.0618
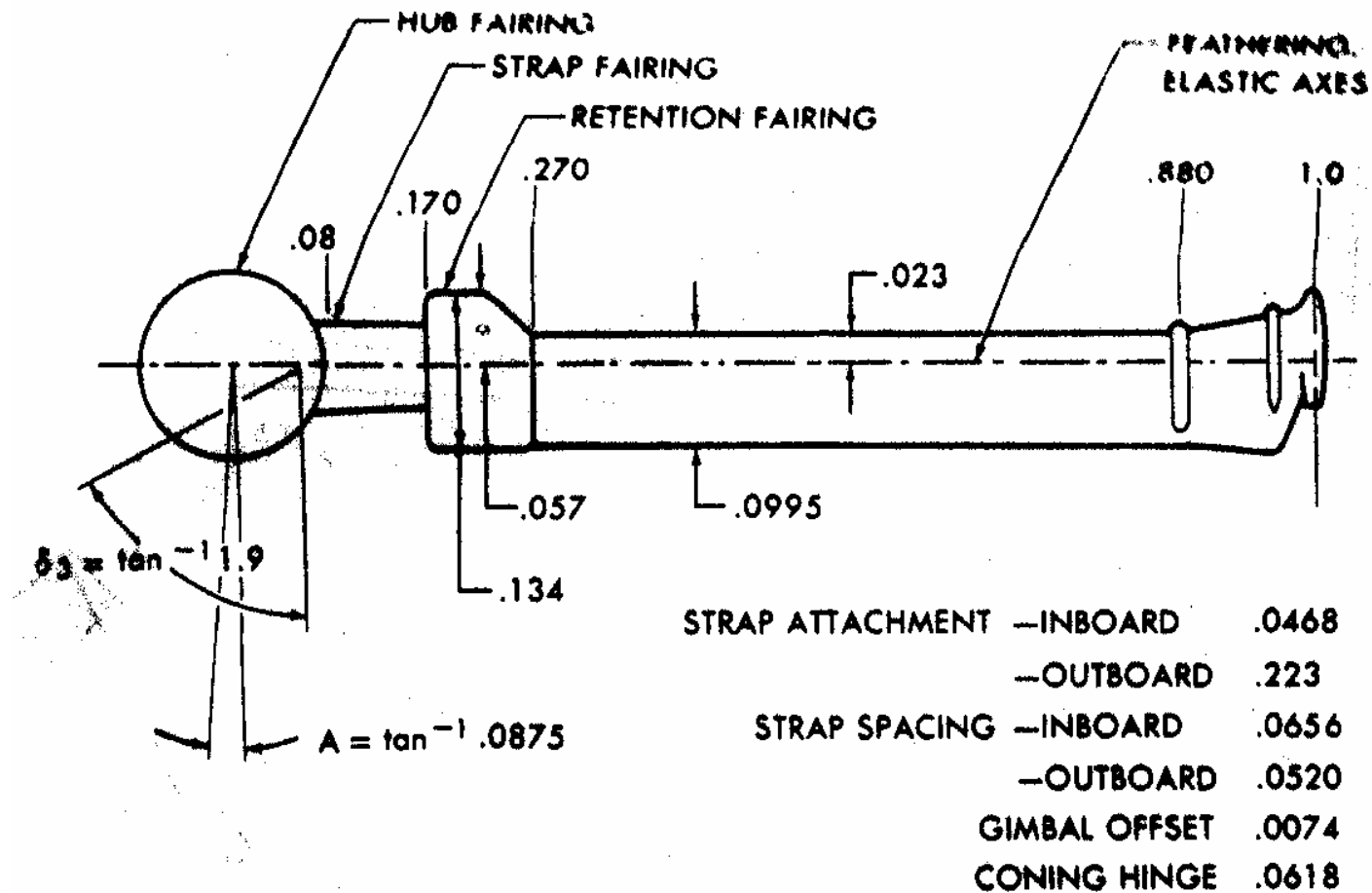
The Model 3 Provided Performance (As Well As Instability) Data. Tested At P = 0 To Study Effect Of "Strap Retention Fairing."
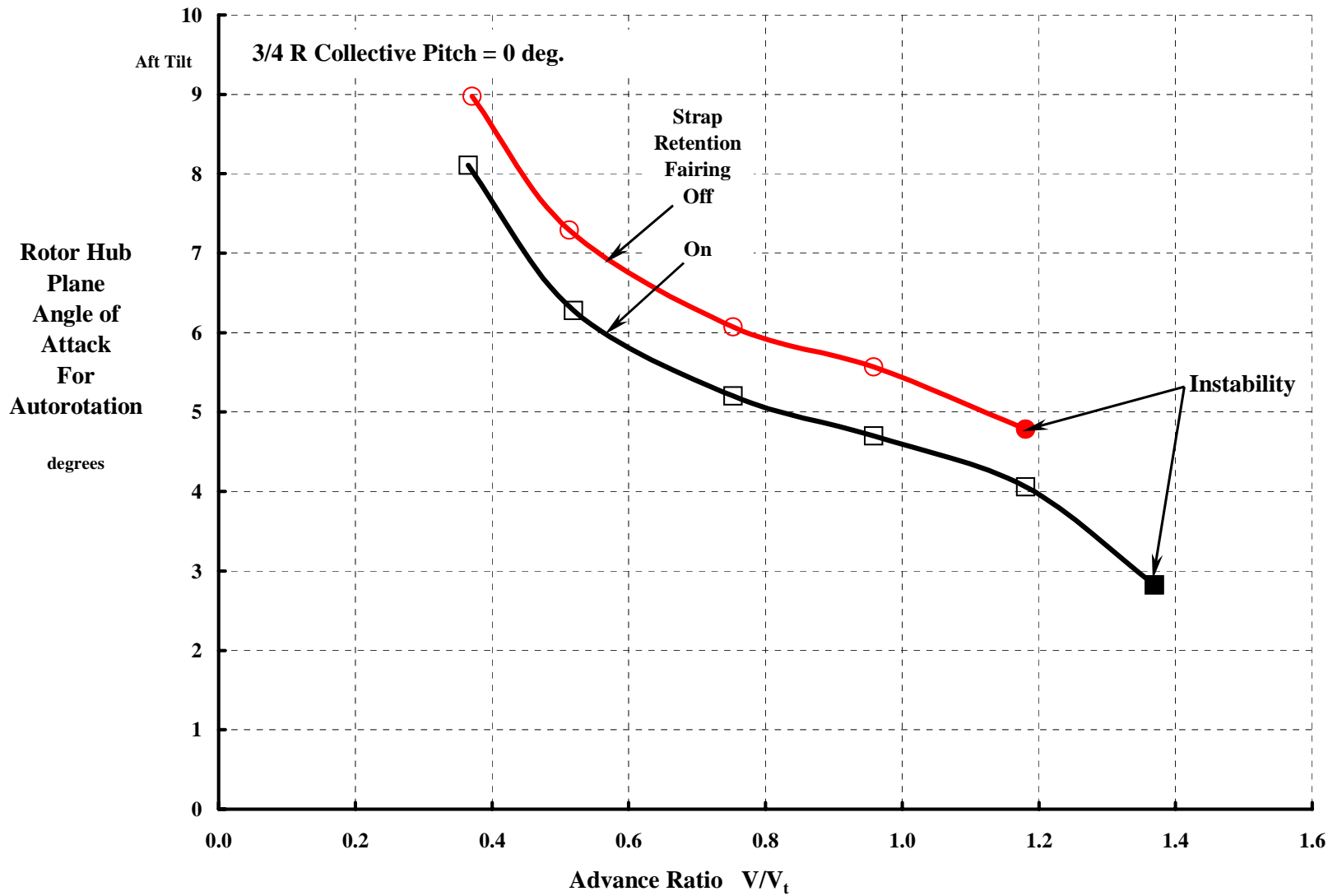
The Cuff Fairing Delayed The Instability To A Higher μ.

Rotor Lift Coefficient In Autorotation

3/4 R Collective Pitch = 0 deg.

$C_T/\sigma = 0.071$

Strap Retention Fairing On

$C_T/\sigma = 0.079$

Off

$C_T/\sigma = 0.108$

$C_T/\sigma = 0.153$

$C_T/\sigma = 0.196$

$C_T/\sigma = 0.215$

Instability

$$C_L = \frac{L}{\frac{1}{2}\rho V^2 \pi R^2} = \frac{2}{\mu^2}\left(\frac{T}{\rho \pi R^2 V_t^2}\right) = \frac{2}{\mu^2}C_T = \frac{2\sigma}{\mu^2}\left(\frac{C_T}{\sigma}\right)$$

Advance Ratio V/V_t
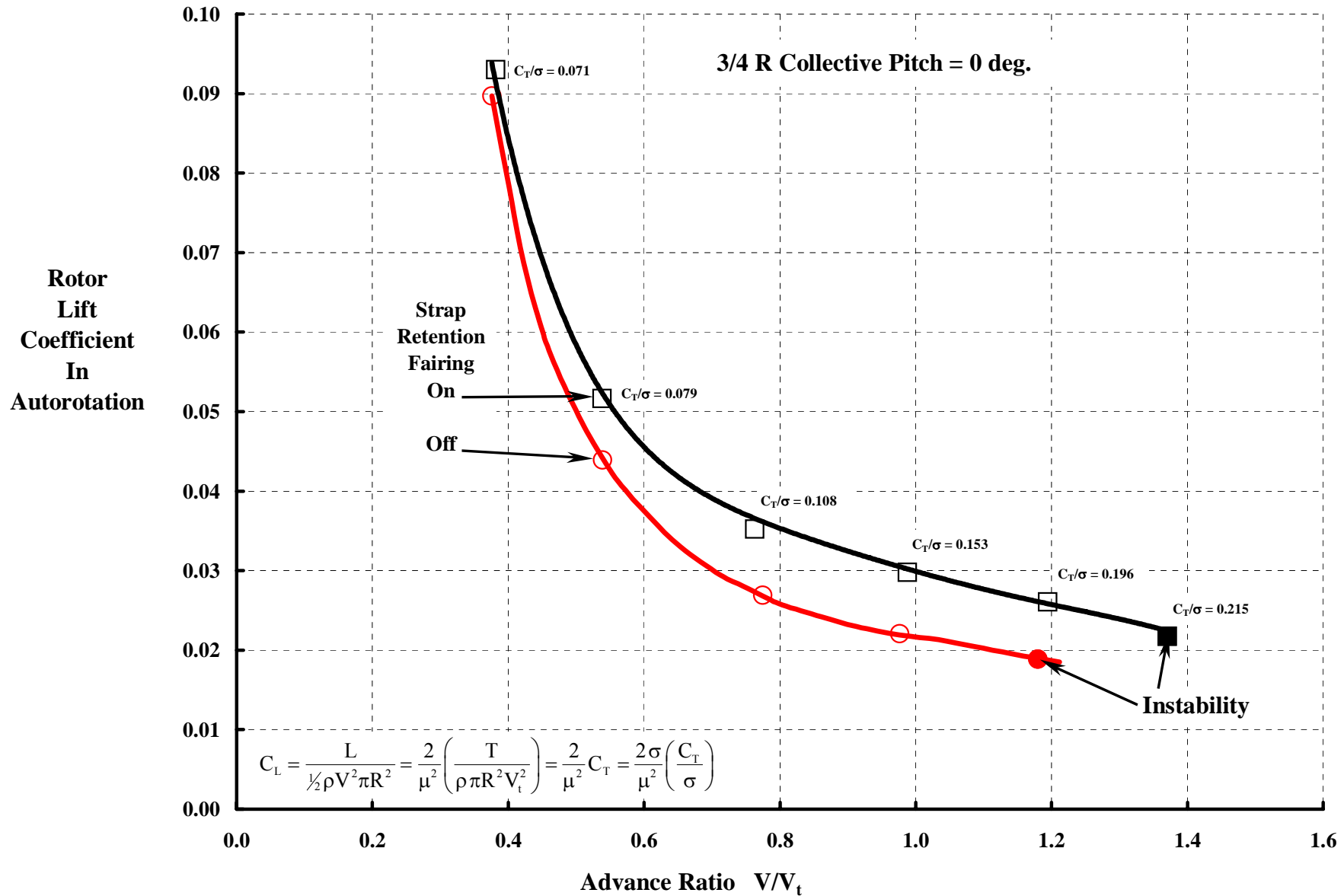
The Cuff Fairing Really Improved Blades Alone Performance.
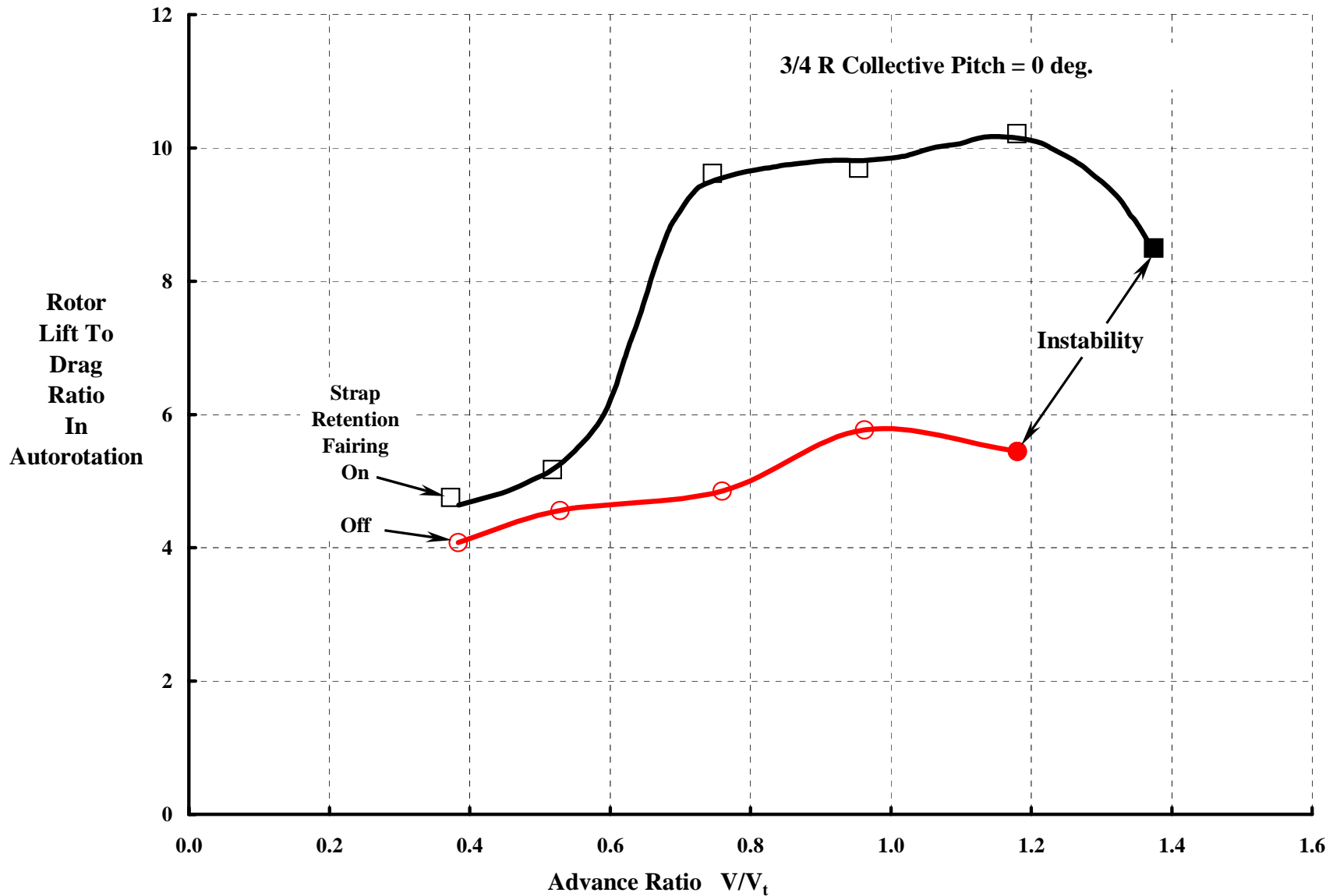
3/4 R Collective Pitch = 0 deg.

Rotor Lift To Drag Ratio In Autorotation

Strap Retention Fairing On

Off

Instability

Advance Ratio V/V_t

LET'S REVISIT AUTOGYROS

First Some History

Cierva, Pitcairn, and Kellett Era (1919 to 1941)
Selection of the Helicopter (1942)
Legacy

Some Technology Aspects

What's in a Name?
Fuselages, Wings, Propellers, Rotors and Trim
Rotor Thrust and Flapping Behavior at High Advance Ratio
Limits to Rotor Lift and Propulsion
To Review Then

XV–1 Re–examination

Full Scale Wind Tunnel Test in 40 by 80
Rotor (With & Without Wing)
Complete Aircraft
➤ Rotor Stability In Forward Flight
Phase II Flight Evaluation

Concluding Remarks

The XV–1's 1st Lift Off (Feb. 1954) Was Followed By The 1st Official Flight In July 1954. Airframe Aero Was An Immediate Objective.

Airplane Flight - 12⁵ knots

Ref: Marks, Marvin D. "Flight Test Development of XV–1 Convertiplane" Paper presented at the AHS Third Annual Western Forum, Dallas, Texas, October 8, 1956. See also, J. of the AHS, Volume 2, No. 1. Photo courtesy of David Peters (from Kurt Hohenemser files)

The XV–1 Phase II Flight Evaluation Was Conducted Between 12 April 1956 And 2 May 1956. Thirty-four Flights Yielded $9^{\pm}$ hours Flight Time.

Photo courtesy of David Peters (from Kurt Hohenemser files)

The Abstract To The Flight Evaluation Report Made 6 Points:

The unloaded rotor principle was found to be a satisfactory convertiplane configuration from the standpoint of flying qualities and operation.

The unloaded rotor does not appear to have any adverse effect on the flight characteristics at high speed in airplane flight and is beneficial in delaying wing stall at low speed.

Transition from helicopter flight to airplane flight was not difficult, but could be simplified with development.

The pitch–cone coupling in this rotor design provides outstanding stability and control characteristics in helicopter flight compared to current designs.

With the exception of the extremely high fuel consumption and the high noise level, the pressure jet system presented no unusual operating problems. Reliability of the burners was marginal.

Numerous deficiencies in performance and control were found, but were primarily attributed to this particular airframe configuration.

Ref: Putnam, V.K. and Eggert, W.W. "Phase II, Flight Evaluation (of the XV–1)" AFFTC–TR-56-35, Feb. 1957. (Also ASTIA AD-112423)

The XV–1 Rotor System, Its Control System And Its Operation Were An Elegant Bit Of Engineering.

The 3 foot Diameter, 1 foot Thick, Elliptical Hub Fairing Enclosed:

a. Top of rotating mast above the pylon
b. Hub "ring"
c. Universal joint gimbal rings (not constant velocity)
d. Root attachments for 2 metal flex strap bundles per blade
e. Spherical bearing for inboard end of hollow torque tube (blade pitch control)
f. Three trailing pitch arms set in helicopter and autogyro configuration for 2.2^o pitch down for 1° cone up and 0.27^o pitch down for 1° flap up. In airplane mode both pitch cone and pitch flap were 2.2^o pitch down for 1° cone or flap up.
g. Swashplate assembly above gimbal rings
h. Three vertical pitch links
i. Plenum distributing air to blades through hollow torque tubes
j. Fuel distribution and burner ignition system
k. Slip ring

The Outboard 14 inch Long, 17 inch Chord, 25% Elliptical Cuff Fairing Enclosed:

a. Outboard attachment fittings for blade
b. Manifold from hollow, torque tube to D spar and two 2 smaller pipes to go out the blade to the tip burner

Note: Completed the transition from elliptical airfoil to blade's 17.5 inch chord, 15 % thick airfoil blade at r/R = 0.283.

The 3 foot Long, 9 inch Chord, 25 % Elliptical Cuff Fairing Enclosed:

a. A 4 inch diameter torque tube
b. Cuff locked to blade and torque tube

Note: The Two laminated metal flex strap bundles per blade (30 straps per bundle, 1.25 inch wide by 1 inch thick) were not enclosed by the elliptical cuff.

The XV–1 Rotor Hub Was Gimbaled,"Bearingless" And Stiff Inplane.

HUB (6 SIDED)

SWASHPLATE
(STAYS ⊥ TO STEM)

TRUSS FRAME TIES OUTER GIMBAL TO HUB

OUTER GIMBAL

SPHERICAL BEARING

HOLLOW TORQUE TUBE (AIR PATH TO BLADE)

LAMINATED STEEL FLEX STRAPS TAKE CF

INNER GIMBAL

SPHERICAL BEARING

AIR

SEAL JOINT (ALLOWS HUB TO TILT)

INTERNAL HYDRAULIC ACTUATOR FOR COLLECTIVE

ROTATING MAST

"STEM" TILTED FOR LAT. & LONG. CYCLIC

LONG. CYCLIC

AIR INPUT FROM COMPRESSORS

LATERAL CYCLIC

FUSELAGE ROOF

Ref: Conversations with Bob Head

Two Laminated, Metal, Flex Strap "Bundles" Retained The Blade To The Hub. A Torque Tube Transmitted Pitch Arm Motion To The Blade. The Cuff Rotated With The Blade And Torque Tube.

HUB

$\delta_3 = 2.2°$ PITCH DOWN FOR 1° CONE OR FLAP

LAMINATED STEEL FLEX STRAP

FAIRING

HOLLOW TORQUE TUBE

AIR DUCT

D SPAR (STEEL)

AIR

Open C Section

SPHERICAL BEARING

AIR DUCT

LAMINATED STEEL FLEX STRAP

PITCH HORN

FAIRING

+15°

Ref: Conversations with Bob Head

In Airplane Mode, the Swashplate Rose and Engaged The "Inner Roof" Of The Hub. (Collective Went To 0° Because Of The Trailing Pitch Arm). The Gimbal & Hub Were Thus Locked To The "Stem" And Cyclic Was Locked Out. Rocking Of The Lower End Of The "Stem" Controlled Hub Plane Incidence. The Rotor Behaved As A Fixed Pitch "Bearingless" Rotor With About 6 % Hinge Offset. Pitch Flap Coupling Was $\delta_3 = 2.2°$ Pitch Down Per 1° Flap Up. A Fly Ball Governor, Tied To Fore & Aft "Stem" Rocking, Controlled Rotor RPM By Hub Plane Angle Of Attack.
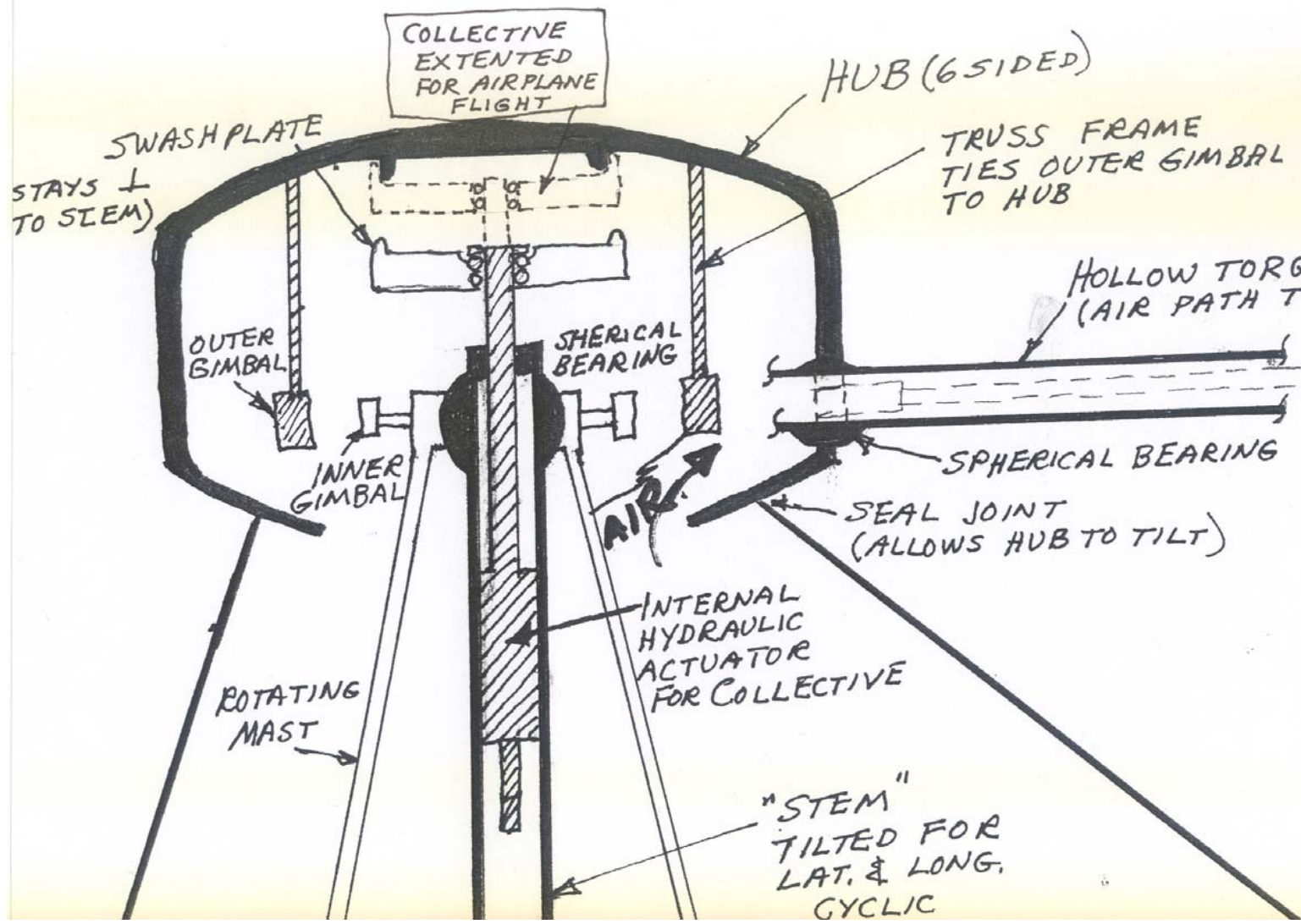
Ref: Conversations with Bob Head

One Of The Two XV–1's Is Stored In A Warehouse At Fort Rucker, Alabama.

Larry Frakes, LTC Franco Villaneuvo, and Tim Smith with help from Fort Rucker Museum maintenance staff found it.

Outboard End Of Torque Tube. Air Passage to Blade
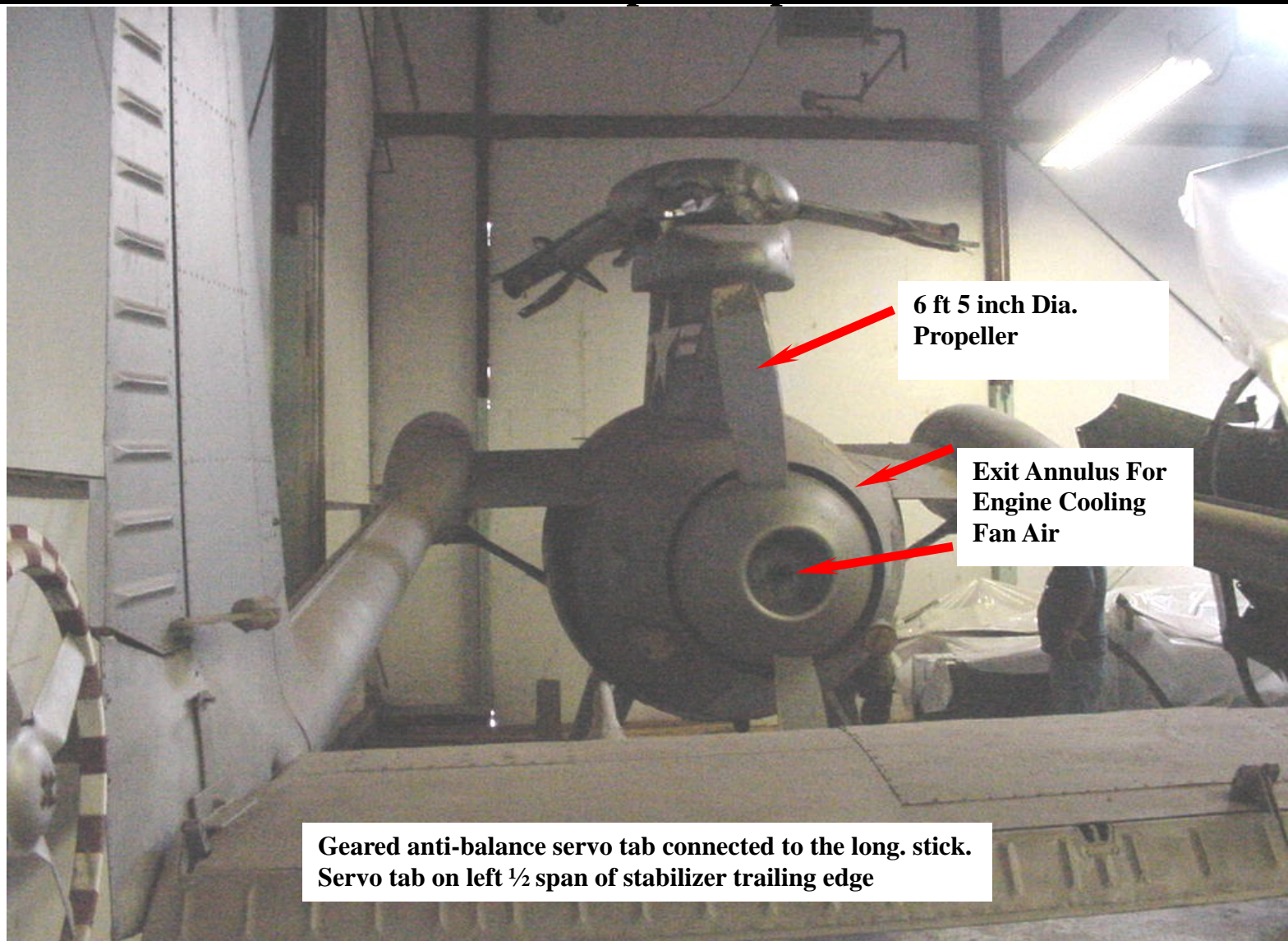
Pylon

Drag Reduction Fairing

Starboard Fuel Tank
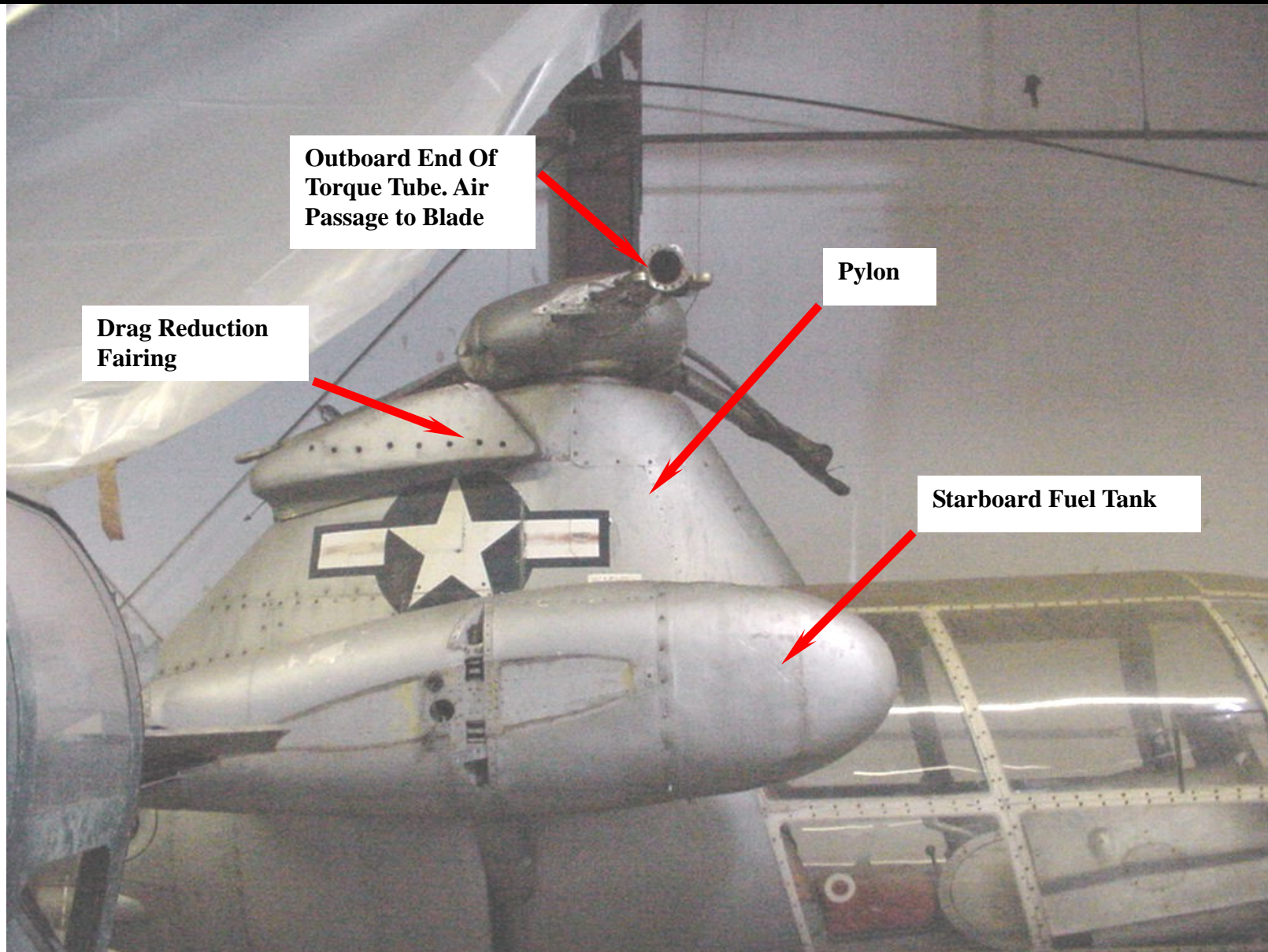
LF-12

Photo courtesy of Larry Frakes, LTC Franco Villaneuvo, and Tim Smith with help from Fort Rucker Museum maintenance staff.

A Torque Tube Transmitted Pitch Arm Motion To The Blade. The Cuff Rotated With The Blade And Torque Tube.

Hollow Torque Tube

Leading Edge, Laminated Steel Tension Torsion Retention Strap Bundle

Inboard Rib Of Blade Retention Fairing

Trailing Edge, Laminated Steel Tension Torsion Retention Strap Bundle

Elliptical Fairing Around Torque Tube
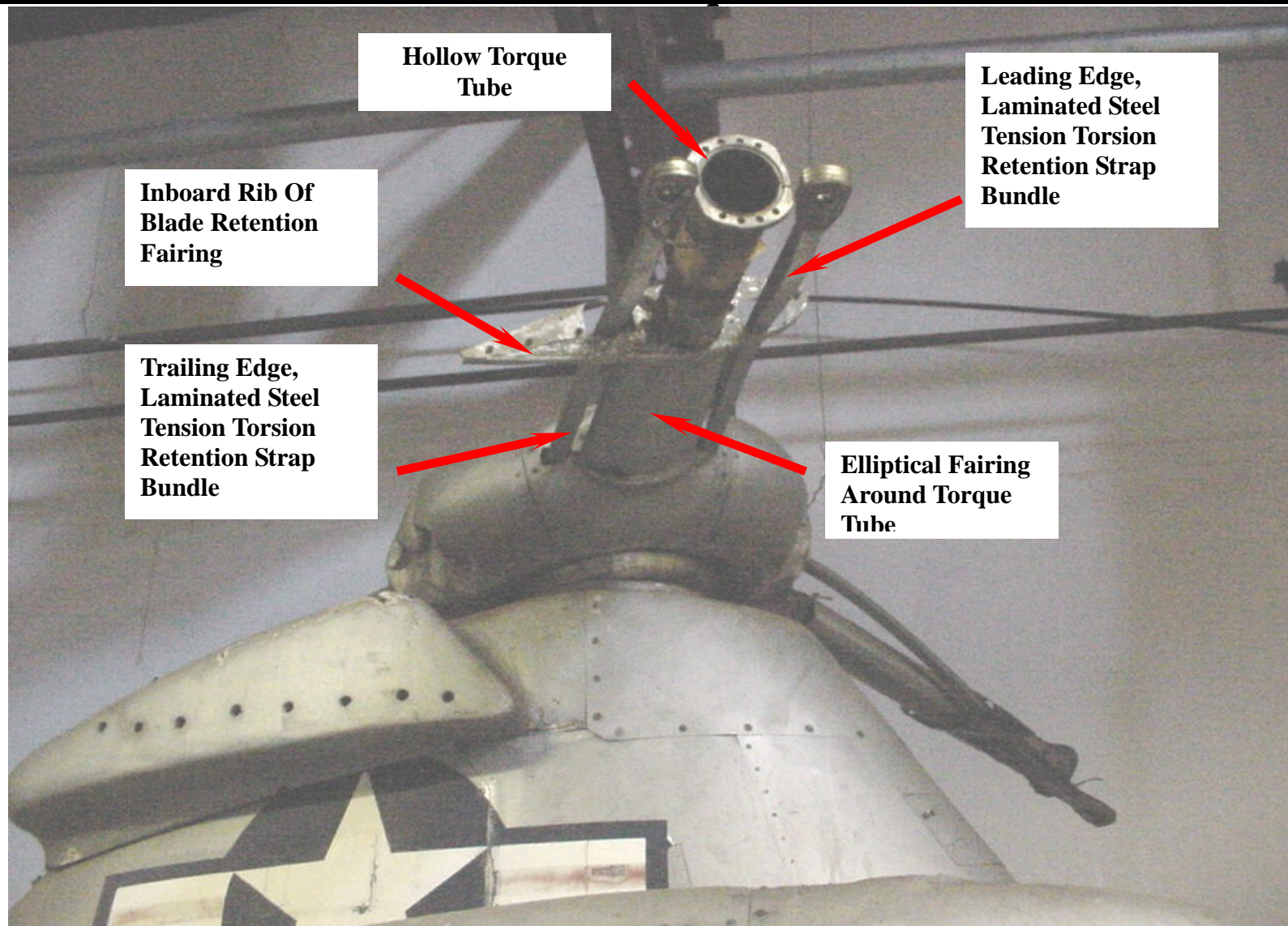
LF-13
Photo courtesy of Larry Frakes, LTC Franco Villaneuvo, and Tim Smith with help from Fort Rucker Museum maintenance staff.

The Two Flex Strap CF Retention Bundles Were Not Enclosed.

Inboard Rib Of Blade Retention Fairing

Starboard Rudder

Starboard Yaw Fan

Elliptical Fairing Around Torque Tube

Trailing Edge, Laminated Steel Tension Torsion Retention Strap Bundle

Prop
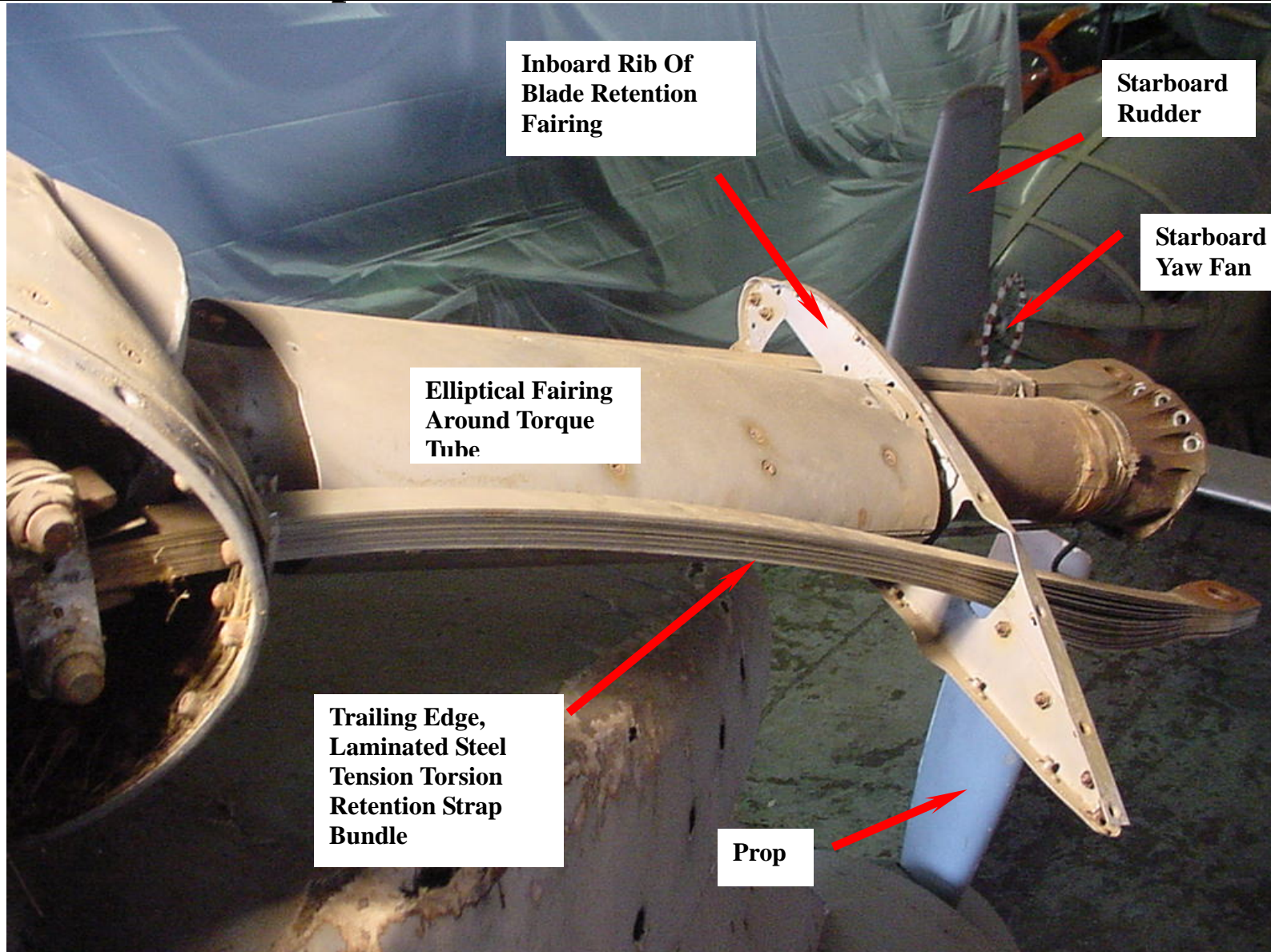
LF-9
Photo courtesy of Larry Frakes, LTC Franco Villaneuvo, and Tim Smith with help from Fort Rucker Museum maintenance staff.

A Spherical Bearing Allowed Torque Tube To Cone & Flap AND Slide In & Out.

6 Sided Hub "Ring"

Spherical Bearing
(Defines Coning &
Flapping Point)

Trailing Edge,
Laminated Steel
Tension Torsion
Retention Strap
Bundle

Torque Tube To
Sherical Bearing
Fitting

Inboard End Of
Hollow Torque
Tube

Access To Bolts
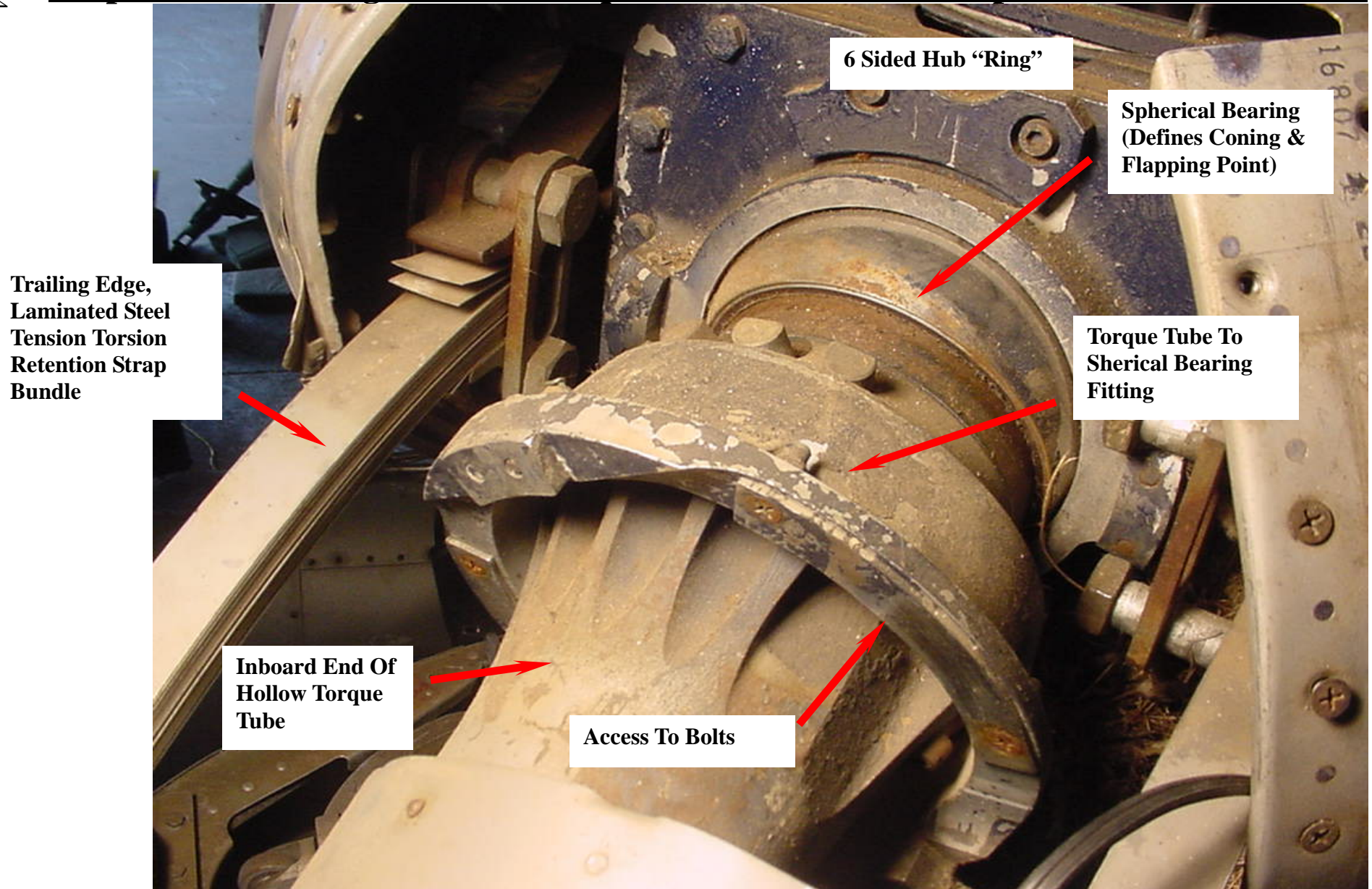
LF-10
Photo courtesy of Larry Frakes, LTC Franco Villaneuvo, and Tim Smith with help from Fort Rucker Museum maintenance staff.

The Fitting Joining The Blade's Steel D–Spar To The Flex Straps & Torque Tube Also Ducted Air To The Spar & Two Smaller Pipes.

Blade
(17.5 inch chord)

Ducts To Aft Two
Air Pipes
(Note 1 ft Ruler)

Bolt Holes For
Flex Straps

Duct To Blade
D–Spar

Blade Root
Fitting

Inboard Rib Of
Blade Retention
Fairing

Tips Of Other Two
Blades. Note Pressure
Jet Exhaust Port
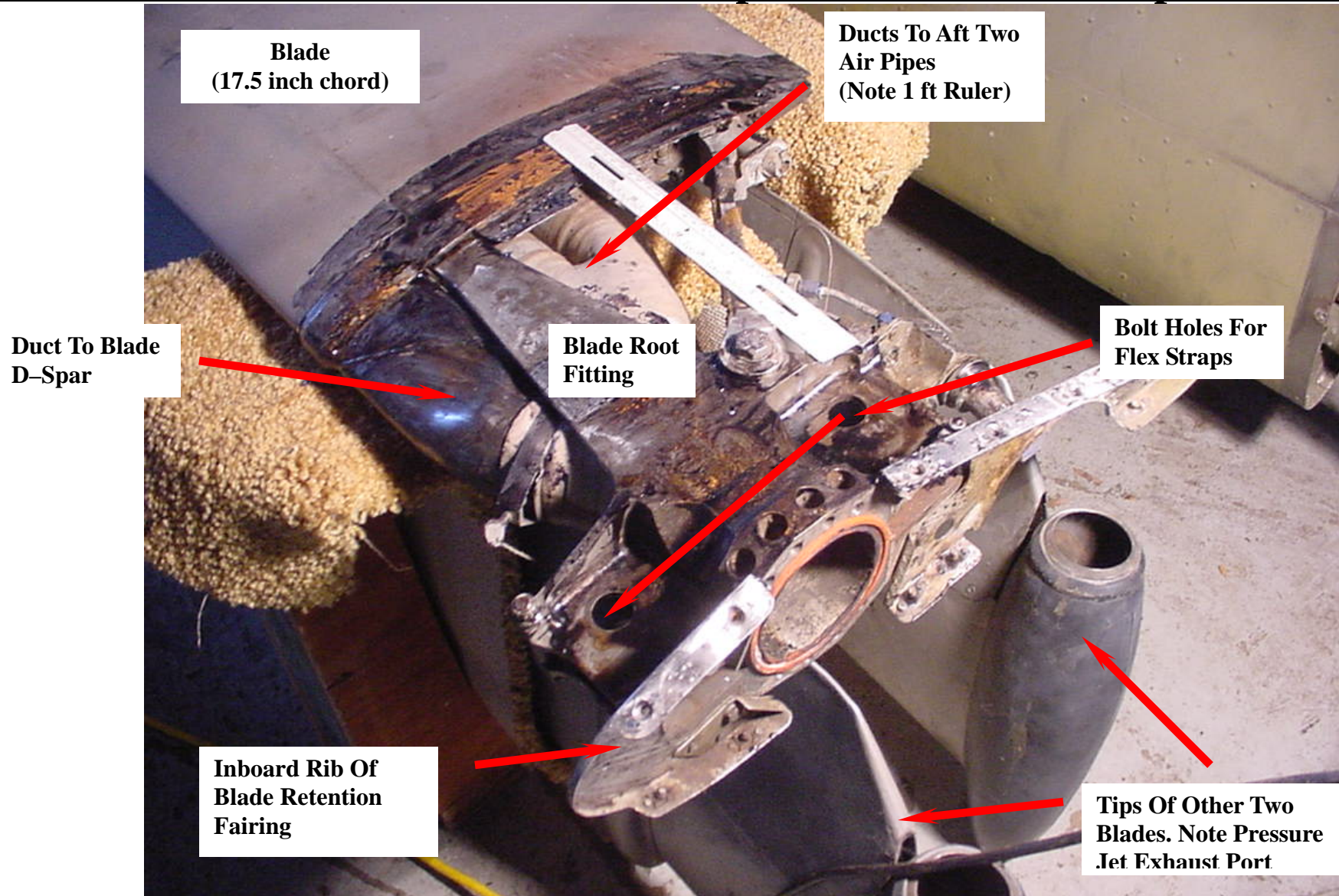
LF-28
Photo courtesy of Larry Frakes, LTC Franco Villaneuvo, and Tim Smith with help from Fort Rucker Museum maintenance staff.

Bob Head (Retired Boeing Mesa) Drew This Sketch At The End Of Our 3rd Meeting. You Can't Believe How Patient, Helpful & Nice He Was.

Ref: Doblhoff, F.L.V., "Part Time Use of Pressure Jets in Rotary Wing Aircraft." 6th Annual Forum of the AHS May 1960

Note: Bob said he thought maximum efficiency occurred when Vjet was twice Vt. Also, if you want to pursue this propulsion system get John Nichols' "The Pressure–Jet Helicopter Propulsion System" HTC–AD 70-81. Mike Scully has a copy of it.
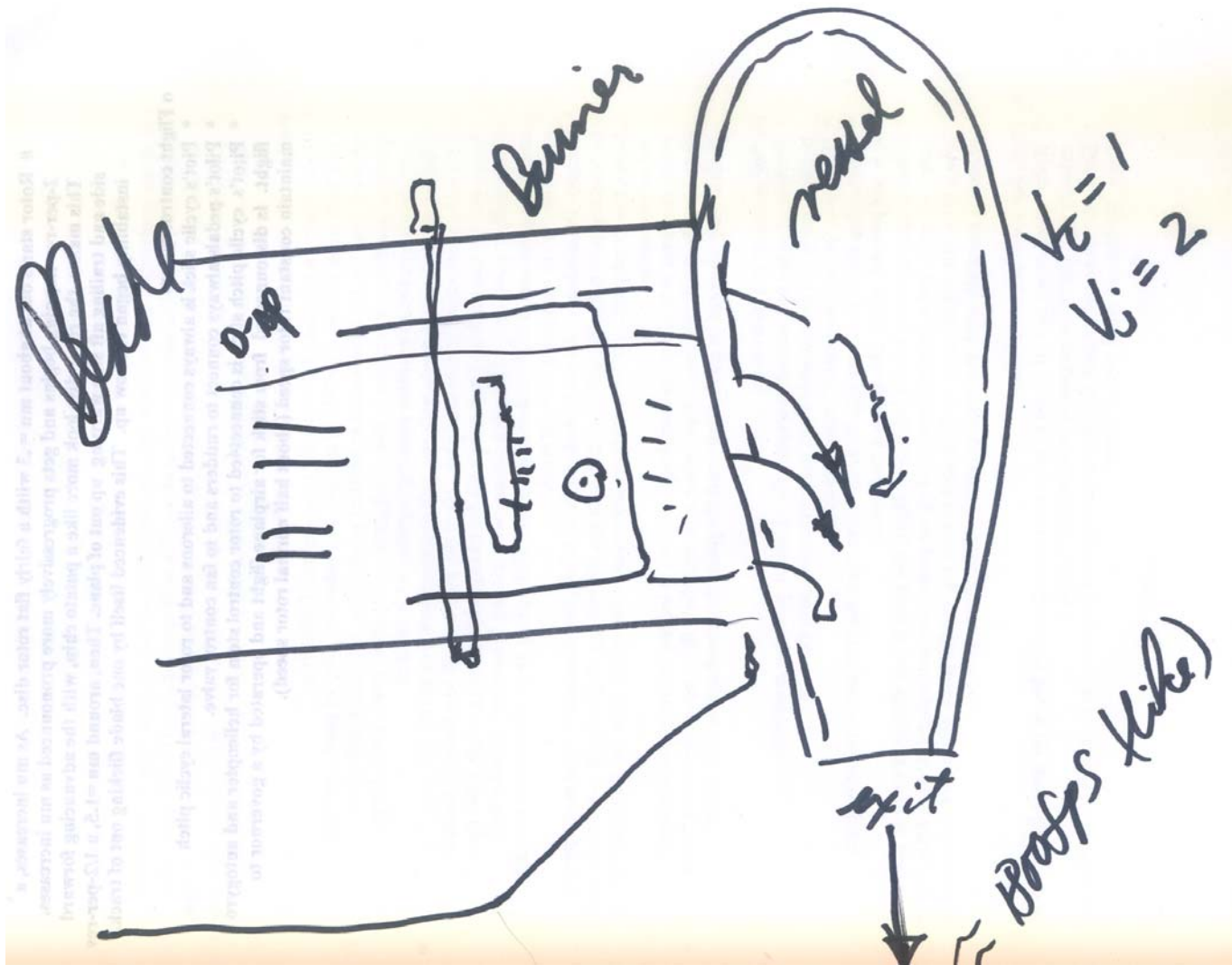
One Of The Pitch Links Was Used To Drive The Swashplate.

Swashplate & Slipring Note Outer Lip Used To Lock Up Hub And Gimbal To "Stem"

"Rigid Pitch Link Used To Drive Swashplate

Upper End Conventional Pitch Link

Bolts Ring For Top Of Hub

Sherical Bearing On Gimbal Center About Which "Stem" Tilted

Upper End Conventional Pitch Link
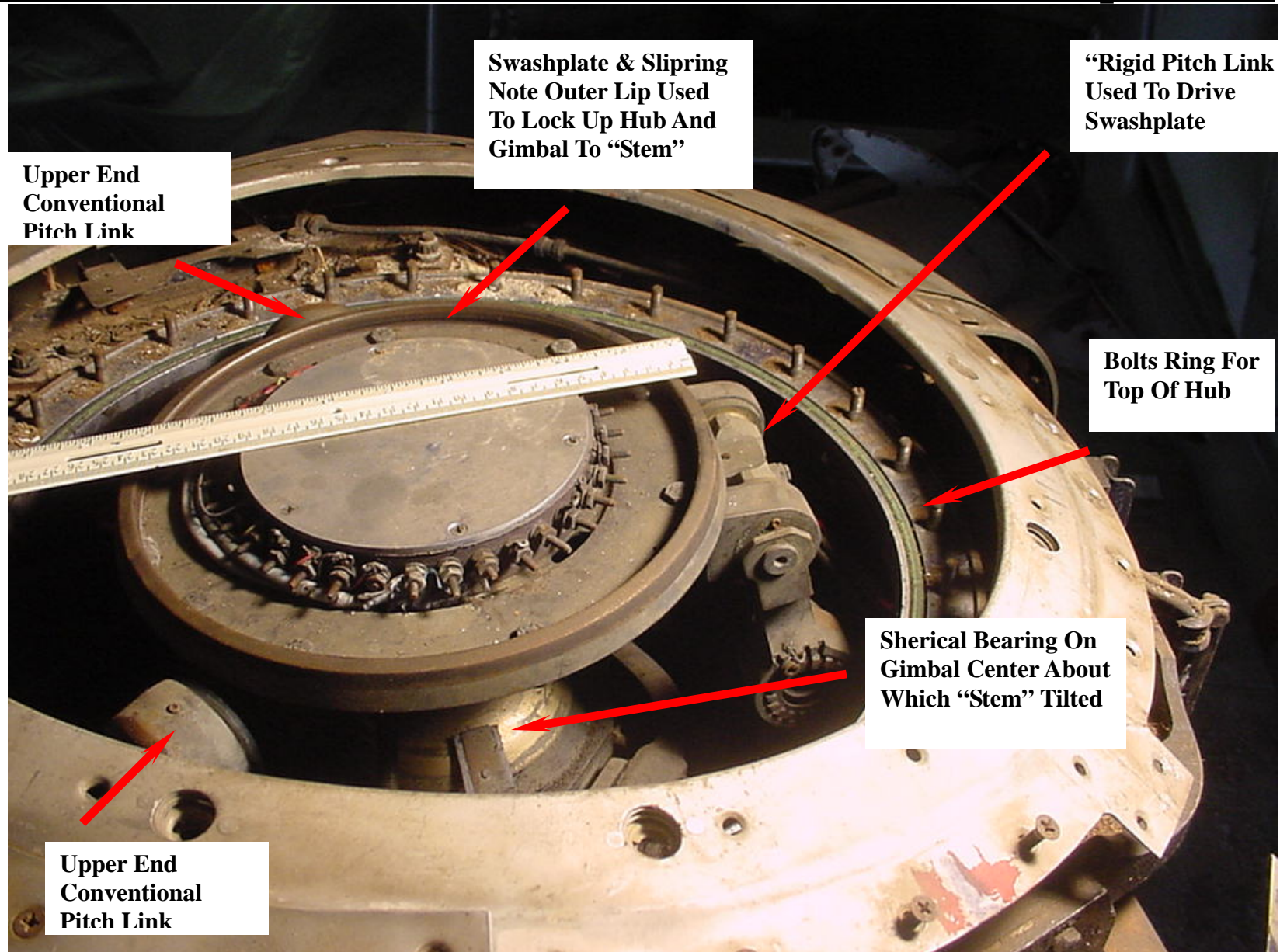
LF-4
Photo courtesy of Larry Frakes, LTC Franco Villaneuvo, and Tim Smith with help from Fort Rucker Museum maintenance staff.

The "Stem" Was A Big Pipe. In Helicopter & Autogyro Modes, It Directly Con–trolled Swashplate Tilt. In Airplane Mode, It Directly Controlled Hub Plane Tilt.

"Rigid" Pitch Link Used To Drive Swashplate

Slipring

Swashplate

The "Stem"
Note: The collective actuator was inside the stem

Sherical Bearing On Gimbal Center About Which The "Stem" Tilted
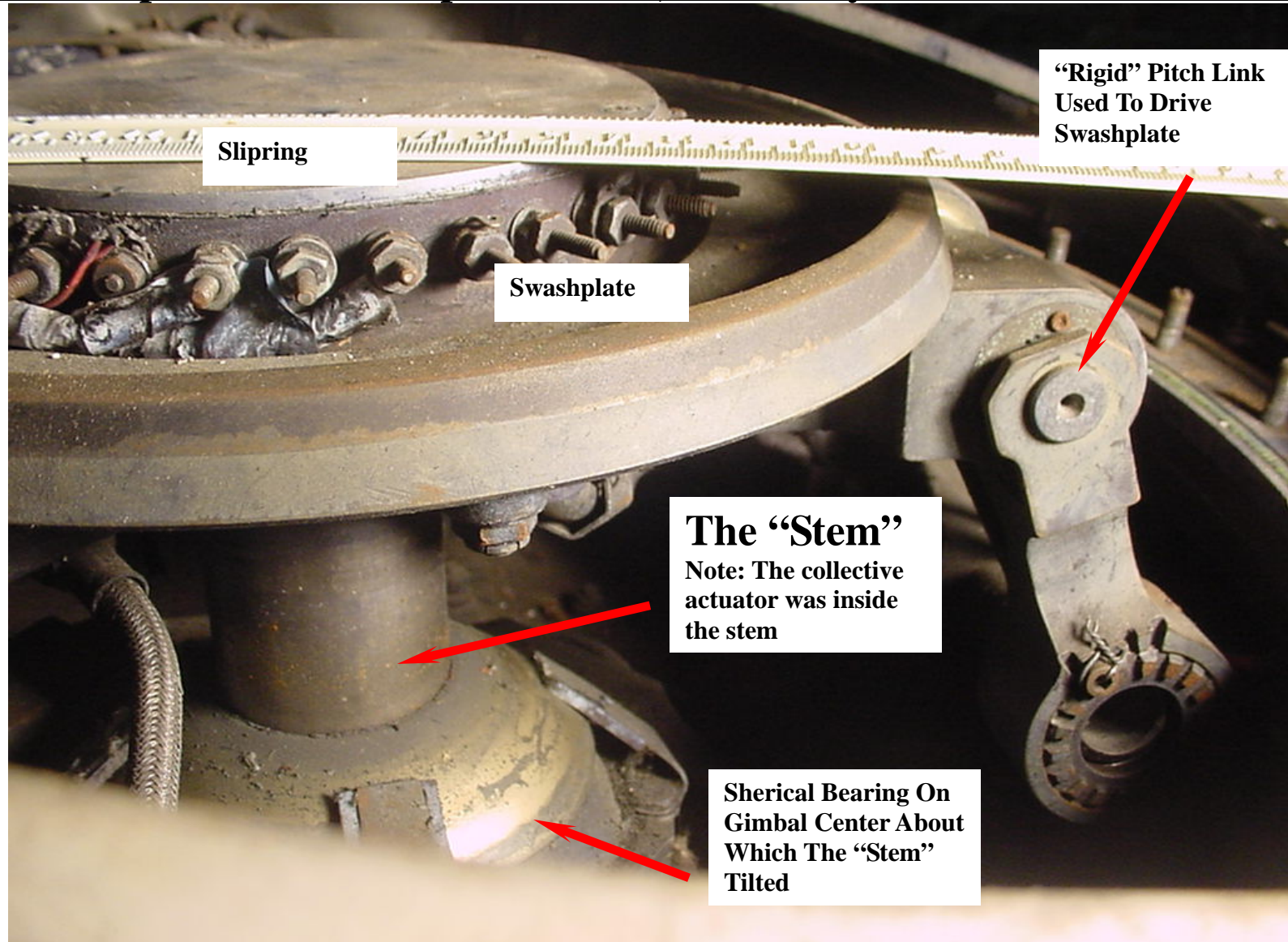
LF-21
Photo courtesy of Larry Frakes, LTC Franco Villaneuvo, and Tim Smith with help from Fort Rucker Museum maintenance staff.

Compressed Air Filled The Inside Of The Hub, Gimbal & Swashplate Volume. Air Got To The Inboard End Of The Hollow Torque Tube And Then Out The Torque Tube To The Blade.

Gimbal Inner Ring Pivot

Gimbal Inner Ring

Upper End Conventional Pitch Link

Lower End Conventional Pitch Link

Pitch Arm Inboard End (Solid Cross section)

Pitch Arm "C" Cross-section

Outer Shell Hub Fairing
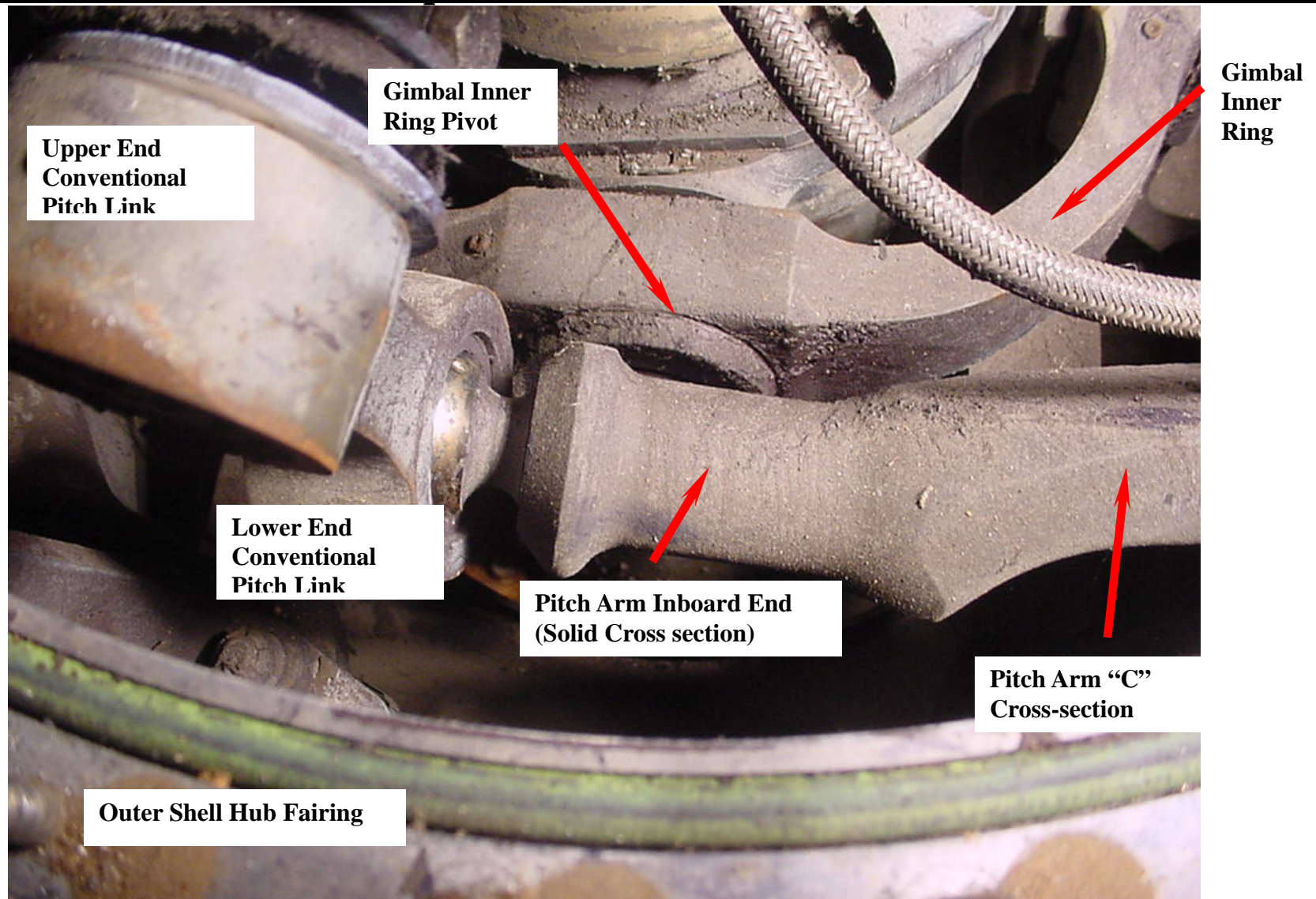
LF-20
Photo courtesy of Larry Frakes, LTC Franco Villaneuvo, and Tim Smith with help from Fort Rucker Museum maintenance staff.

We'll Have To Get Prop Geometry From The Prop. McCauley (1-800-621-7767) Made The 6 ft 5 inch Dia. Fixed Pitch Prop As Experimental But Has No Records.

6 ft 5 inch Dia. Propeller

Exit Annulus For Engine Cooling Fan Air

Geared anti-balance servo tab connected to the long. stick. Servo tab on left ½ span of stabilizer trailing edge

LF-15
Photo courtesy of Larry Frakes, LTC Franco Villaneuvo, and Tim Smith with help from Fort Rucker Museum maintenance staff.

"The Stabilizer Is Essentially A Velocity Sensing Device…..
Its Position Is Relatively Independent Of Angle Of Attack [of the aircraft]."
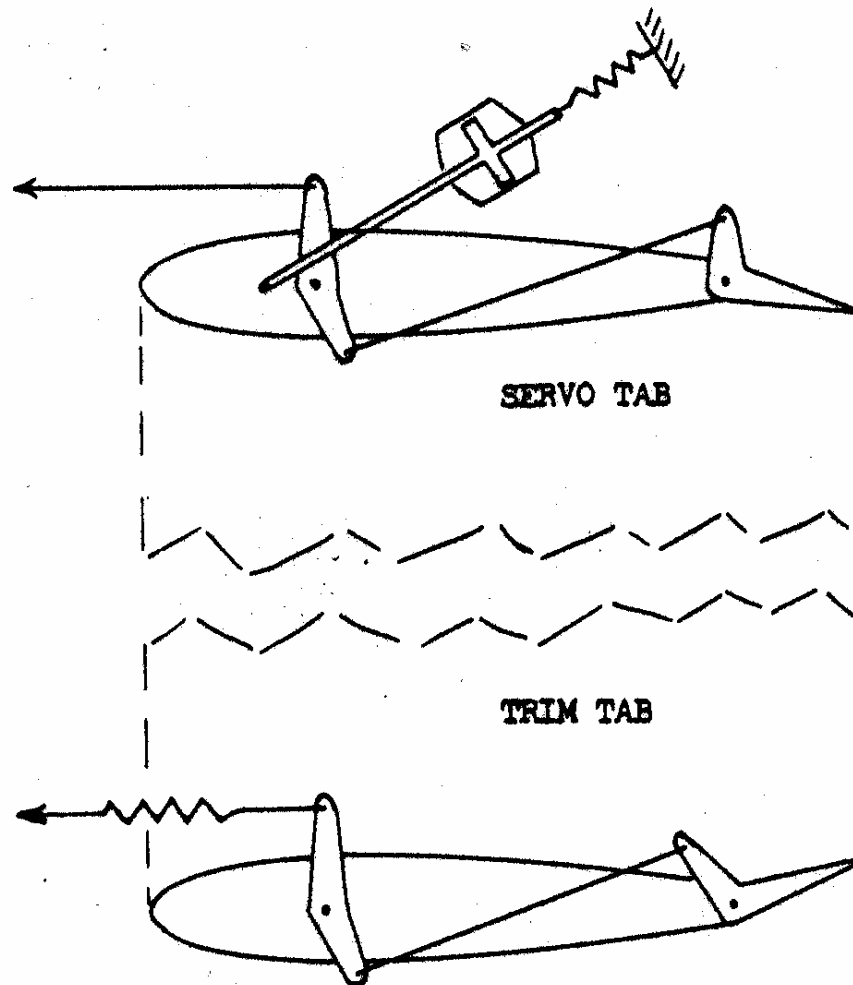
Geared anti-balance servo tab connected to the long. stick.

Servo tab on left half span of stabilizer trailing edge

SERVO TAB

TRIM TAB

Geared anti-balance trim tab connected to a lever to the left of the pilot or an electric switch on the collective stick.

Trim tab on right half span of stabilizer trailing edge

Ref: Marks, Marvin D. "Flight Test Development of XV−1 Convertiplane" Paper presented at the AHS Third Annual Western Forum, Dallas Texas, October 8, 1956. (Also Journal of the AHS, Vol. 2, No. 1, 1957)

The 15 inch Dia. Yaw Fans Were Driven By Hydraulic Motors At Around 6,000 RPM. To Change Thrust, RPM Was Reversed. Directional Control Was Inadequate.

Fan Mounted Directly To Motor.
Hub Dia. = 4.4 inch
Root chord = 1.84 inch
Tip chord = 1.54 inch
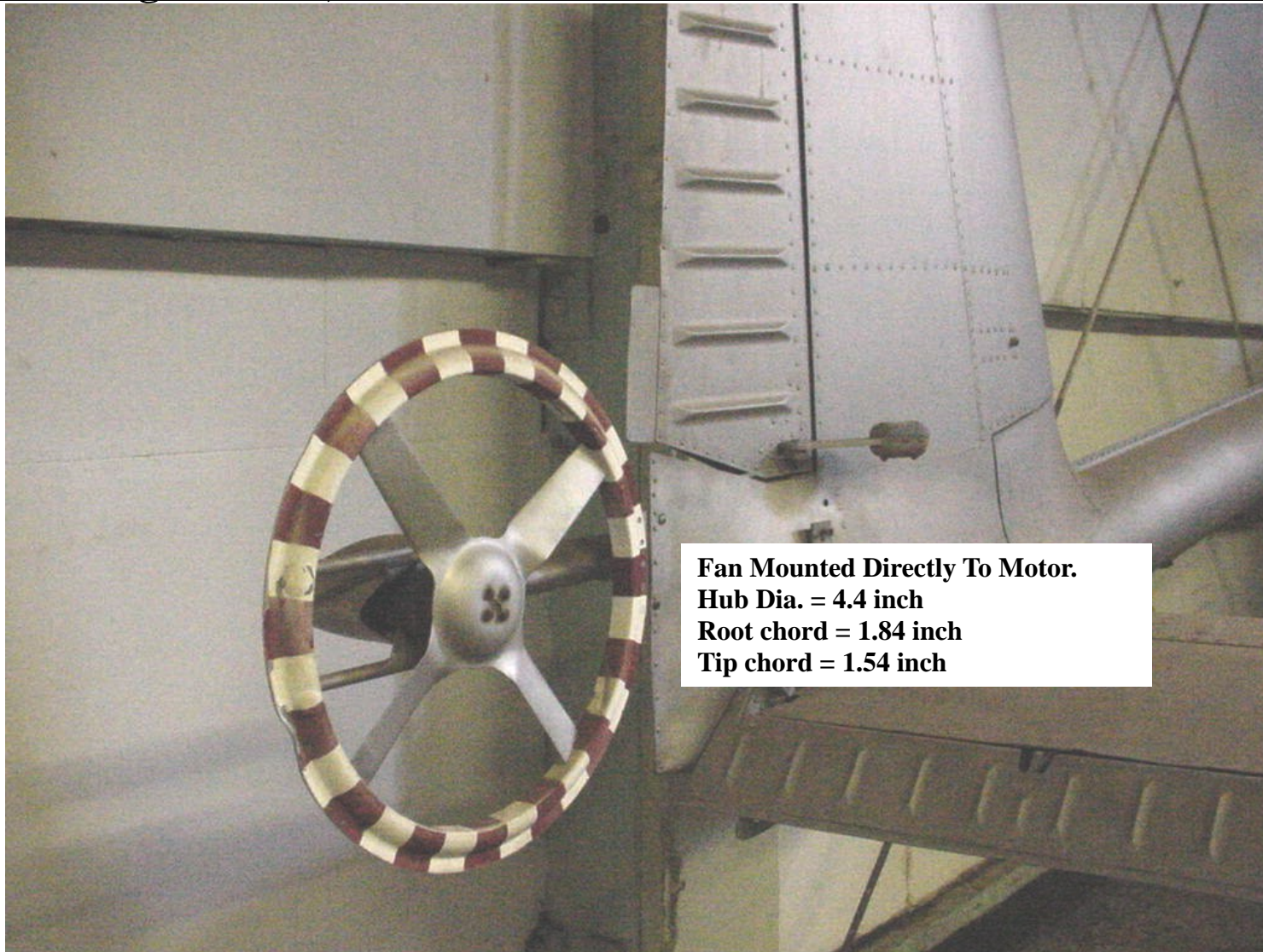
LF-16
Photo courtesy of Larry Frakes, LTC Franco Villaneuvo, and Tim Smith with help from Fort Rucker Museum maintenance staff.

"Take-off, Landing, Hovering And Low Speed Flight Are Accomplished As A Helicopter. Cruise And High Speed Flight Are Made As An Airplane. Autogyro <u>Flight Is Used During Transition From Rotor To Propeller Powered Flight."</u>

Helicopter Flight:

        Rotor Speed – Collective Pitch and Engine Throttle Setting
        Longitudinal – Cyclic Pitch and Horizontal Tail Surface Deflection
        Lateral – Cyclic Pitch and Aileron Deflection
        Directional – Tail Fans With Rudders Increasingly Effective With Forward Speed
        Collective Pitch – Normal Helicopter

Autogyro Flight (transition from helicopter to airplane)

        Rotor Speed – Function of Longitudinal Stick And Tip Path Plane Angle (Varied from 380 rpm at low speeds
                to 300 rpm at high speed)
        Longitudinal – Cyclic Pitch and Horizontal Tail Surface Deflection Through Servo Tab (trim tab separate)
        Lateral – Cyclic Pitch and Aileron Deflection
        Directional – Tail Fans With Rudders Increasingly Effective With Forward Speed
        Collective Pitch – Fixed At Full Down <u>Autogyro</u> <u>Setting</u> <u>Of</u> <u>6 degrees</u>

Airplane Flight (above 90 knots)

        Rotor Speed – Held Constant By Fly Ball Governor Controlling Hub Plane Angle Of Attack. Longitudinal
                Stick & Cyclic Locked Out (Governor set for 185 rpm)
        Longitudinal – Horizontal Tail Surface Deflection Through Servo Tab (trim tab separate)
        Lateral – Aileron Deflection and Hub Plane Lateral Tilt
        Directional – Rudders And Tail Fans At Reduced RPM
        Collective Pitch – Fixed At Full Down <u>Airplane</u> <u>Setting</u> <u>Of</u> <u>0 degrees</u>

Note: A control shift lever was used to obtain airplane flight. When shifted, the lever 1) disconnected long. cyclic from the rotor, 2) reduced pitch to zero and 3) locked rotor hub and gimbal to control stem.

Ref: Putnam, V.K. and Eggert, W.W. "Phase II, Flight Evaluation (of the XV–1)" AFFTC–TR-56-35, Feb. 1957. (Also ASTIA AD-112423)

Rotor Speed Was Well Controlled In All Three Flight Configurations.

Note: When Marks published his paper, the XV–1 V_{max} was classified. Phase II Flight Evaluation showed maximum V_{true} = 148 kts at takeoff power of 550 BHP at sea level, std day.

Helicopter (410)

Autogyro
Trim Tab = -50
Trim Tab = -35

Rotor RPM

Region of "resonant condition." Predominately 3 per rev.

"Vibration at this amplitude is of course unsatisfactory; however, since this is a transient condition lasting only from 5 to 10 seconds, it is considered tolerable."

0.2g

0.7g

0.2g

Airplane
Governor Off
Collective = 0°
Hub Plane = +2.5° wrt To Airframe

Airplane (185)

Governor Contacts Front Stop

Airspeed Ratio V/V_{max}

Ref: Marks, Marvin D. "Flight Test Development of XV–1 Convertiplane"

The XV–1 Had Positive Static Longitudinal Stability Above 60 knots. The Trim Tab Could Be Used To Reposition The Stick For Comfort.
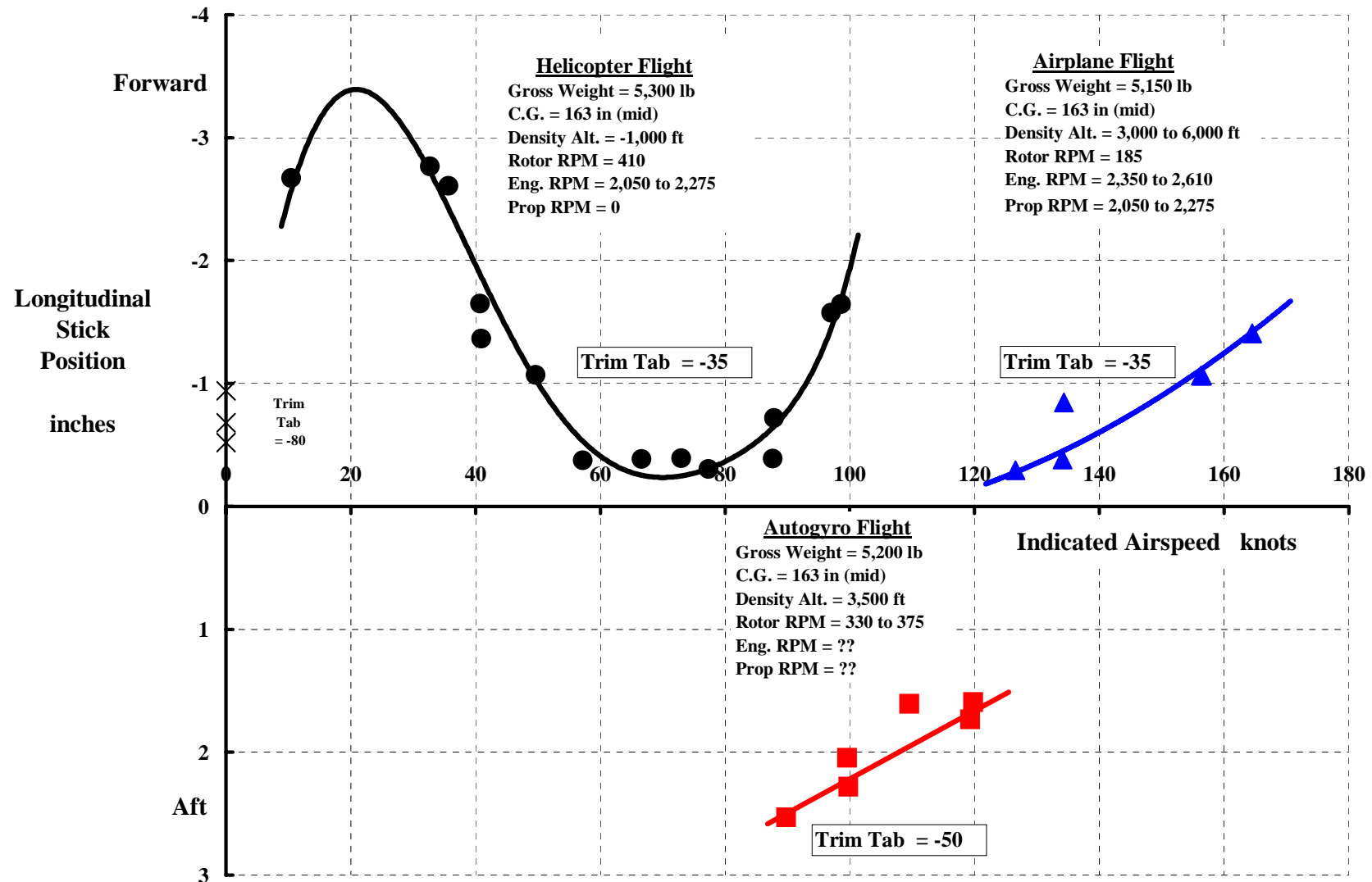
Ref: Putnam, V.K. and Eggert, W.W. "Phase II, Flight Evaluation (of the XV–1)" AFFTC–TR-56-35, Feb. 1957. (Also ASTIA AD-112423)

Very Little Lateral Stick Was Required To Trim The XV–1.

Helicopter Flight
Gross Weight = 5,300 lb
C.G. = 163 in (mid)
Density Alt. = -1,000 ft
Rotor RPM = 410
Eng. RPM = 2,050 to 2,275
Prop RPM = 0

Airplane Flight
Gross Weight = 5,150 lb
C.G. = 163 in (mid)
Density Alt. = 3,000 to 6,000 ft
Rotor RPM = 185
Eng. RPM = 2,350 to 2,610
Prop RPM = 2,050 to 2,275

Autogyro Flight
Gross Weight = 5,200 lb
C.G. = 163 in (mid)
Density Alt. = 3,500 ft
Rotor RPM = 330 to 375
Eng. RPM = ??
Prop RPM = ??

Lateral Stick Position inches

Right

Left

Indicated Airspeed   knots

Very Little Pedal Displacement Was Required To Trim The XV–1.

Helicopter Flight
Gross Weight = 5,300 lb
C.G. = 163 in (mid)
Density Alt. = -1,000 ft
Rotor RPM = 410
Eng. RPM = 2,050 to 2,275
Prop RPM = 0

Airplane Flight
Gross Weight = 5,150 lb
C.G. = 163 in (mid)
Density Alt. = 3,000 to 6,000 ft
Rotor RPM = 185
Eng. RPM = 2,350 to 2,610
Prop RPM = 2,050 to 2,275

Autogyro Flight
Gross Weight = 5,200 lb
C.G. = 163 in (mid)
Density Alt. = 3,500 ft
Rotor RPM = 330 to 375
Eng. RPM = ??
Prop RPM = ??

Pedal Position inches — Right / Left

Indicated Airspeed   knots

Pitch Rate Response To Aft Stick Showed Good Dynamic Stability. But, There Was Accompanying Roll Rate That Was Not Explained.

Helicopter Flight
Gross Weight = 5,300 lb
C.G. = 163 in (mid)
Density Alt. = 4,000 ft
Calibrated Airspeed = 87 kts
Trim Tab = -40
Rotor RPM = 410
Eng. RPM = ??
Prop RPM = 0
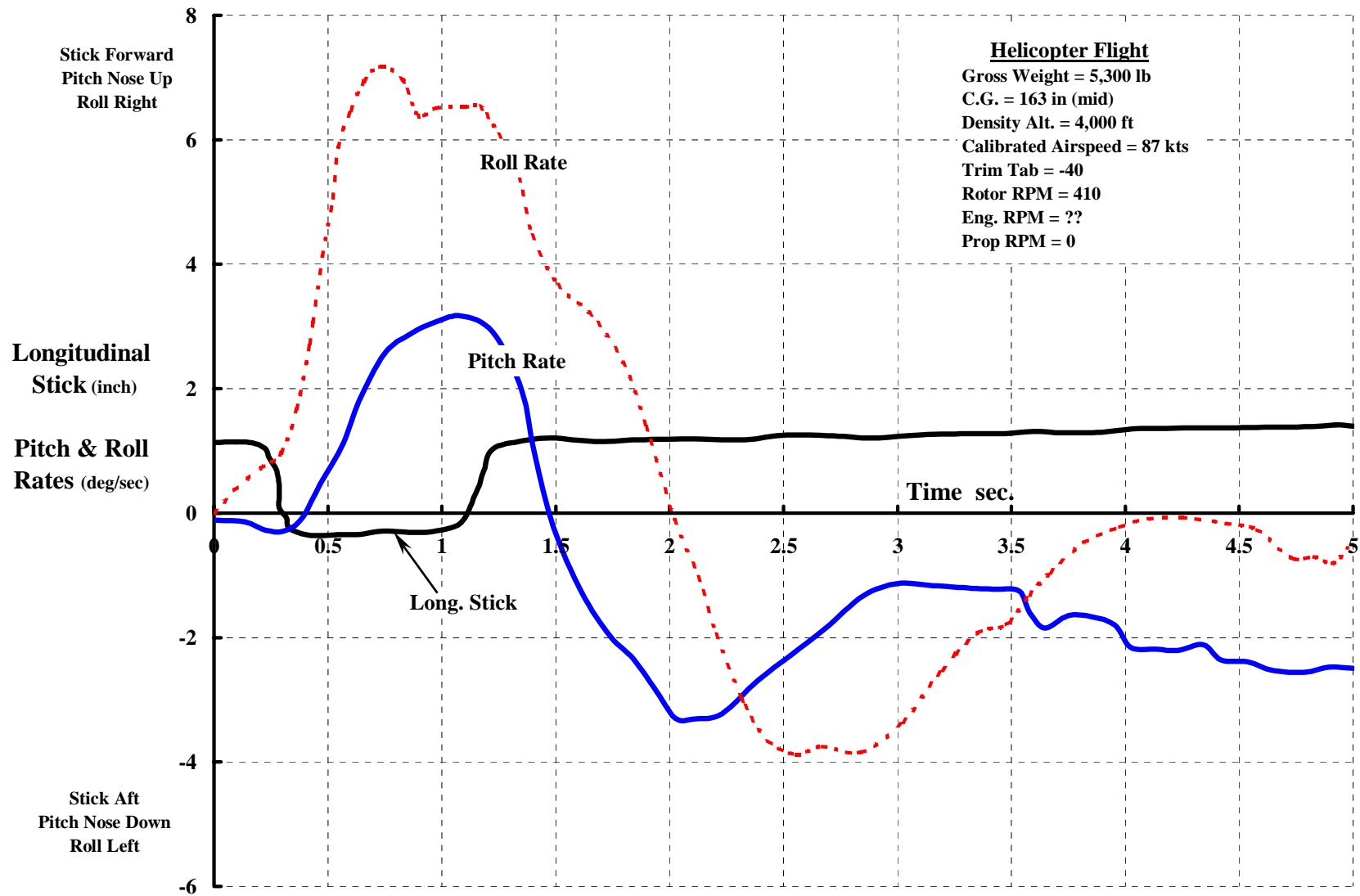
Pitch Rate – Accompanied By Roll Rate – After An Aft Stick Input Was Just As Typical In Autogyro And Airplane Flight Modes.
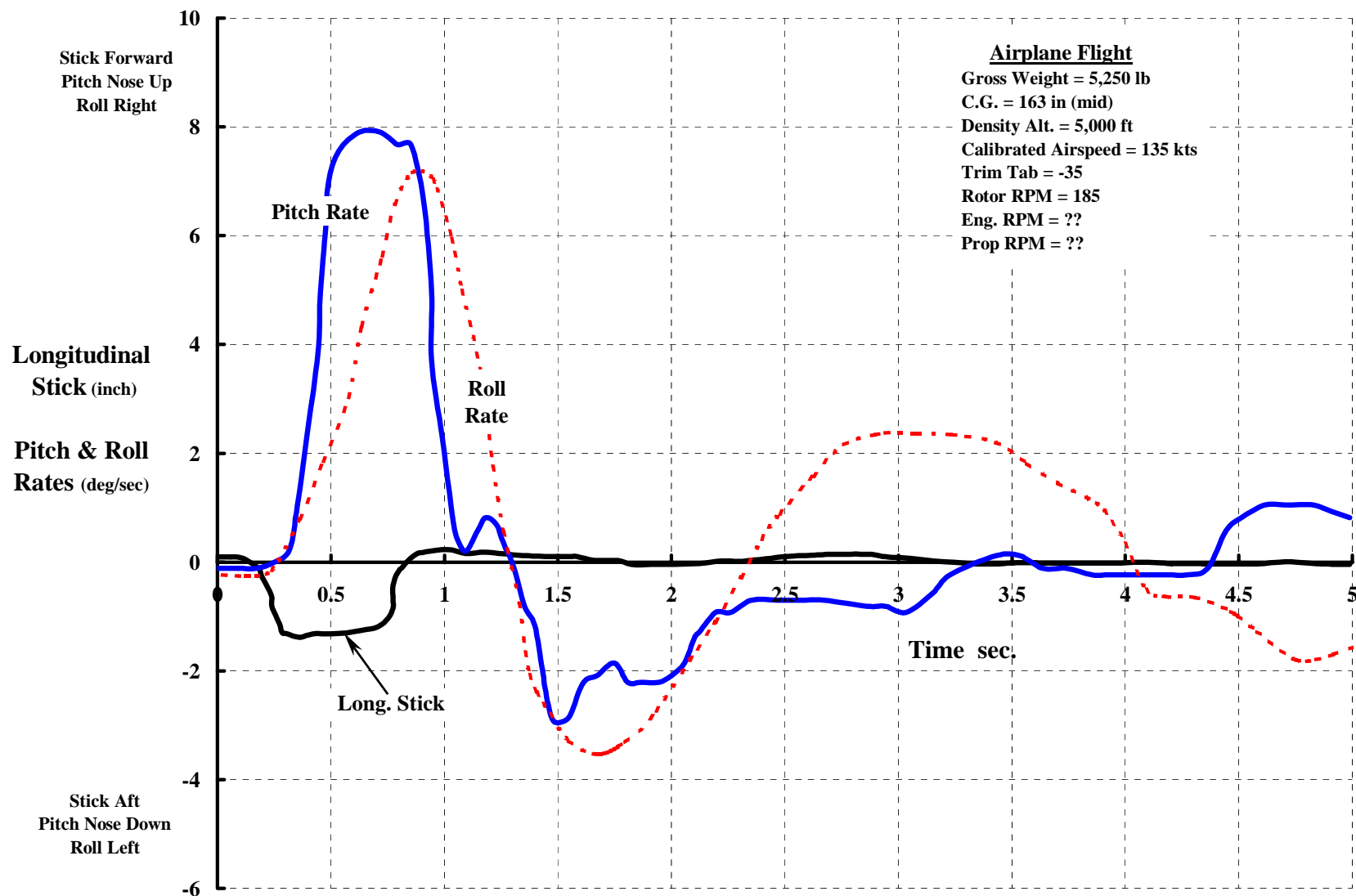
This Level Of 1P Vibration At The Pilot's Station Might Not Be Acceptable Today.
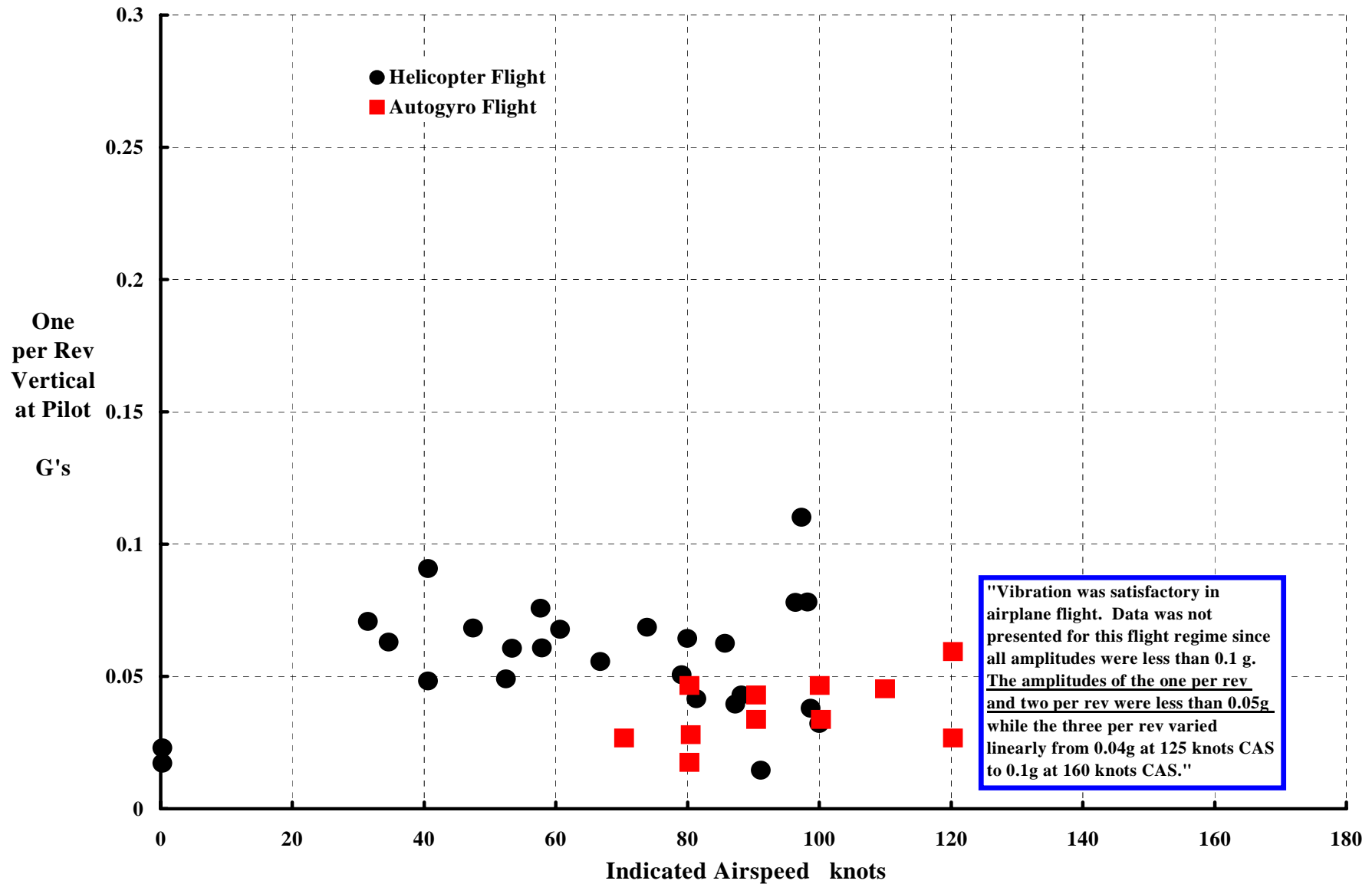
Ref: Putnam, V.K. and Eggert, W.W. "Phase II, Flight Evaluation (of the XV–1)"

This Level Of 2P Vibration At The Pilot's Station From A 3 Bladed Rotor Is Very High,

Two per Rev Vertical at Pilot Station

G's

- ● Helicopter Flight
- ■ Autogyro Flight

Indicated Airspeed   knots

"Vibration was satisfactory in airplane flight. Data was not presented for this flight regime since all amplitudes were less than 0.1 g. The amplitudes of the one per rev and two per rev were less than 0.05g while the three per rev varied linearly from 0.04g at 125 knots CAS to 0.1g at 160 knots CAS"

3P Vibration At The Pilot's Station Was Unacceptable Above 80 knots In Helicopter & Autogyro Flight. Vibration Was OK In Airplane Flight.

Three per Rev Vertical at Pilot Station

G's

● Helicopter Flight
■ Autogyro Flight
▲ Airplane Flight

"Vibration was satisfactory in airplane flight. Data was not presented for this flight regime since all amplitudes were less than 0.1 g. The amplitudes of the one per rev and two per rev were less than 0.05g while the three per rev varied linearly from 0.04g at 125 knots CAS to 0.1g at 160 knots CAS."

Indicated Airspeed   knots

"The Influence Of Stick Motions On Inplane Loads Has Been The Major Blade Loads Problem." Increasing The Inplane Stiffness Of The Flex Straps Helped.

Note: No radius station given for where these loads were measured.

BLADE VERTICAL BENDING MOMENTS
(FIGURE XIV)
(ALTERNATING)

A - HELICOPTER
B - AUTOGIRO
C - AIRPLANE

BENDING MOMENT - IN. LB.

BLADE INPLANE BENDING MOMENTS
(FIGURE XV)
(ALTERNATING)

BENDING MOMENT - IN. LB.
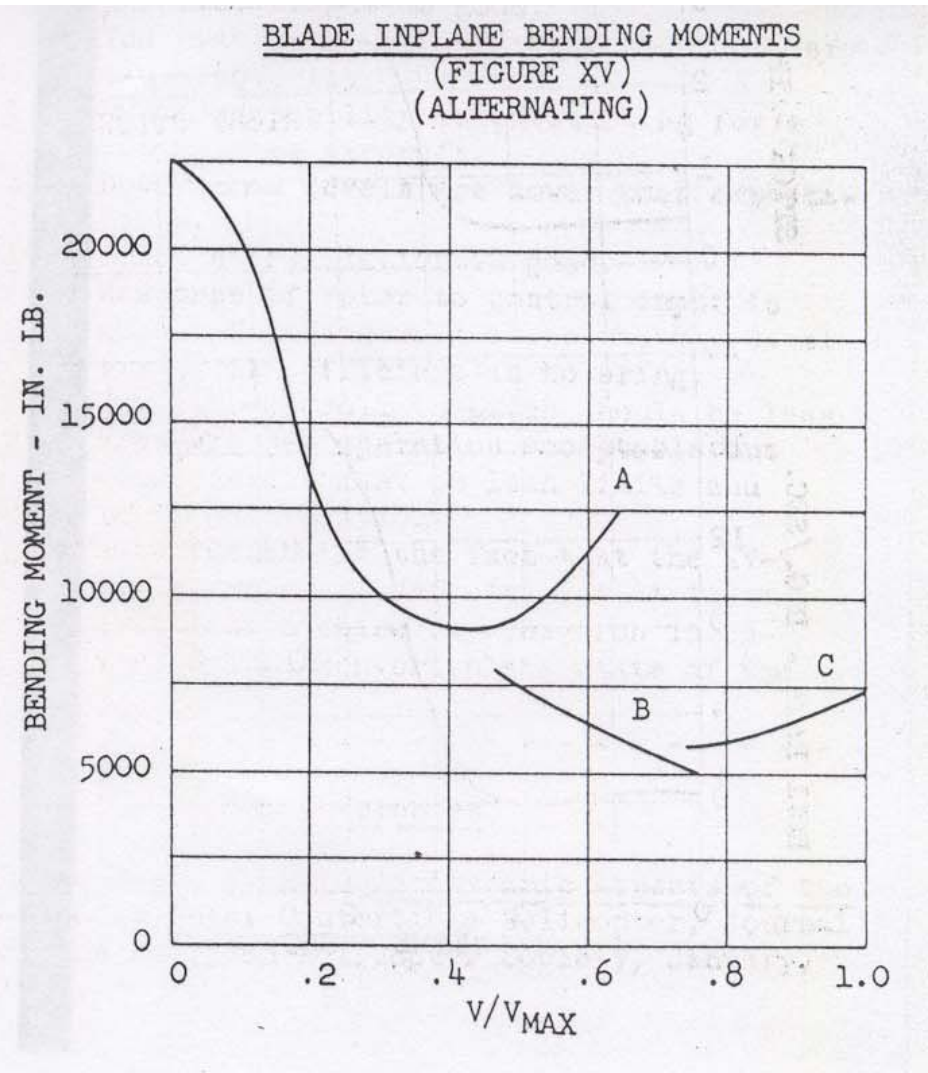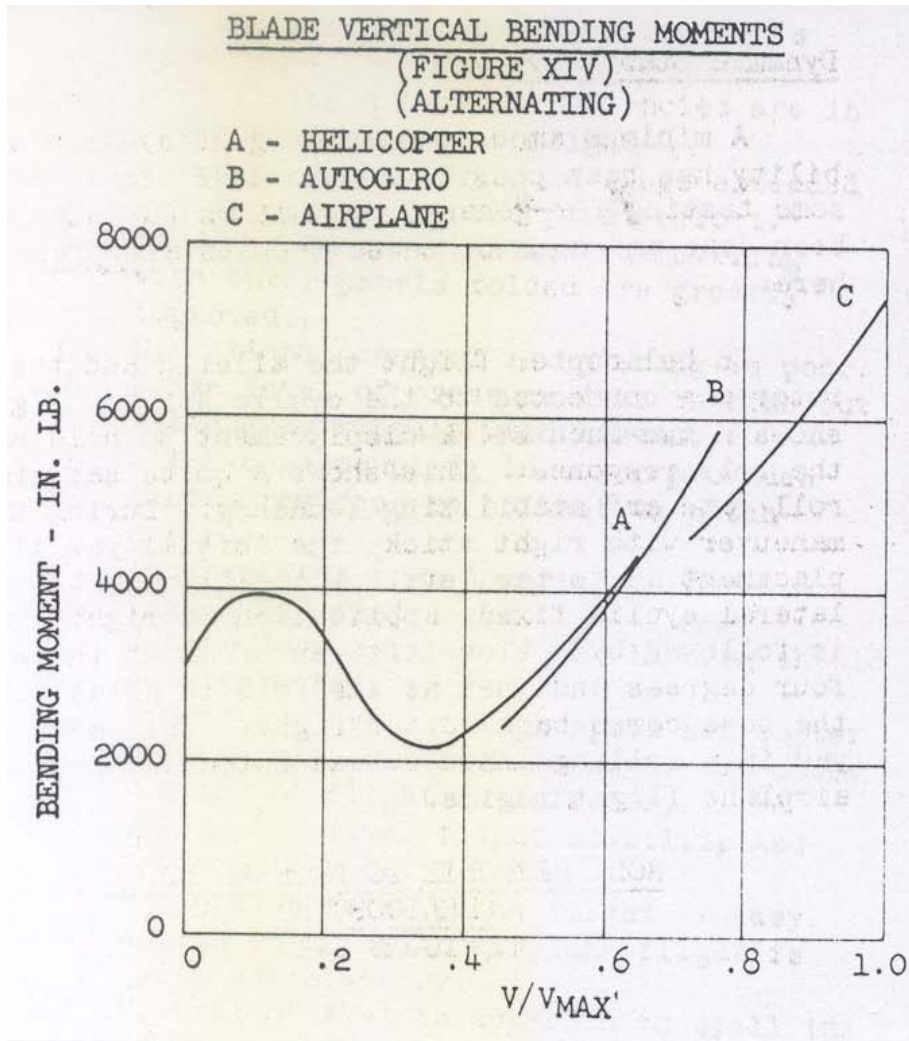
Ref: Marks, Marvin D. "Flight Test Development of XV–1 Convertiplane"

Prior To Modification (A'), The Control Stem's Bending Frequency Was Just Above 3 Per Rev. Four Pounds Removed From The Stem's Bottom Cut Loads In Half.

ALTERNATING CONTROL MOMENTS
(FIGURE XIII)

A - HELICOPTER   A' - HELICOPTER
B - AUTOGIRO   (PRIOR TO MODIFICATION)
C - AIRPLANE
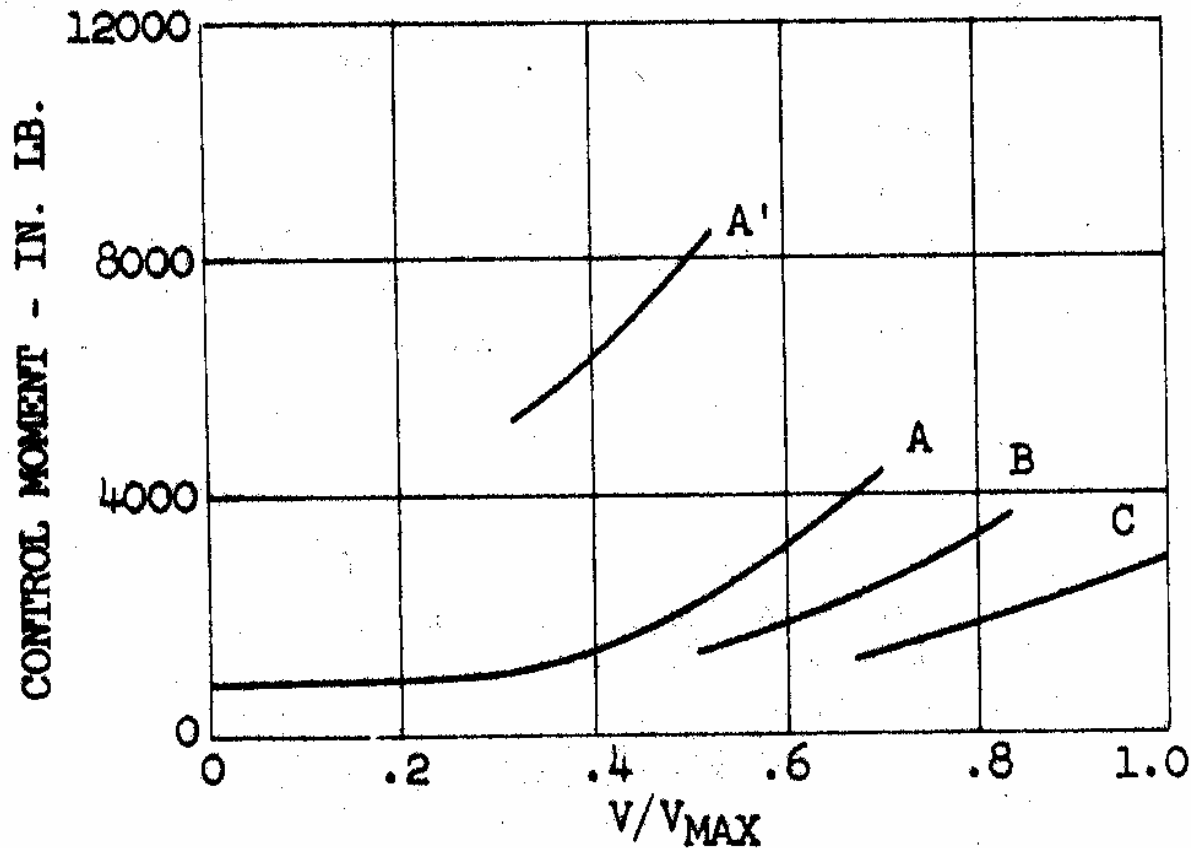
"An Intense Sound Pressure Level Was Found To Exist Out To A Radius Of Approximately 80 feet From The XV–1 While Hovering Near The Ground."

Notes: "Subjective comments made by several personnel exposed to this noise indicated that within a radius of 30 feet, one's reaction is to 'turn and run' even when protective devices for the ears are worn." A level of 116 db was recorded in the cockpit. Noise from the helicopter remained above 90 decibels at distances estimated to be as much as one-half mile away.

Overall Sound Pressure Level decibels (Ref: 0.0002 microbars)

Distance From Aircraft   feet

Notes:
a. Hovering
b. Winds 5 to 10 knots
c. Temperature = 39° F
d. Background Sound Level = 60 db
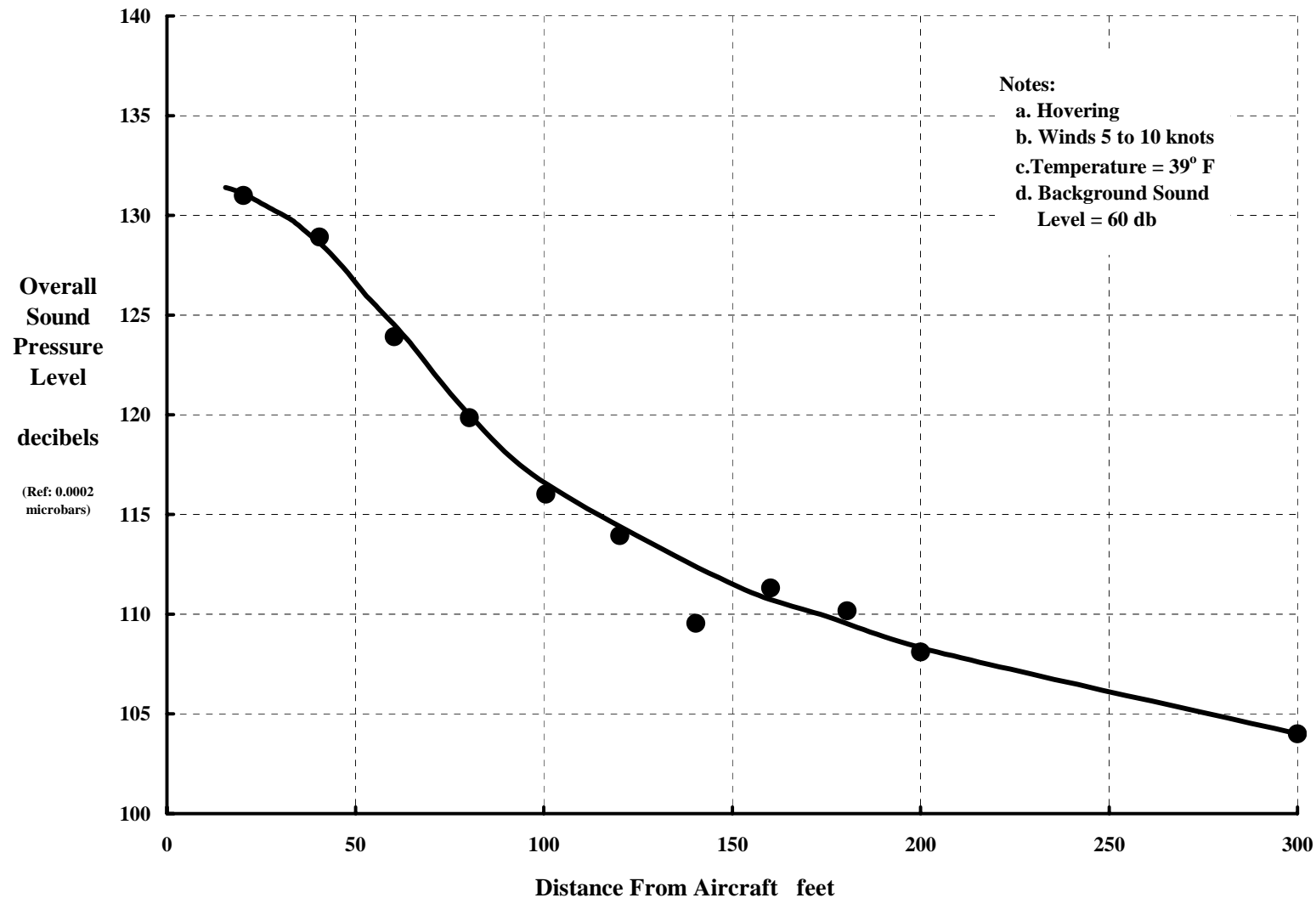
Ref: Putnam, V.K. and Eggert, W.W. "Phase II, Flight Evaluation (of the XV–1)"

Kurt Hohenemser Provided This Estimate Of Performance Based On The 40-by 80-ft WT Test. He Included Corrections For WT Strut Interference And For "Improvements In Aerodynamic Design Made Since Conducting The Wind Tunnel Tests." Helicopter Power Req'd. Based On Analysis.

Note: When Hohenemser gave his paper at the 11th AHS Forum in 1955, the XV–1 V_{max} was classified. Phase II Flight Evaluation showed maximum V_{true} = 148 kts at takeoff power of 550 BHP (i.e. N_{eng}) at sea level, standard day.

FIG. 2

XV-1 standard day level flight power required and power available.
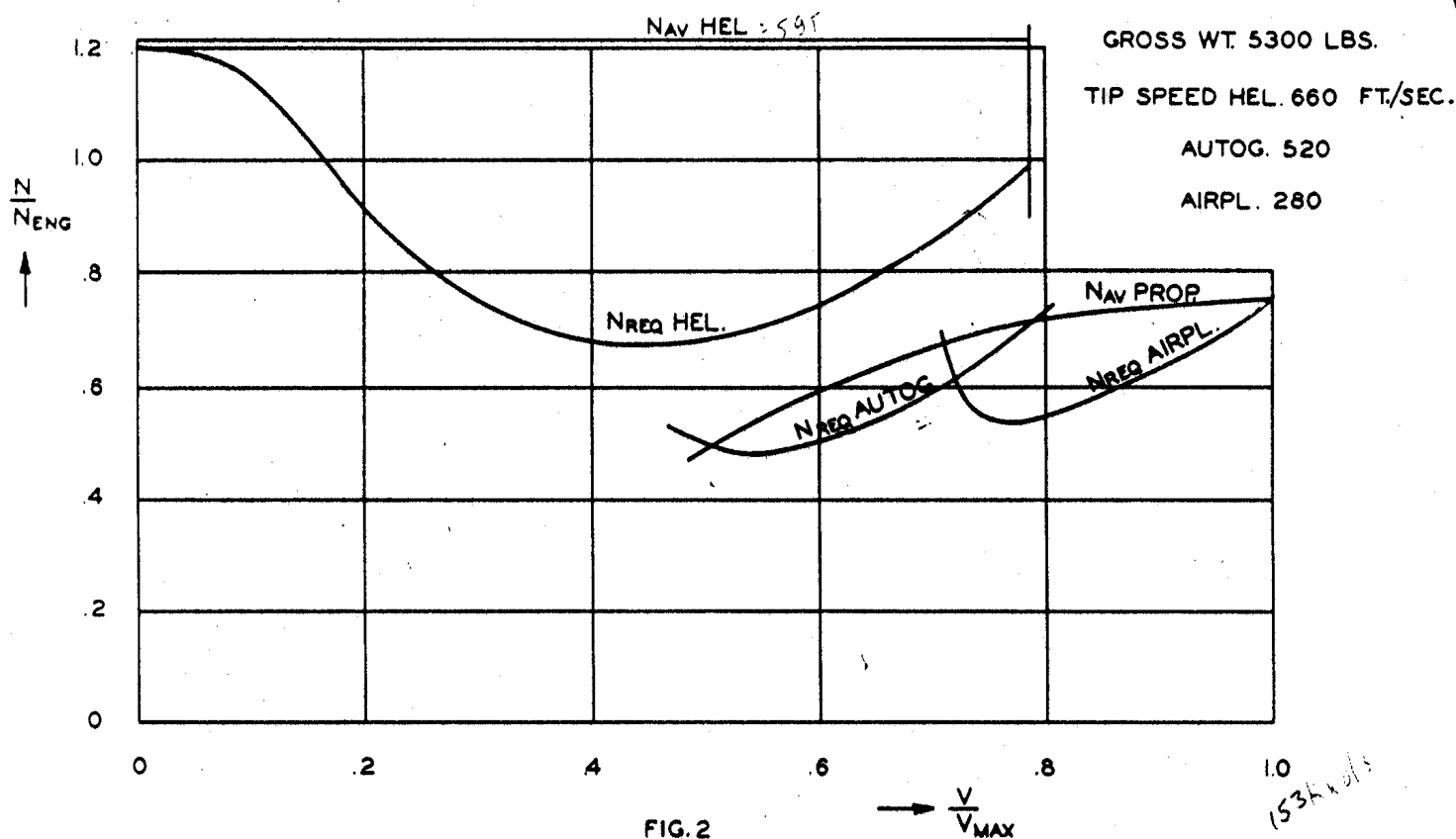
Harris Dimensional Horsepower Version Of Hohenemser Estimate.
Assumes N_{eng} = Engine TO BHP = 550hp And V_{max} = 148 knots.

Note: Also assumes cooling fan + accessories power = 50 hp

Engine Takeoff Brake Horsepower Rating (550)

$$\text{Prop Thrust HP}_{avail} = \eta_P \left(\begin{array}{l} \text{Eng BHP} \\ -\text{Cooling Fan} \\ -\text{Accessories} \end{array} \right)$$

Horsepower

Sea Level,
Standard Day

Helicopter
Engine BHP Req'd.
1. Calculated as if a
   normal helicopter
   with shaft driven rotor.
2. Includes cooling fan
   & accessories

Autogyro & Airplane
Thrust HP Req'd.
1. Derived from full scale
   40-by 80-ft. WT test.
2. **DOES NOT** include cooling
   fan & accessories

True Airspeed   knots

The XV–1's Propeller Efficiency Really Was Not Firmly Established.

Note: XV–1 data assumes engine RPM = 2,450 at sea level on a standard day.

Propeller
Propulsive
Efficiency

(SL, Std. Day)

η_P

**Harris Low Side
View For XV-1
Prop Based On
Fig. 30 Of MAC
Report No. 3599**

(See Seminar pgs. 118, 119 & 120)

**Harris Interpretation Of
XV-1 Prop Efficiency
Using Hohenemser's
THP_avail**

Assumes:
 a) Engine TO BHP = 550 hp
 b) Cooling fan &
   accessories of 50 hp

**Prop Efficiency
Used By
Wayne Weisner
In Estimating
Kellett XO-60
Autogyro
Performance**

True Airspeed   knots

Harris Dimensional Brake Horsepower Version Of Hohenemser Estimate. Assumes N_{eng} = Engine TO BHP = 550hp And V_{max} = 148 knots.

Engine Brake Horsepower

Sea Level, Standard Day

Engine Takeoff Brake Horsepower Rating (550)

Helicopter
Engine BHP Req'd.
1. Calculated as if a normal helicopter with shaft driven rotor.
2. Includes cooling fan & accessories of 50 hp

Autogyro & Airplane
Engine BHP Req'd.
1. Derived from full scale 40-by 80-ft. WT test.
2. Includes cooling fan & accessories of 50 hp
3. Includes Hohenemser's propeller efficiency

$$\text{Eng.BHP}_{req'd.} = \frac{\text{THP}_{req'd.}}{\eta_P} + \text{HP}_{Cooling} + \text{HP}_{Acc.}$$

True Airspeed   knots

Prediction Of Autogyro & Airplane Flight Performance Was Darn Good.
(It's Too Bad The Aircraft Was Underpowered & The Prop Was Too Small.)

Note: A proposal to re–engine with a turbine did not get supported.

Autogyro
Phase II Flight
Evaluation Report,
Discussion, pg 17
Note: Harris guess

Airplane
Phase II Flight
Evaluation Report,
Fig. No. 23, pg 48
Note:Adjusted for slight
descent at 148 and 161 knots
points

Engine TO BHP (550)

Engine
Brake
Horsepower

Sea Level,
Standard Day

Autogyro & Airplane
Engine BHP Req'd.
1. Derived from full scale
   40-by 80-ft. WT test.
2. Includes cooling fan &
   accessories of 50 hp
3. Includes propeller efficiency

True Airspeed   knots

Helicopter Flight With Pressure Jet Tip Drive Takes A Lot Of Fuel.

A-171
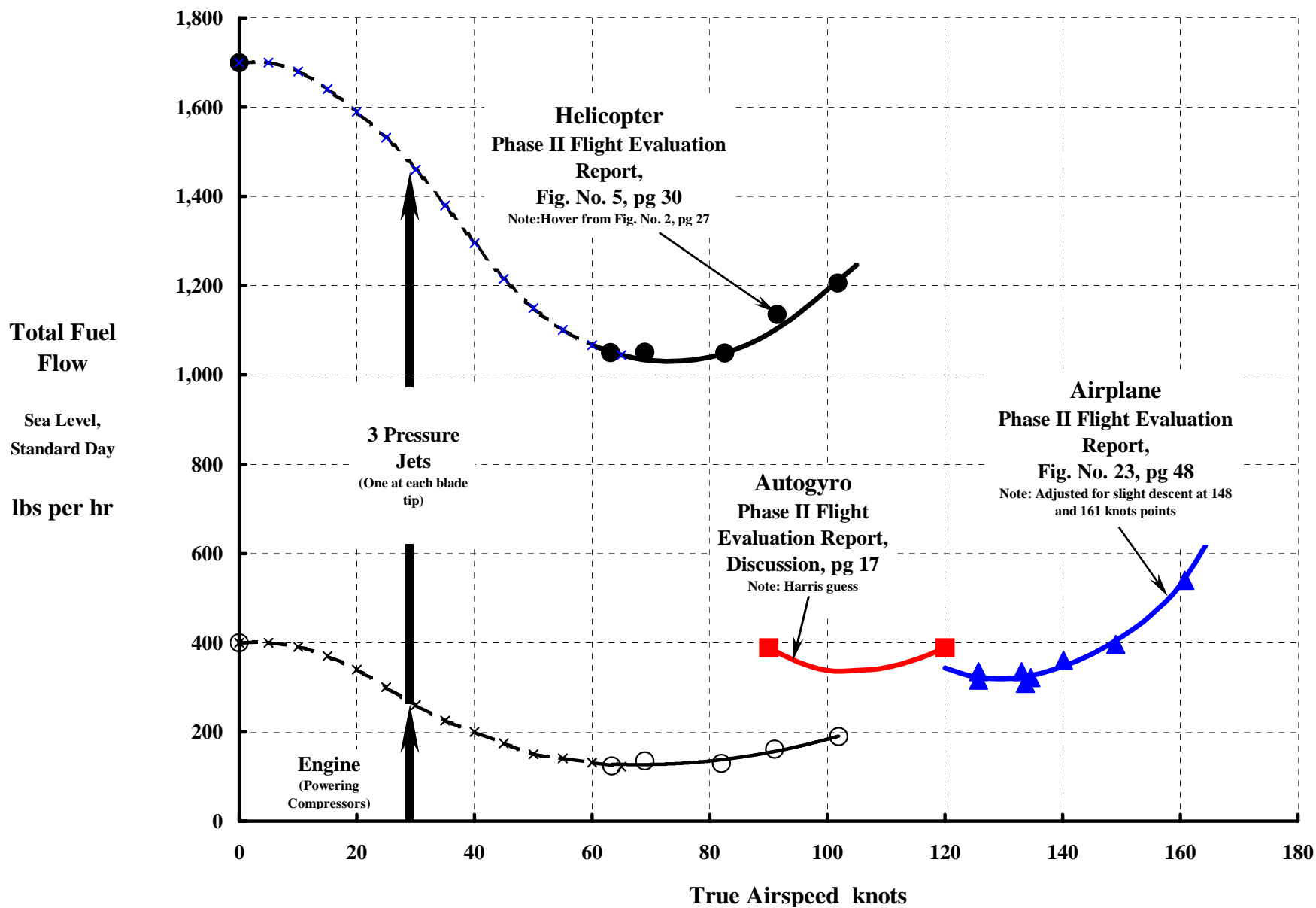
The Phase II Report Said The XV–1 Did Not Compare Well Versus "a typical fixed wing specific range of 1.1 nautical miles per pound of fuel at similar gross weight."
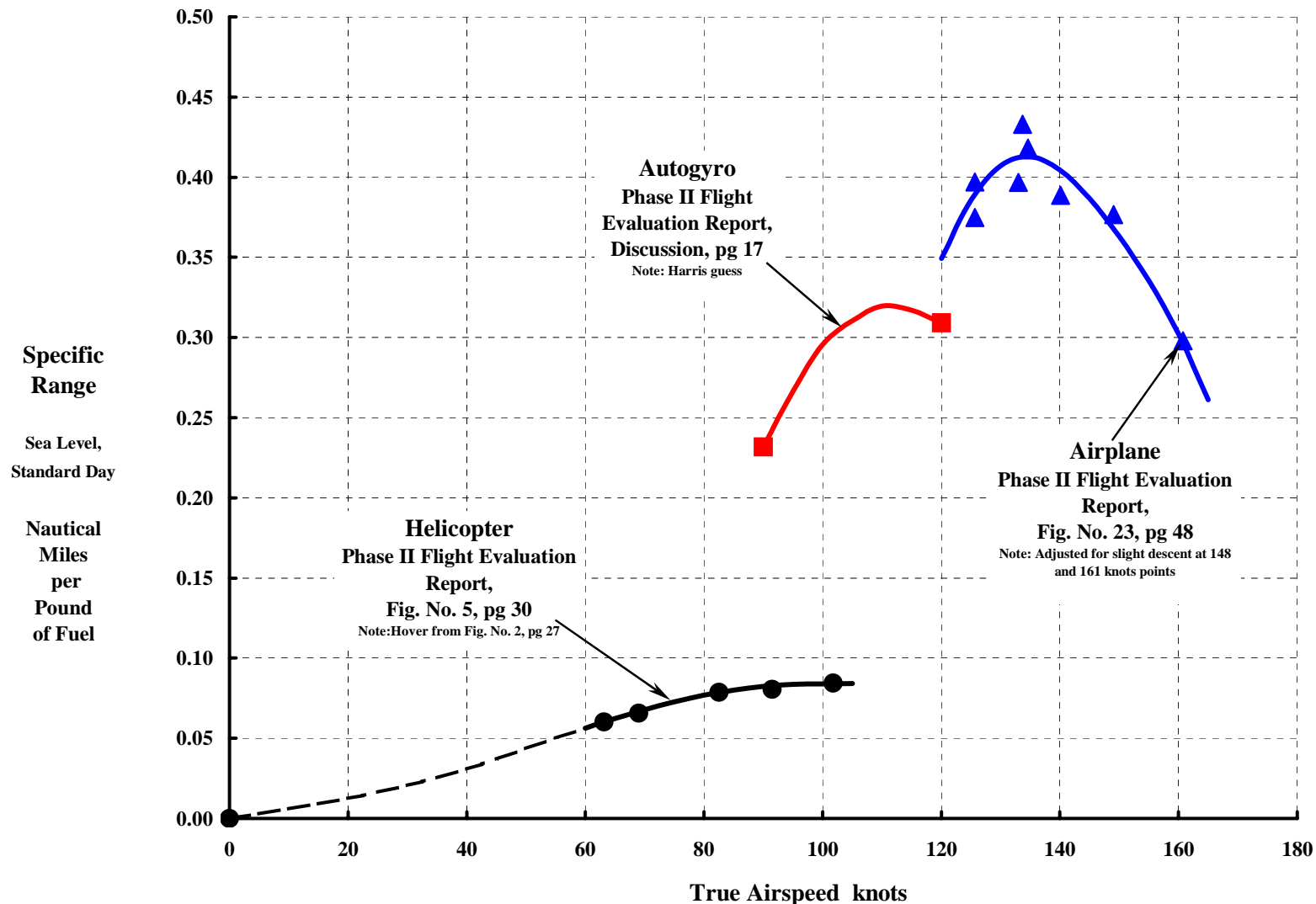
<u>Overall, The Evaluation Report Had Favorable Conclusions.</u>

1. The positive lateral and longitudinal stability provided by this rotor design is outstanding compared to current operational helicopters. Control sensitivity, however, is insufficient for precise control of the aircraft, particularly at low speeds.

2. The rotor induced vibration level above 80 knots in helicopter flight is unsatisfactory.

3. Directional control power is inadequate at low speeds.

4. Folding the wings is effective in improving hovering performance.

5. The reliability of the pressure jet burners installed is considered marginal as a result of inconsistency in lean limits between burners and susceptibility to power fluctuation in certain flight conditions.

6. The noise level from the pressure jet burners is such that protection (ear plugs or ear muffs) will be required at all times for ground crew within the immediate area of the aircraft.

7. Conversion procedures are not difficult but some simplification appears possible.

8. Stability and control in airplane flight are good. The unloaded rotor does not have any adverse effect on the flight characteristics of the aircraft.

9. Good control and a satisfactory vibration level were exhibited at the maximum speeds attained during airplane flight. The unloaded rotor configuration appears to have good high speed potential.

10. In airplane flight this rotor is capable of unloading the fixed wing as speed is decreased, thus delaying wing stall. This is potentially a very useful feature.

11. With some development it appears that one trim setting could be used for all flight regimes.

12. This airframe configuration appears to have caused many undesirable flight characteristics. The most important of these are as follows:

    a. Arbitrary rolling and lateral movement in hover as caused by the rotor wash over the airframe.
    b. Yawing tendency in transition.
    c. Large trim changes required from hover to forward flight.
    d. Static longitudinal instability during transition [from hover to about 60 kts.]
    e. Insufficient static directional stability, particularly in helicopter flight.
    f. Low frequency vibration of the aircraft in sideslip in airplane flight.

The Evaluation Report's Recommendations Were Encouraging:

It is recommended that the XV-1 be utilized to the fullest extent in the development of the unloaded rotor principle, the pressure jet system, and the pitch-cone coupled rotor system for application to future designs.

A minimum of XV-1 flight time should be expended in solution of problems associated with this particular airframe configuration. In particular the following should be accomplished immediately on the XV-1:

1. Determine, by using various control ratios, satisfactory control sensitivities for this rotor design.

2. Investigate means of simplifying conversion procedures.

3. Determine minimum airspeed that can be attained by unloading the fixed wing with the rotor in airplane flight, and stability and control characteristics in this flight condition.

4. Develop technique required for use of one trim setting for all flight regimes.

5. Investigate the cause and determine means of eliminating the vibration at high speed in helicopter flight.

6. Investigate the cause and determine means of eliminating the pitch roll coupling experienced during all dynamic longitudinal stability tests.

Also, Marks, in his AHS Journal paper (Vol. 2, No. 1–1957), summarized development and flight testing of the XV–1 with 23 additional points.

A Pretty Impressive Team If You Ask Me!

Photo courtesy of Dave Peters from Kurt Hohenemser file. Note: Bob Head could not see Kurt Hohenemser, Fred Doblhoff or himself in picture.

EPILOGUE–The XV-1 Rotor Went On The Model 120. The Rotor Was Also Scaled Up To 75 feet For XHCH; Ground Tests Were Done.

Photos courtesy of Bob Head. Note: Ft Rucker has one XV–1 and the Air & Space Museum has the other.

Model 120

XHCH

LET'S REVISIT AUTOGYROS

First Some History

Cierva, Pitcairn, and Kellett Era (1919 to 1941)
Selection of the Helicopter (1942)
Legacy

Some Technology Aspects

What's in a Name?
Fuselages, Wings, Propellers, Rotors and Trim
Rotor Thrust and Flapping Behavior at High Advance Ratio
Limits to Rotor Lift and Propulsion
To Review Then

XV–1 Re–examination

Full Scale Wind Tunnel Test in 40 by 80
Rotor (With & Without Wing)
Complete Aircraft
Rotor Stability In Forward Flight
Phase II Flight Evaluation

→ Concluding Remarks

Think What Could Be Done With The XV–1 Concept Today.

Note: The red dotted line covers the Phase II Report "a typical fixed wing specific range of 1.1 n.m. per lb of fuel at similar gross weight."

$$SR = 3.50 \left(\frac{TOGW}{1,000} \right)^{-1.0}$$

$$SR = 5.75 \left(\frac{TOGW}{1,000} \right)^{-1.0}$$

$$SR = 2.15 \left(\frac{TOGW}{1,000} \right)^{-1.0}$$

YOH-6A
April 6,1966
World Record
TOGW = 3,235 lb
Fuel Used = 1,850 lb
Range = 1,978 n.m.
Ref: 23rd AHS Forum No. 125

UH-1H (T800)
April 22,1993
TOGW = 9,916 lb
Fuel Used = 4,101 lb
Range = 1,492 n.m.
Ref: 50th AHS Forum page 601 to 612

McDonnell XV-1
(at SL Std. Day)

Airplane
Autogyro
Helicopter

Note:Several hundred helicopter data points from Harris file

Specific Range

Nautical Miles per Pound of Fuel

10

1

0.1

0.01

100

1,000

10,000

100,000

Take Off Gross Weight pounds

LIST_ONE.xls

And I Also Think That:

It appears doubtful that we can dig enough up on the Rotodyne to have a good data base – unless someone in England comes through.

A solution to the pressure jet tip propulsion system noise and fuel consumption problems may not exist. I vote for a shaft driven main rotor. Additionally, the XV–1 blade thickness, tip jet size, inboard cuff around torque tube–but exposed blade retention flex straps–translated to an average blade C_{do} of 0.0124 at flat pitch in whirl testing and more like a C_{do} of 0.019 in forward flight, virtually twice that of today's helicopters.

The Lockheed AH–56 Cheyenne needs to be re–examined. It had the lowest drag hub I've ever seen. Couple it's blade retention / pitch change configuration with Hohenemser's very high pitch–flap approach and the rotor system should be a snap – even out to 1.2 advance ratio. Of course, we'd need a fly by "something" control system.

The interference drag between a faired hub (i.e., like the XV–1) and a pylon is 2 or 3 times what you might think,

There is little need to dream if the base aircraft (fuselage, wing, pylon, hub and propulsive system) can't produce a maximum L/D of 12 to 15. Given this L/D breakthrough, the lowest solidity rotor that can do the helicopter job will do fine.

The stiff inplane approach makes a lot of sense. But slowing the rotor RPM down and passing through blade resonance's suggests that vibration isolation will be required. Five to 10 seconds of airframe shutter (0.7g) at 2 per rev (or 3 or 4 per rev) isn't good enough.

The transition from helicopter to airplane flight and back must be transparent. Loosing 1,000 to 1,500 feet as the underpowered XV–1 did is not an option.

Extravagant – even excessive – claims by management, program offices, marketing, engineering and/or manufacturing are out and out lies. Even overly optimistic claims are very, very undesirable.

<u>Acknowledgements</u>

Supplemental Data And Charts

1. The Production Cierva C.30 $D/q = 7.57$ ft^2. It's TOGW = 1,800 lbs.

Rotor hub
$D/q = 0.84$ ft^2

Wind screens
$D/q = 0.38$ ft^2

Pylon $D/q = 0.84$ ft^2

Engine and exhaust ring
$D/q = 1.43$ ft^2

Undercarriage and its wheels
$D/q = 2.44$ ft^2

I-CIER

Tail wheel
$D/q = 0.13$ ft^2

Tail plane
$D/q = 0.59$ ft^2

Fuselage, with vertical fins
$D/q = 0.93$ ft^2

Ref. Hufton, P.A. et al, "General Investigation into the Characteristics of the C.30 Autogiro", R & M No. 1859, March 1939

1. The Complete 1/8 Scale Model Of The Cierva C.30 Autogiro.
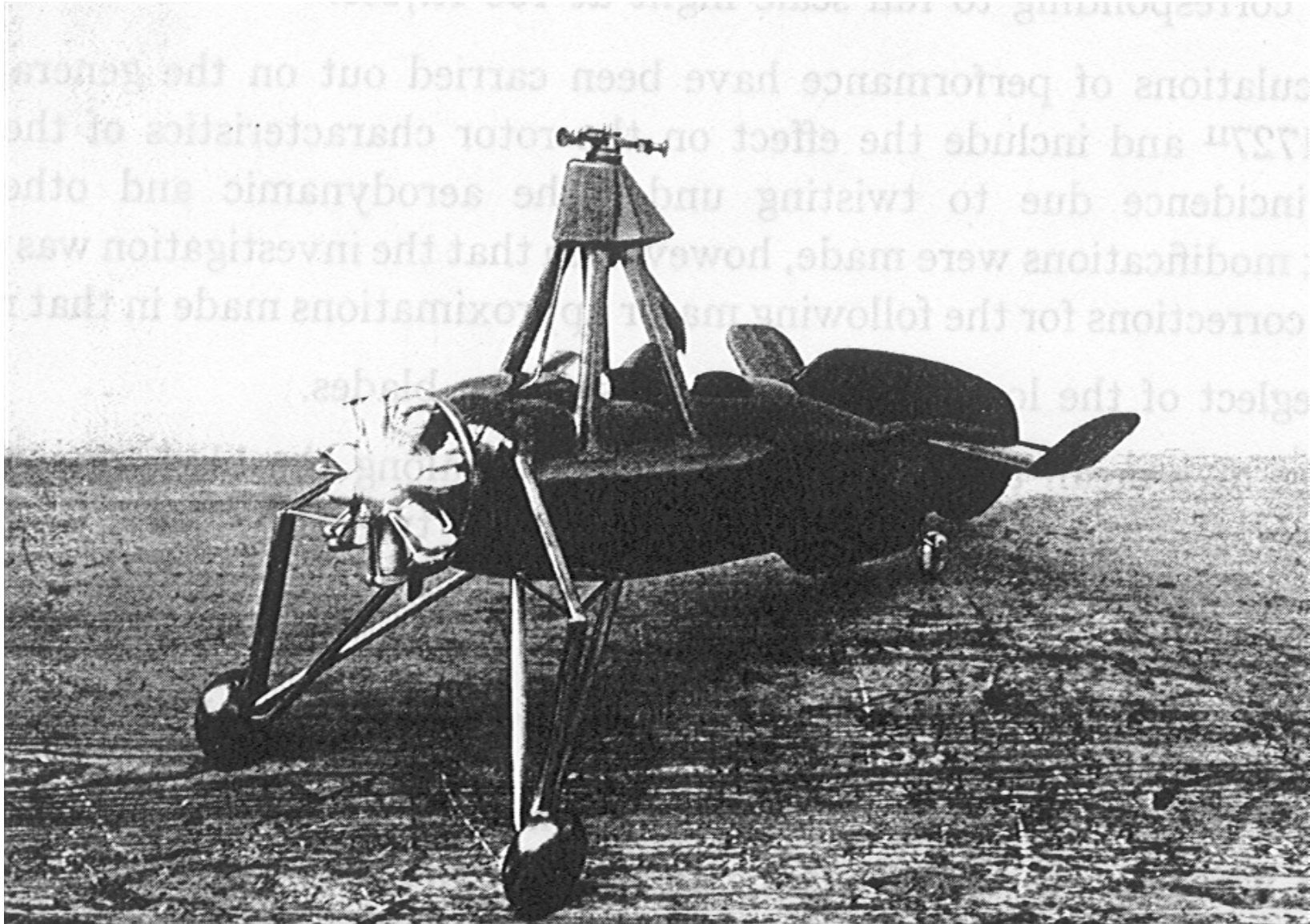
1. C.30 1/8 Scale Model Wind Tunnel Data From R & M 1859.

TABLE 12
Tests on a 1 /8 scale model of the C.30 Autogiro (without rotor) in 7 ft. No. 3 Wind Tunnel
Complete Model tested at 60 ft./sec. (corrected for Spindle and wires drag)

	Incidence (degrees)	Lift (lb.)	Drag (lb.)	Pitching Moment (lb.-ft.)	Lift (lb.)	Drag (lb.)	Pitching Moment (lb.-ft.)	Lift/q (lb.)	Drag/q (lb.)	Pitching Moment/q (lb.-ft.)
					Equivalent full scale at 100 ft./sec.			**Harris Calculated** q = 11.89		
Complete model	-4	-0.603	0.7039	0.555	-107.1	125.1	790	-9.01	10.52	66.44
	-2	-0.347	0.6888	0.25	-61.6	122.3	356	-5.18	10.29	29.94
	0	-0.149	0.6676	0.041	-26.5	118.8	58	-2.23	9.99	4.88
	2	0.001	0.6628	-0.141	0.2	117.9	-200	0.02	9.92	-16.82
	4	0.151	0 .6705	-0.287	26.8	119.2	-409	2.25	10.03	-34.40
	6	0.364	0 .6839	-0.48	64.7	121.5	-683	5.44	10.22	-57.44
	8	0.561	0.7005	-0.672	99.8	124.6	-956	8.39	10.48	-80.40
	10	0.727	0.7401	-0.85	129.3	131.5	-1210	10.87	11.06	-101.77
	14	0.999	0.8204	-1.063	177.6	145.9	-1513	14.94	12.27	-127.25
	18	1.13	1.0372	-1.21	200.8	184.2	-1721	16.89	15.49	-144.74
	22	1.225	1.245	-1.28	217.8	221.4	-1321	18.32	18.62	-111.10
	26	1.198	1.35	-1.13	212.8	240	-1608	17.90	20.19	-135.24
Tailplane removed. 60 ft./sec.										
	-4	-0.118	0.6459	-0.045	-21	115	-64	-1.77	9.67	-5.38
	0	-0.125	0.6241	0.027	-22.2	110.9	38	-1.87	9.33	3.20
	2	-0.133	0.6155	0.038	-23.6	109.4	54	-1.98	9.20	4.54
	6	-0.088	0.61	0.094	-15.6	108.6	134	-1.31	9.13	11.27
	10	-0.05	0.6241	0.127	-8.9	110.9	181	-0.75	9.33	15.22
	14	-0.017	0.6609	0.198	-3.2	117.6	282	-0.27	9.89	23.72
	18	0.048	0.6942	0.239	8.5	123.2	340	0.71	10.36	28.60
	22	0.137	0.7317	0.266	24.4	130.1	378	2.05	10.94	31.79
	26	0.211	0.7865	0.312	37.5	139.9	444	3.15	11.77	37.34

1. C.30 1/8 Scale Model Wind Tunnel Data From R & M 1859.

TABLE 13

Model tested at 0° incidence over a range of wind speed

	Wind Speed (ft./sec.)	Lift (lb.)	Drag (lb.)	Pitching Moment (lb.-ft.)	Equivalent full scale at 100 ft./sec. Lift (lb.)	Drag (lb.)	Pitching Moment (lb.-ft.)	Harris Calculated q = 11.89 Lift/q (lb.)	Drag/q (lb.)	Pitching Moment/q (lb.-ft.)
Complete model	40	-0.049	0.3074	0.021	-19.6	123	67	-1.65	10.34	5.63
	50	-0.096	0.4708	0.031	-24.6	120.6	64	-2.07	10.14	5.38
	60	-0.144	0.6625	0.031	-25.6	117.9	44	-2.15	9.92	3.70
	70	-0.23	0.8824	0.062	-30	115.2	65	-2.52	9.69	5.47
	80	-0.333	1.1354	0.093	-33.3	113.5	74	-2.80	9.55	6.22
	90	-0.441	1.4071	0.155	-34.8	111.1	97	-2.93	9.34	8.16
Tailplane removed	40	-0.038	0.2892	0.01	-15.2	115.7	32	-1.28	9.73	2.69
	50	-0.071	0.4395	0.01	-18.2	112.5	20	-1.53	9.46	1.68
	60	-0.12	0.6211	0.016	-21.3	110.4	23	-1.79	9.29	1.93
	70	-0.191	0.8227	0.037	-25	107.4	39	-2.10	9.03	3.28
	80	-0.263	1.0606	0.016	-26.3	106.1	13	-2.21	8.92	1.09
	90	-0.355	1.3132	0.048	-28	103.9	30	-2.35	8.74	2.52
Rotor hub also removed	60	-0.099	0.5641	-0.031	-17.6	100.2	-44	-1.48	8.43	-3.70
	90	-0.325	1.1827	-0.062	-25.7	93.5	-39	-2.16	7.86	-3.28
Engine and exhaust ring also removed	40	-0.038	0.2168	-0.01	-15.2	86.7	-32	-1.28	7.29	-2.69
	50	-0.067	0.336	-0.021	-17.2	86.1	-43	-1.45	7.24	-3.62
	60	-0.114	0.4663	-0.021	-20.3	83	-30	-1.71	6.98	-2.52
	70	-0.182	0.6158	-0.031	-23.8	80.5	-32	-2.00	6.77	-2.69
	80	-0.263	0.7882	-0.041	-26.3	78.8	-33	-2.21	6.63	-2.78
	90	-0.357	0.9746	-0.052	-28.2	77	-33	-2.37	6.48	-2.78
Undercarriage also removed	40	-0.02	0.0946	0.064	-8	37.8	203	-0.67	3.18	17.07
	50	-0.023	0.1439	0.081	-5.9	36.8	166	-0.50	3.10	13.96
	60	-0.023	0.2043	0.091	-4.1	36.4	129	-0.34	3.06	10.85
	70	-0.036	0.2725	0.122	-4.7	35.6	127	-0.40	2.99	10.68
	80	-0.056	0.3486	0.163	-5.6	34.9	130	-0.47	2.94	10.93
	90	-0.076	0.4234	0.205	-6	33.5	130	-0.50	2.82	10.93
Windscreens also removed	60		0.1794			31.9			2.68	
	90		0.3632			28.7			2.41	
Rotor pylon and tailwheel also removed (	40	-0.009	0.0364	0.027	-3.6	14.6	86	-0.30	1.23	7.23
	50		0.054			13.8			1.16	
	60		0.0758			13.5			1.14	
	70		0.0997	0.072		13.1	75		1.10	6.31
	80		0.1285			12.9			1.08	
	90	-0.058	0.163	0.13	-4.6	12.9	82	-0.39	1.08	6.90

1. C.30 1/8 Scale Model Wind Tunnel Data From R & M 1859.

TABLE 15
Drag of 1 /8 scale C.30 autogiro model in the compressed air tunnel

					Equivalent full scale at 100 ft./sec.	Harris Calculated q = 11.89		
Density (slug per cubic feet)	Wind Speed (f t./sec.)	Log log(.125* V*Density /0.00237)	Model Scale D/q (sq. ft.)	Drag (lb.)		Lift/q (lb.)	Drag/q (lb.)	Pitching Moment/q (lb.-ft.)
0.00234	79.3	-0.004079	0.1544	117.2			9.86	
0.00355	50.0	-0.01262	0.1542	117.1			9.85	
0.00355	62.4	0.0283982	0.1527	115.8			9.74	
0.00355	74.9	0.0595149	0.1472	111.8			9.40	
0.00355	84.8	0.0794656	0.1476	112.0			9.42	
0.00682	36.0	0.0462018	0.1493	113.3			9.53	
0.00682	43.2	0.0760685	0.1462	111.0			9.34	
0.00682	50.4	0.0998106	0.1406	106.7			8.97	
0.00682	57.6	0.1193775	0.1394	105.9			8.91	
0.00682	68.4	0.1433278	0.1348	102.2			8.60	
0.00682	79.6	0.1634176	0.1332	101.1			8.50	
0.00979	48.1	0.144602	0.1341	101.9			8.57	
0.00979	60.1	0.1737161	0.1283	97.5			8.20	
0.00979	72.2	0.1963093	0.1231	93.5			7.86	
0.00979	72.2	0.1963093	0.1223	92.9			7.81	
0.00979	87.0	0.2181319	0.1189	90.3			7.59	
0.01765	40.3	0.1970631	0.1043	79.2			6.66	
0.01765	51.5	0.2254937	0.1186	90.0			7.57	
0.01765	64.8	0.2505374	0.1135	86.2			7.25	
0.01765	80.7	0.2731819	0.1118	84.9			7.14	

2. I Like Glauert's Quartic Roots Displayed This Way.
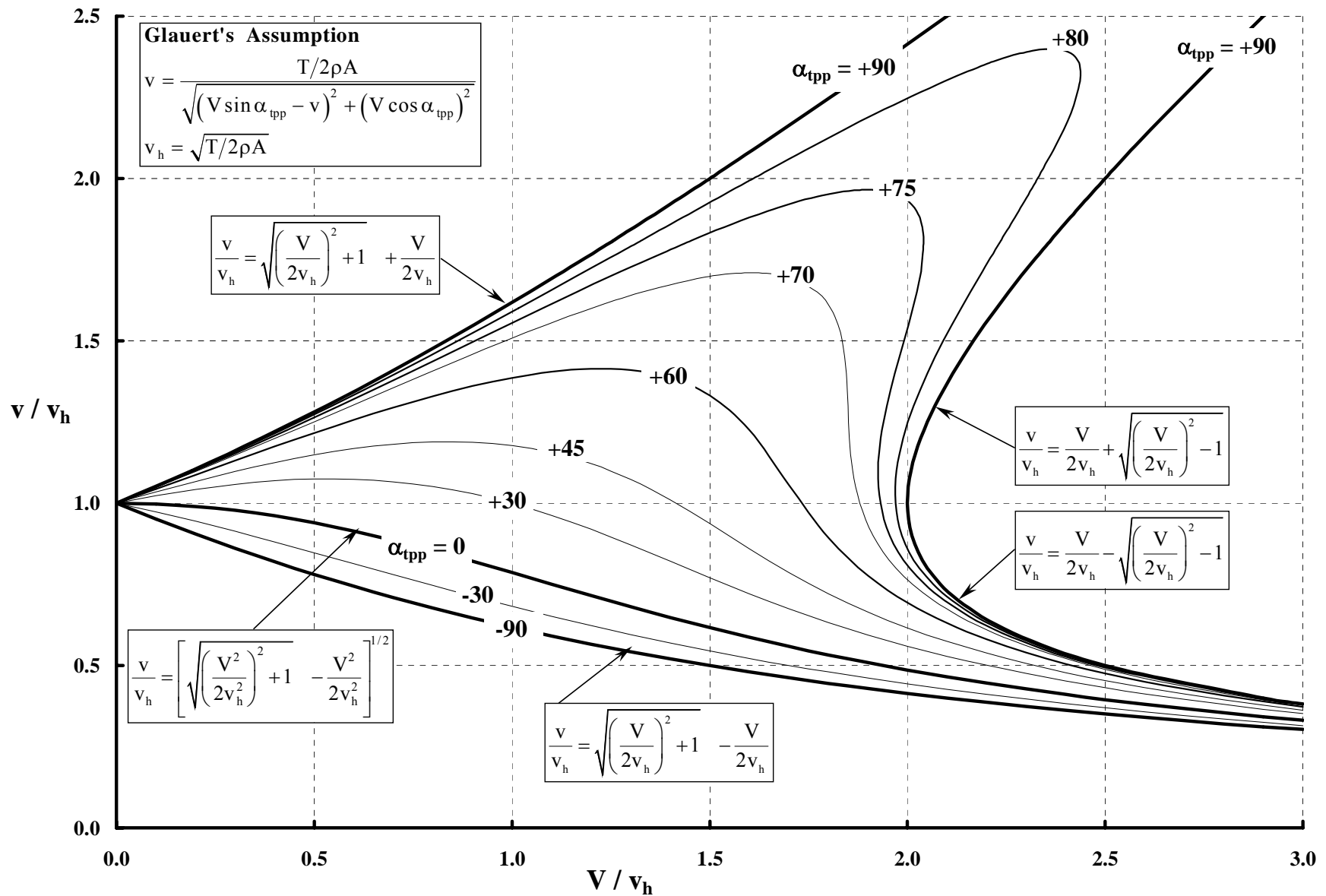
3. Glauert's Quartic Can Be Made to Follow Just 1 Root.

Glauert's Assumption

$$v = \frac{T/2\rho A}{\sqrt{\left(V\sin\alpha_{tpp} - v\right)^2 + \left(V\cos\alpha_{tpp}\right)^2}}$$

$$v_h = \sqrt{T/2\rho A}$$

$$\frac{v}{v_h} = \sqrt{\left(\frac{V}{2v_h}\right)^2 + 1} + \frac{V}{2v_h}$$

$$\frac{v}{v_h} = \frac{V}{2v_h} - \sqrt{\left(\frac{V}{2v_h}\right)^2 - 1}$$

$$\frac{v}{v_h} = \left[\sqrt{\left(\frac{V^2}{2v_h^2}\right)^2 + 1} - \frac{V^2}{2v_h^2}\right]^{1/2}$$

$$\frac{v}{v_h} = \sqrt{\left(\frac{V}{2v_h}\right)^2 + 1} - \frac{V}{2v_h}$$

$\alpha_{tpp} = +90$, $+80$, $+75$, $+70$, $+60$, $+45$, $+30$, $\alpha_{tpp} = 0$, -30, -90

v / v_h (vertical axis), **V / v_h** (horizontal axis)
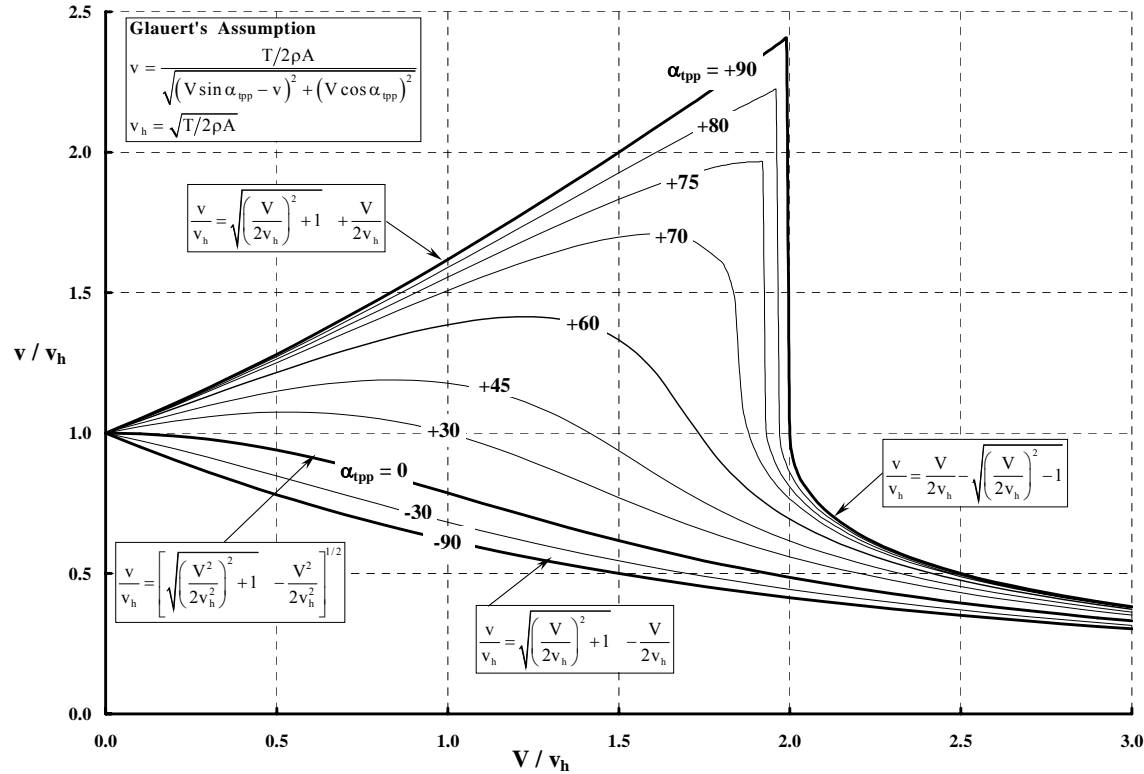
Solve $v^4 - 2\sin\alpha Vv^3 + V^2v^2 - 1 = 0$ To Give A Jump

$$G = V^8\cos^2\alpha - V^4 - 18V^4\cos^2\alpha + 27V^4\cos^4\alpha + 16$$

$$F = V^2\frac{V^4 - 18 + 54\cos^2\alpha}{1,728}$$

$$H = \frac{\sqrt{3}}{288}\sqrt{|G|}$$

$$A + B = \begin{cases} \sqrt[3]{F+H} + \sqrt[3]{F-H} & ,G > 0 \\ 2\left\{\sqrt[6]{F^2 + H^2}\right\}\left\{\cos\left[\frac{1}{3}\arccos\left(\frac{F}{\sqrt{F^2 + H^2}}\right)\right]\right\} & ,G < 0 \end{cases}$$

$$C = \frac{V^2\left(3\cos^2\alpha - 1\right)}{12}$$

$$D = \sqrt{\left[2\sqrt{\left(A+B\right)^2 + C\left(A+B\right) + C^2 - 3AB}\right] - \left(A+B+2C\right)}$$

$$v = D + \frac{V}{2}\sin\alpha - \sqrt{\left(A+B\right) - C}$$

Ref. My files (1) MathCad file labeled "Glauert DESCENT CODE.mcd" and (2) EXCEL file labeled "Quartic Solution.xls"

4. Converting Power From Torque × Ω To Force × V.

The lightly loaded propeller is a relatively uncomplicated device to picture as the following two sketches, Figures C and D, suggest. A representative blade element at some radius station, r , will have an airfoil shaped cross-section as shown in Figure C. This blade element is acted upon by two axial velocities. The prime velocity is flight speed, V. The secondary velocity is the axial component of the induced velocity, v_i. The inplane velocity is dominated by shaft rotational speed times the radius station, Ωr. The inplane component of the induced velocity is frequently called the swirl velocity. This swirl velocity is not shown in the sketches. For the lightly loaded propeller, the induced velocity is considered very much smaller than either V or Ωr.
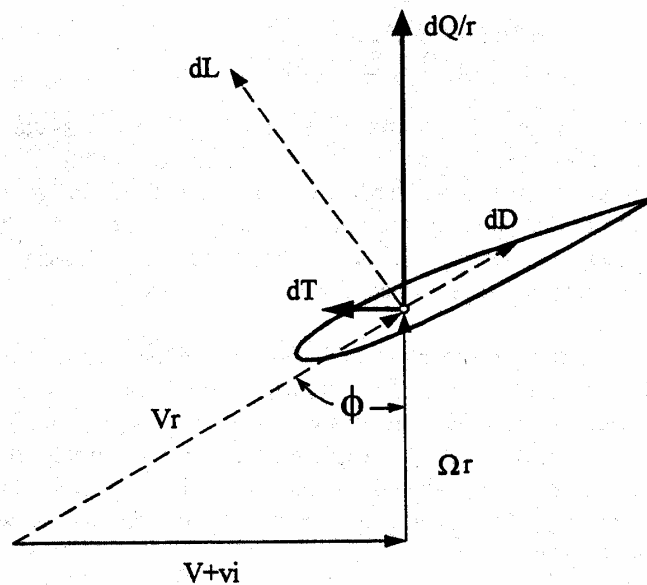
Figure C. Blade Element Sketch
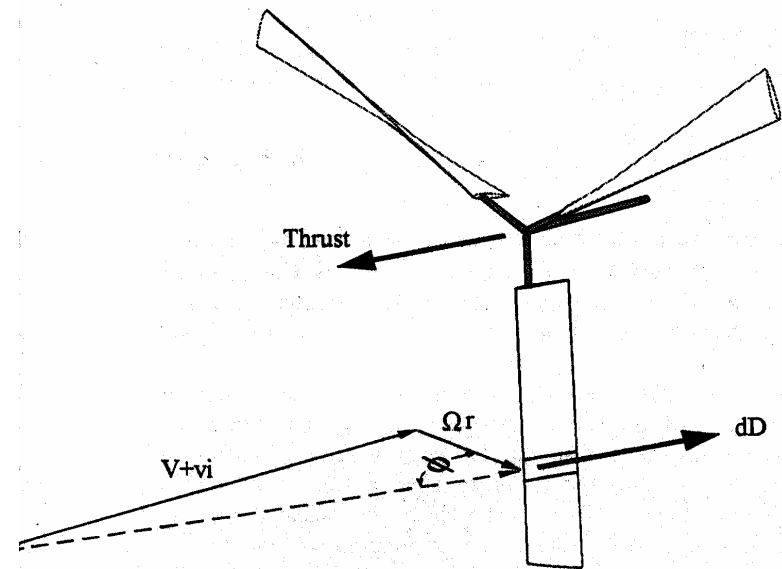
Figure D. Sketch of Prop–rotor

These simple schematics can first be used to derive the power equation introduced in this Seminar. To begin with, the thrust acts parallel to the shaft. The inplane force times the radius station gives a torque about the shaft. Power is torque times shaft rotational speed denoted as Ω. However, power can also be calculated as a force times a velocity. Three basic equations are immediately apparent from the blade element diagram. That is

Ref. 2. Harris, F.D., "Performance Analysis of Two Early NACA High Speed Propellers With Application to Civil Tiltrotor Configurations", NASA Contractor Report 196702, August 1996

4. Converting Power From Torque $\times$ Ω To Force $\times$ V. (Continued)

$$dT = dL\cos\phi - dD\sin\phi$$

$$dQ = r\left(dL\sin\phi + dD\cos\phi\right)$$

$$dP = \Omega\,dQ = \Omega r\left(dL\sin\phi + dD\cos\phi\right)$$

The transfer from calculating power as $Q\,\Omega$ to a force times velocity proceeds as follows:

a. First solve for dL from dT and substitute the result into the dP equation.

$$dL = \frac{dT + dD\sin\phi}{\cos\phi}$$

$$dP = \Omega r\left[\left(\frac{dT + dD\sin\phi}{\cos\phi}\right)\sin\phi + dD\cos\phi\right]$$

b. Next, expand the dP expression collecting the primary forces dT and dD

$$dP = \Omega r\frac{\sin\phi}{\cos\phi}\,dT + \Omega r\left[\frac{\sin^2\phi}{\cos\phi} + \cos\phi\right]dD$$

$$dP = \Omega r\frac{\sin\phi}{\cos\phi}\,dT + \Omega r\left[\frac{1}{\cos\phi}\right]dD$$

c. Then, recognize that the velocity vector diagram defines Ωr in two ways. Thus,

$$\Omega r = V_r\cos\phi \quad \text{and} \quad V + v_i = V_r\sin\phi \quad \text{or} \quad V_r = \frac{V + v_i}{\sin\phi}$$

But then a **second** definition of Ωr comes by **eliminating** V_r

$$\Omega r = \frac{V + v_i}{\sin\phi}\cos\phi \quad \text{or} \quad \Omega r\frac{\sin\phi}{\cos\phi} = V + v_i$$

as well as $\dfrac{\Omega r}{\cos\phi} = V_r$

4. Converting Power From Torque × Ω To Force × V. (Concluded)

d. Now, substitute the two ways of expressing Ωr into the power equation to get

$$dP = \left(V + v_i\right) dT + V_r \ dD$$

e. Finally, integrate the elemental dP over the blade span. If the induced velocity is assumed uniform, it follows that the total power accounting for all blades is

$$P = T V + T v_i + b\int_{root}^{tip} V_r \ dD$$

and with the integral term called profile power, P_o

$$P = T V + T v_i + P_o$$

The preceding logic reduces the performance problem to calculating the profile power, P_o , while conceding that the error in induced power will be small. It is not always easy to accurately estimate profile power, particularly when the resultant velocity at a blade element is transonic or supersonic or when there are large areas of separated flow. However, profile power can be closely approximated rather simply in many more cases than one might expect.

5. Converting From Torque × Ω To Force × V Using Gessow & Myers Equations From "Aerodynamics of the Helicopter."

The five basic equations provided in Chapter 8 are reproduced here with slight modifications. (The Fourier series for flapping is in autogyro notation of $\beta = a_0 - a_1 \cos\psi - b_1 \sin\psi$):

Eq. (16) $\quad \dfrac{2C_T}{\sigma a} = \dfrac{\theta}{3} + \dfrac{1}{2}\mu^2\theta + \dfrac{1}{2}\lambda \qquad$ where $\lambda = \dfrac{V\sin\alpha - v_i}{V_t}$ and $\mu = \dfrac{V\cos\alpha}{V_t}$

Eq. (36) $\quad a_0 = \dfrac{\gamma}{2}\left[\dfrac{\theta}{4}\left(1+\mu^2\right) + \dfrac{\lambda}{3}\right] \qquad$ where $\gamma = \dfrac{\rho\, a\, c\, R^4}{I_{flap}}$ and $I_{flap} \approx \dfrac{m\, R^3}{3}$

Eq. (37) $\quad a_1 = \dfrac{\mu\left(\frac{8}{3}\theta + 2\lambda\right)}{1 - \frac{1}{2}\mu^2} \qquad\qquad b_1 = \dfrac{4\mu\, a_0}{3\left(1 + \frac{1}{2}\mu^2\right)}$

Eq. (45) $\quad \dfrac{2C_Q}{\sigma a} = \dfrac{C_{do}}{4a}\left(1+\mu^2\right) + \left\{ -\dfrac{1}{3}\lambda\theta - \dfrac{1}{2}\lambda^2 - \dfrac{1}{8}\left(a_1^2+b_1^2\right) - \dfrac{1}{2}\mu^2\left(\dfrac{a_0^2}{2} + \dfrac{3}{8}a_1^2 + \dfrac{1}{8}b_1^2\right) - \dfrac{1}{2}\mu\lambda\, a_1 + \dfrac{1}{3}\mu\, a_0\, b_1 \right\}$

Eq. (56) $\quad \dfrac{2C_H}{\sigma a} = \dfrac{\mu\, C_{do}}{2a} + \left\{ +\dfrac{1}{3}\theta\, a_1 - \dfrac{1}{2}\mu\lambda\theta + \dfrac{3}{4}\lambda\, a_1 + \dfrac{1}{4}\mu\, a_1^2 - \dfrac{1}{6}a_0\, b_1 + \dfrac{1}{4}\mu\, a_0^2 \right\}$

You first see in the torque equation the $-\dfrac{1}{2}\lambda^2$ term, which can be replaced by $-\dfrac{2C_T}{\sigma a}\lambda + \dfrac{1}{3}\theta\lambda + \dfrac{1}{2}\mu^2\theta\lambda$ to give

Eq. (45) $\quad \dfrac{2C_Q}{\sigma a} = \dfrac{C_{do}}{4a}\left(1+\mu^2\right) + \left\{ -\dfrac{1}{3}\lambda\theta + \left[-\dfrac{2C_T}{\sigma a}\lambda + \dfrac{1}{3}\theta\lambda + \dfrac{1}{2}\mu^2\theta\lambda\right] - \dfrac{1}{8}\left(a_1^2+b_1^2\right) - \dfrac{1}{2}\mu^2\left(\dfrac{a_0^2}{2} + \dfrac{3}{8}a_1^2 + \dfrac{1}{8}b_1^2\right) - \dfrac{1}{2}\mu\lambda\, a_1 + \dfrac{1}{3}\mu\, a_0\, b_1 \right\}$

and this reduces to

Eq. (45) $\quad \dfrac{2C_Q}{\sigma a} = \dfrac{C_{do}}{4a}\left(1+\mu^2\right) + \left\{ -\dfrac{2C_T}{\sigma a}\lambda + \dfrac{1}{2}\mu^2\theta\lambda - \dfrac{1}{8}\left(a_1^2+b_1^2\right) - \dfrac{1}{2}\mu^2\left(\dfrac{a_0^2}{2} + \dfrac{3}{8}a_1^2 + \dfrac{1}{8}b_1^2\right) - \dfrac{1}{2}\mu\lambda\, a_1 + \dfrac{1}{3}\mu\, a_0\, b_1 \right\}$

Next, you see the term, $\dfrac{1}{2}\mu^2\theta\lambda$, in the torque equation and see that that term is in the H–force equation when the H–force equation is multiplied by μ. Thus, the torque equation becomes

5. Converting From Torque × Ω To Force × V (Concluded).

Eq. (45)
$$\frac{2C_Q}{\sigma a} = \frac{C_{do}}{4a}\left(1+\mu^2\right) + \left\{ \begin{array}{l} -\frac{2C_T}{\sigma a}\lambda + \left[-\frac{2C_H}{\sigma a}\mu + \frac{\mu C_{do}}{2a}\mu + \left\{+\frac{1}{3}\theta\,a_1 + \frac{3}{4}\lambda\,a_1 + \frac{1}{4}\mu\,a_1^2 - \frac{1}{6}a_0\,b_1 + \frac{1}{4}\mu\,a_0^2\right\}\mu\right] \\[3mm] -\frac{1}{8}\left(a_1^2 + b_1^2\right) - \frac{1}{2}\mu^2\left(\frac{a_0^2}{2} + \frac{3}{8}a_1^2 + \frac{1}{8}b_1^2\right) - \frac{1}{2}\mu\lambda\,a_1 + \frac{1}{3}\mu\,a_0\,b_1 \end{array} \right\}$$

which, upon collecting terms reduces to

Eq. (45)
$$\frac{2C_Q}{\sigma a} = \frac{C_{do}}{4a}\left(1+\mu^2\right) + \frac{\mu^2\,C_{do}}{2a} - \frac{2C_T}{\sigma a}\lambda - \frac{2C_H}{\sigma a}\mu + \left\{ \begin{array}{l} \left[\frac{1}{3}\mu\theta\,a_1 + \frac{3}{4}\mu\lambda\,a_1 + \frac{1}{4}\mu^2\,a_1^2 - \frac{1}{6}\mu\,a_0\,b_1 + \frac{1}{4}\mu^2\,a_0^2\right] \\[3mm] -\frac{1}{8}\left(a_1^2 + b_1^2\right) - \frac{1}{2}\mu^2\left(\frac{a_0^2}{2} + \frac{3}{8}a_1^2 + \frac{1}{8}b_1^2\right) - \frac{1}{2}\mu\lambda\,a_1 + \frac{1}{3}\mu\,a_0\,b_1 \end{array} \right\}$$

But when the equations for a_0, a_1, and b_1 are substituted in the { } portion, the { } portion equals zero. This transforms the torque equation to

Eq. (45)
$$\frac{2C_Q}{\sigma a} = \frac{C_{do}}{4a}\left(1+\mu^2\right) + \frac{\mu^2\,C_{do}}{2a} - \frac{2C_T}{\sigma a}\lambda - \frac{2C_H}{\sigma a}\mu$$

A collection of terms gives

Eq. (45)
$$\frac{2C_Q}{\sigma a} = \frac{C_{do}}{4a}\left(1+3\mu^2\right) - \frac{2C_T}{\sigma a}\lambda - \frac{2C_H}{\sigma a}\mu$$

and multiplying through by $\sigma\,a/2$ gives

Eq. (45)
$$\frac{Q}{\rho A V_t^2 R} = C_Q = \frac{\sigma C_{do}}{8}\left(1+3\mu^2\right) - C_T\,\lambda - C_H\,\mu = C_P = \frac{(P = Q\Omega)}{\rho A V_t^3}$$

Multiplying through by $\rho A V_t^3$ gives

Eq. (45)
$$P = \frac{\rho A V_t^3\,\sigma C_{do}}{8}\left(1+3\mu^2\right) - T\left(V\sin\alpha - v_i\right) - H V\cos\alpha$$

which can be regrouped to see induced power as $T\,v_i$ and profile power as $\dfrac{\rho A V_t^3\,\sigma C_{do}}{8}\left(1+3\mu^2\right)$ and so

Eq. (45)
$$P = T\,v_i - \left(T\sin\alpha + H\cos\alpha\right)V + \frac{\rho A V_t^3\,\sigma C_{do}}{8}\left(1+3\mu^2\right)$$

But rotor drag equals $\left(T\sin\alpha + H\cos\alpha\right)$ so

Eq. (45)
$$P = T\,v_i - D V + \frac{\rho A V_t^3\,\sigma C_{do}}{8}\left(1+3\mu^2\right)$$

6. The General Thrust and Rolling Moment Equations In The Tip Path Plane Coordinate System Are:

$$\frac{2C_T}{\sigma a} = \frac{1}{2\pi} \int_0^{2\pi} \int_{x_c}^1 \left(\alpha\, U_T^2\right) dx\, d\psi = \theta_0 \left(T_{\theta o}\right) + \theta_t \left(T_{\theta t}\right) + \lambda_{tpp} \left(T_{\lambda tpp}\right) - \left(B_{1C} + a_{1S}\right)\left(T_{B1C}\right)$$

$$\frac{2C_{Roll}}{\sigma a} = \frac{-1}{2\pi} \int_0^{2\pi} \int_{x_c}^1 \left(\alpha\, U_T^2\right)\left(x \sin\psi\right) dx\, d\psi = -\theta_0 \left(RM_{\theta o}\right) - \theta_t \left(RM_{\theta t}\right) - \lambda_{tpp} \left(RM_{\lambda tpp}\right) + \left(B_{1C} + a_{1S}\right)\left(RM_{B1C}\right)$$

If the rolling moment is set equal to zero (i.e., a balanced rotor), then feathering in the tip path plane becomes

$$\left(B_{1C} + a_{1S}\right) = \frac{\theta_0 \left(RM_{\theta o}\right) + \theta_t \left(RM_{\theta t}\right) + \lambda_{tpp} \left(RM_{\lambda tpp}\right)}{\left(RM_{B1C}\right)}$$

The thrust equation for a balanced rotor (i.e., $\dfrac{2C_{Roll}}{\sigma a} = 0$) then becomes

$$\frac{2C_T}{\sigma a} = \theta_0 \left(T_{\theta o} - T_{B1C}\frac{RM_{\theta o}}{RM_{B1C}}\right) + \theta_t \left(T_{\theta t} - T_{B1C}\frac{RM_{\theta t}}{RM_{B1C}}\right) + \lambda_{tpp} \left(T_{\lambda tpp} - T_{B1C}\frac{RM_{\lambda tpp}}{RM_{B1C}}\right)$$

6. The Coefficients Required By The Thrust Equation Are:

If $xc \leq \mu$, $\Delta1 = \arcsin\dfrac{xc}{\mu}$ otherwise $\Delta1 = \dfrac{\pi}{2}$ and if $\mu \leq 1$, $\Delta2 = \dfrac{\pi}{2}$ otherwise $\Delta2 = \arcsin\dfrac{1}{\mu}$

$$T\theta o := \frac{\mu^3}{9\cdot\pi}\cdot\left[6\cdot\cos(\Delta2) + 2\cdot(\cos(\Delta1))^3 - 2\cdot(\cos(\Delta2))^3 - 6\cdot\cos(\Delta1)\right] + \frac{\mu^2}{9\cdot\pi}\cdot(9\cdot\Delta2 - 9\cdot\cos(\Delta2)\cdot\sin(\Delta2) + 9\cdot xc\cdot\cos(\Delta1)\cdot\sin(\Delta1) - 9\cdot xc\cdot\Delta1) \ldots$$

$$+ \frac{\mu}{9\cdot\pi}\cdot\left(-18\cdot xc^2\cdot\cos(\Delta1) + 18\cdot\cos(\Delta2)\right) + \frac{1}{9\cdot\pi}\cdot\left(6\cdot\Delta2 - 6\cdot xc^3\cdot\Delta1\right)$$

$$T\theta t := \frac{\mu^4}{48\cdot\pi}\cdot\left[3\cdot\Delta1 + 5\cdot\cos(\Delta2)\cdot\sin(\Delta2) - 2\cdot(\cos(\Delta2))^3\cdot\sin(\Delta2) - 5\cdot\cos(\Delta1)\cdot\sin(\Delta1) + 2\cdot(\cos(\Delta1))^3\cdot\sin(\Delta1) - 3\cdot\Delta2\right] \ldots$$

$$+ \frac{\mu^2}{48\cdot\pi}\cdot\left(-24\cdot xc^2\cdot\Delta1 + 24\cdot\Delta2 + 24\cdot xc^2\cdot\cos(\Delta1)\cdot\sin(\Delta1) - 24\cdot\cos(\Delta2)\cdot\sin(\Delta2)\right) + \frac{\mu}{48\cdot\pi}\cdot\left(64\cdot\cos(\Delta2) - 64\cdot xc^3\cdot\cos(\Delta1)\right) \ldots$$

$$+ \frac{1}{48\cdot\pi}\cdot\left(-24\cdot xc^4\cdot\Delta1 + 24\cdot\Delta2\right)$$

$$TB1C := \frac{\mu^3}{12\cdot\pi}\cdot\left[-3\cdot\Delta1 - 5\cdot\cos(\Delta2)\cdot\sin(\Delta2) + 2\cdot(\cos(\Delta2))^3\cdot\sin(\Delta2) + 5\cdot\cos(\Delta1)\cdot\sin(\Delta1) - 2\cdot(\cos(\Delta1))^3\cdot\sin(\Delta1) + 3\cdot\Delta2\right] \ldots$$

$$+ \frac{\mu^2}{12\cdot\pi}\cdot\left[8\cdot xc\cdot(\cos(\Delta1))^3 + 24\cdot\cos(\Delta2) - 24\cdot xc\cdot\cos(\Delta1) - 8\cdot(\cos(\Delta2))^3\right] \ldots$$

$$+ \frac{\mu}{12\cdot\pi}\cdot\left(12\cdot xc^2\cdot\cos(\Delta1)\cdot\sin(\Delta1) + 12\cdot\Delta2 - 12\cdot xc^2\cdot\Delta1 - 12\cdot\cos(\Delta2)\cdot\sin(\Delta2)\right) + \frac{1}{12\cdot\pi}\cdot\left(-8\cdot xc^3\cdot\cos(\Delta1) + 8\cdot\cos(\Delta2)\right)$$

$$T\lambda tpp := \frac{\mu^2}{2\cdot\pi}\cdot(\Delta2 - \Delta1 + \cos(\Delta1)\cdot\sin(\Delta1) - \cos(\Delta2)\cdot\sin(\Delta2)) + \frac{\mu}{2\cdot\pi}\cdot(-4\cdot xc\cdot\cos(\Delta1) + 4\cdot\cos(\Delta2)) + \frac{1}{2\cdot\pi}\cdot\left(-2\cdot xc^2\cdot\Delta1 + 2\cdot\Delta2\right)$$

For μ = 2 and xc = 0.16, $T\theta o = 1.26738365981258$ $T\theta t = 0.866765988909496$ $TB1C = 1.6346633252304$ $T\lambda tpp = 1.12305764679466$

6. The Coefficients Required By The Rolling Moment Equation Are:

If $xc \le \mu$, $\Delta1 = \arcsin\dfrac{xc}{\mu}$ otherwise $\Delta1 = \dfrac{\pi}{2}$ and if $\mu \le 1$, $\Delta2 = \dfrac{\pi}{2}$ otherwise $\Delta2 = \arcsin\dfrac{1}{\mu}$

$$RM\theta o := \frac{\mu^4}{90\cdot\pi}\cdot\left[15\cdot\cos(\Delta1) - 10\cdot(\cos(\Delta1))^3 - 15\cdot\cos(\Delta2) + 10\cdot(\cos(\Delta2))^3 - 3\cdot(\cos(\Delta2))^5 + 3\cdot(\cos(\Delta1))^5\right] \dots$$

$$+ \frac{\mu^2}{90\cdot\pi}\cdot\left[90\cdot\cos(\Delta2) - 30\cdot(\cos(\Delta2))^3 - 90\cdot xc^2\cdot\cos(\Delta1) + 30\cdot xc^2\cdot(\cos(\Delta1))^3\right] \dots$$

$$+ \frac{\mu}{90\cdot\pi}\cdot\left(60\cdot\Delta2 - 60\cdot xc^3\cdot\Delta1 - 60\cdot\cos(\Delta2)\cdot\sin(\Delta2) + 60\cdot\cos(\Delta1)\cdot xc^3\cdot\sin(\Delta1)\right) + \frac{1}{90\cdot\pi}\cdot\left(45\cdot\cos(\Delta2) - 45\cdot xc^4\cdot\cos(\Delta1)\right)$$

$$RM\theta t := \frac{\mu^5}{720\cdot\pi}\cdot\left[-15\cdot\Delta1 - 33\cdot\cos(\Delta2)\cdot\sin(\Delta2) + 26\cdot(\cos(\Delta2))^3\cdot\sin(\Delta2) - 8\cdot(\cos(\Delta2))^5\cdot\sin(\Delta2) + 15\cdot\Delta2 - 26\cdot(\cos(\Delta1))^3\cdot\sin(\Delta1) + 8\cdot(\cos(\Delta1))^5\cdot\sin(\Delta1) + 33\cdot\cos(\Delta1)\cdot\sin(\Delta1)\right] \dots$$

$$+ \frac{\mu^2}{720\cdot\pi}\cdot\left[160\cdot(\cos(\Delta1))^3\cdot xc^3 - 160\cdot(\cos(\Delta2))^3 + 480\cdot\cos(\Delta2) - 480\cdot xc^3\cdot\cos(\Delta1)\right] + \frac{\mu}{720\cdot\pi}\cdot\left(-360\cdot xc^4\cdot\Delta1 + 360\cdot\Delta2 + 360\cdot xc^4\cdot\cos(\Delta1)\cdot\sin(\Delta1) - 360\cdot\cos(\Delta2)\cdot\sin(\Delta2)\right) \dots$$

$$+ \frac{1}{720}\cdot\frac{\left(288\cdot\cos(\Delta2) - 288\cdot xc^5\cdot\cos(\Delta1)\right)}{\pi}$$

$$RMB1C := \frac{\mu^4}{288\cdot\pi}\cdot\left[15\cdot\Delta1 + 33\cdot\cos(\Delta2)\cdot\sin(\Delta2) - 26\cdot(\cos(\Delta2))^3\cdot\sin(\Delta2) + 8\cdot(\cos(\Delta2))^5\cdot\sin(\Delta2) - 15\cdot\Delta2 + 26\cdot(\cos(\Delta1))^3\cdot\sin(\Delta1) - 8\cdot(\cos(\Delta1))^5\cdot\sin(\Delta1) - 33\cdot\cos(\Delta1)\cdot\sin(\Delta1)\right] \dots$$

$$+ \frac{\mu^2}{288\cdot\pi}\cdot\left[180\cdot xc^2\cdot\cos(\Delta1)\cdot\sin(\Delta1) - 108\cdot xc^2\cdot\Delta1 + 108\cdot\Delta2 - 180\cdot\cos(\Delta2)\cdot\sin(\Delta2) + 72\cdot(\cos(\Delta2))^3\cdot\sin(\Delta2) - 72\cdot xc^2\cdot(\cos(\Delta1))^3\cdot\sin(\Delta1)\right] \dots$$

$$+ \frac{\mu}{288\cdot\pi}\cdot\left[128\cdot(\cos(\Delta1))^3\cdot xc^3 - 384\cdot xc^3\cdot\cos(\Delta1) + 384\cdot\cos(\Delta2) - 128\cdot(\cos(\Delta2))^3\right] + \frac{1}{288\cdot\pi}\cdot\left(72\cdot xc^4\cdot\cos(\Delta1)\cdot\sin(\Delta1) + 72\cdot\Delta2 - 72\cdot xc^4\cdot\Delta1 - 72\cdot\cos(\Delta2)\cdot\sin(\Delta2)\right)$$

$$RM\lambda tpp := \frac{\mu^3}{24\cdot\pi}\cdot\left[-3\cdot\Delta2 + 3\cdot\Delta1 - 5\cdot\cos(\Delta1)\cdot\sin(\Delta1) + 2\cdot(\cos(\Delta1))^3\cdot\sin(\Delta1) + 5\cdot\cos(\Delta2)\cdot\sin(\Delta2) - 2\cdot(\cos(\Delta2))^3\cdot\sin(\Delta2)\right] \dots$$

$$+ \frac{\mu}{24\cdot\pi}\cdot\left(-12\cdot xc^2\cdot\Delta1 + 12\cdot xc^2\cdot\cos(\Delta1)\cdot\sin(\Delta1) + 12\cdot\Delta2 - 12\cdot\cos(\Delta2)\cdot\sin(\Delta2)\right) + \frac{1}{24\cdot\pi}\cdot\left(-16\cdot xc^3\cdot\cos(\Delta1) + 16\cdot\cos(\Delta2)\right)$$

For $\mu = 2$ and $xc = 0.16$, $RM\theta o = 0.983892731582208$ $RM\theta t = 0.68894324169276$ $RMB1C = 0.563956586470527$ $RM\lambda tpp = 0.205879694256279$

6. For The Classical Case Where $x_c = 0$ and $\mu \le 1$:

$$\Delta1 := 0 \qquad\qquad \Delta2 := \frac{\pi}{2}$$

For $\mu = 0.75$ and xc = 0

$$T\theta o := \frac{-4}{9\cdot\pi}\cdot\mu^3 + \frac{1}{2}\cdot\mu^2 + \frac{1}{3}$$

$$T\theta o = 0.554900229673873$$

$$T\theta t := \frac{-1}{32}\cdot\mu^4 + \frac{1}{4}\cdot\mu^2 + \frac{1}{4}$$

$$T\theta t = 0.3807373046875$$

$$TB1C := \frac{1}{8}\cdot\mu^3 + \frac{1}{2}\cdot\mu$$

$$TB1C = 0.427734375$$

$$T\lambda tpp := \frac{1}{4}\cdot\mu^2 + \frac{1}{2}$$

$$T\lambda tpp = 0.640625$$

$$RM\theta o := \frac{4}{45\cdot\pi}\cdot\mu^4 + \frac{1}{3}\cdot\mu$$

$$RM\theta o = 0.258952465548919$$

$$RM\theta t := \frac{1}{96}\cdot\mu^5 + \frac{1}{4}\cdot\mu$$

$$RM\theta t = 0.189971923828125$$

$$RMB1C := \frac{-5}{192}\cdot\mu^4 + \frac{3}{16}\cdot\mu^2 + \frac{1}{8}$$

$$RMB1C = 0.22222900390625$$

$$RM\lambda tpp := \frac{-1}{16}\cdot\mu^3 + \frac{1}{4}\cdot\mu$$

$$RM\lambda tpp = 0.1611328125$$

6. For The Less Well Known Case Where $x_c = 0$ and $\mu \geq 1$:

$$\Delta 1 := 0 \qquad \Delta 2 := \operatorname{asin}\left(\frac{1}{\mu}\right)$$

For $\mu = 2.0$ and $xc = 0$

$$T\theta o := \frac{1}{9 \cdot \pi} \cdot \left[\left(4 \cdot \mu^2 + 11\right) \cdot \left(\mu^2 - 1\right)^{\frac{1}{2}} - 4 \cdot \mu^3 + \left(6 + 9 \cdot \mu^2\right) \cdot \operatorname{asin}\left(\frac{1}{\mu}\right) \right]$$

$$T\theta o = 1.29999597983412$$

$$T\theta t := \frac{1}{16 \cdot \pi} \cdot \left[\left(14 + \mu^2\right) \cdot \left(\mu^2 - 1\right)^{\frac{1}{2}} + \operatorname{asin}\left(\frac{1}{\mu}\right) \cdot \left(8 + 8 \cdot \mu^2 - \mu^4\right) \right]$$

$$T\theta t = 0.870245007349516$$

$$TB1C := \frac{1}{12 \cdot \pi} \cdot \left[\left(13 \cdot \mu + \frac{2}{\mu}\right) \cdot \left(\mu^2 - 1\right)^{\frac{1}{2}} + \operatorname{asin}\left(\frac{1}{\mu}\right) \cdot \left(12 \cdot \mu + 3 \cdot \mu^3\right) \right]$$

$$TB1C = 1.9071566813657$$

$$T\lambda tpp := \frac{1}{2 \cdot \pi} \cdot \left[3 \cdot \left(\mu^2 - 1\right)^{\frac{1}{2}} + \operatorname{asin}\left(\frac{1}{\mu}\right) \cdot \left(2 + \mu^2\right) \right]$$

$$T\lambda tpp = 1.32699334313269$$

$$RM\theta o := \frac{-1}{90 \cdot \pi} \cdot \left[-8 \cdot \mu^4 + 8 \cdot \mu^3 \cdot \left(\mu^2 - 1\right)^{\frac{1}{2}} - 56 \cdot \mu \cdot \left(\mu^2 - 1\right)^{\frac{1}{2}} - \frac{12}{\mu} \cdot \left(\mu^2 - 1\right)^{\frac{1}{2}} - 60 \cdot \operatorname{asin}\left(\frac{1}{\mu}\right) \cdot \mu \right]$$

$$RM\theta o = 1.00572695315891$$

$$RM\theta t := \frac{1}{144 \cdot \pi} \cdot \left[\left[\left(\frac{16}{\mu}\right) + 62 \cdot \mu - 3 \cdot \mu^3\right] \cdot \left(\mu^2 - 1\right)^{\frac{1}{2}} + \left(72 \cdot \mu + 3 \cdot \mu^5\right) \cdot \operatorname{asin}\left(\frac{1}{\mu}\right) \right]$$

$$RM\theta t = 0.691274449344122$$

$$RMB1C := \frac{-1}{288 \cdot \pi \cdot \mu} \cdot \left[\left(8 - 158 \cdot \mu^2 - 15 \cdot \mu^4\right) \cdot \left[\frac{\left(\mu^2 - 1\right)}{\mu^2}\right]^{\frac{1}{2}} + \left(15 \cdot \mu^5 - 108 \cdot \mu^3 - 72 \cdot \mu\right) \cdot \operatorname{asin}\left(\frac{1}{\mu}\right) \right]$$

$$RMB1C = 0.566274449344122$$

$$RM\lambda tpp := \frac{1}{8 \cdot \pi} \cdot \left[\left(2 + \mu^2\right) \cdot \left[\frac{\left(\mu^2 - 1\right)}{\mu^2}\right]^{\frac{1}{2}} + \left(4 \cdot \mu - \mu^3\right) \cdot \operatorname{asin}\left(\frac{1}{\mu}\right) \right]$$

$$RM\lambda tpp = 0.206748335783172$$

7. Thrust and Feathering Equations in Terms of α_{tpp} and θ_0

If the rolling moment is set equal to zero (i.e., a balanced rotor), then feathering in the tip path plane becomes

$$\left(B_{1C} + a_{1S}\right) = \frac{\left(RM_{\theta o}\right)\theta_0 + \left(RM_{\theta t}\right)\theta_t + \left(RM_{\lambda tpp}\right)\lambda_{tpp}}{\left(RM_{B1C}\right)}$$

This value of $B_{1C} + a_{1S}$ is substituted into the thrust equation, resulting in

$$\frac{2C_T}{\sigma a} = \left(T_{\theta o} - T_{B1C}\frac{RM_{\theta o}}{RM_{B1C}}\right)\theta_0 + \left(T_{\theta t} - T_{B1C}\frac{RM_{\theta t}}{RM_{B1C}}\right)\theta_t + \left(T_{\lambda tpp} - T_{B1C}\frac{RM_{\lambda tpp}}{RM_{B1C}}\right)\lambda_{tpp}$$

Now

$$\alpha_{tpp} = \alpha_{shaft} + a_{1S} \quad \text{and} \quad \lambda_{tpp} = \mu\tan\alpha_{tpp} - \frac{v}{V_t} \approx \mu\,\alpha_{tpp} - \left(\frac{\sigma a}{2}\frac{K_T}{2\mu}\right)\frac{2C_T}{\sigma a} \quad \text{if} \quad \mu > 0.15$$

The empirical non-uniform downwash factor is $K_T = 1.075 + 10\left[\tanh\left(5\mu^3\right)\right]$

So that

$$\frac{C_T}{\sigma} = \left\{\frac{\frac{a}{2}\left(T_{\theta o} - T_{B1C}\frac{RM_{\theta o}}{RM_{B1C}}\right)}{1 + \left(\frac{\sigma a}{2}\frac{K_T}{2\mu}\right)\left(T_{\lambda tpp} - T_{B1C}\frac{RM_{\lambda tpp}}{RM_{B1C}}\right)}\right\}\theta_0 + \left\{\frac{\frac{a}{2}\left(T_{\theta t} - T_{B1C}\frac{RM_{\theta t}}{RM_{B1C}}\right)}{1 + \left(\frac{\sigma a}{2}\frac{K_T}{2\mu}\right)\left(T_{\lambda tpp} - T_{B1C}\frac{RM_{\lambda tpp}}{RM_{B1C}}\right)}\right\}\theta_t + \left\{\frac{\frac{a}{2}\left(\mu T_{\lambda tpp} - \mu T_{B1C}\frac{RM_{\lambda tpp}}{RM_{B1C}}\right)}{1 + \left(\frac{\sigma a}{2}\frac{K_T}{2\mu}\right)\left(T_{\lambda tpp} - T_{B1C}\frac{RM_{\lambda tpp}}{RM_{B1C}}\right)}\right\}\alpha_{tpp}$$

or in abbreviated form

$$\frac{C_T}{\sigma} = \left\{\frac{\partial C_T/\sigma}{\partial\theta_0}\right\}\theta_0 + \left\{\frac{\partial C_T/\sigma}{\partial\theta_t}\right\}\theta_t + \left\{\frac{\partial C_T/\sigma}{\partial\alpha_{tpp}}\right\}\alpha_{tpp}$$

7. Thrust and Feathering Equations in Terms of α_{tpp} and θ_0

Next, the feathering equation can be expanded as

$$\left(B_{1C} + a_{1S}\right) = \frac{RM_{\theta o}}{RM_{B1C}}\theta_0 + \frac{RM_{\theta t}}{RM_{B1C}}\theta_t + \frac{\mu\,RM_{\lambda tpp}}{RM_{B1C}}\alpha_{tpp} - \frac{RM_{\lambda tpp}}{RM_{B1C}}\left(\frac{\sigma K_T}{2\mu}\right)\frac{C_T}{\sigma}$$

Substituting the thrust equation and collecting terms then gives

$$\left(B_{1C} + a_{1S}\right) = \left\{\frac{RM_{\theta o}}{RM_{B1C}} - \frac{RM_{\lambda tpp}}{RM_{B1C}}\left(\frac{\sigma K_T}{2\mu}\right)\left(\frac{\partial C_T/\sigma}{\partial \theta_0}\right)\right\}\theta_0 + \left\{\frac{RM_{\theta t}}{RM_{B1C}} - \frac{RM_{\lambda tpp}}{RM_{B1C}}\left(\frac{\sigma K_T}{2\mu}\right)\left(\frac{\partial C_T/\sigma}{\partial \theta_t}\right)\right\}\theta_t$$

$$+ \left\{\frac{\mu\,RM_{\lambda tpp}}{RM_{B1C}} - \frac{RM_{\lambda tpp}}{RM_{B1C}}\left(\frac{\sigma K_T}{2\mu}\right)\left(\frac{\partial C_T/\sigma}{\partial \alpha_{tpp}}\right)\right\}\alpha_{tpp}$$

or in abbreviated form

$$\left(B_{1C} + a_{1S}\right) = \left\{\frac{\partial\left(B_{1C} + a_{1S}\right)}{\partial \theta_0}\right\}\theta_0 + \left\{\frac{\partial\left(B_{1C} + a_{1S}\right)}{\partial \theta_t}\right\}\theta_t + \left\{\frac{\partial\left(B_{1C} + a_{1S}\right)}{\partial \alpha_{tpp}}\right\}\alpha_{tpp}$$

8. Classical Thrust and Flapping Equations in Shaft Axis Ref. System

The thrust and flapping equations can also be referred to the shaft axis system because

$$\alpha_{tpp} = \alpha_{shaft} + a_{1S} \quad \text{and} \quad \lambda_{tpp} = \mu \tan\left(\alpha_{shaft} + a_{1S}\right) - \frac{v}{V_t} \approx \lambda_S + \mu\, a_{1S}$$

First, rewrite the tip path plane feathering equation to obtain the 1st harmonic longitudinal flapping. Then substitute for λ_{tpp} to see

$$a_{1S} = \frac{\left(RM_{\theta o}\right)\theta_0 + \left(RM_{\theta t}\right)\theta_t + \left(RM_{\lambda tpp}\right)\left(\lambda_S + \mu\, a_{1S}\right) - \left(RM_{B1C}\right)B_{1C}}{\left(RM_{B1C}\right)}$$

Now solve for longitudinal flapping, which gives

$$a_{1S} = \left\{\frac{RM_{\theta o}}{RM_{B1C} - \mu\, RM_{\lambda tpp}}\right\}\theta_0 + \left\{\frac{RM_{\theta t}}{RM_{B1C} - \mu\, RM_{\lambda tpp}}\right\}\theta_t + \left\{\frac{RM_{\lambda tpp}}{RM_{B1C} - \mu\, RM_{\lambda tpp}}\right\}\lambda_S - \left\{\frac{RM_{B1C}}{RM_{B1C} - \mu\, RM_{\lambda tpp}}\right\}B_{1C}$$

or, in abbreviated form

$$a_{1S} = \left\{A\theta_0\right\}\theta_0 + \left\{A\theta_t\right\}\theta_t + \left\{A\lambda_S\right\}\lambda_S - \left\{AB_{1C}\right\}B_{1C}$$

For the case where xc = 0 and $\mu < 1$, 1st harmonic longitudinal flapping classically appears as

$$a_{1S} = \frac{\lambda_S\left(2\mu - \frac{1}{2}\mu^3\right) + \theta_0\left(\frac{8}{3}\mu + \frac{32}{45\pi}\mu^4\right) + \theta_t\left(2\mu + \frac{1}{12}\mu^5\right) - B_{1C}\left(1 + \frac{3}{2}\mu^2 - \frac{5}{24}\mu^4\right)}{1 - \frac{1}{2}\mu^2 + \frac{7}{24}\mu^4}$$

In a similar fashion, the thrust equation transfers to the shaft axis system as

8. Classical Thrust and Flapping Equations in Shaft Axis Ref. System

$$\frac{2C_T}{\sigma a} = \left(T_{\theta o}\right)\theta_0 + \left(T_{\theta t}\right)\theta_t + \left(T_{\lambda tpp}\right)\left(\lambda_S + \mu\,a_{1S}\right) - \left(B_{1C} + a_{1S}\right)\left(T_{B1C}\right)$$

which collects to

$$\frac{2C_T}{\sigma a} = \left(T_{\theta o}\right)\theta_0 + \left(T_{\theta t}\right)\theta_t + \left(T_{\lambda tpp}\right)\lambda_S - \left(T_{B1C}\right)B_{1C} + \left(\mu\,T_{\lambda tpp} - T_{B1C}\right)a_{1S}$$

In the preceding thrust equation, the coefficient of a_{1S} is not zero. That is,

$$\left(\mu\,T_{\lambda tpp} - T_{B1C}\right) \approx \frac{1}{8}\mu^3 \ \text{ for } \ \mu \le 1 \ \text{ and for } \ \mu \ge 1 \quad \left(\mu\,T_{\lambda tpp} - T_{B1C}\right) \approx \frac{1}{8} + \frac{1}{5}\left(\mu^2 - 1\right) + \frac{1}{500}\left(\mu^2 - 1\right)^2$$

Substituting for longitudinal flapping and collecting terms can be done. The lengthy result is :.

$$\frac{2C_T}{\sigma a} = \left\{T_{\theta o} + \frac{RM_{\theta o}\left(\mu\,T_{\lambda tpp} - T_{B1C}\right)}{RM_{B1C} - \mu\,RM_{\lambda tpp}}\right\}\theta_0 + \left\{T_{\theta t} + \frac{RM_{\theta t}\left(\mu\,T_{\lambda tpp} - T_{B1C}\right)}{RM_{B1C} - \mu\,RM_{\lambda tpp}}\right\}\theta_t$$

$$+ \left\{T_{\lambda tpp} + \frac{RM_{\lambda tpp}\left(\mu\,T_{\lambda tpp} - T_{B1C}\right)}{RM_{B1C} - \mu\,RM_{\lambda tpp}}\right\}\lambda_S - \left\{T_{B1C} + \frac{RM_{B1C}\left(\mu\,T_{\lambda tpp} - T_{B1C}\right)}{RM_{B1C} - \mu\,RM_{\lambda tpp}}\right\}B_{1C}$$

The thrust equation thus reduces to

$$\frac{2C_T}{\sigma a} = \left\{T_1\right\}\theta_0 + \left\{T_2\right\}\theta_t + \left\{T_3\right\}\lambda_S - \left\{T_4\right\}B_{1C}$$

For the case where xc = 0 and $\mu < 1$, the four constants are given as

8. Classical Thrust and Flapping Equations in Shaft Axis Ref. System

$$T_1 = \frac{1}{3}\left\{1 + \frac{3}{2}\mu^2 - \frac{4}{3\pi}\mu^3 + \mu^4\left(\frac{1 + \frac{4}{15\pi}\mu^3}{1 - \frac{1}{2}\mu^2 + \frac{7}{24}\mu^4}\right)\right\}$$

$$T_2 = \frac{1}{4}\left\{1 + \mu^2 - \frac{1}{8}\mu^4 + \mu^4\left(\frac{1 + \frac{1}{24}\mu^4}{1 - \frac{1}{2}\mu^2 + \frac{7}{24}\mu^4}\right)\right\}$$

$$T_3 = \frac{1}{2}\left\{1 + \frac{1}{2}\mu^2 + \frac{1}{2}\mu^4\left(\frac{1 - \frac{1}{4}\mu^4}{1 - \frac{1}{2}\mu^2 + \frac{7}{24}\mu^4}\right)\right\}$$

$$T_4 = \frac{\mu}{2}\left\{1 + \frac{1}{4}\mu^2 + \frac{1}{4}\mu^2\left(\frac{1 + \frac{3}{2}\mu^2 - \frac{5}{24}\mu^4}{1 - \frac{1}{2}\mu^2 + \frac{7}{24}\mu^4}\right)\right\}$$

9. Thrust and Flapping Equations in Terms of α_{shaft} and θ_0

In the thrust equation, λ_S can be replaced by

$$\lambda_S = \mu \tan \alpha_S - \frac{v}{V_t} \approx \mu \, \alpha_S - \left(\frac{\sigma a}{2} \frac{K_T}{2\mu} \right) \frac{2C_T}{\sigma a} \quad \text{if} \quad \mu > 0.15$$

The empirical non-uniform downwash factor is $K_T = 1.075 + 10 \left[\tanh \left(5\mu^3 \right) \right]$

and the thrust equation becomes

$$\frac{2C_T}{\sigma a} = \{T_1\} \theta_0 + \{T_2\} \theta_t + \{T_3\} \left[\mu \, \alpha_S - \left(\frac{\sigma a}{2} \frac{K_T}{2\mu} \right) \frac{2C_T}{\sigma a} \right] - \{T_4\} B_{1C}$$

Solving this expression for C_T/σ gives

$$\frac{C_T}{\sigma} = \left\{ \frac{a}{2} \frac{T_1}{1 + \dfrac{\sigma a}{2} \dfrac{K_T}{2\mu} T_3} \right\} \theta_0 + \left\{ \frac{a}{2} \frac{T_2}{1 + \dfrac{\sigma a}{2} \dfrac{K_T}{2\mu} T_3} \right\} \theta_t + \left\{ \frac{a}{2} \frac{\mu \, T_3}{1 + \dfrac{\sigma a}{2} \dfrac{K_T}{2\mu} T_3} \right\} \alpha_S - \left\{ \frac{a}{2} \frac{T_4}{1 + \dfrac{\sigma a}{2} \dfrac{K_T}{2\mu} T_3} \right\} B_{1C}$$

which, when abbreviated, is

$$\frac{C_T}{\sigma} = \{\overline{T_1}\} \theta_0 + \{\overline{T_2}\} \theta_t + \{\overline{T_3}\} \alpha_S - \{\overline{T_4}\} B_{1C}$$

For flapping, λ_S can be replaced by

$$\lambda_S \approx \mu \, \alpha_S - \left(\frac{\sigma \, K_T}{2\mu} \right) \frac{C_T}{\sigma} = \mu \, \alpha_S - \left(\frac{\sigma \, K_T}{2\mu} \right) \left[\{\overline{T_1}\} \theta_0 + \{\overline{T_2}\} \theta_t + \{\overline{T_3}\} \alpha_S - \{\overline{T_4}\} B_{1C} \right]$$

and, in abbreviated form

9. Thrust and Flapping Equations in Terms of α_{shaft} and θ_0

$$a_{1S} = \left\{ \frac{\partial a_{1S}}{\partial \theta_0} \right\} \theta_0 + \left\{ \frac{\partial a_{1S}}{\partial \theta_t} \right\} \theta_t + \left\{ \frac{\partial a_{1S}}{\partial \alpha_S} \right\} \alpha_S - \left\{ \frac{\partial a_{1S}}{\partial B_{1C}} \right\} B_{1C}$$

where the coefficients are:

$$\frac{\partial a_{1S}}{\partial \theta_0} = \left\{ \frac{1}{RM_{B1C} - \mu\, RM_{\lambda tpp}} \right\} \left\{ RM_{\theta o} - \left(\frac{\sigma K_T}{2\mu} \right) \left(RM_{\lambda tpp} \right) \{ \overline{T}_1 \} \right\}$$

$$\frac{\partial a_{1S}}{\partial \theta_t} = \left\{ \frac{1}{RM_{B1C} - \mu\, RM_{\lambda tpp}} \right\} \left\{ RM_{\theta t} - \left(\frac{\sigma K_T}{2\mu} \right) \left(RM_{\lambda tpp} \right) \{ \overline{T}_2 \} \right\}$$

$$\frac{\partial a_{1S}}{\partial \lambda_S} = \left\{ \frac{1}{RM_{B1C} - \mu\, RM_{\lambda tpp}} \right\} \left\{ \mu RM_{\lambda tpp} - \left(\frac{\sigma K_T}{2\mu} \right) \left(RM_{\lambda tpp} \right) \{ \overline{T}_3 \} \right\}$$

$$\frac{\partial a_{1S}}{\partial B_{1C}} = \left\{ \frac{1}{RM_{B1C} - \mu\, RM_{\lambda tpp}} \right\} \left\{ RM_{B1C} - \left(\frac{\sigma K_T}{2\mu} \right) \left(RM_{\lambda tpp} \right) \{ \overline{T}_4 \} \right\}$$

10. Jenny, Arcidiacono & Smith Tables From Linearized Theory

TABLE I - ARTICULATED ROTOR
FLAPPING DERVIATIVES

μ	$\gamma = \dfrac{\rho a c R^4}{I_{flap}}$	$\dfrac{\partial a_{1S}}{\partial \theta_0}$	$\dfrac{\partial a_{1S}}{\partial \theta_t}$	$\dfrac{\partial a_{1S}}{\partial \lambda_S}$	$\dfrac{\partial a_{1S}}{\partial (1/R\Omega^2)}$	$\dfrac{\partial b_{1S}}{\partial \theta_0}$	$\dfrac{\partial b_{1S}}{\partial \theta_t}$	$\dfrac{\partial b_{1S}}{\partial \lambda_S}$	$\dfrac{\partial b_{1S}}{\partial (1/R\Omega^2)}$
1.0	15.0	2.80	2.68	1.936	1.912	4.900	2.502	3.910	-58.1
1.5	15.0	7.32	5.30	3.076	-14.510	22.850	17.851	13.040	-117.9
1.8	15.0	66.50	55.35	35.400	-308.100	382.350	305.020	185.740	-1333.8
1.0	10.0	3.78	2.65	1.943	1.699	3.300	1.742	2.570	-53.5
1.5	10.0	6.61	4.72	2.584	-14.120	13.520	10.492	7.500	-99.3
1.8	10.0	19.49	15.50	8.950	-101.610	70.510	55.840	33.110	-351.8
1.0	5.0	3.77	2.63	1.951	1.062	1.672	0.908	1.265	-48.8
1.5	5.0	6.07	4.02	1.990	-9.750	5.720	4.396	3.031	-76.9
1.8	5.0	8.79	6.42	2.920	-39.000	14.260	11.130	6.230	-128.8
2.0	5.0	19.01	14.32	6.470	-95.400	34.130	26.670	13.210	-238.6
1.0	2.3	3.72	2.59	1.930	0.516	0.762	0.418	0.572	-46.6
1.5	2.3	5.36	3.70	1.733	-4.930	2.410	1.845	1.247	-67.1
1.8	2.3	6.75	4.69	1.778	-16.880	4.720	3.650	1.960	-85.6
2.0	2.3	8.32	5.85	2.041	-28.400	7.170	5.540	2.610	-101.3
2.2	2.3	11.73	8.51	2.870	-66.700	13.450	10.400	4.370	-152.8
2.5	2.3	48.16	36.47	12.400	-343.400	64.260	49.800	18.110	-559.

TABLE I - ARTICULATED ROTOR
FLAPPING DERVIATIVES (Cont'd.)

μ	$\gamma = \dfrac{\rho\, ac\, R^4}{I_{flap}}$	$\dfrac{\partial a_{2S}}{\partial \theta_0}$	$\dfrac{\partial a_{2S}}{\partial \theta_t}$	$\dfrac{\partial a_{2S}}{\partial \lambda_S}$	$\dfrac{\partial a_{2S}}{\partial (1/R\Omega^2)}$	$\dfrac{\partial b_{2S}}{\partial \theta_0}$	$\dfrac{\partial b_{2S}}{\partial \theta_t}$	$\dfrac{\partial b_{2S}}{\partial \lambda_S}$	$\dfrac{\partial b_{2S}}{\partial (1/R\Omega^2)}$
1.0	15.0	1.736	1.048	1.181	-10.167	-0.1915	-0.2690	0.0647	-8.670
1.5	15.0	9.498	7.599	5.358	-46.530	5.0360	2.2510	1.9106	-19.830
1.8	15.0	221.326	176.470	107.262	-769.500	67.7370	54.0030	33.6650	-240.480
1.0	10.0	1.218	0.784	0.766	-6.024	-0.1134	-0.1594	0.0383	-7.710
1.5	10.0	5.050	3.828	2.522	-30.180	3.2670	1.4600	1.2359	-19.290
1.8	10.0	34.824	27.473	16.053	-169.170	14.8920	11.8720	7.1010	-79•30
1.0	5.0	0.639	0.435	0.373	-1.882	-0.0354	-0.0498	0.0119	-4.810
1.5	5.0	1.614	1.166	0.626	-10.420	1.1280	0.5040	0.4281	-13.330
1.8	5.0	4.577	3.469	1.712	-32.460	2.8580	2.2780	1.1420	-30.440
2.0	5.0	11.515	8.916	4.217	-377.670	7.6530	6.0730	3.1920	-59.500
1.0	2.3	0.295	0.204	0.167	-0.421	-0.0079	-0.0111	0.0026	-2.340
1.5	2.3	0.567	0.393	0.168	-2.420	0.2620	0.1174	0.0996	-6.740
1.8	2.3	0.982	0.697	0.235	-6.460	0.5690	0.4530	0.2820	-13.180
2.0	2.3	1.429	1.034	0.331	-11.410	1.0500	0.8330	0.4380	-17.700
2.2	2.3	2.810	2.080	0.699	-22.700	2.5100	1.9750	0.8860	-31.500
2.5	2.3	15.760	11.980	4.120	-123.600	16.9300	13.0900	4.7540	-143.900

10. Jenny, Arcidiacono & Smith Tables From Linearized Theory

TABLE I - ARTICULATED ROTOR

FLAPPING DERVIATIVES (Cont'd.)

μ	$\gamma = \dfrac{\rho a c R^4}{I_{flap}}$	$\dfrac{\partial \beta_0}{\partial \theta_0}$	$\dfrac{\partial \beta_0}{\partial \theta_t}$	$\dfrac{\partial \beta_0}{\partial \lambda_S}$	$\dfrac{\partial \beta_0}{\partial (1/R\Omega^2)}$
1.000	15.0	4.242	2.092	3.501	-54.800
1.500	15.0	16.299	12.858	9.649	-91.300
1.800	15.0	222.850	177.780	108.280	-777.600
1.000	10.0	2.867	1.450	2.315	-52.100
1.500	10.0	9.599	7.516	5.516	-76.200
1.800	10.0	41.720	33.050	19.625	-208.600
1.000	5.0	1.453	0.752	1.148	-49.400
1.500	5.0	4.035	3.121	2.204	-57.900
1.800	5.0	8.690	6.790	3.828	-79.000
2.000	5.0	19.070	14.960	7.507	-137.600
1.000	2.3	0.663	0.346	0.520	-47.900
1.500	2.3	1.697	1.304	0.901	-50.000
1.800	2.3	2.930	2.270	1.237	-54.300
2.000	2.3	4.150	3.210	1.529	-59.700
2.200	2.3	9.300	7.010	2.750	-83.600
2.500	2.3	32.900	19.140	9.070	-274.200

TABLE II - TEETERING ROTOR
FLAPPING DERVIATIVES

μ	$\tan \delta_3$	$\dfrac{\partial a_{1S}}{\partial \theta_0}$	$\dfrac{\partial a_{1S}}{\partial \theta_t}$	$\dfrac{\partial a_{1S}}{\partial \lambda_S}$	$\dfrac{\partial a_{1S}}{\partial \beta_{PC}}$	$\dfrac{\partial b_{1S}}{\partial \theta_0}$	$\dfrac{\partial b_{1S}}{\partial \theta_t}$	$\dfrac{\partial b_{1S}}{\partial \lambda_S}$	$\dfrac{\partial b_{1S}}{\partial \beta_{PC}}$
1.0	0	3.76	2.62	1.955	0	0	0	0	1.0120
1.5	0	5.31	3.65	1.677	0	0	0	0	1.3840
2.0	0	6.75	4.59	1.361	0	0	0	0	1.6780
2.5	0	8.21	5.55	1.128	0	0	0	0	2.0570
3.0	0	9.69	6.52	0.958	0	0	0	0	2.4240
1.0	0.268	3.10	2.16	1.613	0.661	-0.832	-0.579	-0.432	0.8350
1.5	0.268	4.11	2.83	1.299	1.134	-1.103	-0.759	-0.348	1.0440
2.0	0.268	5.17	3.52	1.043	1.466	-1.386	-1.153	-0.279	1.2860
2.5	0.268	6.27	4.24	0.862	1.812	-1.680	-1.136	-0.231	1.5710
3.0	0.268	7.40	4.98	0.732	2.13	-1.982	-1.335	-0.196	1.8510
1.0	0.577	1.89	1.32	0.985	0.870	-1.094	-0.763	-0.568	0.5090
1.5	0.577	2.26	1.55	0.713	1.341	-1.305	-0.898	-0.411	0.5730
2.0	0.577	2.79	1.90	0.563	1.705	-1.612	-1.571	-0.325	0.6940
2.5	0.577	3.37	2.28	0.463	2.099	-1.947	-1.316	-0.267	0.8440
3.0	0.577	3.97	2.67	0.393	2.47	-2.296	-1.546	-0.227	0.9950

10. Jenny, Arcidiacono & Smith Tables From Linearized Theory

TABLE III - ARTICULATED ROTOR THRUST DERVIATIVES

$\gamma = \dfrac{\rho a c R^4}{I_{flap}}$	μ	$\dfrac{1}{a}\dfrac{\partial C_T/\sigma}{\partial \lambda_S}$	$\dfrac{1}{a}\dfrac{\partial C_T/\sigma}{\partial \theta_0}$	$\dfrac{1}{a}\dfrac{\partial C_T/\sigma}{\partial \theta_t}$
15.0	1.0	0.483	0.554	0.370
15.0	1.5	1.124	2.101	1.412
15.0	1.8	11.582	23.995	19.720
10.0	1.0	0.482	0.556	0.411
10.0	1.5	1.013	1.874	1.062
10.0	1.8	3.336	7.107	5.572
5.0	1.0	0.482	0.566	0.375
5.0	1.5	0.879	1.658	1.080
5.0	1.8	1.458	3.262	2.352
5.0	2.0	3.080	8.102	6.052
2.3	1.0	0.480	0.555	0.374
2.3	1.5	0.822	1.473	0.970
2.3	1.8	1.101	2.506	1.736
2.3	2.0	1.398	3.687	2.595
2.3	2.2	2.019	7.428	4.433
2.3	2.5	8.229	29.195	23.255

TABLE IV - TEETERING ROTOR THRUST DERVIATIVES

μ	$\dfrac{1}{a}\dfrac{\partial C_T/\sigma}{\partial \lambda_S}$	$\dfrac{1}{a}\dfrac{\partial C_T/\sigma}{\partial \theta_0}$	$\dfrac{1}{a}\dfrac{\partial C_T/\sigma}{\partial \theta_t}$
1.0	0.472	0.558	0.376
1.5	0.808	1.456	0.984
2.0	1.139	3.079	2.075
2.5	1.463	5.647	3.797
3.0	1.785	4.399	2.990

11. Rotor Minimum Profile Power, Torque and H–Force

It is possible to conceive of a rotor system made up of rotor blades whose airfoil is a classical flat plate. This rotor system can be rotated in edgewise flight at zero shaft tilt. The blades can be assumed to have no twist, be of constant chord, and be at zero collective pitch. Furthermore, a turbulent boundary layer for a flat plate seems to be a rational assumption from which to calculate blade element drag.

With the preceding thoughts in mind, the skin friction drag coefficient of a flat plate is available from experiments and is on the order of

$$C_{do} = \frac{0.144}{(\text{Re ynold's Number})^{1/5}} = \frac{0.144}{(LV/\nu)^{1/5}}$$

In the case of a rotating flat plate, the characteristic velocity is simply the resultant velocity at a blade element

$$V = V_t \sqrt{(x + \mu \sin \psi)^2 + (\mu \cos \psi)^2} = V_t \sqrt{U^2}$$

which accounts for both chordwise and spanwise flow at a given radial station, $x = r/R$.

Though incorrect, it is expeditious to take the reference length as $L = c$, the chord of the rectangular blade. With these assumptions, the drag coefficient becomes

$$C_{do} = \frac{0.144}{(c V_t/\nu)^{1/5}} \frac{1}{(\sqrt{U^2})^{1/5}} = \frac{0.144}{RN_t^{1/5}} (\sqrt{U^2})^{-1/5}$$

A blade element clearly experiences a yawed flow angle, Λ, which has sine and cosine magnitudes of

$$\cos \Lambda = \frac{x + \mu \sin \psi}{\sqrt{U^2}} \quad \text{or} \quad \sin \Lambda = \frac{\mu \cos \psi}{\sqrt{U^2}}$$

11. Rotor Minimum Profile Power, Torque and H–Force

The profile power coefficient may now be calculated as

$$C_{Po} = \frac{P_o}{\rho \pi R^2 V_t^3} = \left(\frac{bc}{\pi R}\right)\left[\frac{0.144}{(RN_t)^{1/5}}\right]\frac{1}{4\pi}\int_0^{2\pi}\int_0^1 \left(\sqrt{U^2}\right)^{-1/5}\left(\sqrt{U^2}\right)^3 dx\ d\psi$$

Curve fitting the numerically integrated results out to μ = 1.5 gives

$$\frac{C_{Po}}{\sigma} = \left[\frac{0.144}{(RN_t)^{1/5}}\right]\left(\frac{5}{38}\right)\left(1 + 4.287951587\mu^2 + 1.157562393\mu^4 - 0.107300944\mu^6\right)$$

In a similar manner, the minimum torque and H–Force coefficients are calculated as

$$C_{Qo} = \frac{Q_o}{\rho \pi R^2 V_t^2 R} = \left(\frac{bc}{\pi R}\right)\left[\frac{0.144}{(RN_t)^{1/5}}\right]\frac{1}{4\pi}\int_0^{2\pi}\int_0^1 \left(\sqrt{U^2}\right)^{-1/5}\left(\sqrt{U^2}\right)^2 \cos\Lambda\ x\ dx\ d\psi$$

$$C_{Ho} = \frac{H_o}{\rho \pi R^2 V_t^2} = \left(\frac{bc}{\pi R}\right)\left[\frac{0.144}{(RN_t)^{1/5}}\right]\frac{1}{4\pi}\int_0^{2\pi}\int_0^1 \left(\sqrt{U^2}\right)^{-1/5}\left(\sqrt{U^2}\right)^2 \sin(\psi + \Lambda)\ dx\ d\psi$$

and fitting the numerically integrated results out to μ = 1.5 gives

$$\frac{C_{Qo}}{\sigma} = \left[\frac{0.144}{(RN_t)^{1/5}}\right]\left(\frac{5}{38}\right)\left(1 + 1.1309711465\mu^2 - 0.3152844123\mu^4 + 0.0493605492\mu^6\right)$$

$$\frac{C_{Ho}}{\sigma} = \left[\frac{0.144}{(RN_t)^{1/5}}\right]\left(0.3888891\mu\right)\left(1 + 0.07776825\mu + 0.67796130\mu^2 - 0.29175304\mu^3 + 0.05276101\mu^4\right)$$

11. Rotor Minimum Profile Power, Torque and H–Force

Consider using the Sikorsky S–76 as an illustration of what the range in minimum profile power might be. The required dimensional data for this helicopter rotor are:

      a. Blades $= 4$
      b. Radius $= 22.0$ ft
      c. Chord $= 1.28$ ft
      d. Solidity $= 0.07476$
      e. Tip speed $= 676$ fps
      f. Kinematic viscosity $= 0.0001564$ ft^2/sec
      g. Tip Reynold's Number $= 5,532,480$
      h. Nominal $C_{do} = 0.008500$

On a C_{Po} / σ basis, the range appears to be:

Classical
$$\frac{C_{Po}}{\sigma} = \frac{C_{do}}{8}\left(1 + 3\mu^2 + \frac{3}{8}\mu^4\right) = 0.0010625\left(1 + 3\mu^2 + \frac{3}{8}\mu^4\right)$$

Cierva
$$\frac{C_{Po}}{\sigma} = \frac{C_{do}}{8}\left(1 + 4\mu^2 + \mu^4\right)$$

Harris
$$\frac{C_{Po}}{\sigma} = 0.001062\left(1 + 4.65\mu^2 + 4.15\mu^4 - \mu^6\right)$$

Flat Plate
$$\frac{C_{Po}}{\sigma} = \left[\frac{0.144}{\left(RN_t\right)^{1/5}}\right]\left(\frac{5}{38}\right)\left(1 + 4.287951587\mu^2 + 1.157562393\mu^4 - 0.107300944\mu^6\right)$$

$$= 0.000849\left(1 + 4.287951587\mu^2 + 1.157562393\mu^4 - 0.107300944\mu^6\right)$$

These four cases are graphed on the next page. An additional figure, taken from the noted reference, illustrates the basis of Harris' approximation. Juan de la Cierva's approximation (in modern form) was obtained from his unpublished work that was edited by Dr. J.A.J. Bennett and titled "Engineering Theory of the Autogiro, Volume I (see page 10).

11. Rotor Minimum Profile Power, Torque and H–Force
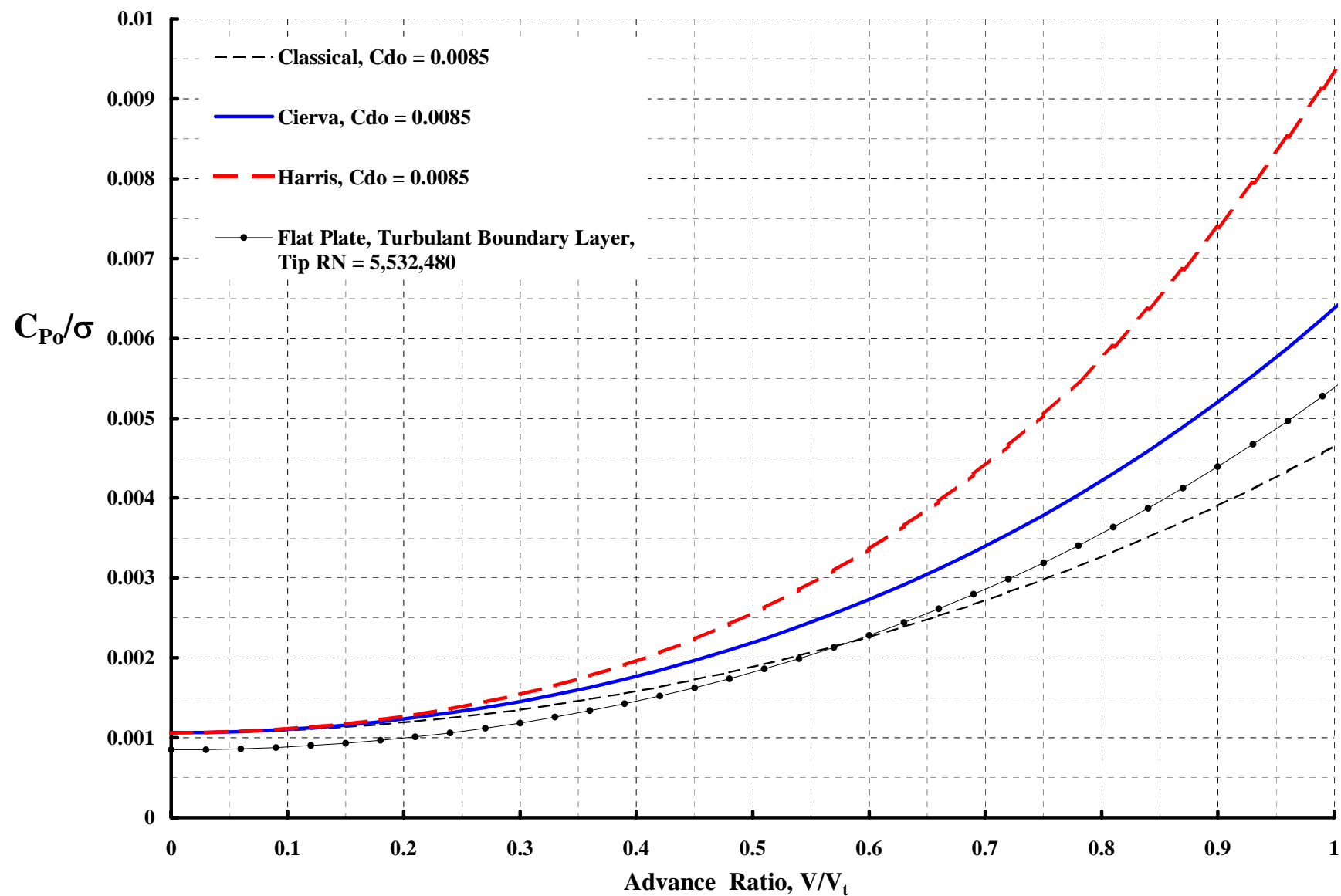
The chart plots C_{Po}/σ versus advance ratio μ.

Legend:

REF	NOTES
◁ 32	ALL TIPS
△ 31	34 FT $\theta_t = -7.7$
⊡ 30	H-34 $\theta_t = 0$
⊙ 48	AGB
◇ 30	34 FT $\theta_t = -1.7$

$$\frac{C_{Po}}{\sigma} = \frac{C_{do}}{8}\left(1 + 4.65\mu^2 + 4.15\mu^4 - \mu^6\right)$$

$C_{do} = 0.01$

$C_{do} = 0.0085$

$$\frac{C_{Po}}{\sigma} = \frac{C_{do}}{8}\left(1 + 3\mu^2\right)$$

$C_{do} = 0.0085$

ADVANCE RATIO, μ
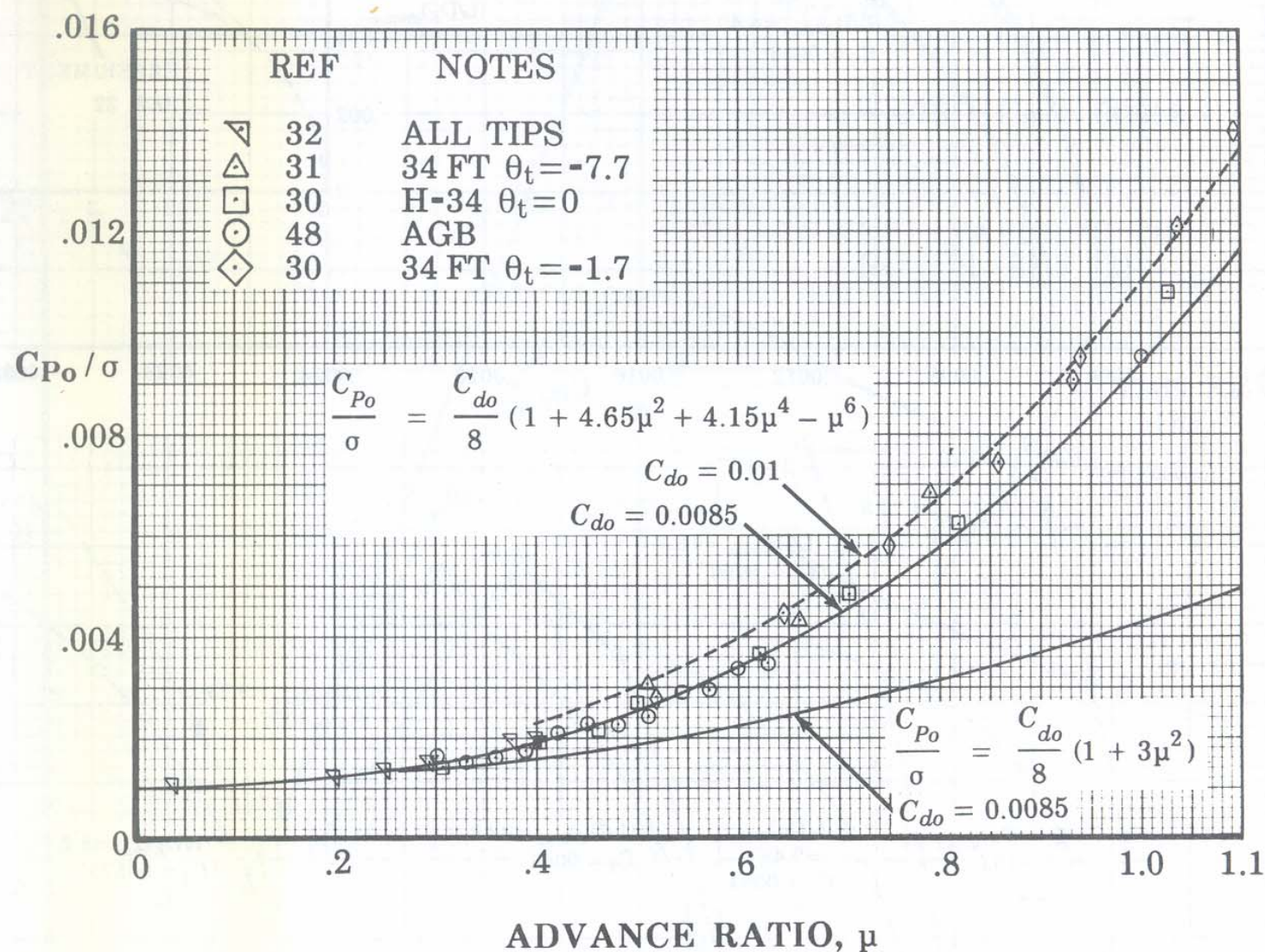
Ref.: Figure 26 of "Rotary Wing Aerodynamics–Historical Perspective and Important Issues", F.D. Harris Paper Given at AHS Southwest Region Specialists' Meeting on Aerodynamics and Aeroacoustics, Feb. 25-27, 1987. Chairman Tom Wood of Bell Helicopter

12. Graphs of Rotor Induced Power versus Thrust at μ = 0.5

Advance Ratio = 0.5
S-76, Vt = 670 fps

Legend and fit equations:

- ○ Mu = 0.5, Coll. = 0 deg. $y = 5.450E{+}02x^3 - 6.238E{-}01x^2 + 7.151E{-}03x + 2.572E{-}05$
- ■ Mu = 0.5, Coll. = 1 deg. $y = 4.799E{+}02x^3 - 2.869E{-}01x^2 + 6.324E{-}03x + 2.372E{-}05$
- △ Mu = 0.5, Coll. = 2 deg. $y = 3.539E{+}02x^3 + 1.060E{+}00x^2 + 1.116E{-}03x + 2.732E{-}05$
- ✕ Mu = 0.5, Coll. = 3 deg. $y = 5.204E{+}02x^3 - 1.490E{+}00x^2 + 1.170E{-}02x + 1.257E{-}05$
- ✶ Mu = 0.5, Coll. = 4 deg. $y = 5.336E{+}02x^3 - 1.145E{+}00x^2 + 5.339E{-}03x + 2.862E{-}05$
- ● Mu = 0.5, Coll. = 10 deg. $y = 3.924E{+}03x^3 - 7.589E{+}01x^2 + 5.348E{-}01x - 1.197E{-}03$
- ─── Glauert

$$C_L = \frac{Rotor\ Lift}{\rho\,\pi\,R^2 V_t^2}$$

$$C_{Pi} = \frac{Induced\ Power}{\rho\,\pi\,R^2 V_t^3}$$

$$Glauert's\ P_i = Tv_i \approx T\,\frac{T}{2\rho\pi R^2 V}$$

$$Or\ \ C_{Pi} \approx \frac{C_L^2}{2\mu}$$

Rotor Induced Power Coefficient

C_{Pi}

Rotor Lift Coefficient C_L

Computed with CAMRAD II

12. Graphs of Rotor Induced Power versus Thrust at μ = 0.6

Legend:
- ○ Mu = 0.6, Coll. = 0 deg. — $y = 1.562E{+}01x^3 + 3.824E{+}00x^2 - 1.089E{-}04x + 4.428E{-}05$
- ■ Mu = 0.6, Coll. = 1 deg. — $y = 1.596E{+}02x^3 + 3.460E{+}00x^2 - 8.189E{-}04x + 4.257E{-}05$
- △ Mu = 0.6, Coll. = 2 deg. — $y = -1.446E{+}02x^3 + 7.207E{+}00x^2 - 1.561E{-}02x + 5.847E{-}05$
- × Mu = 0.6, Coll. = 3 deg. — $y = -1.246E{+}02x^3 + 6.874E{+}00x^2 - 1.606E{-}02x + 6.102E{-}05$
- ✳ Mu = 0.6, Coll. = 4 deg. — $y = 7.242E{+}02x^3 - 3.755E{+}00x^2 + 2.536E{-}02x + 8.923E{-}06$
- ● Mu = 0.6, Coll. = 10 deg. — $y = 1.040E{+}03x^3 - 9.362E{+}00x^2 + 4.800E{-}02x + 9.429E{-}06$
- —— Glauert

Advance Ratio = 0.6 S-76 Vt = 670 fps

Y-axis: Rotor Induced Power Coefficient C_{Pi}

X-axis: Rotor Lift Coefficient C_L

12. Graphs of Rotor Induced Power versus Thrust at μ = 0.7

○ Mu = 0.7, Coll. = 0 deg.	$y = 8.225E+02x^3 - 2.399E+00x^2 + 1.739E-02x + 4.540E-05$
■ Mu = 0.7, Coll. = 1 deg.	$y = 6.946E+02x^3 - 1.528E-01x^2 + 8.091E-03x + 5.450E-05$
△ Mu = 0.7, Coll. = 2 deg.	$y = -6.275E+02x^3 + 1.363E+01x^2 - 3.755E-02x + 1.010E-04$
✕ Mu = 0.7, Coll. = 3 deg.	$y = -2.099E+03x^3 + 3.039E+01x^2 - 9.964E-02x + 1.756E-04$
✱ Mu = 0.7, Coll. = 4 deg.	$y = 1.474E+02x^3 + 4.592E+00x^2 - 7.330E-03x + 7.308E-05$
● Mu = 0.7, Coll. = 10 deg.	$y = 1.991E+03x^3 - 2.945E+01x^2 + 1.923E-01x - 2.931E-04$
▬ Glauert	

Advance Ratio = 0.7 S-76 Vt = 670 fps

Rotor Induced Power Coefficient C_{Pi}

Rotor Lift Coefficient C_L

12. Graphs of Rotor Induced Power versus Thrust at $\mu = 0.8$

Legend and equations:

- ○ Mu = 0.8, Coll. = 0 deg. $y = 7.296E{+}02x^3 - 5.931E{-}01x^2 + 9.790E{-}03x + 7.208E{-}05$
- ■ Mu = 0.8, Coll. = 1 deg. $y = 8.192E{+}02x^3 - 7.180E{-}01x^2 + 8.711E{-}03x + 7.507E{-}05$
- △ Mu = 0.8, Coll. = 2 deg. $y = 5.686E{+}02x^3 + 1.183E{+}00x^2 + 5.546E{-}03x + 7.741E{-}05$
- ✕ Mu = 0.8, Coll. = 3 deg. $y = -3.421E{+}02x^3 + 1.046E{+}01x^2 - 2.394E{-}02x + 1.106E{-}04$
- ✳ Mu = 0.8, Coll. = 4 deg. $y = -8.450E{+}01x^3 + 8.923E{+}00x^2 - 2.370E{-}02x + 1.222E{-}04$
- ◆ Mu = 0.8, Coll. = 10 deg. $y = 1.083E{+}01x^2 - 6.149E{-}02x + 2.699E{-}04$
- — Glauert

Advance Ratio = 0.8 S-76 Vt = 670fps

Axis labels: Rotor Induced Power Coefficient C_{Pi} (vertical); Rotor Lift Coefficient C_L (horizontal)

12. Graphs of Rotor Induced Power versus Thrust at μ = 0.9

Legend and equations shown on graph:

- ○ Mu = 0.9, Coll. = 0 deg. $y = 3.350E+00x^2 + 2.472E-03x + 9.447E-05$
- ■ Mu = 0.9, Coll. = 1 deg. $y = 4.888E+00x^2 - 4.329E-03x + 1.061E-04$
- △ Mu = 0.9, Coll. = 2 deg. $y = 3.377E+00x^2 + 5.513E-03x + 1.006E-04$
- × Mu = 0.9, Coll. = 3 deg. $y = 1.768E+00x^2 + 1.666E-02x + 9.501E-05$
- ✳ Mu = 0.9, Coll. = 4 deg. $y = 5.739E+00x^2 - 1.258E-03x + 1.252E-04$
- ▬ Glauert

Advance Ratio = 0.9 S-76 Vt = 670 fps

Y-axis: Rotor Induced Power Coefficient C_{Pi}

X-axis: Rotor Lift Coefficient C_L

13. The Propulsive Force Required To Overcome The Drag Of An Autorotating Rotor.

Autogyros and their variants carry the aircraft gross weight (or a portion of the gross weight) on a lifting rotor. The rotor is generally not powered and simply autorotates. Figure 1 illustrates a sketch of the concept. Though not shown, a fixed wing can, in fact, be included in the configuration to carry the greater percentage of the gross weight in high speed flight. The propulsive force overcoming the aircraft's drag can be provided by a propeller or some other device. Furthermore, this propulsive device need not necessarily provide all of the horizontal force required for equilibrium because the rotor, given a little power, can provide some propulsive force to achieve force equilibrium in the flight path direction. However, the general design direction evolved over the past several decades has been towards a completely unloaded rotor both in lift and propulsive force.

A key factor in the performance of the autogyro and its variants is the propulsive force required to overcome the drag of the autorotating rotor. The drag of the autorotating rotor can most easily be derived from the familiar power equation of a helicopter. This fundamental equation, derived from elementary blade element theory in Supplemental Data and Charts, Item 5, is

$$\text{Rotor Power}\left(P_{Req'd.}\right) = \text{Induced Power}\left(P_i\right) + \text{Propulsive Power}\left(XV\right) + \text{Profile Power}\left(P_0\right)$$

In the helicopter's case the rotor is tilted forward to provide a propulsive force (X) *along the flight path* at velocity (V). For autogyros and their variants, the rotor is inclined at a positive tip path plane angle of attack (α_{tpp}) as shown in Figure 1. While the sketch is drawn to infer level flight, any climb or descent could have been shown as a part of $\alpha_{tpp.}$

For the autorotating (or nearly autorotating) rotor, it is convenient to think of the rotor propulsive force (X) as negative drag (D) in which case

$$P_{Req'd.} = P_i + \left(-DV\right) + P_0$$

and this allows the rotor drag to be expressed as

$$D_R = \frac{P_i + P_0 - P_{Req'd.}}{V} = T_R \sin\alpha_{tpp} + H_R \cos\alpha_{tpp}$$

13. The Propulsive Force Required To Overcome The Drag Of An Autorotating Rotor.

It is well to keep in mind that for an autogyro, the flight path velocity can never be zero or the rotor would not autorotate. In the preceding expression, as V approaches zero, the numerator goes to zero because shaft power is required (i.e., the autogyro must become a helicopter or "hang" on its propeller with a non-rotating rotor–if the engine was powerful enough). In short, as V→0, D→0/0. Thus, to define drag as V→0, it is better to calculate drag as $D = T_R \sin\alpha_{tpp} + H_R \cos\alpha_{tpp}$ in which case the answer will depend on the assumption about α_{tpp}. This general point was illustrated for the autogyro by Wheatley who did gliding tests of a Pitcairn PCA-2 autogyro. His NACA TR-434 report provided data that was shown on page 11 in the body of this document. Of course, with the propeller powered, the rate of descent could be reduced to zero (i.e., steady level flight) for speeds above 20 knots. The PCA-2 only had a 300 hp engine and a 10.5 foot diameter prop so the aircraft began to descend at low speed even with full power. Interestingly, with a 20 knot head wind, the PCA-2 could be landed "vertically" and with a very gentle touch down.
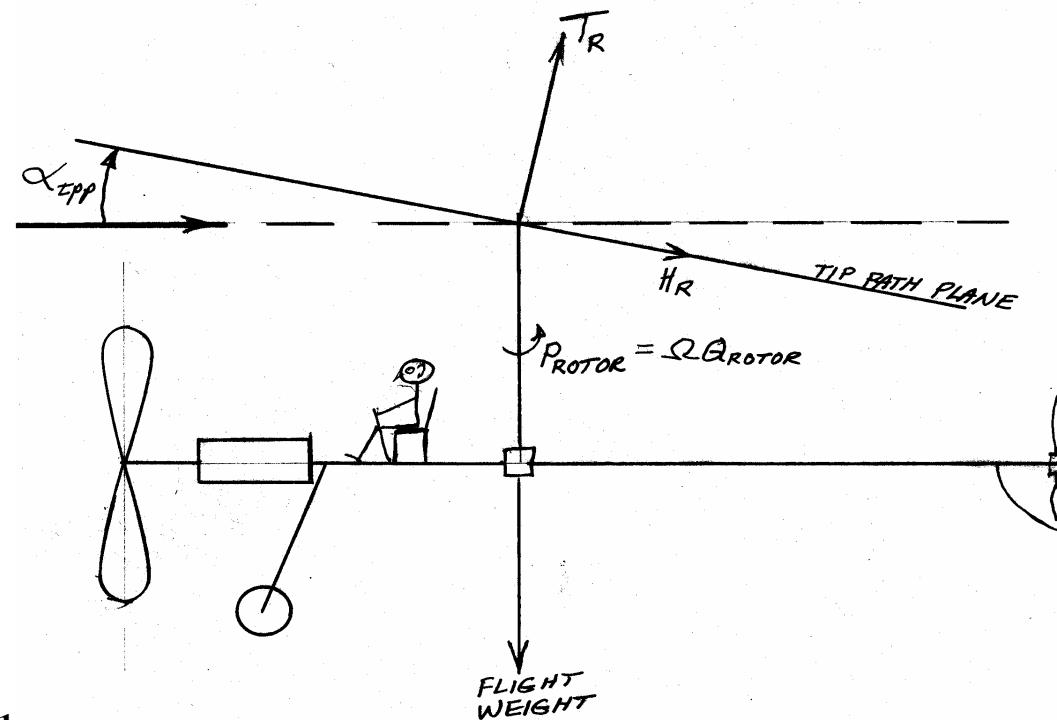
Figure 1

13. The Propulsive Force Required To Overcome The Drag Of An Autorotating Rotor.

The rotor, at a slightly positive α_{tpp} and carrying a small amount of lift, will autorotate and no input power to the rotor shaft will be required (i.e., $P_{Req'd.} = 0$). Though not obvious from the preceding expression for rotor drag, if $\alpha_{tpp} = 0$ and rotor lift is zero, then shaft power will be required in the amount ΩQ_0 and the propulsive device must provide a force equal to H_0. But if the rotor is truly in autorotation with some slight lift and slightly positive α_{tpp}, an accelerating or negative torque is created to overcome Q_0. This accelerating torque is created by the upward flow of air through the rotor disc, which adds a drag load on the propulsive device of magnitude $\Omega Q_0/V$. For actual autorotation then, the helicopter's profile power (when divided by V) becomes the autogyro's profile drag (D_o) and, referring to Supplemental Data and Charts, Item 11, is simply

$$D_o = \frac{P_o}{V} = \frac{\Omega Q_o}{V} + H_o \approx \left(\rho\pi R^2 V_t^3\right)\left(\frac{\sigma C_{do}}{8}\right)\left(1 + 4.65\mu^2 + 4.15\mu^4 - \mu^6\right)\left(\frac{1}{V}\right)$$

The helicopter's rotor induced power (P_i) in high speed forward flight becomes the autogyro's induced drag, which is frequently approximated by ideal wing theory times a K_i as

$$D_i = \frac{P_i}{V} \approx K_i \frac{L^2}{2\rho\pi R^2 V^2} \quad \text{if} \ \ V \gg 0$$

Limited computations with CAMRAD II using an S–76 rotor model *with zero twist and a prescribed wake* suggest that

$$K_i = 1 - 29.332\mu + 92.439\mu^2 - 51.746\mu^3 \quad \text{for} \ \ 0.5 \le \mu \le 1.0$$

and for advance ratios at and below 0.5,

$$K_i = 1.075\cosh\left(6.76\mu^2\right) \quad \text{for} \ \ \mu \le 0.5$$

are adequate approximations to the more correct calculation, which should be made using free wake methodology.

Consider next the following numerical example with the input tabulated below. Note that two tip speeds are defined in this numerical example so that a crude picture of the winged autogyro's performance can be described. The higher $V_t = 600$ fps allows the rotor to operate at $C_T/\sigma = 0.1$ when the rotor carries all the gross weight (10,000 lbs) at sea level on a standard day in the takeoff speed range.

13. The Propulsive Force Required To Overcome The Drag Of An Autorotating Rotor.

After takeoff and with sufficient forward speed, the wing may carry 9,000 lbs of weight leaving the rotor to carry 1,000 lbs. At this point the rotor $C_T/\sigma = 0.01$ because the tip speed is still at 600 ft/sec and the aircraft is still at sea level. Finally, the transition to winged autogyro flight is completed by reducing tip speed to 300 ft/sec. At this point, $C_T/\sigma = 0.04$ with the aircraft still at sea level. In the winged autogyro mode, or, if you prefer, the airplane mode, the sky is the limit.

Parameter	Symbol	Value
Gross weight	GW	10,000 lb
Rotor Lift	L	1,000 lb
Radius	R	22 ft
Blade chord	c	1.29 ft
No. of blades	b	4
Tip speed 1	V_t	600 ft/sec
Tip speed 2	V_t	300 ft/sec
Density	ρ	0.002378 slug/ft^3
Solidity	$\sigma = bc/\pi R$	0.07476
Airfoil drag coeff.	C_{do}	0.0100

Figure 2 shows the calculated rotor drag (D) in pounds as a function of forward speed (V) in knots for three conditions representative of an autogyro having an autorotating rotor and a wing, which can unload the rotor lift. Note that the speed range below 50 knots has not been addressed since the aircraft could have any number of configurations from helicopter to jump takeoff for this very low speed range. (Keep in mind that profile drag due to lift that comes from operating the nearly unloaded rotor at $C_T/\sigma = 0.04$ rather than $C_T/\sigma = 0$ is not yet included in Figure 2. Therefore, calculations with a comprehensive code can be expected to increase the rotor drag above that shown in Figure 2.) Finally, at 180 knots and $V_t = 300$ ft/sec, advance ratio is one and any number of aeroelastic instabilities lay in waiting for the rotor after $\mu = 1$.

Finally, the rotor drag can be expressed as a parasite drag by dividing drag by dynamic pressure (i.e., D/q in sq. ft.). The results from Figure 2 are shown in D/q form in Figure 3.

13. The Propulsive Force Required To Overcome The Drag Of An Autorotating Rotor.
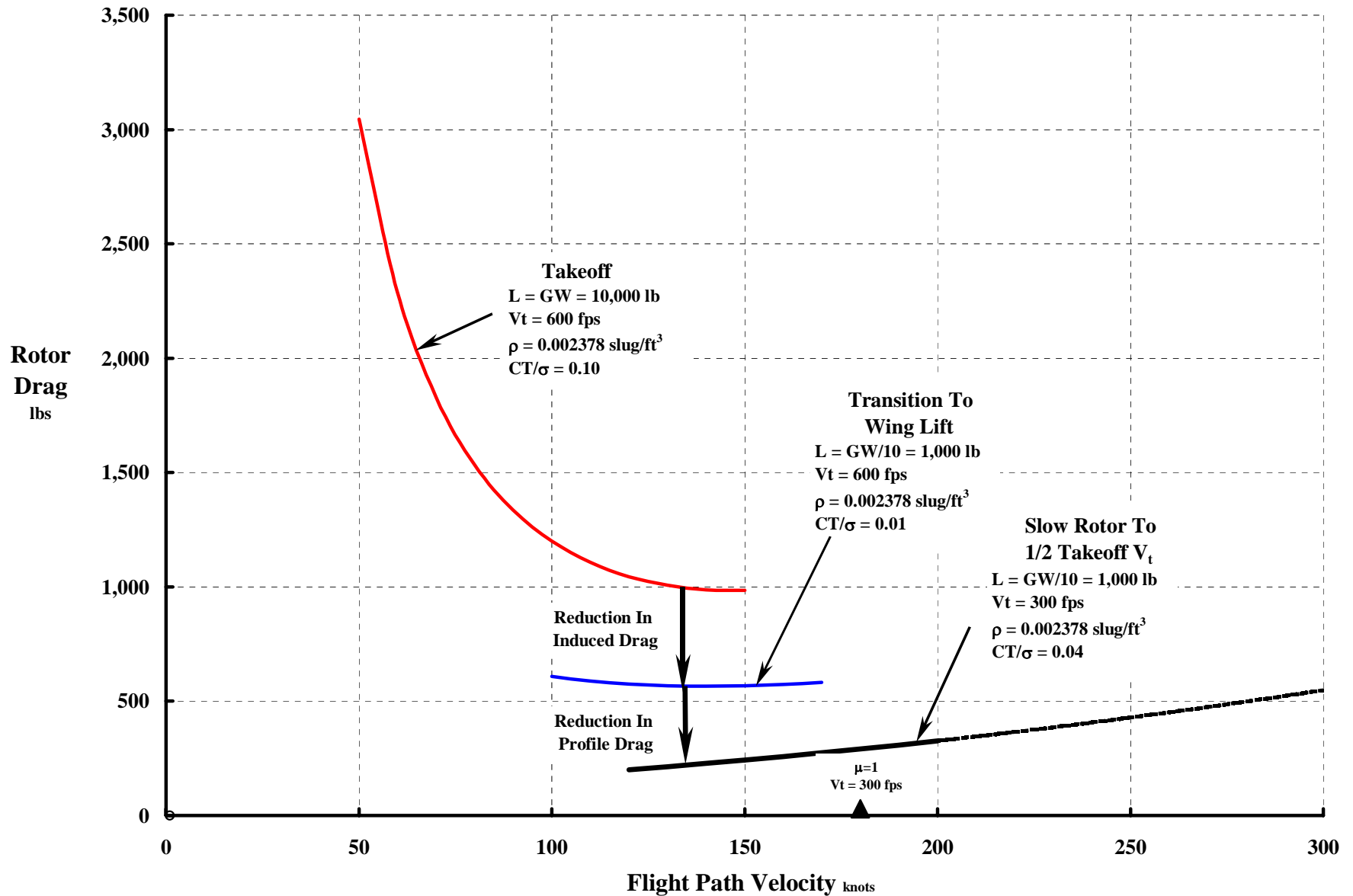
Figure 2. Sample result for 10,000 pound winged autogyro.

13. The Propulsive Force Required To Overcome The Drag Of An Autorotating Rotor.

Takeoff
L = GW = 10,000 lb
Vt = 600 fps
ρ = 0.002378 slug/ft³
CT/σ = 0.10

Transition To Wing Lift
L = GW/10 = 1,000 lb
Vt = 600 fps
ρ = 0.002378 slug/ft³
CT/σ = 0.01

Slow Rotor To 1/2 Takeoff V$_t$
L = GW/10 = 1,000 lb
Vt = 300 fps
ρ = 0.002378 slug/ft³
CT/σ = 0.04

Reduction In Induced Drag

Reduction In Profile Drag

μ=1
Vt = 300 fps
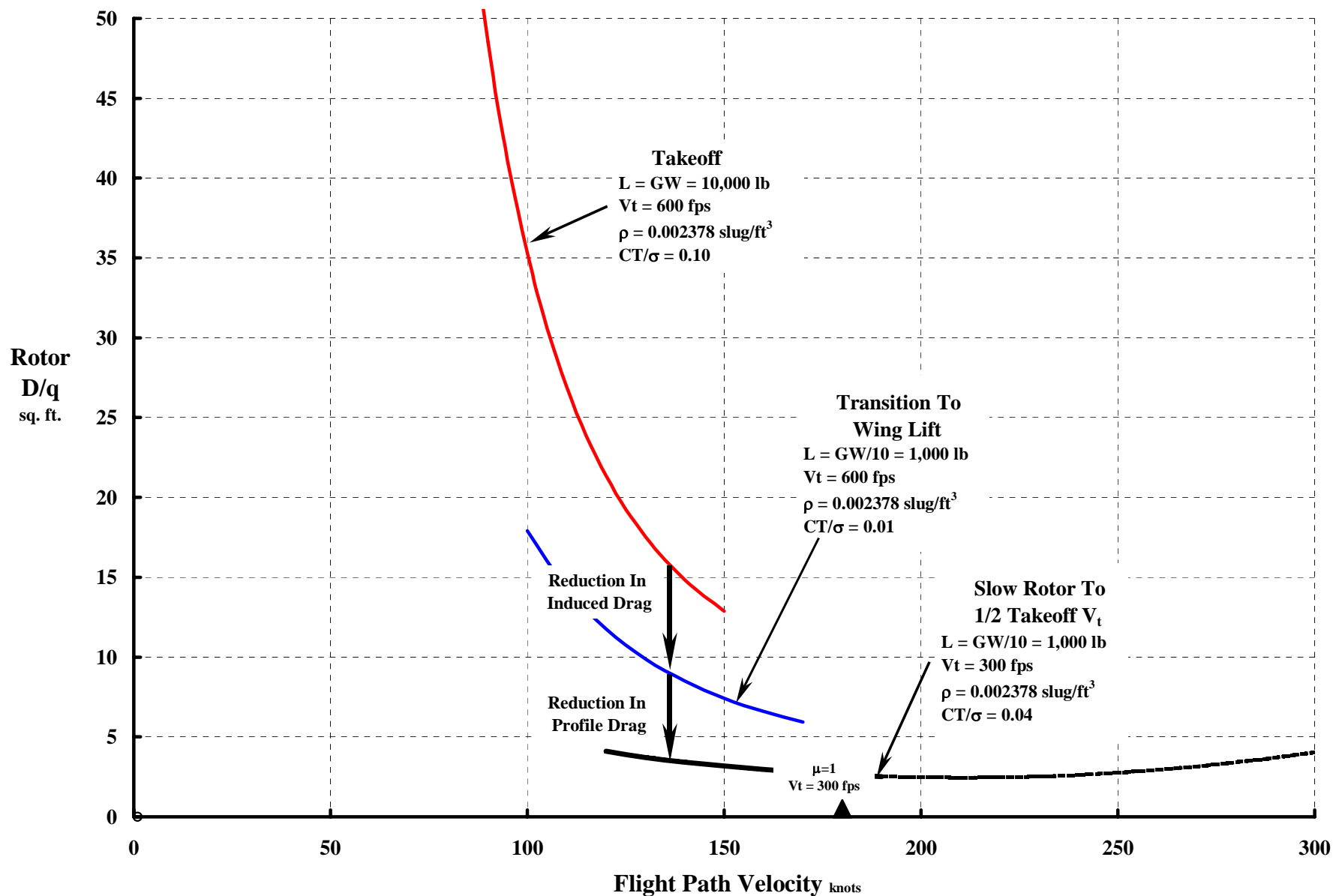
Figure 3. Sample result for 10,000 pound winged autogyro

13. The Propulsive Force Required To Overcome The Drag Of An Autorotating Rotor.

Figure 3 raises an interesting point about the value of D/q in the limit of a very slowly turning rotor. In 1966 I published a paper[1] that examined issues dealing with radial flow effects. In that paper, I offered the profile power μ function as $(1 + 4.65\mu^2 + 4.15\mu^4 - \mu^6)$ which was a curve fit of tabulated results up to $\mu = 1.0$ from computations carried out to $\mu = 3.0$. A portion of that table is included at the end of this Item 13. (An adequate curve fit up to $\mu = 3.0$ would be $(1 + 5.2003\mu^2 + 2.8777\mu^4 - 0.1788\mu^6 - 0.0202844\mu^8 + 0.0052625\mu^{10} - 0.0002735\mu^{12})$. Several assumptions were incorporated in the theory leading to this result as my paper[1] detailed. Briefly, the assumptions were:

a. $Cd_\Lambda = \dfrac{C_{do}}{\cos^{1/5}\Lambda}$ (increases C_d with yawed flow angle)

b. Reverse flow $C_{do} = 2$ times Normal flow C_{do}

c. Blade Element $V_{BE} = \sqrt{(\Omega r)^2 + 2(\Omega r)V\sin\Lambda + V^2}$

Later,[2] I published confirmation – at least to my satisfaction – that my suggested function was good enough for preliminary design *provided compressibility was not a factor*.

One of the results of the 1966 paper was the asymptotic behavior of minimum profile rotor drag. The result, for a slowly turning rotor (i.e. $\mu = 3$), was that

$$\frac{D_o}{q} = 1.3(2R)^2\sigma C_{do} \quad \text{for } \mu = 3 \text{ and close enough for higher } \mu\text{'s}$$

In rotor notation this result becomes

$$\frac{C_{Do}}{\sigma} = \frac{C_{Po}/\sigma}{\mu} = \frac{D_o}{\rho A V_t^2 \sigma} = \frac{2}{\pi}\left(\frac{D_{E_{min}}}{q\,d^2\sigma C_{do}} = 1.3 \text{ per Table}\right)\mu^2 C_{do} = 0.8276\mu^2 C_{do}$$

---

[1] See Harris, "Preliminary Study of Radial Flow Effects on Rotor Blades" AHS Journal of July 1966.
[2] Ref.: Figure 26 of "Rotary Wing Aerodynamics–Historical Perspective and Important Issues", F.D. Harris Paper Given at AHS Southwest Region Specialists' Meeting on Aerodynamics and Aeroacoustics, Feb. 25-27, 1987. Chairman Tom Wood of Bell Helicopter

13. The Propulsive Force Required To Overcome The Drag Of An Autorotating Rotor.

Table 1. Harris 1966 Radial Flow Solution $Cd_o = 0.01$

Advance Ratio	$\dfrac{2C_{Ho}}{\sigma Cd_o}$	$\dfrac{2C_{Qo}}{\sigma Cd_o}$	$\dfrac{2C_{Po}}{\sigma Cd_o}$	$\dfrac{D_o}{qD^2\sigma Cd_o}$	$\dfrac{C_{Do}}{\sigma}$
0.0	0.00000	0.2500	0.2500	∞	∞
0.1	0.07762	0.2540	0.2617	205.00	0.01309
0.2	0.16240	0.2657	0.2982	29.20	0.00746
0.3	0.26720	0.2846	0.3647	10.60	0.00608
0.4	0.37780	0.3099	0.4610	5.66	0.00576
0.5	0.52300	0.3406	0.6050	3.80	0.00605
0.6	0.69400	0.3755	0.7940	2.88	0.00662
0.7	0.89000	0.4135	1.0380	2.38	0.00741
0.8	1.11600	0.4532	1.3500	2.07	0.00844
0.9	1.38000	0.4933	1.7350	1.87	0.00964
1.0	1.66700	0.5324	2.1990	1.73	0.01100
1.1	2.03260	0.5695	2.8050	1.65	0.01275
1.2	2.41000	0.6042	3.4960	1.59	0.01457
1.3	2.82140	0.6362	4.3140	1.54	0.01659
1.4	3.24500	0.6653	5.2080	1.49	0.01860
1.5	3.70000	0.6916	6.2420	1.45	0.02081
1.6	4.20000	0.7147	7.4350	1.43	0.02323
1.7	4.73000	0.7348	8.7760	1.40	0.02581
1.8	5.30000	0.7516	10.2920	1.39	0.02859
1.9	5.90000	0.7652	11.9750	1.37	0.03151
2.0	6.50000	0.7749	13.7750	1.35	0.03444
2.1	7.20000	0.7817	15.9020	1.35	0.03786
2.2	7.90000	0.7857	18.1660	1.34	0.04129
2.3	8.60000	0.7864	20.5660	1.33	0.04471
2.4	9.35000	0.7840	23.2240	1.32	0.04838
2.5	10.09200	0.7783	26.0080	1.31	0.05202
2.6	11.00000	0.7691	29.3690	1.31	0.05648
2.7	11.84400	0.7565	32.7350	1.31	0.06062
2.8	12.77900	0.7406	36.5230	1.31	0.06522
2.9	13.76000	0.7212	40.6400	1.31	0.07007
3.0	14.68730	0.6986	44.7610	1.30	0.07460

V/STOL Aircraft and Propulsion Concepts
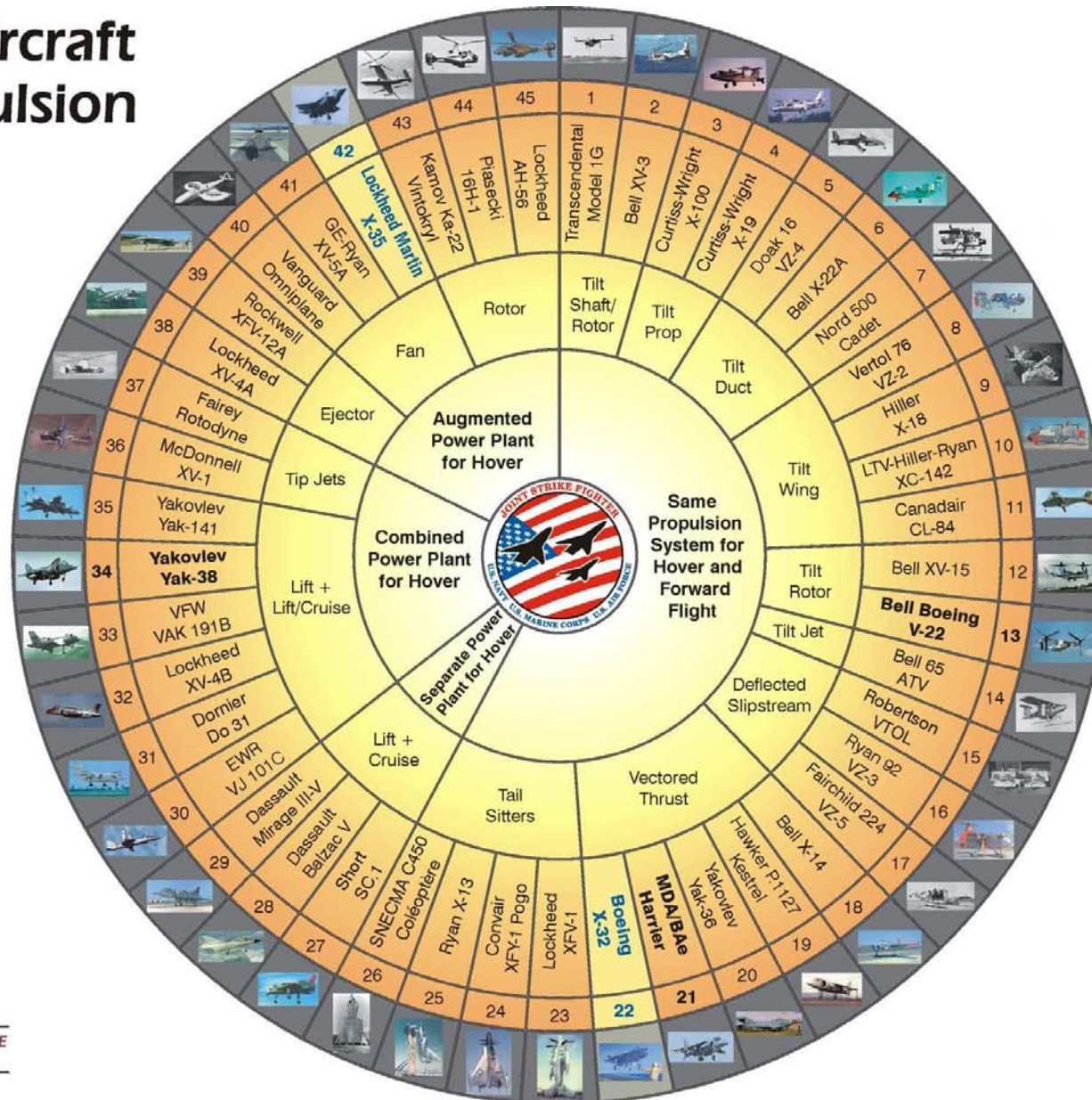
ANSER
A NOT-FOR-PROFIT PUBLIC SERVICE
RESEARCH INSTITUTE
http://www.anser.org

15. Additional Notes Provided by Mr. Robert Head (Retired Boeing Mesa)

XV–1 "CONVERTIPLANE"

McDonnell Aircraft Corp.
Mid-1950s

Robert Head, May 2003

These reminiscences are about 50 years old, so they may have some gaps. The basic airframe came from an early post-World War II commercial airplane program for a four-place airplane in the "Bonanza" and "Navion" class. The pitch/cone rotor was invented by Kurt Hohenemser in Germany during WW II. The tip jet propulsion system was invented by Fred Doblhoff in Austria during WW II. Both of these gentlemen were brought to McDonnell at the end of the War. Doblhoff told me that quick, definitive action was one thing he admired about a dictatorship. He said he conceived the tip jet concept; wrote a 10-page proposal; went to Berlin to see the Minister of R&D who read the proposal, asked a few questions, stamped "Approved" on it; and said go do it. Not at all like the good old American free enterprise system of request for proposal, proposal, conferences, modified proposal, best and final offer, and a contract (maybe).

The XV-1 was the first in a series of rotorcraft that used the XV-1 concept:
      a. XV-1 with a 31.5 foot diameter main rotor
      b. Model 120 that used a slightly modified XV-1 rotor, a flying crane fuselage. and three gas turbine
             compressors;
      c. Model XHCH-1 which had a 75 foot diameter rotor, a flying crane fuselage, and twin turboshaft engines that
             drove a pair of axial flow compressors.

The XV-1 was designed for three modes of flight:
      Helicopter – rotor powered, propeller stopped, full cyclic and collective pitch control by the
             pilot. The Model 120 and XHCH-1 were projected to fly only in this mode.
      Autogyro – rotor autorotates at full rpm, propeller is powered, rotor autorotates under full cyclic
             pitch control by the pilot, but at a low fixed collective pitch
      Airplane – rotor autorotates at half-speed, propeller is powered, pilot controls only lateral cyclic
             pitch, rudders, and ailerons. Collective pitch is locked at zero degrees,
             longitudinal cyclic pitch is disconnected from the pilot's control, governor
             controls longitudinal cyclic pitch for a constant rpm.

The aerodynamic controls operate in all flight modes without disconnection or limited operating range. The horizontal tail is mounted between the two tailbooms, is full-floating, spring-loaded nose up and pivoted at a point behind the aerodynamic center. The control tab is half-span, connected as a anti-balance tab, and operated by the pilot in all flight modes The balance tab is half-span, connected as an anti-balance tab, with a spring cartridge in the tab mechanism that makes horizontal tail fly itself into a more nose-down attitude as the convertiplane flies faster.

Directional control is by a pair of rudders that are permanently connected to the pilot's pedals, and by a pair of small diameter fixed-pitch fans at the end of the tail-booms. They change direction of rotation and rpm as the pilot operates the pedals to modulate the directional control moment.

The power system consisted of a radial reciprocating engine that drove a differential transmission that, in turn, drove either a drive shaft for the pusher propeller or twin centrifugal compressors for powering the main rotor. The compressed air from the two compressors was combined in the hub which served as a plenum for distributing the compressed air to the three rotor blade-root torque tubes. At the outboard ends of the torque tubes, a trifurcated duct divided the air into three air delivery tubes that ran the length of the blades, one through the leading edge spar and two in the trailing edge fairing. At the outboard end of the blade, the air was directed into the inboard end of the combustion nozzle which had an airfoil-shaped section that continued the blade contour out to the aft- facing thrust nozzle. The inboard portion of the nozzle assembly contained a flame-holder, a fuel spray-bar, and a spark plug to ignite the fuel/air mixture.

The design of the XV-1 tip jets was such that they could not be reignited in flight if they happened to flame out. Consequently, the tip jets were constantly "on" throughout each flight. They were not producing any appreciable thrust – just consuming lots of fuel. This design problem was solved for the Model 120 and the XHCH-1; their tip jet's fuel could be turned on and off at will.

The XV-1's rotor support system consisted of steel cone with its large end "down", and a double-row ball bearing at the bottom to allow the rotor to turn, lift and to accept side forces, and also drive generators and hydraulic pumps. The upper end of the mast had an internal spherical bearing that guided the "control stem", and provided support for an external, concentric gimbal ring to attach the hub.

The control stem had a "swashplate" at its top end. The control stem telescoped using an internal hydraulic actuator for collective pitch control. The control stem swung back and forth and side to side for cyclic pitch control. The control stem had a ball bearing near its top to allow the lower portion to stay fixed in rotation with respect to the airframe, and the top end to spin with the rotor.

The hub body was a hollow steel, six-sided ring. It had three holes in its sides for the blades, these holes being lined with spherical bearings that served as flap/feather bearings and as gas seals to prevent escape of the propulsion gas –

they were designed to accommodate the blade's spanwise stretching that it encountered going from stopped to full rpm. The hub was supported by the gimbal that was attached to this hub ring. Adjacent to each blade hole in this ring were a pair of lugs for bolting on the laminated blade retention straps.

The bottom plate of the hub bolted to the hub ring and also to a spherical seal ring known colloquially as the "salad bowl". This provided a gas seal as the hub tilted. (A concentric duct around the outside of the drive cone provided a gas path up to the salad bowl.) A top plate bolted to the hub ring and sealed off the plenum that was the hub body. There was a raised ring on the inside of the hub top plate that engaged the top of the swashplate for "airplane" flight. (More about this later.)

The blades were each attached to the hub by a pair of laminated steel straps, one forward and one aft of the torque tube. They attached to the blade at the outboard tip of the torque tube. This arrangement resulted in a rotating system with an in-plane natural frequency on the order of 1.3 per rev, a condition in which it is impossible to encounter ground resonance. The heavy, stiff blades gave the rotor a very high inertia. There was a picture of a mechanic sitting on a blade about half-way out to the tip with no visible blade bending.

In an inadvertent almost crash landing, the Model 120 helicopter was flipped nose-up and rolled well to the side. The pilot managed to pull the helicopter up, level it, and land safely. The damage was a bent landing gear and blade scuff marks on the top of one fuel tank. The rotor was down to about half-rpm near the top of its climb. Without the high inertia in this rotor, the consequences would have been much more severe.

Some details about the control system and the Pitch/cone and pitch/flap hub mechanism:
>Blade pivots in the side of the hub for flapping and feathering.
>Pitch arm trails behind its blade in the plane of rotation. Tip of pitch arm has spherical bearing for attachment to vertical pitch links. Two pitch links have spherical bearing connections to the swashplate – the other has a plain hinge at the top end to keep the swashplate aligned with the hub.
>The pitch arm cross section transitions, going inboard, from cylindrical in the flapping hinge region, to a "C" section to allow the entry of compressed air into the blade root, and then into a clevis for attaching the pitch link.

When in the helicopter mode with the hub unlocked and free to tilt, the pitch/cone mechanism comes into play. Here the hub will tilt to whatever angle is demanded by the blades. Then as the blades change their coning angle, cone up – blade feather nosedown. The pitch change with coning takes place about a line connecting the center of the rotor and the end of the pitch arm. The blades all must cone together to make this concept work.

Because the pitch arm for each blade trails its blade, the swashplate must move upward to produce zero collective pitch. As the swashplate moves up, the locking rings engage to make the hub follow the swashplate. So this single

motion reduces collective pitch to 0 degrees and locks the hub to the control system for autorotation. When the rotor is in this pitch/flap mode, the hub is locked to the swashplate and they must both tilt together, Then when any one blade flaps up or down, the blade individually changes its pitch angle, and the pitch/flap mechanism is in place.

Pitch/cone rotor characteristics:
- A pitch/cone rotor can almost overcome the classical pitching instability – geometrically it's not possible to fit the mechanism for this condition into the hub.
- Helicopter has a "cushioned" riding quality.
- Alternating blade loads are significantly lower than for conventional helicopter.
- It is not possible to get into ground resonance.
- When engine power is lost in helicopter flight, the pilot is not obligated to push the collected pitch down immediately. With no power, the rotor slows down a little, blades lose a little lift, blades cone upward and reduce collective pitch angle, and autorotation proceeds normally with the rotor spinning a little more slowly.

Pitch/flap rotor characteristics:
- Rotor slows down to half speed to keep the rotor advancing blade tip speed below sonic velocity and the rotor advance ratio within bounds
- Rotor shows an increasing flapping instability as advance ratio increases (observations from McDonnell wind tunnel tests):
- Rotor starts out at about $\mu = 0.3$ with a fairly flat rotor disc. As μ increases, a 2-per-rev flapping begins and gets progressively more pronounced as μ increases. This makes the rotor disc look more like a potato chip, with the advancing forward side and trailing aft side warping up out of plane. Then, around $\mu =1.5$, a 1/2-per-rev instability began to show up. This evidenced itself by one blade flicking out of track.

Flight control system characteristics:
- Pilot's cyclic stick is always connected to ailerons, horizontal tail, and to rotor lateral cyclic pitch
- Pilot's pedals always connect to rudders and to fan control valve.
- Pilot's cyclic pitch stick is connected to rotor control stem for helicopter and autogyro flight. Is disconnected from stick for airplane flight and operated by a governor to maintain constant rotor speed (about half normal rotor speed).

<u>**ADDITIONAL THOUGHTS ABOUT XV–1 "CONVERTIPLANE"**</u>
Robert Head, June 2003

<u>**A. Schemes for power plant configuration:**</u>
XV-1 and Rotodyne style
> Compressor supplies "cold" (300 deg) temperature compressed air to afterburners (1800 deg) in tip jets
> Propeller(s) provide cruise thrust
> Small fans provide steering control in XV-1. Differential propeller thrust steers Rotodyne

Boeing X-50 "Dragonfly", Canard Rotor Wing style
> Turbofan engine supplies "warm" (800 deg) temperature gas to either jets at the blade tips (no afterburning) or
>> to an aft-facing cruise thrust nozzle
> Sideward-facing steering jets are bled off the main gas stream

Hughes XV-9 Hot Cycle style
> Turbojet engine supplies "hot" (1400 deg) temperature gas to jet nozzles at the blade tips or to an aft-facing
>> cruise thrust nozzle
> Sideward-facing steering jets are bled off the main gas stream

Doman Helicopter (commercially marketed in 1950's)
> Mechanical torque delivered to the rotor or to a propulsion fan. Since the hub must tilt to achieve pitch-cone
>> effect, the drive shaft into the rotor must have a flexible joint to allow the shaft to bend.
> A constant-speed universal joint is probably too big to fit inside the rotor mast; a Hookes Joint would allow the
>> hub tilting but also produce an unfortunate two-per-rev torque oscillation at rotor speed frequency. This
>> torque oscillation would be minimized if the drive shaft rpm were many times that of the rotor speed.
>> Doman helicopters showed the way to overcome this problem in the 1950s by running a high speed,
>> low-torque shaft into the rotor hub and having a couple of sets of planetary gears in the hub above the
>> plane of the blades to get down to the desired rotor rpm.

B. XV-1 Flight Regimes
> Helicopter – Rotor powered and fully controlled by the pilot – propeller is stopped and locked – horizontal tail
>> and ailerons are controlled by the pilot – control shift lever is in the "up position
> Autogyro – Rotor autorotates at low collective pitch setting – propeller is powered – horizontal tail, ailerons,
>> and rotor lateral cyclic pitch are controlled by the pilot – control shift lever is in the "up" position with a
>> <u>minimum</u> collective pitch setting locked at 6 degrees

Airplane – Rotor autorotates at half speed – pitch control lever is in the "down" position and the collective pitch angle is locked at 0 degrees – rotor hub is locked to rotor longitudinal cyclic pitch control – it is disconnected from the pilot's cyclic stick and operated by a flyball governor to maintain constant rotor rpm – propeller is powered – horizontal tail, ailerons, and rotor lateral cyclic pitch are controlled by the pilot

C. XV-1 Flight Control System

Rotor cyclic and collective pitch angles and control shift are controlled by hydraulic power system

Ailerons, rudders, and horizontal tail are manually operated

All Cockpit Controls appear to be conventional, and act in the conventional way. The major difference is the Control Shift lever which is mounted alongside the collective pitch stick, and outboard of it.

The Shift lever has two positions: "Up" which limits the minimum collective pitch angle to six degrees (which is the collective pitch angle for "autogyro" flight and for autorotation if the engine power is interrupted in "helicopter" flight), and locks the longitudinal control mechanism (longitudinal cyclic pitch stick to longitudinal rotor control stem) which is the conventional control configuration for helicopters. The rotor hub is free to tilt to allow the "pitch/cone" effect. "Down" which locks the collective pitch angle at zero degrees, and, in turn, locks the rotor hub to the control stem to allow the rotor to act in the "pitch/flap" mode for high-speed cruise flight. The rotor longitudinal cyclic pitch mechanism is connected to a flyball governor to maintain rotor rpm at approximately one-half the helicopter rpm.

D. Cockpit Controls

Cyclic Pitch Stick ---- moves left/right, forward/aft

Pedals --- moves left/right

Collective Pitch Stick --- moves up/down

Control Pitch Stick Shift Lever --- moves up/down

E. Control Connections

Lateral cyclic pitch stick is always connected to the rotor lateral cyclic pitch mechanism, and to the wing-mounted ailerons

Longitudinal cyclic pitch stick is always connected to the control tab on the horizontal tail. It is always connected to the rotor longitudinal cyclic pitch mechanism in "helicopter" flight and in "autogyro" flight. It disconnects from the rotor longitudinal cyclic pitch-mechanism in "airplane" flight – the rotor cyclic pitch is then controlled by a governor to maintain constant rotor speed

F. Pitch/Cone and Pitch/Flap Rotor Ride Qualities

In both the pitch/cone and pitch/flap modes of flight the lifting rotor's lift curve is significantly lower than that for a conventional rotor which, in turn, is significantly lower than that for a fixed wing. This results in a very smooth ride in turbulent air.

MORE POINTS ABOUT THE XV–1 "CONVERTIPLANE"
Robert Head
June 2003

Icing is not a problem. The hot gas running through the hub and blades melts off any ice that may have formed while parked in a freezing rain, and will keep ice from forming on the blades in helicopter flight. If ice collects while in airplane or autogyro flight, convert to helicopter flight to melt the ice.

In the early 1950s, the XV-1 rotor was made primarily of steel because it was the only structural material available that could provide the strength necessary at the elevated temperature. Nowadays titanium or high-temperature composites such as carbon/carbon could handle the operational conditions at reduced weight.

The rotor could be started and stopped in a high wind on the ground. Start with the rotor collective pitch in its zero position with the hub locked to the control stem. Then as the rotor starts turning, if a gust hits one blade and that blade tends to rise, its pitch/flap coupling forces the blade into a nose-down attitude which develops a "down" flapping force on that blade which opposes the upward gust force and keeps the rotor in track. This effect makes it unnecessary to incorporate "flap-up" stops.

In the hub-free mode the rotor blades are self-tracking. If one blade has a little too much pitch angle compared with the others which makes that blade fly higher than the other blades, that blade will force the hub tilt away from the "up" blade. The pitch/cone coupling will make the "high" blade fly "down" and the other blades fly "up" until the blades are all flying in track, but with the rotor blades flying in a slightly tilted tip-path plane.

A Type of Lifting Rotor with Inherent Stability

KURT HOHENEMSER*

McDonnell Aircraft Corporation

SUMMARY

The more important of the forward flight aerodynamic characteristics of a rotor type are presented where the collective blade pitch angle is kinematically coupled with the collective flapping or coning angle, while no coupling is provided between cyclic flapping and cyclic pitch angles. The rotor with pitch-cone change may be designed to have positive static stability as compared to the negative static stability of the conventional fixed-pitch rotor; partial blade stall during pull-ups or upward gusts may be avoided in spite of a high and economic thrust coefficient in steady flight, and no adjustment of the collective pitch control is required for the transition from powered flight to autorotation. The rotor with pitch-cone change, because of its inherent stability, promises, without recourse to external stabilizing devices, appreciably improved flying qualities of the helicopter.

DISCUSSION

IT IS GENERALLY KNOWN that the conventional lifting rotor with hinged or tetering blades has characteristics that produce, in forward flight of the helicopter, longitudinal instability unless external stabilizing surfaces or other stabilizing devices are provided.[1, 2, 6, 7] We first discuss the main parameters responsible for the longitudinal control and stability characteristics of the helicopter.

Fig. 1 shows a schematic side view of a lifting rotor with hinged or tetering blades. V is the direction of the relative air speed; α measures the attitude of the control plane or plane of zero cyclic feathering with respect to the direction of flow, positive if inclined backwards; and a_1 measures the backward inclination of the tip path plane with respect to the control plane. The thrust vector T is approximately perpendicular to the tip path plane and, in the undisturbed flight condition, is assumed to pass through the aircraft center of gravity. x and z are body fixed reference axes through the c.g., x pointing into the direction of undisturbed flight and z perpendicular to x downwards. Changes of forward flight speed and of attitude produce the following three pitching moments about the c.g.:

An increase in forward flight speed V without change of attitude α causes an increase in a_1 or a backward inclination of the thrust vector T producing a tail-heavy pitching moment about the c.g. In other words, *the lifting rotor has positive velocity stability.*

A slow increase in attitude angle α without change of flight speed V also causes an increase in a_1 or a back-

ward inclination of the thrust vector T relative to the fuselage producing a tail-heavy pitching moment about the c.g. In other words, *the lifting rotor is statically unstable.* The fact that the lifting rotor is unstable with change of attitude was obscured for some time by the stable stick travel observed in most helicopter types, which means that an increase in steady flight speed requires a more forward position of the control stick. For the airplane, a stable stick travel is an indication of static stability. This is not true for the helicopter, where a stable stick travel may be produced by the velocity stability in spite of instability with change of attitude.

A rapid increase in attitude angle α without change of flight speed V causes a decrease in a_1 or a forward inclination of the thrust vector T relative to the fuselage, producing a nose-heavy pitching moment about the c.g. proportional to the rate of change of attitude. In other words, *the lifting rotor has positive pitch damping.*

Finally, an increase in attitude angle α produces an increase in thrust T. The increase in attitude angle α may also be described as an additional downward velocity component of the helicopter $\dot{z}$, and we may state that *the lifting rotor has positive vertical damping.*

Although there is a total of nine longitudinal stability derivatives, numerical evaluation of the complete equations of motion has shown that only the four derivatives just mentioned are of major influence on the flying qualities of the helicopter. The effect of these four derivatives is the following:

The velocity stability is, as was mentioned before, mainly responsible for a stable stick travel. The velocity stability should, however, be kept in moderate limits, because the frequency of the long-period oscillation of the helicopter increases with increased velocity stability, and a low frequency is desirable from a point of view of flying characteristics.
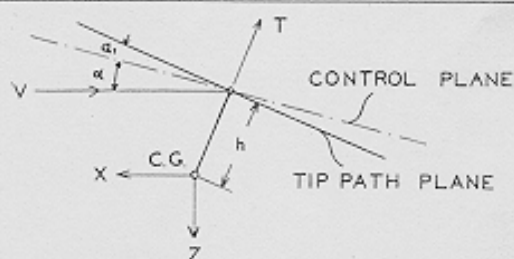

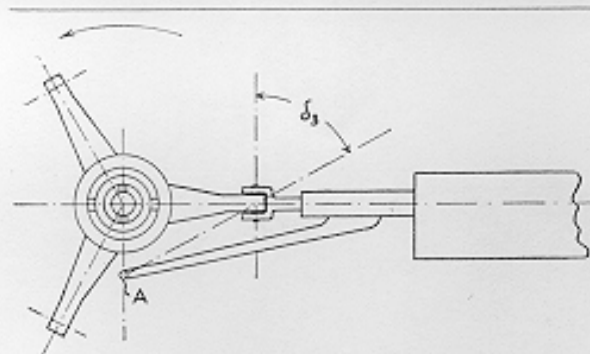FIG. 1. Schematic side view of lifting rotor.

555

FIG. 2.   Plan view of rotor hub with pitch-cone change.

Static stability is necessary for damping the long-period oscillation. The instability of most helicopters is not obvious under normal flight conditions, because the period of the instable oscillation is so long that the pilot has ample time to correct any tendencies of self-excitation. If, however, because of a wrong c.g. location or a lack of forward stick travel, the pilot encounters a condition where he runs out of forward longitudinal control, the instability becomes obvious, and dangerous flight conditions with extreme and uncontrollable attitude changes occur. It may be noted here that a pitch governor keeping the rotor speed constant increases the static instability of the helicopter, and for this reason such a governor should be avoided.

The pitch damping, which is proportional to the blade moment of inertia, has a marked effect on the flying characteristics of the helicopter. The higher the pitch damping, the longer and more damped is the oscillation period of the helicopter. Therefore, lifting rotors with either heavy blades or heavy tip weights of jet engines or rotor types, with artificially increased pitch damping like the Bell and Hiller rotors, require less attention by the pilot than conventional rotor types. An increase in pitch damping, however, slows down the control response, and the pitch damping therefore should not be excessive.

The vertical damping is responsible for the load factors produced by gusts. A low vertical damping is desirable from a point of view of smooth flight and also of good dynamic stability.

One method of correcting the static instability of the conventional lifting rotor is to compensate it by the positive static stability produced by a stabilizing surface or by an appropriate fuselage shape. In spite of difficulties caused by the rotor downwash, satisfactory stabilization has been achieved in some cases by stabilizing surfaces at least for a limited speed range. However, the better method seems to be the elimination of the unstable moments at the source rather than their compensation by an additional device.

Another method of correcting the static instability of the conventional lifting rotor would be the use of large δ_3 angles for the horizontal blade hinge axes. By

this method, a_1 could be almost completely eliminated and the tip path plane would always coincide with the control plane. This method would, however, not only eliminate the static instability but also eliminate the two other pitching moment derivatives—the velocity stability and the pitch damping—both of which are extremely important, as has been indicated before.

A third method, which is the main subject of this paper, not only leaves the velocity stability and the pitch damping unimpaired but also provides positive static stability for the lifting rotor. The method consists in coupling the collective blade pitch angle with the collective blade flapping or coning angle, while no coupling is provided between cyclic pitch and cyclic flapping angles. One manner of realizing this method is shown in Fig. 2, which is a plane view of a rotor hub with pitch-cone change. The hub is universally hinged at the rotor shaft, and the blades are individually hinged to the hub at a distance from the rotor center. The blade pitch arm extends opposite to the direction of rotation to the rotor center and is operated in a conventional manner by vertical links attached to the points A.

The tip path plane of this rotor may be inclined by an angle a_1 with respect to the control plane without affecting the blade pitch. Any increase in coning angle a_0, however, produces a decrease in blade pitch angle proportional to tan δ_3. The complication of the hub and hinge assembly by having a universal center hinge and additional outer flap hinges is, as compared to the conventional rotor, more than offset by the elimination of drag hinges and their dampers, which are unnecessary in this design, and by the compactness and simplicity of the control mechanism. In case of a jet-driven rotor, the center universal hinge may be replaced by a self-aligning bearing, and the design, shown in Fig. 2, lends itself especially well to jet-driven lifting rotors.

The following comparison between the conventional fixed-pitch rotor and the rotor with pitch cone-change is made on the basis of a simplified analysis following Bailey's N.A.C.A. Report[2] but using a constant profile drag coefficient of the blade of 0.012. The rotor is assumed to have rectangular untwisted blades with a blade solidity of 0.06 and a blade inertia coefficient of 10.

Fig. 3, upper portion, shows, for an advance ratio μ of 0.35, the coning angle a_0 against attitude angle α of the control plane for different blade pitch angles θ.

Fig. 3, lower portion, shows the backward tip path plane inclination a_1 against α. For any given blade pitch angle θ, the backward tip path plane inclination increases with α, causing static instability of the lifting rotor.

Now assume, as an example, that blade pitch angle θ and coning angle a_0 are related by the equation

$$\theta = 24 - 2.7\, a_0$$

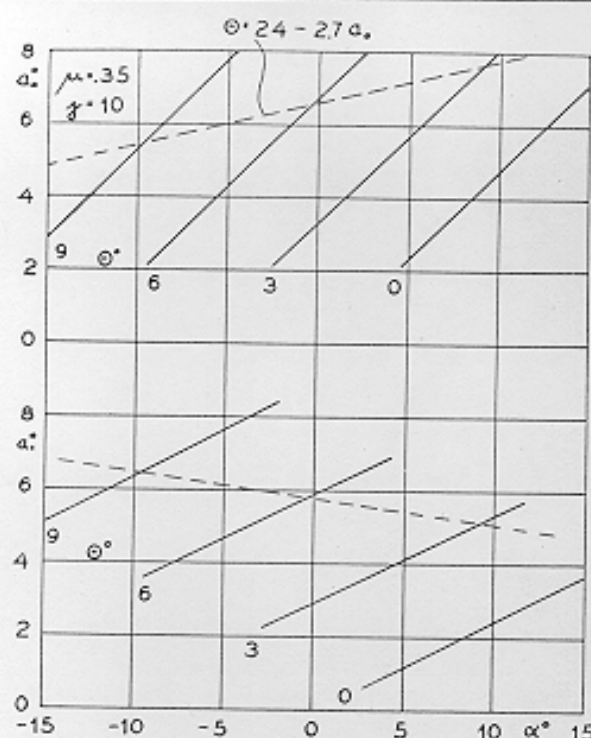which is valid for a δ_3 angle of 70° and for a coning

A-238

FIG. 3. Coning angle a_0 and tip path plane inclination a_1 against α with blade pitch angle θ as parameter for advance ratio $\mu = 0.35$. Dashed lines for sample rotor with pitch-cone change.
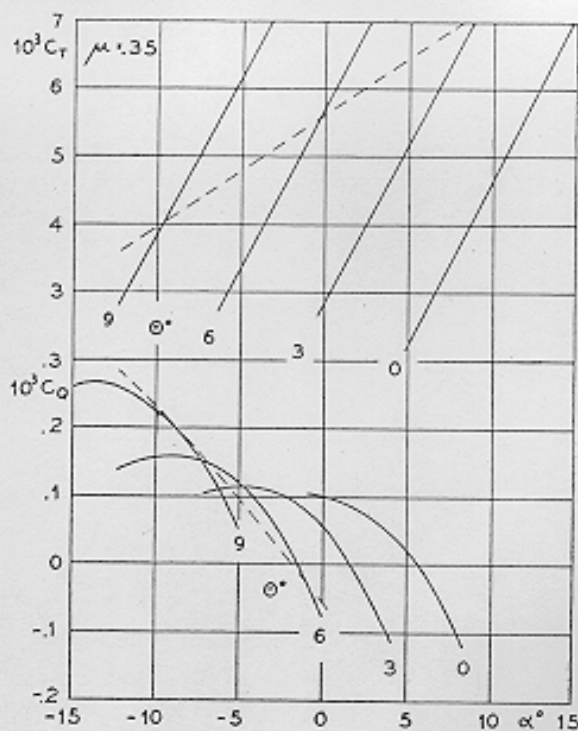

FIG. 4. Thrust coefficient c_T and torque coefficient c_Q against α with blade pitch angle θ as parameter for advance ratio $\mu = 0.35$. Dashed lines for sample rotor with pitch-cone change.

angle a_0 of 5.5° belonging to a pitch angle θ of 9°. Points corresponding to this equation are connected in Fig. 3 by dashed lines. The higher the coning angle a_0, the lower the pitch angle θ. The dashed line in the lower part of Fig. 3 gives the change of a_1 with α, and it is seen that the slope is reversed as compared to the conventional rotor with fixed blade pitch angle θ. The rotor with pitch-cone change may be designed so that it provides positive static stability.

Fig. 4, upper portion, shows the thrust coefficient c_T against α for different blade pitch angles θ and for the same advance ratio as before, $\mu = 0.35$. The dashed line belongs to the sample rotor with pitch-cone change. It is seen that the increase of thrust with increased attitude angle α is considerably reduced as compared to the rotor with fixed blade pitch.

Fig. 4, lower portion, shows the torque coefficient of a lifting rotor against α for different blade pitch angles θ. The dashed line, belonging to the rotor with pitch-cone change, does not show the curved character of the fixed-pitch lines and has a fairly constant slope.

Diagrams similar to those presented here for an advance ratio of $\mu = 0.35$, were also developed for other advance ratios. The result is a complete comparison between the fixed-pitch rotor and the rotor with pitch-cone change, as shown in the following diagrams. The three quantities—backward inclination of tip path plane with respect to control plane a_1, thrust coefficient c_T, and torque coefficient c_Q—are plotted for both rotor
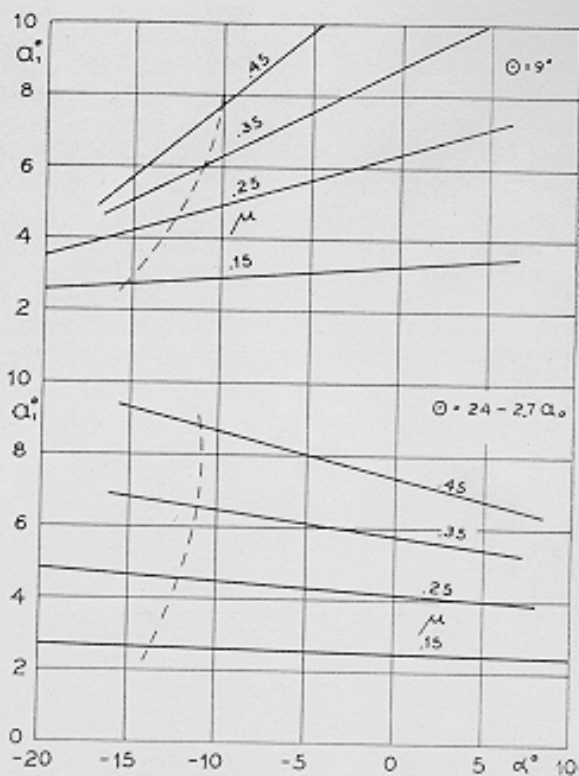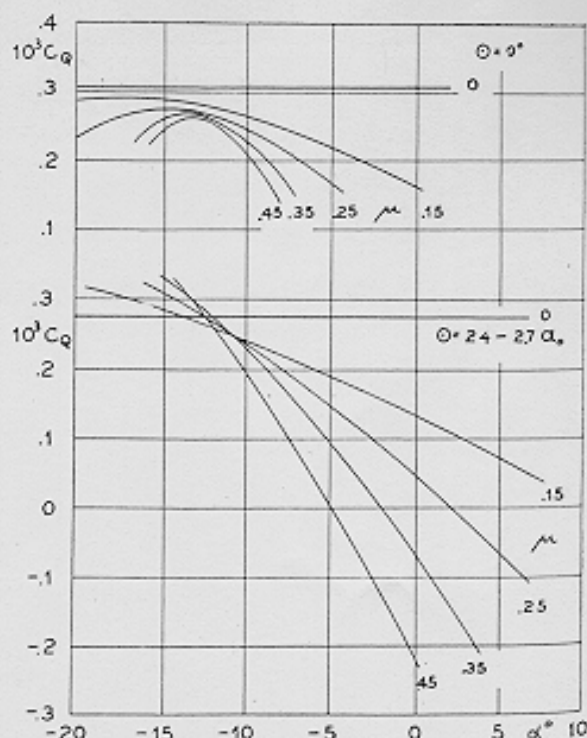

FIG. 5. Comparison between fixed-pitch rotor (above) and rotor with pitch-cone change (below). Tip path plane inclination a_1 against α with advance ratio μ as parameter. Dashed lines for constant c_Q/c_T equal to c_Q/c_T in hovering.

A-239
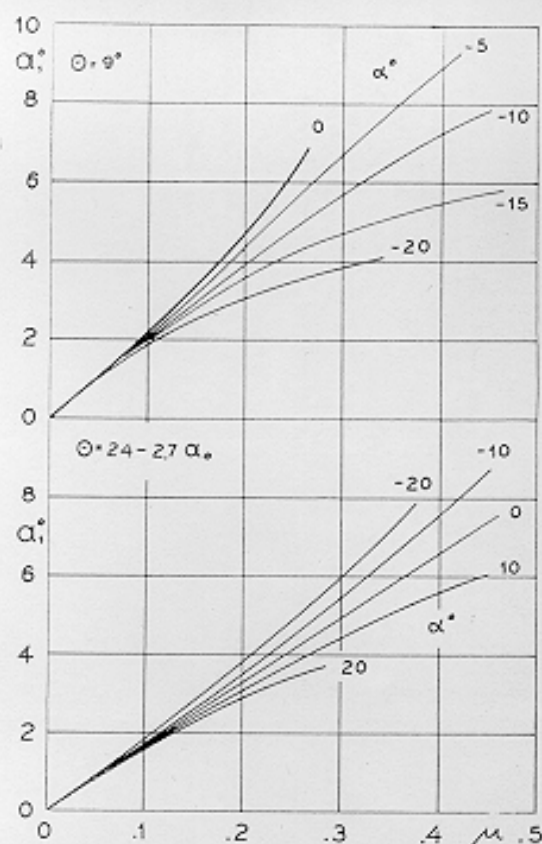
FIG. 6.   Same as Fig. 5, except with μ as abscissa.
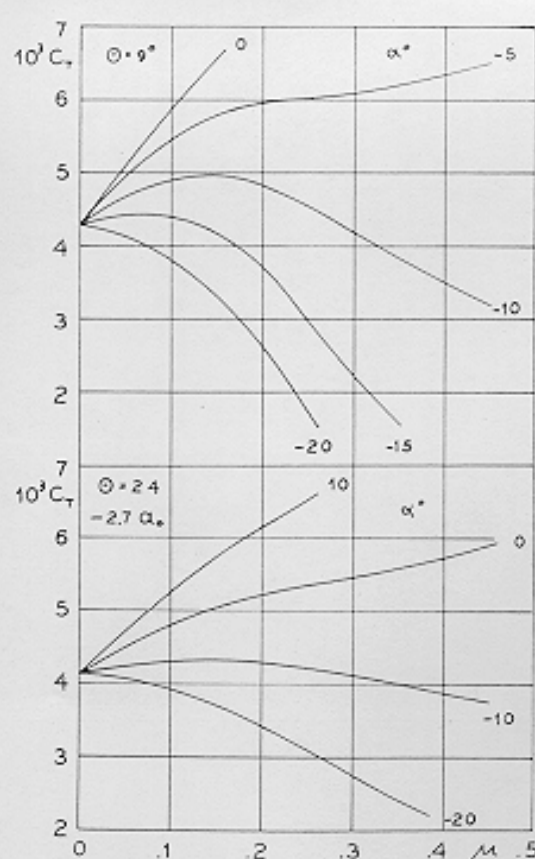
FIG. 8.   Same as Fig. 7, except with μ as abscissa and α as parameter.
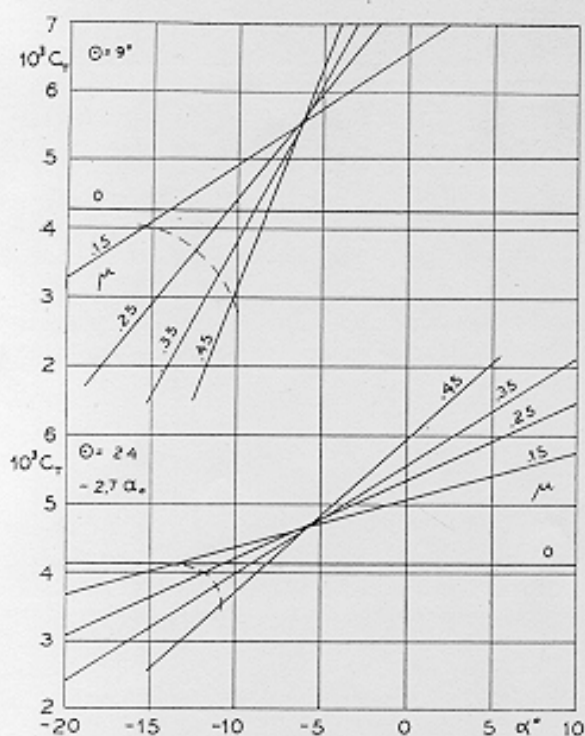
FIG. 7.   Comparison between fixed-pitch rotor (above) and rotor with pitch-cone change (below).   Thrust coefficient c_T against α with advance ratio μ as parameter.   Dashed lines for constant c_Q/c_T equal to c_Q/c_T in hovering.

FIG. 9.   Comparison between fixed-pitch rotor (above) and rotor with pitch-cone change (below).   Torque coefficient c_Q against α with advance ratio μ as parameter.

A-240

types against α with μ as parameter and against μ with α as parameter. The upper part of each figure contains the fixed-pitch rotor characteristics, assuming a pitch angle of $\theta = 9°$; the lower part of each figure contains the characteristics of the rotor with pitch-cone change.

Fig. 5 shows the comparison for the tip path plane inclination a_1 against α with μ as parameter. This is the most important part of the comparison, since it shows the reversal of the slopes of the $a_1 - \alpha$ curves for all μ values. The fixed-pitch rotor is statically instable in the whole range; the rotor with pitch-cone change is statically stable under all conditions.

Fig. 6 shows the same characteristics in a different presentation—namely, a_1 against μ with α as parameter. The main character of the $a_1 - \mu$ curves is the same in both cases, indicating that the velocity stability of both rotor types will be of the same order of magnitude.

Fig. 7 shows the comparison for the thrust coefficient c_T against α with μ as parameter. The slope of all $c_T - \alpha$ curves is appreciably smaller for the rotor with pitch-cone change than for the fixed-pitch rotor.

Fig. 8 shows the same characteristics in a different presentation—namely, c_T against μ with α as parameter.

Fig. 9 shows the comparison for the torque coefficient c_Q against α with μ as parameter.

FIG. 11. Vertical damping $- Z_{\dot{z}}$ and velocity stability $\bar{M}_{\dot{x}}$ against advance ratio μ for constant c_Q/c_T equal to c_Q/c_T in hovering. 1 for fixed pitch, $\theta = 9°$; 2 for sample rotor with pitch-cone change, $\theta = 24 - 2.7a_3$. Solid curves for constant torque; dashed curves for constant rotor speed.

Fig. 10 gives the same set of values in a different presentation—namely, c_Q against μ with α as parameter.

The data given in these diagrams are sufficient for establishing a theoretical comparison between the flying characteristics of the fixed-pitch rotor and those of the rotor with pitch-cone change. The main improvement accomplished by the pitch-cone change is the positive static stability instead of the negative static stability of the fixed-pitch rotor. But there are also other improvements, the most important of which is the elimination of partial blade stall at high forward speeds, especially during maneuvers. Partial blade stall has proved to be a severe limitation of the lifting rotor, and it is accompanied by heavy vibrations and reduction or loss of control. The main parameter controlling the blade stall is the thrust coefficient. Performancewise, it is most economic to operate at a high thrust coefficient and close to the condition of beginning blade stall.[4] In this case, however, pull-ups and upward gusts cause large portions of the blades to stall. The rotor with pitch-cone change reaches, during maneuvers and gusts, considerable lower thrust coefficients than the fixed-pitch rotor (see Fig. 7), and blade stall may therefore be avoided in spite of a high and economic thrust coefficient in steady flight.
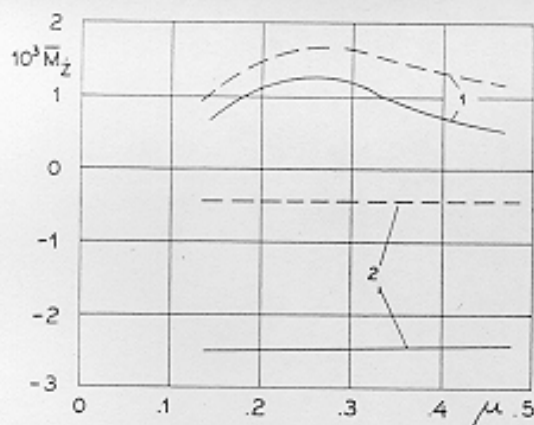

FIG. 10. Same as Fig. 9, except with μ as abscissa and α as parameter.

FIG. 12.   Static stability $-\bar{M}_z$ against advance ratio μ for same conditions as in Fig. 11.

A further improvement of the rotor with pitch-cone change as compared to the fixed-pitch rotor is its capability of autorotation without adjustment of the collective pitch control, which is a desirable safety feature.

Finally, a quantitative comparison of stability derivatives of the two rotor types is of interest. Fig. 11 shows the vertical damping $\bar{Z}_z$ and the velocity stability $\bar{M}_z$ against μ for conditions with a power input equal to the hovering power. The solid lines have been computed under the assumption of constant torque and varying rotor speed, which is practically fulfilled in the case of slow oscillations of a helicopter without rotor speed governor. The dashed lines have been computed under the assumption of constant rotor speed and varying torque, which is approximately fulfilled in the case of rapid motions of the helicopter when the inertia of the rotor prevents corresponding rapid changes of the rotor speed or in the case of a rotor speed governor controlling the engine output. Curves 1 belong to the fixed-pitch rotor, and curves 2 belong to the rotor with pitch-cone change. The vertical damping $\bar{Z}_z$ is nearly the same in both cases if the torque is kept constant. This indicates that, for relatively slow pull-ups or in turns, the two rotor types will have the same vertical load factors. For constant rotor speed, however, the rotor with pitch-cone change has a considerably reduced vertical damping $\bar{Z}_z$, indicating a reduced sensitivity to sudden gusts.

The velocity stability of the rotor with pitch-cone change is increased as compared to the fixed-pitch rotor, indicating a greater forward stick travel with increased forward speed. The increased velocity stability produces an increased frequency of the helicopter oscillation, which is not desirable. The δ_3 angle should, therefore, stay in the limits required for achieving static stability and should not be unnecessarily high.

The pitch damping has not been plotted because it is the same for both types of rotor.

Fig. 12 shows the static stability derivative $\bar{M}_z$ for both rotor types, also against μ. Positive $\bar{M}_z$ is equivalent to static instability. The improvement by the rotor with pitch-cone change is especially great in the case of constant torque (solid lines).

Static stability is a necessary but not sufficient requirement for dynamic stability. Whether or not the helicopter is dynamically stable depends mainly on the fuselage moment of inertia. Fig. 13 indicates the maximum moment of inertia allowable in order to obtain dynamic stability with the rotor with pitch-cone change. The solid line represents the case of constant torque; the dashed line represents the case of constant r.p.m. In spite of the smaller static stability, the maximum allowable moment of inertia is larger in the case of constant r.p.m. than in the case of constant torque. If the inertia of the fuselage stays within these limits, the helicopter with pitch-cone change will be longitudinally stable, without any stabilizing surface or stabilizing device, only by its own inherent stability. Fig. 13 indicates that the rotor stability increases with forward speed. Of course, the fuselage must have a shape so that its pitching moment derivatives do not offset the stability derivatives of the rotor proper. But even if the inherent stability of the rotor with pitch-cone change is not sufficient to overcome destabilizing effects of the fuselage, the use of this rotor type seems to promise appreciably improved flying qualities of the helicopter.

To sum up the main characteristics of the rotor with pitch-cone change:

(1) Positive static stability instead of negative static stability of the fixed-pitch rotor.

(2) Possibility of avoiding partial blade stall during pull-ups or upward gusts in spite of a high and economic thrust coefficient in steady flight.

(3) Elimination of collective pitch adjustment for the transition from powered flight to autorotation.

(4) Considerable mitigation of loads caused by sudden gusts.

(5) Increase in velocity stability.

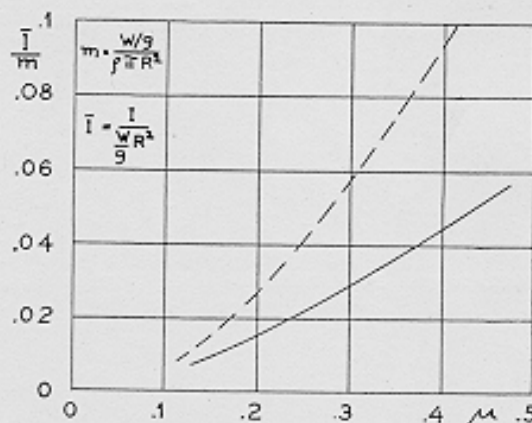(6) Unimpaired damping in pitch of the helicopter.

FIG. 13.   Maximum allowable helicopter moment of inertia about pitching axis against μ for dynamic stability when using sample rotor with pitch-cone change. Solid lines for constant torque; dashed lines for constant rotor speed.

(7) Unimpaired vertical maneuvering load factors if the rotor speed is allowed to vary without interference of a rotor speed governor.

(8) Possibility of attaining dynamic longitudinal stability in forward flight without stabilizing surfaces or other stabilizing devices.

We were mainly concerned here with the longitudinal stability of the rotor with pitch-cone change. Other problems related to this type of rotor (such as lateral stability, rotor speed oscillations, and coning angle oscillations) have been investigated and will be presented separately.

SYMBOLS

V = velocity of undisturbed flight

α = attitude angle of control plane (plane of zero cyclic pitch) with respect to flight velocity; positive if helicopter is inclined backwards

a_1 = angle of backward inclination of the tip path plane with respect to the control plane

T = thrust vector, assumed to be perpendicular to the tip path plane

x, z = body fixed reference axes, x pointing in the direction of undisturbed flight and z perpendicular to x downwards

a_0 = collective flapping or coning angle

δ_3 = angle between outer kinematic flapping axis and tangential direction

δ = profile drag coefficient of blade

γ = $c\rho a R^4/I_B$ = blade inertia coefficient

c = blade chord

ρ = air density

a = slope of blade lift coefficient against blade angle of attack (assumed to be 5.7)

R = rotor radius

I_B = blade moment of inertia about horizontal hinge

σ = $bc/\pi R$ = blade solidity

b = number of blades

θ = blade pitch angle

c_T = $T/\rho\Omega^2\pi R^4$ = thrust coefficient

Ω = angular rotor speed

c_Q = $Q/\rho\Omega^2\pi R^5$ = torque coefficient

Q = rotor torque; positive if engine puts power into rotor

μ = $V\cos\alpha/\Omega R$ = advance ratio

$\lambda\Omega R$ = speed of axial flow through rotor

$A\ldots K$ = functions of μ tabulated in Table 1

$\dot{x}, \dot{z}$ = small disturbance velocities in direction of x axis and of z axis

$\dot{\alpha}$ = small disturbance angular velocity about pitching axis

W = gross weight of helicopter

g = acceleration of gravity

Z = force in direction of z axis

M = pitching moment; positive if tail heavy

I = helicopter moment of inertia about pitching axis

$Z_{\dot{z}}$ = $\partial Z/\partial\dot{z}$ \} derivatives
$M_{\dot{x}}$ = $\partial M/\partial\dot{x}$

m = $(w/g)/\rho RA$ = mass coefficient

A = rotor disc area

C_L = $W/(V^2/2)\rho A \approx 2C_T/\mu^2$ = rotor lift coefficient

t = time

$\bar{M}_{\dot{z}}$ = $M_{\dot{z}}/AR\rho v$ = velocity stability

$-\bar{M}_{\dot{z}}$ = $-M_{\dot{z}}^2/AR\rho v$ = static stability

$-\bar{M}_{\dot{\alpha}}$ = $-M_{\dot{\alpha}}/AR^2\rho v$ = pitch damping

$-\bar{Z}_{\dot{z}}$ = $-Z_{\dot{z}}/A\rho v$ = vertical damping

I = $I/(w/g)R^2$ = dimensionless helicopter moment of inertia about pitching axis

A/E = coefficients of frequency equations

q_c = $Q/AR(\rho/2)v^2 = 2c_Q/\mu^2$ = torque coefficient

$q_{c\mu}$ = $\partial q_c/\partial\mu$ \} derivatives
$q_{c\alpha}$ = $\partial q_c/\partial\alpha$

c_M = $M/AR(\rho/2)V^2$ = pitching moment coefficient

$C_{M\mu}$ = $\partial c_M/\partial\mu$ \} derivatives
$c_{M\alpha}$ = $\dfrac{\partial c_M}{\partial\alpha}$

h = distance between rotor hub and helicopter c.g.

$\bar{h}$ = h/R = dimensionless distance

AERODYNAMIC ROTOR CHARACTERISTICS

According to reference 3, the following equations are available for determining the thrust coefficient c_T, the torque coefficient c_Q, the backward inclination of the tip path plane with respect to the control plane a_1, and the coning angle a_0 as functions of the three independent variables α, μ, and θ:

$$\alpha = (\lambda/\mu) + (c_T/2\mu^2), \quad (\lambda = -\sqrt{c_T/2} \text{ for hovering})$$
$$2c_T/a\sigma = A\lambda + B\theta$$
$$2c_Q/a\sigma = (C/a)\delta - D\lambda^2 - E\lambda\theta - F\theta^2$$
$$a_1 = G\lambda + H\theta$$
$$a_0/\gamma = I\lambda + K\theta$$

The rotor is assumed to have untwisted rectangular blades with a blade solidity of $\sigma = 0.06$, with a lift coefficient slope of $a = 5.7$, with a constant profile drag coefficient of $\delta = 0.012$, and with a blade inertia coefficient of $\gamma = 10$. The values for the coefficients $A\ldots K$ as functions of μ are given in reference 3 for a tip-loss factor of 0.97 and are summarized in Table 1.

TABLE 1

μ	0	0.15	0.25	0.35	0.45
A	0.470	0.476	0.487	0.504	0.529
B	0.300	0.315	0.333	0.361	0.399
C	0.250	0.256	0.266	0.280	0.299
D	0.470	0.502	0.558	0.646	0.766
E	0.300	0.369	0.490	0.689	0.986
F	0	0.022	0.066	0.145	0.276
G	0	0.322	0.543	0.777	1.026
H	0	0.418	0.715	1.041	1.405
I	0.150	0.152	0.153	0.154	0.155
K	0.110	0.113	0.118	0.124	0.133

The four quantites a_0, a_1, c_T, and c_Q against α, with θ as parameter, are plotted in Figs. 3 and 4 for $\mu = 0.35$. Similar plots have been obtained for the other advance ratios μ listed in Table 1. The assumption of a constant profile drag coefficient provides approximately correct c_Q curves only in a limited range. In reality, the downward trend of the $c_Q - \alpha$ curves with increasing α, as shown in Fig. 4, is ultimately reversed.

In Figs. 4 and 9, the c_Q curves are only plotted in a range for which a reasonable approximation is expected.

The rotor with pitch-cone change is assumed to have a δ_3 angle of 70°. The reduction in pitch angle $\Delta\theta$ produced by an increase in coning angle Δa_0 is

$$\Delta\theta = \tan\delta_3 \Delta a_0 = 2.7 \Delta a_0$$

A-243

The pitch setting is assumed to result in a blade pitch angle of $\theta = 9°$ at a coning angle $a_0 = 5.5°$. The relation between θ and a_0, therefore, reads

$$\theta = 24 - 2.7a_0$$

Introducing this relation in the $a_0 - \alpha$ diagram, Fig. 3, upper portion, gives correlated values α, μ, and θ for the rotor with pitch-cone change and reduces the number of independent variables from three to two. The three quantities a_1, c_T, and c_Q may now be determined as functions of α and μ and may be compared to the corresponding functions for a fixed-pitch rotor, as is shown in Figs. 6 to 10, assuming $\theta = 9°$ for the fixed-pitch rotor.

LONGITUDINAL STABILITY

Using as reference axes body axes through the center of gravity, the x axis pointing in the direction of undisturbed flight (see Fig. 1), the equations of longitudinal motion of the helicopter for a disturbance from level flight read, if only the more important terms are retained (see reference 5, page 5),

$$(W/g)\ddot{x} + W \int \dot{\alpha}\,dt = 0$$

$$(W/g)\,(\dot{z} - \dot{\alpha}V) = \dot{z}Z_{\dot{z}}$$

$$I\dot{\alpha} = \dot{x}M_{\dot{z}} + \dot{z}M_{\dot{z}} + \dot{\alpha}M_{\dot{\alpha}}$$

$\dot{\alpha}$ is the pitching disturbance velocity, and $\dot{x}$ and $\dot{z}$ are the disturbance velocities in x and z direction.

These three equations express the force equilibrium in x and z direction and the moment equilibrium about the pitching axis.

$\dot{z} - \dot{\alpha}V$ is the vertical acceleration in space which is different from $\dot{z}$ because of the angular velocity $\dot{\alpha}$ and the translational velocity V of the reference coordinate system. The three pitching moment derivatives $M_{\dot{z}}$, $-M_{\dot{z}}$, and $-M_{\dot{\alpha}}$ are velocity stability, static or attitude stability, and pitch damping. The force derivative $-Z_{\dot{z}}$ is the vertical damping.

In a system of dimensionless quantities, using the rotor radius R as unit of length, the aircraft mass W/g as unit of mass, and the quantity mR/V as unit of time with $m = (W/g)/\rho AR$, the above equations read

$$\ddot{x} + (m/2)\,c_L \int \dot{\alpha}\,d\bar{t} = 0$$

$$\ddot{z} - \dot{\alpha}m = \dot{z}\bar{Z}_{\dot{z}}$$

$$\bar{I}\dot{\alpha} = \dot{x}\bar{M}_{\dot{z}} + \dot{z}\bar{M}_{\dot{z}} + \dot{\alpha}\bar{M}_{\dot{\alpha}}$$

The dimensionless quantities (symbols with a bar) are determined by the following equations:

Velocity stability, $\bar{M}_{\dot{z}} = M_{\dot{z}}/AR\rho V$

Static stability, $-\bar{M}_{\dot{z}} = (M_{\dot{z}}/AR\rho V)$

Pitch damping, $-\bar{M}_{\dot{\alpha}} = -(M_{\dot{\alpha}}/AR^2\rho V)$

Vertical damping, $-\bar{Z}_{\dot{z}} = -(Z_{\dot{z}}/A\rho V)$

Further,

$$\bar{V} = m; \quad \dot{\bar{z}} = (m/V)\dot{z}$$

$$\dot{\bar{\alpha}} = (mR/V)\dot{\alpha}; \quad \bar{I} = I/(w/g)R^2$$

$$\bar{g} = \frac{m^2}{V^2}\,Rg = \frac{m}{2}\,\frac{W}{(V^2/2)A\rho} = \frac{m}{2}\,c_L$$

$$\bar{t} = (V/mR)t$$

The longitudinal motion is stable if all coefficients of the frequency equation

$$A\bar{\lambda}^4 + B\bar{\lambda}^3 + C\bar{\lambda}^2 + D\bar{\lambda} + E = 0$$

are positive and if

$$BCD - AD^2 - B^2E > 0$$

In most cases the middle term is negligible and the stability criterion reduces to

$$CD - BE > 0$$

The coefficients of the frequency equation read

$$A = \bar{I}; \quad B = -\bar{M}_{\dot{\alpha}} - \bar{Z}_{\dot{z}}\bar{I}$$

$$C = \bar{M}_{\dot{\alpha}}\bar{Z}_{\dot{z}} - \bar{M}_{\dot{z}}m; \quad D = (m/2)c_L\bar{M}_{\dot{z}}$$

$$E = -(m/2)c_L\bar{M}_{\dot{z}}\bar{Z}_{\dot{z}}$$

Inserting these expressions in the simplified stability criterion gives

$$-\bar{M}_{\dot{z}} - (\bar{I}/m)\bar{Z}_{\dot{z}}^2 > 0$$

For zero moment of inertia of the helicopter, the longitudinal motion is stable if velocity stability, static stability, pitch damping, and vertical damping are positive. For finite moment of inertia, the longitudinal motion is stable if this moment of inertia is smaller than the value corresponding to the equation

$$\bar{I}/m = -\bar{M}_{\dot{z}}/\bar{Z}_{\dot{z}}^2$$

This quantity is for the rotor with pitch-cone change plotted against μ in Fig. 13.

STABILITY DERIVATIVES

During attitude or velocity changes of the helicopter the aerodynamic rotor torque varies. The change in rotor speed depends on the engine characteristics for fixed throttle position. Two alternative assumptions will be made: (A) constant engine torque; (B) constant engine r.p.m. The assumption of constant torque is approximately valid for reciprocating engines and for pressure jets at the wing tips. Actually, the torque of a reciprocating engine with fixed throttle position will slightly increase with r.p.m. because of the effect of the blower, and the torque of a pressure jet will slightly decrease with r.p.m. In case a r.p.m. governor is connected to the power regulation, the assumption (B) is valid. Actually, the rotor moment of inertia is also of some importance. For slow attitude or velocity changes of the helicopter, however, the rotor moment of inertia may be neglected, and the constant torque

A-244

assumption will be a good approximation. For rapid changes of attitude and velocity, the constant r.p.m. assumption is valid. The stability derivatives are first given under assumption (A) of constant torque.

The torque coefficient q_c is defined by the equation

$$Q = q_c A R (\rho/2) (V + \dot{x})^2$$

where q_c depends on μ and α. Partial differentiation with respect to $\dot{x}$ and $\dot{z}$, together with the identity $\alpha_i = 1/V$, and considering $\dot{x} \ll V$,

$$(V/2)\mu_{\dot{z}} = -q_c/q_{c\alpha}$$

$$(V/2)\mu_{\dot{x}} = -(1/2)(q_{c\alpha}/q_{c\mu})$$

The pitching moment coefficient c_M (function of α and μ) is defined by the equation

$$M = c_M A R (\rho/2)(V + \dot{x})^2$$

and partial differentiation with respect to $\dot{x}$ and $\dot{z}$, considering $c_M = 0$ for the steady flight state, $\alpha_i = 1/V$, $\dot{x} \ll V$, and the two above equations for $\mu_{\dot{z}}$ and $\mu_{\dot{x}}$, results in

Velocity stability, $\bar{M}_{\dot{z}} = \dfrac{M_{\dot{z}}}{A R \rho V} = -\dfrac{q_c}{q_{c\mu}} c_{M\mu}$

Static stability, $-\bar{M}_{\dot{z}} = -\dfrac{M_{\dot{z}}}{A R \rho V} =$

$$-\frac{1}{2}\left(c_{M\alpha} - \frac{q_{c\alpha}}{q_{c\mu}} c_{M\mu}\right)$$

Similiarly, following from

$$Z = c_L A (\rho/2)(V + \dot{x})^2$$

by partial differentiation and by using the above given expressions for α_i and $\mu_{\dot{z}}$,

Vertical damping, $-\bar{Z}_{\dot{z}} = -\dfrac{Z_{\dot{z}}}{A \rho V} = \dfrac{1}{2}\left(c_{L\alpha} - \dfrac{q_{c\alpha}}{q_{c\mu}} c_{L\mu}\right)$

Finally,

Pitch damping, $-\bar{M}_{\dot{\alpha}} = -\dfrac{M_{\dot{\alpha}}}{A R^2 \rho V} = -\dfrac{c_{M\alpha}}{2}\dfrac{V}{R}$

According to Fig. 1, assuming that the thrust passes in the undisturbed steady flight condition through the c.g. of the helicopter, and approximating thrust by lift force, the derivatives of the pitching moment coefficient read

$$c_{M\dot{\alpha}} = c_L a_{1\dot{\alpha}} \bar{h}$$
$$c_{M\alpha} = c_L a_{1\alpha} \bar{h}$$
$$c_{M\mu} = c_L a_{1\mu} \bar{h}$$

where $\bar{h} = h/R$. Substituting

$$q_c = 2c_Q/\mu^2; \quad q_{c\alpha} = 2c_{Q\alpha}/\mu^2$$
$$q_{c\mu} = (2/\mu^2)[c_{Q\mu} - (2c_Q/\mu)]$$

$$c_L = 2c_T/\mu^2; \quad c_{L\alpha} = 2c_{T\alpha}/\mu^2$$
$$c_{L\mu} = (2/\mu^2)[c_{T\mu} - (2c_T/\mu)]$$

and using further the approximation

$$a_{1\dot{\alpha}} = -(16\mu/\gamma)(R/V)$$

(see reference 5), the expressions for our four derivatives in terms of the coefficients plotted in Figs. 6 to 10 read

Velocity stability, $\bar{M}_{\dot{z}} = \dfrac{c_Q}{(2c_Q/\mu) - c_{Q\mu}} \dfrac{2c_T}{\mu^2} a_{1\mu}\bar{h}$

Static stability, $-\bar{M}_{\dot{z}} = -\dfrac{\bar{h} c_T}{\mu^2} \times$

$$\left[a_{1\alpha} + \frac{c_{Q\alpha}}{(2c_Q/\mu) - c_{Q\mu}} a_{1\mu}\right]$$

Vertical damping, $-\bar{Z}_{\dot{z}} = -\dfrac{1}{\mu^2} \times$

$$\left[c_{T\alpha} + \frac{c_{Q\alpha}}{(2c_Q/\mu) - c_{Q\mu}}\left(c_{T\mu} - \frac{2c_T}{\mu}\right)\right]$$

Pitch damping, $-\bar{M}_{\dot{\alpha}} = -16 c_T \bar{h}/\gamma\mu$

Under the assumption (B) of constant r.p.m., one obtains, with $\mu_{\dot{z}} = \mu/V$ and $\mu_{\dot{x}} = 0$, the following derivatives:

Velocity stability, $\bar{M}_{\dot{z}} = \dfrac{\mu}{2} c_{M\mu} = \dfrac{c_T a_{1\mu} \bar{h}}{\mu}$

Static stability, $-\bar{M}_{\dot{z}} = -\dfrac{1}{2} c_{M\alpha} = -\dfrac{\bar{h} c_T}{\mu^2} a_{1\alpha}$

Vertical damping, $-\bar{Z}_{\dot{z}} = -c_{T\alpha}/\mu^2$

Pitch damping, unchanged

A comparison of the three derivatives $\bar{M}_{\dot{z}}$, $\bar{M}_{\dot{z}}$, and $\bar{Z}_{\dot{z}}$ for the rotor with pitch-cone change and for the fixed-pitch rotor, for constant torque, and for constant rotor speed is given in Figs. 11 and 12. The pitch damping is not plotted because it is almost the same for both rotor types.

The flight conditions assumed for the curves of Figs. 11 and 12 are defined by the assumption of a rotor torque equal to the torque in hovering and of a rotor thrust equal to the thrust in hovering. In terms of coefficients this means that

$$c_Q/c_T = c_{Q0}/c_{T0}$$

where c_{Q0} and c_{T0} are the torque and thrust coefficients in hovering.

These conditions are indicated in Figs. 6 to 10 by dashed lines. For appropriate values of parasite drag of the helicopter, these conditions are also level flight conditions. The main parameters for these conditions may be taken from Tables 2 and 3.

A-245

TABLE 2

Constant Pitch Rotor

μ	$\alpha°$	$\theta°$	$c_T\,10^3$	$c_Q\,10^3$	$a_1°$
0.15	−15.4	9	4.05	0.290	2.8
0.25	−12.6	9	3.70	0.265	4.6
0.35	−11.1	9	3.35	0.240	6.1
0.45	−10.3	9	3.00	0.215	7.7

TABLE 3

Rotor with Pitch-Cone Change

μ	$\alpha°$	$\theta°$	$c_T\,10^3$	$c_Q\,10^3$	$a_1°$
0.15	−13.6	8.8°	4.10	0.275	2.7
0.25	−12.0	9.1	4.00	0.268	4.6
0.35	−11.1	9.5	3.85	0.258	6.4
0.45	−11.0	9.9	3.50	0.235	8.4

REFERENCES

[1] Reeder, J. P., and Gustafson, F. B., *Notes on Flying Qualities of Helicopters*, presented at the Fourth Annual Forum of the American Helicopter Society, April, 1948.

[2] Stewart, W., *Flight Testing of Helicopters*, Journal of The Royal Aeronautical Society, Vol. 52, No. 449, pp. 261–304, May, 1948.

[3] Bailey, F. J., Jr., *A Simplified Theoretical Method of Determining the Characteristics of a Lifting Rotor in Forward Flight*, N.A.C.A. Report No. 716, 1941.

[4] Gustafson, F. B., and Gessow, A., *Effect of Blade Stalling on the Efficiency of a Helicopter Rotor as Measured in Flight*, N.A.C.A. T.N. No. 1250, 1947.

[5] Hohenemser, K., *Longitudinal Stability of the Helicopter in Forward Flight*, A.M.C. Translation No. F-TS-688-RE, August, 1946.

[6] Gustafson, F. B., Amer, K. B., Haig, C. R., and Reeder, J. P., *Longitudinal Flying Qualities of Several Single-Rotor Helicopters in Forward Flight*, N.A.C.A. T.N. No. 1983, 1949.

[7] Gessow, A., and Amer, K. B., *An Introduction to the Physical Aspects of Helicopter Stability*, N.A.C.A. T.N. No. 1982, 1949.

Periodic Motions of a Rectangular Wing Moving at Supersonic Speed

[4] Evvard, J. C., *A Linearized Solution for Time-dependent Velocity Potentials Near Three-dimensional Wings at Supersonic Speeds*, N.A.C.A. T.N. No. 1699, September, 1948.

[5] Miles, J. W., *On the Oscillating Rectangular Airfoil at Supersonic Speeds*, Journal of the Aeronautical Sciences, Vol. 16, No. 6, p. 381, June, 1949.

[6] Garrick, I. E., and Rubinow, S. I., *Flutter and Oscillating Air Forces Calculations for an Airfoil in a Two-dimensional Supersonic Flow*, N.A.C.A. T.N. No. 1158, 1946.

[7] Miles, J. W., *The Aerodynamic Forces on an Oscillating Airfoil at Supersonic Speeds*, Journal of the Aeronautical Sciences, Vol. 14, No. 6, pp. 531–538, June, 1947.

[8] von Borbely, S., *Aerodynamic Forces on a Harmonically Oscillating Wing at Supersonic Velocity (Two-dimensional Case)*, R.T.P. Translation No. 2019, British Ministry of Aircraft Production (from Z.A.M.M., Vol. 22, pp. 190–205, 1942).

[9] Schwarz, L., *Untersuchung einiger mit den Zylinder-funktionen nullter Ordnung verwandter Funktionen*, Luftfahrtforschung, Vol. 20, pp. 340–372, February, 1944.

[10] Busemann, A., *Infinitesimale kegelige Überschallströmung*, Luftfahrtforschung, Vol. 20, pp. 105–121, 1943 (also available as N.A.C.A. T.M. No. 1100, 1947).

[11] Li, Ting-Yi, *Periodic Supersonic Motions of a Thin Wing of Finite Span*, Ph.D. Thesis, California Institute of Technology, 1950.

I.A.S. Nineteenth Annual Meeting

Authors wishing to have papers considered for presentation at this meeting should submit outlines or short abstracts to the Meetings Committee, 2 East 64th St., New York 21, N.Y., no later than September 15, 1950.

A-246

THIS PAGE INTENTIONALLY BLANK

REPORT DOCUMENTATION PAGE

Form Approved
OMB No. 0704-0188

The public reporting burden for this collection of information is estimated to average 1 hour per response, including the time for reviewing instructions, searching existing data sources, gathering and maintaining the data needed, and completing and reviewing the collection of information. Send comments regarding this burden estimate or any other aspect of this collection of information, including suggestions for reducing this burden, to Department of Defense, Washington Headquarters Services, Directorate for Information Operations and Reports (0704-0188), 1215 Jefferson Davis Highway, Suite 1204, Arlington, VA 22202-4302. Respondents should be aware that notwithstanding any other provision of law, no person shall be subject to any penalty for failing to comply with a collection of information if it does not display a currently valid OMB control number.
PLEASE DO NOT RETURN YOUR FORM TO THE ABOVE ADDRESS.

1. REPORT DATE (DD-MM-YYYY)	2. REPORT TYPE	3. DATES COVERED (From - To)
31-10-2003	Contractor Report	Jun 2002 - Oct 2003

4. TITLE AND SUBTITLE
An Overview of Autogyros and the McDonnell XV-1 Convertiplane

5a. CONTRACT NUMBER

5b. GRANT NUMBER
NAG2-1597

5c. PROGRAM ELEMENT NUMBER

6. AUTHOR(S)
Franklin D. Harris

5d. PROJECT NUMBER

5e. TASK NUMBER

5f. WORK UNIT NUMBER
SAT292004D

7. PERFORMING ORGANIZATION NAME(S) AND ADDRESS(ES)
University of Maryland
Dept. of Aerospace Engineering
College Park, MD 20742

8. PERFORMING ORGANIZATION REPORT NUMBER
A-0310910

9. SPONSORING/MONITORING AGENCY NAME(S) AND ADDRESS(ES)
National Aeronautics and Space Administration
Washington, DC 20546-0001

10. SPONSORING/MONITOR'S ACRONYM(S)
NASA

11. SPONSORING/MONITORING REPORT NUMBER
NASA/CR-2003-212799

12. DISTRIBUTION/AVAILABILITY STATEMENT
Unclassified-Unlimited
Subject Category - 05
Distribution: Non-Standard   Available: NASA CASI (301)621-0390

13. SUPPLEMENTARY NOTES
Point of Contact: William Warmbrodt, Ames Research Center, MS 215-1
            Moffett Field, CA 94035-1000; (650)604-5642

14. ABSTRACT

This report and its lengthy appendix first reviews early autogyro history. The period from Juan de la Cierva's invention in the early1920s through to the U. S. Army Air Corps' choice, in 1943, of the helicopter instead of the more fully developed autogyro, is examined from a technical point of view. With this historical background in hand, simple aerodynamic technology for rotors, wings, propeller, and fuselages is provided for reference.

The McDonnell XV-1 convertiplane development and its program are discussed in detail, with particular emphasis on the wind tunnel and flight testing that was accomplished with two prototype aircraft in the early 1950s. The tip drive rotor system with its ingeniously designed hub was well suited to high speed rotorcraft. The configuration was conceived by Kurt Hohenemser and Fred Dubloff. Many photographs taken of the XV-1 stored at Fort Rucker are included in this report's appendix.

15. SUBJECT TERMS
Rotorcraft, Autogyro, Aerodynamics, XV-1

16. SECURITY CLASSIFICATION OF:			17. LIMITATION OF ABSTRACT	18. NUMBER OF PAGES	19b. NAME OF RESPONSIBLE PERSON
a. REPORT	b. ABSTRACT	c. THIS PAGE			William Warmbrodt
U	U	U	UU	282	19b. TELEPHONE NUMBER (Include area code) (650) 604-5642

Standard Form 298 (Rev. 8-98)
Prescribed by ANSI Std. Z39-18